Iron and Phosphorus Cycling under Ferruginous Conditions

Jennifer Thompson

Submitted in accordance with the requirements for the degree of
Doctor of Philosophy

The University of Leeds
Earth Surface Science Institute
School of Earth and Environment

January, 2018

The candidate confirms that the work submitted is her own and that appropriate credit has been given where reference has been made to the work of others.

Assertion of moral rights (optional):

Acknowledgements

Firstly I must thank my supervisors Simon Poulton, Romain Guilbaud and Mike Krom, who's guidance, knowledge and support have been constant throughout. Simon's door has always been open for moments of puzzled head scratching and his enthusiasm for the project has been unwavering throughout the years. I must sincerely thank Romain for the hours spent in the lab, training me in the initial stages of the project, without it I suspect progress would have been much slower! Mike, thank you for always asking the difficult question and for providing knowledge on the intricacies of phosphorus cycling.

I would also like to say a huge thank you to the technical staff who have supported me (scientifically and motivationally!), particularly Stephen Reid for analysing my "mucky" solutions, Lesley Neve for help with XRD and Andy Connelly for his ever smiling face at the end of a long day.

My time at Leeds would not have been anywhere near as enjoyable without being surrounded by the very social Cohen Geochemistry group, and a big thank you must go to the SCR crew who have always been there for lunch, laughs, rants and afternoon ice cream. Particular thanks must go to Kathy and Mark, my "scientific family", having you guys in the lab with me provided a huge amount of entertainment. Andy and Julie, thanks for putting me up and providing me with many takeaways over the last year or so, you've made the final push so much more bearable! Ais, what can I say? I echo your thanks for the food and the Lego, and would like to add my appreciation for the endless kitchen dancing and generally keeping me alive!

Finally I must thank my friends and family for being so incredibly supportive from start to finish. Suzie and Andy for never failing to believe that I would one day finish and not asking how the write up was going too often. Sam, thank you for putting up with me during the worst times and providing me with some of the best times. I'm not sure you knew what you were getting yourself into when we first met, but thank you for all your love and support (and our home!). Most importantly I must thank my parents. Thank you for teaching me to believe I

can achieve anything I set my mind to and for supporting me when it didn’t always go quite to plan. (Dad, this still doesn’t mean I’m a geologist!)

Abstract

Considering the entirety of Earth's history, the ocean has dominantly been in an anoxic, non-sulphidic state, with the water column containing dissolved iron (termed 'ferruginous'). Despite the significance of such conditions, the cycling of nutrients in ferruginous settings remains poorly understood. Phosphorus (P) is thought to be the ultimate limiting nutrient on geological timescales. Therefore it is essential to constrain the behaviour of P under ferruginous conditions in order to evaluate feedback mechanisms associated with P stimulation of primary productivity, organic carbon burial and ultimately oxygen production. This study aims to further our understanding of iron (Fe) and P cycling under ferruginous conditions, through the investigation of a modern ferruginous lake and ancient sedimentary rocks deposited under ferruginous conditions.

Modifications are made to the SEDEX P sequential extraction method to make it suitable for use with ancient sedimentary rocks and Fe-rich sediments. Using this newly revised method, the previously unidentified magnetite-bound pool of P is shown to have constituted a significant proportion of reactive P in many ancient ferruginous environments, indicating that magnetite may require further consideration when modelling P cycling under ferruginous conditions.

Detailed investigation of the water column and sediments of the ferruginous Lake La Cruz reveals that whilst a substantial amount of P is released from the sediments, the formation of reduced Fe phosphates in the water column exerts a strong control on the vertical extent of the benthic P flux, a process that is most likely enhanced over the deeper water column depths of ancient ferruginous oceans.

P partitioning in ancient sedimentary rocks from the ~1.8 billion year old Animikie Basin reveals that under stable redox environments, ferruginous conditions cause significant drawdown and burial of P, most likely resulting in a P limited water column. Whilst the majority of this P is now present as authigenic calcium phosphates, the presence of magnetite-bound P and

observations of the modern ferruginous Lake La Cruz suggest this was most likely initially drawn down in association with Fe minerals.

Table of Contents

List of Tables

List of Figures

Chapter 1 Introduction

1.1 Evolution of the redox state of the earth

1.1.1 Introduction

The chemical development of the ocean and atmosphere throughout the Precambrian is thought to be critical to the timing of eukaryote evolution and rates of diversification (Lyons et al., 2014). The introduction of free oxygen into the Earth's system is of particular interest; whilst it forms 21% of our atmosphere today, for approximately half of Earth's history, oxygen is thought to have been mostly at levels less than 0.001% of present atmospheric level (PAL) (Lyons et al., 2014). Tracking this vital element through deep time is complex, and we must look to the geological record for fingerprints of the geochemical processes that occurred during this deterministic period of Earth history. Decades of research has suggested that the transition from the anoxic environment of the Archean to the dominantly oxic conditions of the Phanerozoic happened in two significant steps, believed to be bookending the Proterozoic (Figure 1.1).

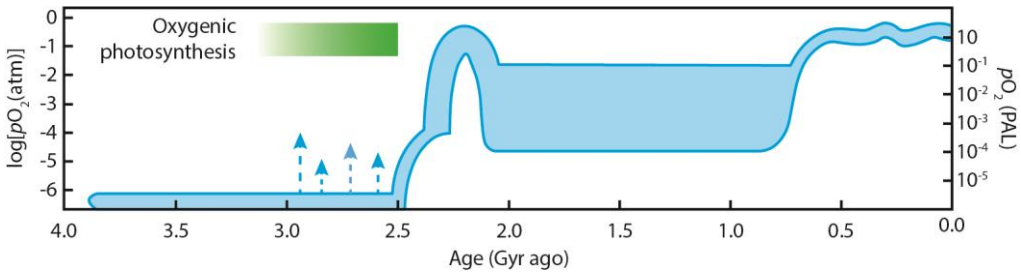

Figure 1.1 Reconstruction of atmospheric O_2 through time (after Lyons et al., 2014)

Two main rises occurred roughly 2.3 billion and 0.8 million years ago, with O_2 concentrations between these two events less well constrained (see Planavsky et al., 2014 and Zhang et al., 2016). Dashed arrows indicate "whiffs" of oxygen prior to 2.5 billion years ago.

The first leap, known as the Great Oxidation Event (GOE), is believed to have occurred approximately 2.47 to 2.32 billion years ago (Holland, 2002), sometime after the evolution of oxygenic photosynthetic organisms. However, atmospheric O_2 appears to have then stabilised at just under 10% PAL for

another billion years, although estimates of atmospheric O_2 during this time still cover a wide range (Planavsky et al., 2014b, Zhang et al., 2016). Whilst this level of atmospheric O_2 was significantly higher than during the Archean, it is generally thought that this was not enough to penetrate more than just the very surface of the ocean. A second rise occurred ~0.58 billion years ago, and only at this point did the deep oceans become oxygenated (Canfield et al., 2008, Canfield et al., 2007, Poulton and Canfield, 2011), allowing for the evolution of large multicellular organisms (Canfield et al., 2007), although evidence of large colonial organisms with a multicellular degree of organisation at 2.1 Ga (Albani et al., 2010) challenges this view . The reason for this intermediate stasis in oxygen concentration during the Proterozoic is still being pursued. It is thought the initial perturbation of the GOE may have been dampened by some feedback mechanism until a threshold was reached at the end of the Proterozoic. In order to determine an explanation, we must first gain a detailed understanding of the biogeochemical processes occurring during this time.

1.1.2 Controls on atmospheric oxygen

Earth's oxygen ultimately comes from photosynthesis (Lyons et al., 2014), but for there to be an appreciable rise in atmospheric concentrations, the global cycle must become perturbed with the sources outweighing the sinks for a time.

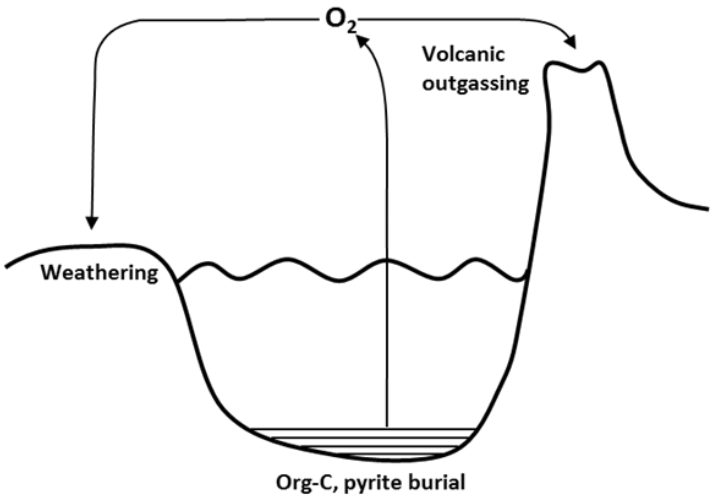

Figure 1.2 Simplified oxygen cycle, representing one source (marine burial of organic C and pyrite) and two sinks (weathering and volcanic outgassing) (Canfield, 2005).

The concept of these sources and sinks (Figure 1.2) and their controls on atmospheric oxygen were first described by Ebelman (1845), but largely lay dormant until it was independently rediscovered by Garrels and Perry (1974) and Holland (1978). Since then, work has continued to investigate the processes involved.

1.1.2.1 Oxygen Sources

It is estimated that 99.9% of the organic matter from primary production on Earth is decomposed (Canfield, 2014), removing oxygen from the atmosphere that was produced during photosynthesis. The 0.1% of organic matter that escapes decomposition and is buried in sediments, ultimately transforming into rocks (organic carbon (C) burial), represents a net source of oxygen to the atmosphere (Figure 1.2). Similarly, respiration of organic matter is commonly carried out by bacterial sulphate reduction, producing hydrogen sulphide. This sulphide will react with iron (if present) to form pyrite (FeS_2), which can then be re-oxidised to sulphate or buried in the sediment. As the pyrite was ultimately formed from the reducing power of organic matter, burial in sediments presents a net source of oxygen to the atmosphere.

1.1.2.2 Oxygen Sinks

Organic matter and pyrite that escape initial oxidation through burial in sediments are entered into the geological rock cycle. Eventually, these rocks are reintroduced to the atmosphere via tectonic uplift and become subject to weathering, where oxygen reacts with the organic matter and pyrite, forming a sink for atmospheric oxygen (Figure 1.2), and thus completing the cycle. The chemically reduced gases produced by volcanoes, such as H_2, H_2S and SO_2, also provide a removal mechanism for oxygen, reacting to form sulphate and water. This final sink (volcanic outgassing) acts independently of any feedbacks within the rest of the oxygen cycle and depends purely on tectonics. However, the two other major processes governing atmospheric oxygen (organic carbon and pyrite burial and oxidative weathering) are intrinsically linked with multiple other complex cycles, on which the redox state of the oceans and sediments have a strong influence.

1.1.3 Organic matter mineralisation

Organic matter mineralisation can occur via a variety of metabolic pathways, each using a different electron acceptor, although when oxygen is absent (anoxic), they all result in reduced rates of organic matter decomposition compared to aerobic respiration (Canfield, 2014). In nature, the order in which these acceptors are utilized can be described simply by the thermodynamics of the process and the energy the organisms are set to gain (Berner, 1980, Froelich et al., 1979, Stumm and Morgan, 1970), and this results in a predictable series of chemical zones in the environment.

1.1.3.1 Chemical zonation

Figure 1.3 demonstrates that the first electron acceptor is typically exhausted before the next is utilised, but it is not uncommon for an overlap in the respiration processes to occur. In an environment with little or no free oxygen, less efficient metabolic pathways are heavily relied upon, and with reduced rates of organic matter decomposition, they result in enhanced concentration of organic carbon being buried. As such, ocean redox itself has a large influence on the balance of the oxygen cycle.

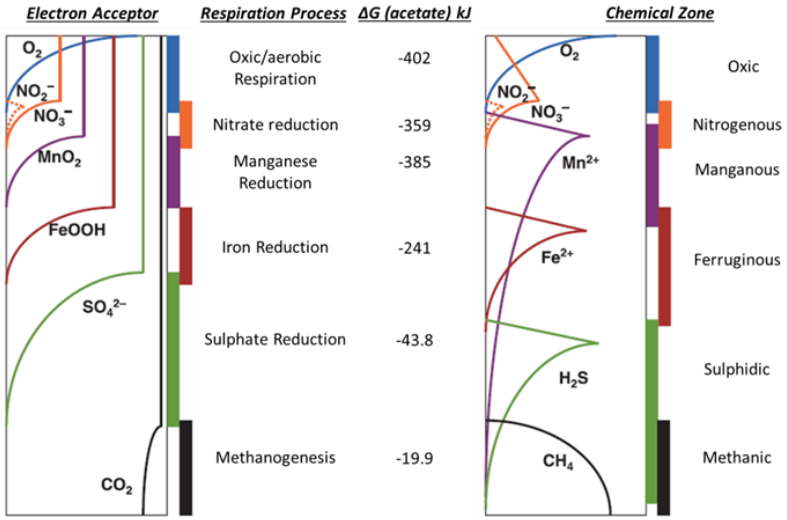

Figure 1.3 A Schematic of the depth distribution of common electron acceptors (left) and the associated chemical zones (right).

The standard Gibbs free energy is given for each respiration process and is based on acetate as an electron donor. Values are standardized to a $4e^-$ transfer equivalent to the oxidation of 1 mole of organic C with an oxidation state of 0 (Canfield and Thamdrup, 2009).

Purely based on the reduced rates of organic carbon mineralisation associated with anaerobic metabolisms, anoxic oceans are self-limiting due to the negative feedback depicted in Figure 1.4. However, ocean anoxia also affects other biogeochemical cycles that influence the cycling of organic matter, and hence oxygen production, the intricacies of which also depend on the type of anoxia.

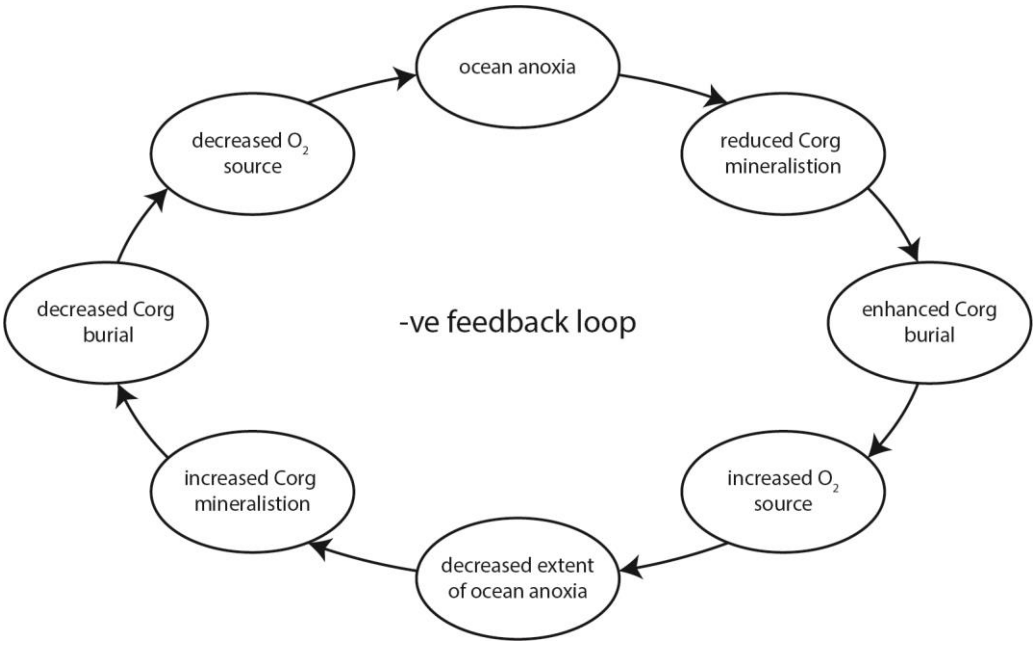

Figure 1.4 A simplified negative feedback on oxygen created by anoxic oceans, based purely on the influence of anaerobic metabolisms. Organic C (Corg).

To understand Earth's atmospheric oxygenation history, we must first constrain the evolution of ocean redox and the associated feedback mechanisms with time, and one of the main ways to track ocean redox through time is by examining the geological rock record.

1.2 Tracking ocean redox

Scientist's views on the redox history of the oceans throughout the Precambrian have varied over time. Until 1998, the prevailing theory was the oceans were anoxic with dissolved iron and no sulphide (termed 'ferruginous') up until the disappearance of banded iron formations (BIFs) by 1.8 Ga, when they became completely oxygenated apart from a few brief instances of iron-rich conditions during "snowball Earth" glaciations nearly a billion years later (Cloud, 1972, Holland, 1984). Canfield (1998), however, challenged this

paradigm that oxygenation of the deep ocean overwhelmed all of the iron sources and led to the demise of BIFs. Instead, they suggested that the deep oceans remained anoxic for another billion years, and it was high concentrations of H_2S that resulted in the cessation of BIFs. In 2008, it was proposed that the supply of sulphate through oxidative weathering, and the capacity to form and bury pyrite in deep ocean settings, was sufficient to consume dissolved Fe for millions of years (Canfield et al., 2008). However, any reduction in the supply of sulphate would decrease the ocean's capacity to lock up Fe as pyrite, allowing ferruginous conditions to return, as hypothesised for ~700 Ga. Until recently, most research has continued with this assumption, that the Paleo- Mesoproterozoic (from 1.8 Ga to 0.75 Ga) ocean was euxinic (anoxic with dissolved sulphide in the water column). Euxinia, however, is an end-member in terms of the redox state of the ocean; in fact there are key stages between fully oxic and euxinic: varying levels of oxygen depletion, and completely anoxic but non-sulphidic. These intermediate redox states can have a significant effect on the biogeochemical cycling that occurs within the water column. Poulton and Canfield (2011) recently suggested a ferruginous water column may have been a dominant feature throughout the Precambrian.

For the oceans to have been euxinic, the sources of sulphide (H_2S) to the ocean would have to exceed those of iron, ensuring excess sulphide after the precipitation of all the ferrous iron as pyrite. However, before the rise of oxygen, sources of sulphide to the oceans were limited to volcanism and hydrothermal vents (Raiswell and Canfield, 2012b),which are both minor fluxes compared to the amount of sulphate (SO_4^{2-}) delivered by rivers in the modern, dominantly oxygenated environment of the Phanerozoic. Iron (Fe) would also have been supplied by hydrothermal vents (along with continental weathering), but for Fe, this would have been a much more significant source on the early Earth. Ancient vents may have had a considerably higher Fe(II)/H_2S ratio than modern ones, exceeding the ratio of pyrite, resulting in a net source of Fe(II) to the oceans (Kump and Seyfried, 2005).

1.2.1 Techniques

Where sediments have been preserved, the redox state of the overlying water column during deposition can be determined. The development of a sequential extraction technique for iron (Poulton and Canfield, 2005) has allowed the

quantification of different fractions of iron, crucially “highly reactive” iron. Highly reactive iron (Fe_{HR}) can be divided into 4 main pools of minerals: iron associated with (1) carbonate minerals (Fe_{carb}), such as ankerite and siderite; (2) ferric (oxyhydr)oxides (Fe_{ox}), such as ferrihydrite, lepidocrocite, goethite and hematite; (3) magnetite (Fe_{mag}); and (4) Fe sulphide (Fe_{py}), generally as pyrite. Fe_{carb}, Fe_{ox} and Fe_{mag} will all react with sulphide post deposition on early diagenetic timescales (months – few years) and therefore when this has occurred, the Fe sulphide extraction procedure of Canfield et al. (1986) should also be used to determine sulphide phases (e.g. pyrite and acid volatile sulphides). The highly reactive Fe pool can therefore be defined as:

$$\mathbf{Fe_{HR} = Fe_{carb} + Fe_{ox} + Fe_{mag} + Fe_{AVS} + Fe_{py}}$$

where Fe_{AVS} is the amount of Fe associated with acid volatile sulphides. The ratio of Fe in these highly reactive pools to total Fe (Fe_{HR}/Fe_T) can reveal if they were deposited in an oxic or anoxic water column (Figure 1.5).

$Fe_{HR}/Fe_T \geq 0.38$ indicates anoxic depositon

$Fe_{HR}/Fe_T \leq 0.22$ indicates oxic deposition

$0.22 < Fe_{HR}/Fe_T > 0.38$ equivoval

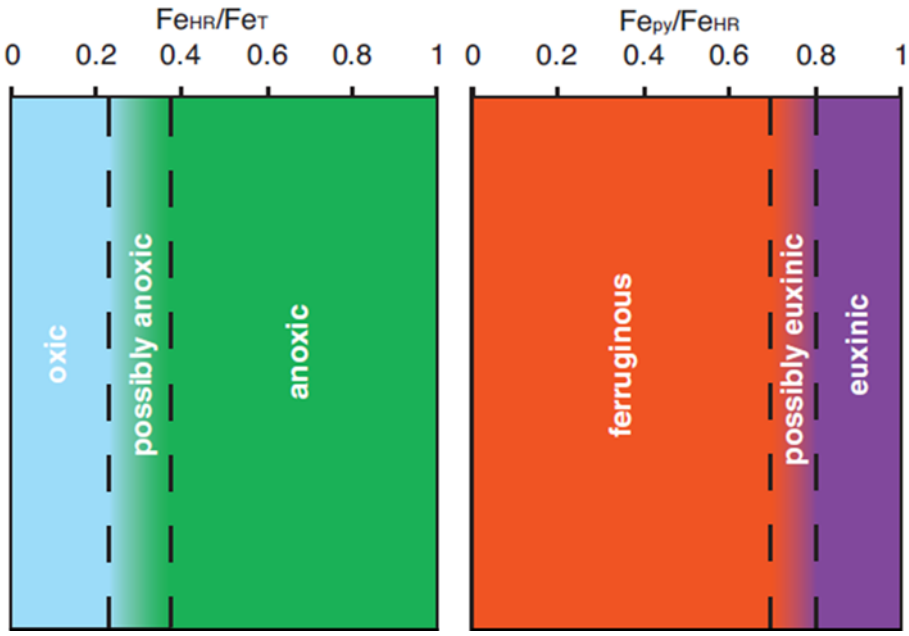

Figure 1.5 A visual representation of the iron speciation parameters used to determine ocean redox. Dashed lines represent the thresholds discussed in the text (Poulton and Canfield, 2011).

These values have emerged from studies on Precambrian, Phanerozoic and modern marine sediments; with sediments depositing from an anoxic water column displaying values >0.38 due to an enrichment in highly reactive Fe, whereas an oxic water column produces ratios less than this. A ratio of 0.22 represents the upper limit of most Phanerozoic sediments deposited under oxic conditions (0.14 ± 0.08, Poulton and Raiswell 2002), and intermediate values between this average and the upper limit of 0.38, may still reflect anoxic deposition where the original Fe_{HR} enrichment has been masked by rapid sedimentation rates (Poulton et al., 2004a, Raiswell and Canfield, 1998) or the conversion of unsulphidised Fe_{HR} to less reactive sheet silicate minerals during diagenesis or metamorphism (Lyons and Severmann, 2006, Poulton et al., 2010, Poulton and Raiswell, 2002). The latter can be evaluated by two methods: comparing the Fe_T/Al ratio with that of average shale (~0.5, see Lyons and Severmann, 2006), with enrichments in Fe_T supporting anoxic deposition; and by determining the pool of poorly reactive sheet silicate minerals using an additional extraction (Poulton et al., 2010).

Sediments that appear to have been deposited under anoxic conditions (Fe_{HR}/Fe_T>0.38), can then be distinguished between euxinic and ferruginous settings based on the degree of sulphidisation of the Fe_{HR} pool (Fe_{py}/Fe_{HR}). Sediments deposited from the water column of the Black Sea suggest a Fe_{py}/Fe_{HR} > 0.8 is indicative of euxinic conditions, however, März et al. (2008) demonstrated that perhaps 0.7 would be a more suitable upper threshold for ferruginous conditions, leaving ratios between 0.7 and 0.8 as somewhat equivocal.

1.2.2 Precambrian redox conditions

Banded Iron Formations (BIFs) are expansive units of chemical sediments comprising of silica- and iron-rich minerals precipitated from seawater, and their occurrence throughout the Archean and the early Paleoproterozoic (Figure 1.6) is indicative of the ferruginous conditions that are thought to have prevailed in the oceans of this period. It is generally agreed that the deposition of BIF required a large flux of Fe to the oceans, and for that dissolved ferrous Fe to be transported over large distances, the oceans had to be anoxic. Sulphide concentrations would also need to be low to prevent the precipitation of Fe sulphides. Rare earth element patterns and neodymium isotope data

from BIF have led to the common assumption that the majority of Fe required for BIF deposition was supplied by hydrothermal vents (Derry and Jacobsen, 1990), although diagenetic recycling of Fe and continental weathering may have also contributed (Li et al., 2015b, Raiswell, 2006). The mechanisms behind BIF deposition, however, are still under debate as the original precipitates are difficult to identify. Even in the most pristine, unweathered examples of BIF, most of the grains (Fe oxides, carbonates silicates and chert) are interpreted to be at least diagenetic and even metamorphic (Rasmussen et al., 2016). BIFs that have undergone weathering and mineralization processes are dominated by secondary Fe oxides.

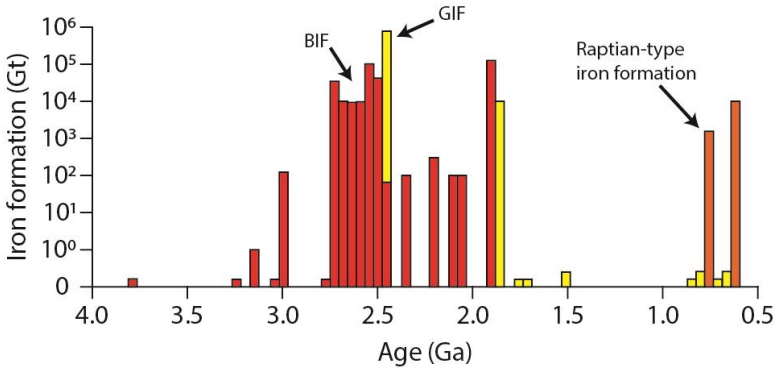

Figure 1.6 Distribution of iron formations through time, modified from Bekker et al. (2010) and Konhauser et al. (2017).

Most deposits before 2.4 Ga are banded iron formations (BIF, red). Between 2.3-0.8 are granular iron formations (GIF, yellow).Orange bars ~0.7 Ga are Raptian-type iron formations associated with glacial deposits.

The most conventional view is that some hematite in BIFs is primary, having formed following the dehydration of the initial precipitate ferrihydrite. As such, there is a large amount of support for an iron oxidising process as the main mechanism for BIF deposition. Prior the Great Oxidation Event, the oxidation of ferrous Fe in seawater is thought to have occurred through photochemical or biologically mediated processes (i.e. photoferrotrophy and cyanobacteria) (Ahn and Buseck, 1990, Bekker et al., 2010, Beukes and Gutzmer, 2008, Cloud, 1968, Kappler et al., 2005, Konhauser et al., 2007a, Konhauser et al., 2002, Sun et al., 2015). In support of this, Fe(II) oxidation by anoxygenic photosynthetic bacteria has been shown to occur in two stratified (year-round,

termed ‘meromictic’) lakes that are thought to be analogues for the Archean ocean (Crowe et al., 2008a, Walter et al., 2014).

As mentioned previously, this conventional theory is based on hematite in BIFs being a primary mineral; however there is uncertainty about this as there is evidence that, in some cases, the hematite may have formed by replacement reactions during post-depositional oxidation (Kaufman et al., 1990, Rasmussen et al., 2014a, Rasmussen et al., 2014b). As a result, an alternative mechanism for BIF deposition has been proposed, based on the primary Fe deposit in at least some BIFs being Fe silicates (Rasmussen et al., 2015, Rasmussen et al., 2016). Indeed, experiments on analogues of Precambrian seawater support the suggestions of inorganic precipitation of Fe silicates (Harder, 1978, Konhauser et al., 2007a, Tosca and Guggenheim, 2014, Tosca et al., 2016).

The answer may not be one mechanism or the other for all BIFs, but rather both processes may have occurred, with the dominant one varying over time and with depositional setting. The two proposed mechanisms do however highlight a need to evaluate the probable primary deposit in each BIF prior to postulating deposition mechanisms and interpreting further geochemical analysis. Recent work by Rasmussen et al. (2016) has shown that using a variety of petrographic techniques and paying attention to the textural evidence surrounding the mineral grains in BIF can help to elucidate the primary phases from those probably formed during late state alteration processes (Rasmussen and Muhling, 2018, Rasmussen et al., 2016).

As seen in Figure 1.6, the occurrence of BIFs during the Archean and particularly the Paleoproterozoic is not constant; and it has been shown to be associated with periods of enhanced volcanism (Isley and Abbott, 1999). The redox structure of the oceans between these pulses is largely unidentified; however, studies of marine shales have provided some evidence for the accumulation of dissolved oxygen along the margins of the Archean ocean (Kendall et al., 2010, Reinhard et al., 2009). The cessation approximately 1.85 Ga ago (apart from short periods in the Neoproterozoic, tied to glaciations), indicates a distinct change in the chemical structure of the oceans. In order for the deposition of BIFs to cease, either the flux of Fe(II) to the oceans must have weakened, or the input of sulphide increased, causing the formation of Fe

sulphides rather than (oxyhydr)oxides, providing that the ocean did not become oxic.

1.2.2.1 Evolution of oxygenic photosynthesis in the Archean?

Whilst there is a range of good evidence for anoxygenic phototrophy in the early Archean, dating back to 3.416 Ga in South Africa (Tice and Lowe, 2004, Tice and Lowe, 2006) and 3.7-.3.8 Ga in Greenland (Czaja et al., 2013), evidence of the presence of cyanobacteria and the evolution of oxygenic photosynthesis prior to the GOE is far more controversial. Stromatolites have previously been interpreted as products of cyanobacteria, with the record stretching back more than 3.4 Ga (Allwood et al., 2006, Hofmann et al., 1999), however the relationship between them and cyanobacteria as since been thrown into question. The discovery of 2-methylhopane biomarkers in Archean rocks was thought to be evidence of cyanobacteria predating the rise of oxygen (Brocks et al., 1999), but subsequent studies recognised that these molecules aren't unique to cyanobacteria. A range of trace metal proxies have been used to suggest "whiffs" of oxygen in Archean surface environments, most notably this has been interpreted from chromium and molybdenum isotopes along with trace metal data in strata from nearly 3 billion years ago (Crowe et al., 2013, Planavsky et al., 2014a). However, interpretation of these signatures remains controversial, not least because there is limited understanding of their geochemical cycles in both modern and ancient environments, but also as many of these "whiff" signatures appear to conflict with independent geochemical O_2 proxies that suggest anoxia.

The idea that oxygenic photosynthesis could evolve more than one billion years prior to the GOE without resulting in an appreciable rise in atmospheric O_2 has recently been tested by Ward et al. (2016) using a simple mathematical approach, taking into account many of the salient features of the major biogeochemical fluxes and reservoirs present in the Archean and early Paleoproterozoic surface environments. They showed that oxygenation following the evolution of oxygenic photosynthesis would have overwhelmed redox buffers within ~100kyrs, suggesting that this unique metabolism most likely arose shortly before the rise of oxygen, rather than hundreds of millions of years before it.

1.2.2.2 Redox structure of the Paleoproterozoic

Poulton et al. (2010) studied a suite of six cores from the 1.88-1.83 billion-year old Animikie group from the Superior region, North America, and they provide a high resolution picture of an ocean margin setting. On analysing the iron speciation, organic C, and sulphur isotope data for the six cores, evidence for a transition from a fully ferruginous water column to euxinic conditions in continental margin settings – extending at least 100km from the palaeoshoreline – is clear; the deep ocean however appeared to remain anoxic and ferruginous throughout.

Analysis of the molybdenum isotope composition (Kendall et al., 2011) of the most proximal core, lead to similar conclusions about the spatial extent of euxinia. Model calculations by Dahl et al. (2011) suggested that due to the efficiency of Mo burial in euxinic environments, no more than a few percent of the seafloor needed to be euxinic to produce the inferred seawater Mo concentration and isotopic signature.

Another reason for proposing that euxinia was restricted to the margins is that globally it would have been difficult to sustain. Whilst Canfield (2004) suggested that euxinic conditions were limited temporally by subduction of sedimentary sulphides, a negative feedback mechanism based on the cycling and removal of Mo under euxinic conditions, has been suggested to restrict conditions spatially (Scott et al., 2008). Removal of this bioessential, redox-sensitive metal would limit primary production, which in itself would limit euxinia.

Until recently, this redox structure of euxinic margins and ferruginous deeper water was thought to persist throughout the Palaeoproterozoic, until the first Neoproterozoic glaciation (~717 million years ago). However, Guilbaud et al. (2015) presented evidence for a global transition from sulphidic to ferruginous mid-depth waters in the earliest Neoproterozoic, coincident with the amalgamation of the supercontinent Rodinia at low latitudes.

1.2.3 Influence of ocean redox on biogeochemical cycles

Despite there being some disagreement about how dominant ferruginous conditions were and the time periods they prevailed, it is now widely accepted that they were a prominent feature of the Precambrian. As a result, to

understand biogeochemical cycling during these periods, it is essential that we know the minerals that existed, and how they interacted with nutrients. Currently, models used to reconstruct biogeochemical cycles of ancient oceans are based on ferrihydrite (Konhauser et al., 2009, Planavsky et al., 2010), which is the dominant precipitate of Fe^{2+} oxidation in oxic oceans. Kappler et al. (2005), however, suggest that other Fe minerals may have greater importance during anaerobic oxidation, an oxidation pathway that would have been significant during the Precambrian. Studies of modern ferruginous systems such as Lake Matano, Indonesia, have identified anoxygenic phototrophic Fe(II)-oxidising bacteria and the mineral green rust as having potentially important roles in iron cycling under ferruginous conditions (Crowe et al., 2008a, Crowe et al., 2008b, Zegeye et al., 2012). Guilbaud et al. (2013), also demonstrated that synthetic carbonate green rust transforms progressively and completely into a mixture of magnetite and siderite when aged under anoxic conditions, suggesting these minerals could also be of significance.

Now the prominent Fe minerals of ferruginous systems are being identified (see Halevy et al., 2017 and Li et al., 2017), we must also consider their interactions with other key biogeochemical elements. Mineralogical controls on phosphorus (P) are of particular interest as P is thought to be the ultimate limiting nutrient on geological timescales (Tyrrell, 1999). Thus the bioavailability of P through time can be considered to exert a key control on organic C production and ultimately, atmospheric oxygenation (Poulton, 2017).

1.3 The phosphorus cycle

1.3.1 The importance of phosphorus

Phosphorus is a key element of life on Earth. As a structural component of all organisms, P forms the backbone of DNA and RNA and is crucial in the transmission of chemical energy through ATP molecules. As such an essential nutrient, the bioavailability of P in the environment has the potential to limit primary productivity. Marine phytoplankton have been observed to have a remarkably constant carbon:nitrogen:phosphorus (C:N:P) ratio of ~106-117:16:1 (Anderson and Sarmiento, 1994, Redfield, 1958). The stability of this ratio suggests an intrinsic link between the three elements. Approximately 80

years ago, Alfred C. Redfield noted that upon the biological depletion of nutrients, no great excess of either N or P remained, suggesting a perfect balance between these two important components (Redfield, 1934). However, large ocean data sets have since revealed that nitrate tends to run out slightly before P in surface waters (see Tyrrell and Law, 1997). As such, it is widely accepted that locally, and on short timescales, nitrate concentrations are the most limiting factor, and hence nitrogen can be described as the “proximate limiting nutrient” (Tyrrell, 1999). However, the “ultimate limiting nutrient” represents the nutrient whose supply rate forces total system productivity over long timescales, and this is commonly assigned to phosphorus (Codispoti, 1989, Redfield, 1958, Tyrrell, 1999, Van Cappellen and Ingall, 1996).

1.3.2 Modern oceanic phosphorus cycling

In its simplest form, the global P cycle (Figure 1.7) has four major processes: (1) tectonic uplift of P-bearing rocks; (2) chemical and physical weathering of those rocks to produce soils, and introduce dissolved and particulate P to rivers; (3) transport of P to lakes and the ocean via rivers; and (4) sedimentation of P from the water column in association with organic matter and minerals and its subsequent burial in the sediments, providing new material for uplift (Ruttenberg, 2003).

However, within the marine realm there are a series of internal, more complex processes that govern the cycling of P. Dissolved P delivered to the oceans by rivers becomes linked the to the marine C and N cycles during fixation of the these elements during photosynthesis in the oceans surface layer, leading to development of the Redfield ratio as discussed above. In the open ocean, beyond the continental shelves and the influence of riverine particulate matter, P is mostly associated with organic matter which is extensively recycled in the upper water column through respiration processes. As particles aggregate and sink, respiration continues with depth, causing P concentrations to build in deeper waters relative to the surface where P is rapidly utilised (e.g. Conley et al., 2002, Luff and Moll, 2004). The majority of particulate P sinking towards the sediments is thought to be in association with organic matter (20-40%), with inorganic particulate P partitioned mainly between ferric (oxyhydr)oxides and apatite (Berner and Rao, 1994, Lebo, 1991, Lucotte and Danglejan, 1983). However, where deep water dissolved P encounters Fe (oxyhydr)oxides

produced by hydrothermal vents, sorptive reactions can result in a substantial removal mechanism. Regardless of its form, sedimentation of particulate P and its eventual burial within sediments is the sole removal mechanism in the marine P cycle (Delaney, 1998, Froelich et al., 1982, Ruttenberg, 1993), and hence has a large control on marine P dynamics.

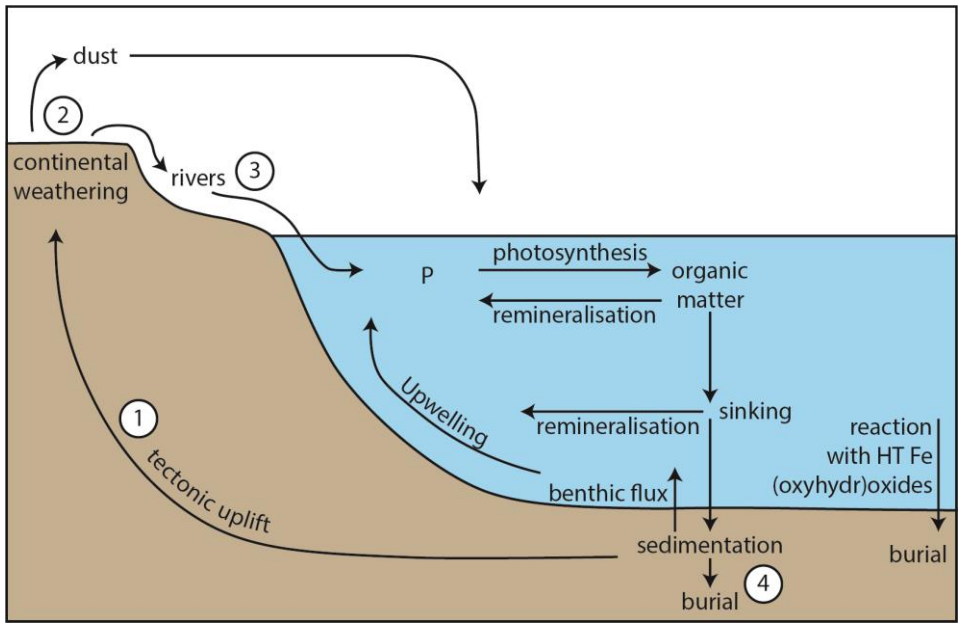

Figure 1.7 A schematic of a simple P cycle

HT stands for hydrothermal. Sorptive removal of P by Fe (oxyhydroxides) originating from hydrothermal vents has been shown to be an important sedimentation mechanism (Wheat et al., 1996)

1.3.2.1 P burial in sediments

The location of marine sediments has a large influence on the forms of P found within them. Coastal shelf and slope environments receive a greater flux of continentally derived P from riverine input compared with the abyssal plains, and this combined with a shorter overlying water column results in the two environments having distinct patterns of sedimentary P partitioning. The proximity of shelf and slope sediments to the delivery of terrigenous P (both organic and inorganic) increases the flux of P and material to the sediment in this environment due to the limited transport of particulate material offshore. The resulting increased sedimentation rates (Filippelli, 1997a,b) can lead to enhanced burial of all forms of P, but when combined with a short overlying

water column (and therefore less respiration of organic matter before deposition) it particularly promotes enhanced burial of organic P.

Authigenic calcium associated P (Ca-P), mostly authigenic apatite, generally dominates sedimentary phosphorus in both coastal and offshore sediments of the modern ocean (Ruttenberg, 2003), but comprises a larger fraction offshore. This is in part due to a weaker flux of Fe-bound, organic and detrital P to sediments away from the coastline; heavy grains of detrital apatite are particularly unlikely to be transported beyond the near-shore zone.

The fractions of P that reach the seafloor, however, do not always represent those that will undergo burial, removing P from the marine P cycle. Within the sediment, microbially-mediated respiration of organic matter can cause the release of a substantial amount of the labile organically-bound P as dissolved inorganic P (DIP) (Anderson et al., 2001, Berner and Rao, 1994, Froelich et al., 1988, Jahnke, 1996, Krom and Berner, 1981, Ruttenberg, 2003). This DIP can efflux from the sediment back into the water column or can undergo further reactions with other sedimentary components. These reactions can include adsorption and/or co-precipitation with Fe (oxyhydr)oxide and carbonate minerals, uptake by bacteria, or transformation to other secondary phases such as authigenic carbonate fluorapatite (CFA) or vivianite (Anschutz et al., 1998, Berner, 1981, Egger et al., 2015, Martens et al., 1978, Rothe et al., 2014, Ruttenberg and Berner, 1993, Slomp et al., 1996b, Van der Zee et al., 2002). The formation of these secondary phases can significantly enhance P burial efficiency, thereby reducing the benthic flux of DIP to the water column and potentially affecting the primary productivity potential of surface waters (Ruttenberg, 2003).

Diagenetic transformations of P within the sediments, particularly in coastal environments, are affected by the chemical, physical and biological conditions of both the sediments and the overlying bottom-water (e.g. Colman and Holland, 2000, Mort et al., 2010, Slomp, 2011), and therefore need to be investigated and constrained for a variety of different environments. Given the influence diagenetic recycling of P can have on primary production and hence ultimately oxygen production, it is paramount that we attempt to understand P cycling throughout Earth’s history, particularly during the evolution of atmospheric oxygen in the Precambrian. P cycling occurring in environments

that reflect the euxinic ocean margins of the Proterozoic, such as the Black Sea, Baltic Sea, and Lake Cadagno, are being increasingly studied (Meyer and Kump, 2008, Mort et al., 2010, Lukkari et al., 2009, Canfield et al., 2010, Dahl et al., 2010, Wirth et al., 2013, Dijkstra et al., 2014), but locations with ferruginous conditions are much harder to come by in the modern, high sulphate world.

1.3.3 P cycling under ferruginous conditions

Due to the high concentration of dissolved Fe(II) in the water column and the enrichment of highly reactive Fe in the sediments, the interaction of iron minerals with P is likely to play an important role in the cycling of P under ferruginous conditions (Bjerrum and Canfield, 2002). Recently in the meromictic Lake Pavin (France), mineralogical analysis of suspended particulate matter has shown vivianite to be the dominant Fe mineral in the ferruginous deep waters, with an amorphous mixed valance Fe-phosphate present in the redoxcline (Busigny et al., 2016, Cosmidis et al., 2014). They suggest, that Fe-oxidation rather than reduction plays an important role in the precipitation of these Fe-phosphates in the water column, due to the persistence of Fe (oxyhydr)oxides throughout the anoxic layer. However, these highly reactive Fe minerals are not present in the sediments below, suggesting reductive Fe dissolution does occur within the sediments. Whilst Cosmidis et al. (2014) provide strong evidence of the importance of Fe-bound P in this ferruginous lake and suggest the involvement of polyphosphate-accumulating microorganisms in the precipitation of Fe-phosphates in the water column of Lake Pavin, our understanding of the P cycle in this system is incomplete, as other pools of phosphorus were not investigated. Fe phosphates appear to be the dominant Fe mineral in this system, but how significant is their role in comparison with organic matter, authigenic apatite and detrital P?

Despite the importance of understanding P cycling under ferruginous conditions, as of yet, a combined analysis of all P and Fe pools in a ferruginous system (both water column and sediments) has not been completed.

1.4 This study

Both ferruginous conditions (Crowe et al., 2008a, Crowe et al., 2008b, Lliros et al., 2015, Zegeye et al., 2012) and phosphorus cycling (Creveling et al., 2014, März et al., 2008, Planavsky et al., 2010, Poulton, 2017, Reinhard et al., 2017) have had increased attention from the scientific community over the last decade, however, some substantial gaps in our knowledge remain, especially when combining the two subjects. This project aims to fill some of these gaps by addressing the following aims and objectives

1.4.1 Aims and objectives

- Determine the partitioning of Fe and P between common operationally defined pools in a ferruginous system.
- Identify what phases influence retention or release of P from sediments in a ferruginous environment.
- Test the current common method for determining P speciation in sediments and its suitability for investigating P in ancient sedimentary rocks, and if necessary, develop a revised extraction scheme.
- Determine whether ferruginous conditions in the Precambrian acted to enhance P retention in sediments, as previously suggested by Bjerrum and Canfield (2002).

1.4.2 Thesis outline

The remainder of this project encompasses work completed with an aim of enhancing our understanding of Fe and P cycling and their interactions under ferruginous conditions by following the aims and objectives outlined above. Following detailed discussion of the standard methods used throughout this project (Chapter 2), Chapter 3 describes testing the suitability of the commonly used SEDEX P speciation method for use with ancient marine sedimentary rocks and Fe-rich modern sediments, and the subsequent development of a revised method. Chapter 4 presents a detailed study of Fe and P systematics in both the water column and sediments of the ferruginous Lake La Cruz (Spain), and discusses how the results may be used to further our understanding of the cycling of these critical elements in ancient ferruginous environments.

Chapter 5 sees the application of the P speciation method developed in Chapter 3 to a suite of ancient sedimentary rocks from the 1.88-1.83 billion-year old Animikie Basin, providing new insights into the availability of P during the transition from a fully ferruginous water column, to euxinic conditions along the continental margin and ferruginous deeper waters. Finally, Chapter 6 provides a summary of the major findings of this work. By linking evidence from a modern ferruginous analogue with data from the geological rock record, an overarching theory about the cycling of Fe and P during ferruginous periods of Earth's history is suggested. Recommendations are then made for the direction of future studies.

Chapter 2 Methodology

2.1 Sample collection and storage

2.1.1 Modern environments

2.1.1.1 Lake La Cruz water column sampling, processing and storage

Prior to sampling, 5 L airtight, concertina style bottles were flushed three times with N_2 gas and stored collapsed in individual N_2 purged bags containing anaerobic atmosphere generating sachets. Water column samples were taken using an on-board peristaltic pump, which pumped water directly from the lake into these expanding bottles via a tap connector until overflowing, when the tap was closed and the hose removed (Figure 2.1). Surface samples were collected first, progressing deeper through the chemocline, retrieving the anoxic samples last to minimise time between the collection and processing of these sensitive samples.

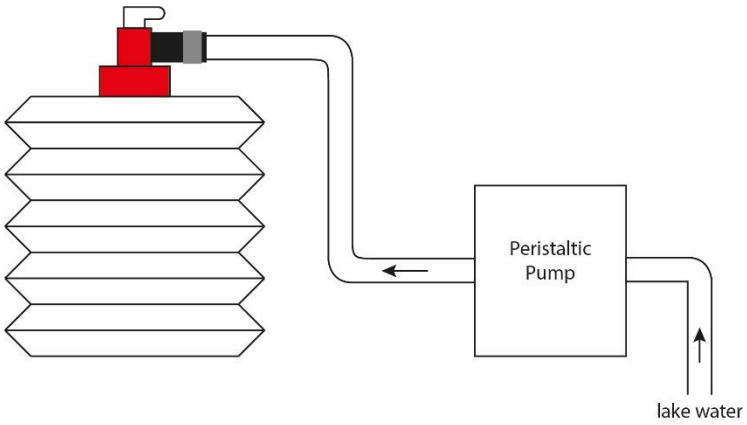

Figure 2.1 Schematic of the water column sampling set up.

Lake water was pumped directly into a deflated N_2 flushed accordion bottle until full.

For each water column sample, subsamples were removed from the 5 L bottles using 10 mL luer lock syringes, both unfiltered and filtered samples were taken for total and dissolved Fe(II), P, S(-II) and SO_4 respectively. Samples were filtered through a filter cartridge (28 mm, 0.2 µm polyethersulfone filter)

attached directly to the syringe. A 50 mL centrifuge tube was also filled with unfiltered water and placed in the freezer for potential future analysis.

For collection of water column particulates, the 5 L sample bottles were then connected to a peristaltic pump that introduced the water to a vacuum filtering set up within a portable anaerobic glove bag filled with N_2 gas (Figure 2.2). The samples were filtered through pre-weighed, large (142 mm diameter), 0.22 µm Isopore™ polycarbonate hydrophilic membranes and the filtrate was collected in 250mL acid cleaned LDPE bottles and frozen for future analysis. The filters themselves were folded and stored in long, 20mL, PTFE-lined rubber disc sealed, Pyrex® culture tubes in the fridge. Multiple filters were collected for each water column sample depth. For some specific redox sensitive samples, an additional unfiltered sample was taken in an airtight vial flushed with N_2, these were then placed in a N_2 flushed air tight container containing an anaerobic atmosphere generating sachet, and stored in the fridge for potential future analysis. A summary of the water column samples taken and how they were stored can be found in Table 2.1.

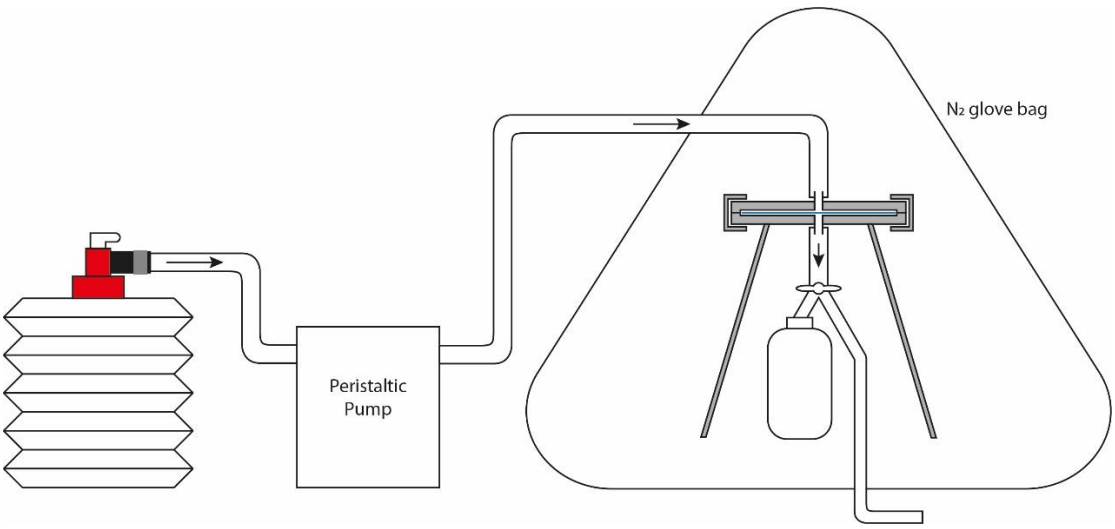

Figure 2.2 Schematic of the water column sample filtering set up.

Water was pumped directly from the accordion bottle into a N_2 filled glove bag where it was filtered.

Table 2.1 Summary of water column sample subsampling and storage.

Sample Purpose	Immediate action	Storage
Total and dissolved Fe(II)	Analysis by the ferrozine method	N/A
Total and dissolved P	Analysis by the phosphomolybdate blue method	N/A
Total and dissolved S(-II)	Fixed with Zn Acetate	Stored in fridge for analysis in Leeds
Total SO4	N/A	Stored in fridge for analysis in Leeds
Total sample for unspecified purpose	50 mL centrifuge tube filled	Stored in freezer
Water column particulates (Ø142 mm filters)	Placed in N_2 filled PTFE rubber disc sealed Pyrex® culture tubes	Stored in fridge
Filtered sample for unspecified purpose	250 mL LDPE bottle filler	Stored in freezer
Anoxic total sample for unspecified purpose	Airtight vial filled and flushed with N_2	Stored in additional N_2 flushed, air tight container in fridge

2.1.1.2 Lake La Cruz sediment sample collection, processing and storage

Three cores of ~30 cm length were retrieved using a gravity corer, sealed with bungs and tape and placed vertically in a cool box for transportation to the temporary laboratory. One core was wrapped and frozen in a vertical position for future work, whilst the remaining two were processed immediately for analysis as follows. Cores were introduced, sealed into a glove bag through a

specially designed seal and secured with a clamp stand (Figure 2.3). The glove bag was then flushed and inflated with N_2 gas to provide an anaerobic atmosphere. The top bung of the core was then removed and the water and unconsolidated surface ooze overlying the compacted sediment core were removed with a large syringe. The core was then gradually extruded in 1-2 cm increments and each sediment slice was transferred to a 50 mL centrifuge tube.

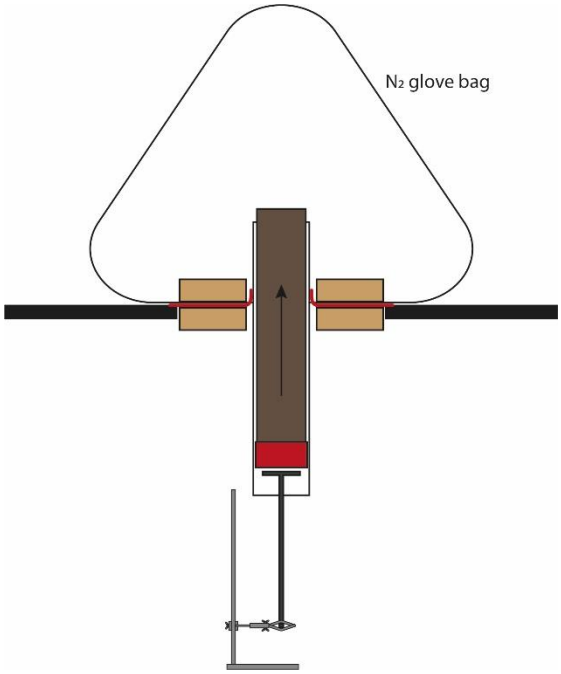

Figure 2.3 Schematic of the core sampling set up.

Cores were extruded through an airtight seal into an N_2 flushed glove bag where they could be processed one slice at a time.

Once the entire core was sliced, two CCS Rhizons® (5 cm flat tip, reinforced with glass fibre wire, poresize 0.15 µm) were inserted into each sediment subsample. 10 mL syringes were then connected via the luer lock to each Rhizon® and the plungers drawn to simultaneously extract and filter the porewaters. These were left to extract over a few hours in the anaerobic atmosphere of the glove bag until adequate volume for analysis had been collected. The Rhizons® were then removed and caps were placed on the sediment samples ready for storage. On removal from the glove bag, the sediment samples were placed in the freezer and aliquots of the porewaters were divided up for immediate analysis of dissolved Fe(II), P and storage of

fixed S(-II) and SO_4 as described for the water column samples. Sediment samples remained frozen during transport back to Leeds, where they were freeze dried and then stored in the freezer.

2.1.1.3 Golfo Dulce sediment collection and storage

Collection and processing of a short core from Golfo Dulce was completed prior to this project and was processed and stored following methods similar to those described above.

2.1.2 Ancient sedimentary rocks

Ancient sedimentary rock samples were collected prior to this project, and taken from well preserved drill cores or from the field (see Table 2.2). Samples were crushed using a disc mill to <63 μm and stored in centrifuge tubes.

Table 2.2 Details of ancient sedimentary rocks sample collection.

Samples	Source
Animikie Basin	Minnesota Department of Natural Rescources, Minnesota Department of Northern Development and Mines, Ontario
North China Craton	Field samples
Timan Region, Russia	Field samples
Saltwick Nab, Yorkshire, UK	Hand specimens taken directly from an exposed outcrop

2.2 Techniques

The standard techniques used to assess the geochemistry of water column particulates and sediments are detailed in this section. A revised method for evaluating phosphorus speciation in ancient sedimentary rocks has been developed as part of this project, details of which can be found in Chapter 4.

2.2.1 Modern phosphorus speciation

The P speciation of water column particulates and sediments was determined using the sequential extraction method (SEDEX) of Ruttenberg (1992). Five operationally defined sedimentary reservoirs of P were extracted by different reagents as detailed in Table 2.3. Extractions were performed on 150-180 mg of freeze dried sediment, or a section of filter paper in the case of water column particulates. The total amount of P extracted by the SEDEX method averaged 82 ± 5% of total P extracted by acid digestion (see section 2.2.4, for details of the method). Between each extraction, samples were centrifuged for 4 minutes at 4000 rpm to separate the sediment and the supernatant, subsamples were then taken for analysis and the excess supernatant discarded prior to the next extraction.

For speciation on water column particulate samples, the filter segments were transferred from the solution to storage tubes with clean tweezers prior to centrifugation, to allow efficient separation of suspended solids from the solution. Once the supernatant had been subsampled for analysis and the remaining solution discarded, the filter segments were then returned to the extraction tube and the storage tube walls were washed into the extraction tube with the following extractant solution to quantitatively transfer any remaining particulates.

Analysis of all extractant solutions - apart from the sodium citrate/bicarbonate/dithionite (CDB – step II) solutions - were analysed for P spectrophotometrically, as described in section 2.3.1.1. The CDB solution causes interferences with this method of analysis, preventing P from being measured this way for step II. Instead, P and Fe concentrations in CDB solutions are determined by inductively coupled plasma – optical emission spectrometry, as detailed in section 2.3.5. The pool of P considered to be biogeochemically “reactive” (P_{reac}) was calculated as the sum of all P reservoirs except P_{det}, i.e.:

$$P_{reac} = P_{sorb} + P_{Fe} + P_{auth} + P_{org}$$

Table 2.3 Sequential extraction steps of the SEDEX method.

Step	Extraction	Target Phase	RSD (%)
I	5 mL 1 M $MgCl_2$ (adjusted to pH 8 with NaOH), shake for 2h x2 5 mL MilliQ water, shake for 2 h x1	$\mathbf{P_{sorb}}$ – Exchangeable or loosely sorbed P	9
II	10 mL 0.3 M Na_3-citrate/ 1.0 M $NaHCO_3$/ 0.14 M Na-dithionite (CDB) (pH 7.6), shake for 8 h 5 mL 1 M $MgCl_2$ (adjusted to pH 8 with NaOH), shake	$\mathbf{P_{Fe}}$ – Easily reducible or reactive ferric Fe-bound P	11
III	10 mL 1 M Na Acetate (adjusted to pH 4 with acetic acid), shake for 6 h 5 mL 1 M $MgCl_2$ (adjusted to pH 8 with NaOH), shake for 2 h x2	$\mathbf{P_{auth}}$ – Authigenic apatite, biogenic hydroxyapatite, $CaCO_3$-bound P	12
IV	10 mL 1 M HCl, shake for 16 h	$\mathbf{P_{det}}$ – Detrital apatite and other inorganic P	28
V	Ash at 550°C 10 mL 1 M HCl, shake for 16 h	$\mathbf{P_{org}}$ – Organic P	16

2.2.2 Modern iron speciation

Fe speciation of sediment samples was assessed using a method developed from the combination of extractions presented in Poulton and Canfield (2005) and Canfield et al. (1986). The resulting procedure separates six operationally defined Fe phases and is described in Table 2.4. Steps I-III were performed sequentially on 50-100 mg of freeze dried sediment. Between each extraction, samples were centrifuged for 4 minutes at 4000 rpm to separate the sediment and the supernatant, subsamples were then taken for analysis and the excess supernatant discarded prior to the next extraction step. Fe(II) in step I solutions was measured spectrophotometrically as detailed in section 2.3.12.3.1.2 and total Fe (i.e. Fe(II)+Fe(III)) for step I, II and III was measured by atomic absorption spectroscopy (AAS), see section 2.3.2. Sulphide bound Fe was determined on a separate split of freeze dried sediment, weighing 0.5-1 g. Sulphide bound Fe was separated into two phases: acid volatile sulphur (Fe_{AVS}) and pyrite (Fe_{Py}), by the two-step HCl and chromous chloride distillation method. The sulphide phases were extracted and trapped as Ag_2S, the mass of which was converted to Fe concentrations assuming the stoichiometry of FeS and FeS_2 (Canfield et al., 1986, Fossing and Jorgensen, 1989).

The pool of highly reducible ferric oxides (Fe_{Ox1}) was calculated as the difference between total Fe and $Fe(II)_{inc.AVS}$ extracted by step I. As the 0.5 M HCl extraction of step I extracts Fe_{AVS} as part of reduced solid phase Fe(II), the unsulphidised pool of Fe(II) was calculated from the subtraction of Fe_{AVS} from $Fe(II)_{inc.AVS}$. The total pool of Fe that is considered to be highly reactive (Fe_{HR}) towards biotic and abiotic reactions in the water column and sediment was calculated as:

$$Fe_{HR} = Fe(II) + Fe_{Ox1} + Fe_{Ox2} + Fe_{mag} + Fe_{AVS} + Fe_{Py}$$

On average Fe_{HR} extracted 70 ± 8% of total Fe determined by acid digestion, the remainder of which is likely to be Fe bound with poorly reactive silicates.

Table 2.4 Modern Fe Speciation.

Sequential extraction steps I-III are taken from Poulton and Canfield (2005). Sequential extractions steps IV-V, taken from Canfield et al. (1986), are preformed on a separate split of sediment. Unsulphidised Fe(II) was calculated by the subtraction of step IV (Fe_{AVS}) from step I ($Fe(II)_{inc.\ AVS}$). The reproducibility (RSD) for each step is given based on replicate sediment samples (n=5).

Step	Extraction	Target Phase	RSD (%)
I	5 mL 0.5 M HCl, shake for 1 h	**$Fe(II)_{inc.\ AVS}$** – Reduced solid phase Fe, including AVS and Fe(II) phosphates	7
		Total Fe measured in this extractant is Fe(II)+Fe(III).	3
		Subtraction of $Fe(II)_{inc.AVS}$ gives:	
		Fe_{Ox1} – Highly reducible ferric oxides such as ferrihydrite	<LOD
I	10 mL of 58.82 g/L Na_3-citrate/ 50 g/L Na-dithionite/ 20 ml/L acetic acid (CDA) (pH 4.8), shake for 2 h	**Fe_{Ox2}** – Reducible ferric oxides such as goethite and hematite	11
III	10 mL of 28.42 g/L ammonium oxalate/ 21.45 g/L oxalic acid, shake for 6 h	**Fe_{mag}** - Magnetite	<LOD
IV	8 mL 50% HCl, boil for 1 h	**Fe_{AVS}** – Acid volatile sulphide	6
V	5 mL 1 M chromous chloride, dissolved in 50% HCl, boil for 1 h	**Fe_{Py}** – Pyrite	8

Fe speciation of water column particulates was determined by applying steps I-III to sections of filter paper. As for P speciation, following each extraction the filter segments were transferred from the solution to storage tubes with clean tweezers prior to centrifugation, to allow efficient separation of suspended solids from the solution. Once the supernatant had been subsampled for analysis and the remaining supernatant discarded, the filter segments were then returned to the extraction tube and the storage tube walls were washed into the extraction tube with the following extractant solution to quantitatively transfer any remaining particulates. Fe_{AVS} and Fe_{Py} could not be determined on water column particulates due to difficulties removing the particulates from the filters, but these Fe pools are likely negligible in the ferruginous water column.

2.2.3 Carbon content

Total carbon (TC) and total organic carbon (TOC) were determined on separate splits of freeze dried sediment. For the analysis of TC, ~200 mg of freeze dried sediment was weighed directly into a combustion boat in preparation for analysis. For the analysis of TOC, weighed samples of freeze dried sediment were pre-treated with 10% (v/v) HCl to remove carbonate phases. 10 mL of acid was added to the sample and shaken briefly by hand, the lid was opened slightly to release CO_2 gas and then tightened, and the sample was then centrifuged. The supernatant was tipped to waste and a further 10 mL of acid was added to the sample. Samples were once again shaken by hand, degassed and then placed on a shaker table overnight (samples were degassed again after 1 h had passed to release any build up of pressure). Following this longer reaction time, samples were degassed and centrifuged with the supernatant tipped to waste. Samples were then washed with repeated additions of MilliQ water, followed by centrifugation and tipping the supernatant to waste, until residual Cl from acid treatment was significantly removed. The decarbonated samples were then placed in a drying cabinet at 50ºC for a minimum of 24 h, and once dry, they were then reweighed in order to calculate the weight loss. Samples were then homogenised with a spatula prior to weighing ~50-100 mg into combustion boats in preparation for analysis. Carbon content of both unaltered and acid washed samples was measured by a LECO C analyser, details of which can be found in section 2.3.6.

Total inorganic carbon (TIC) was calculated as the difference between TC and TOC. Replicate analysis (n=10) of a representative sediment sample gave RSDs of 1% for TC, 4% for TOC and 3% for TIC. Unfortunately, C analysis of water column particulates could not be completed.

2.2.4 Bulk sedimentary digests

Total Fe, Al, Mg, Ca, Mg, P and Mn content of both sediment and water column particulates was determined by acid digestion. For sediment analysis, ~50 mg of freeze dried sediment was weighed into individual porcelain crucibles. For water column particulates, an entire filter with known sample mass was placed loosely folded into individual large porcelain crucibles. All samples were placed in a furnace and heated to ashing point, remaining at 550ºC for 12 h. Once cooled, samples were quantitatively transferred to Teflon beakers with 5 mL concentrated HNO_3. In a specialised fume cupboard, 2 mL of concentrated HF and 2-3 drops of concentrated $HClO_4$ were added to all samples, which were then gently swirled and placed on a hotplate to dry down. Once dry, 2 mL of boric acid (50 g/L) was added to each sample to solubilise aluminium hexafluorates, samples were swirled and returned to the hotplate to evaporate to dryness. Sediment samples were re-dissolved in 5 mL of hot concentrated HNO_3 (or HCl), before being quantitatively transferred and brought to 100 mL volume with MilliQ water in individual volumetric flasks, final concentration 5% (v/v) HNO_3 (or HCl). Water column particulates samples were re-dissolved in 1.5 mL of hot concentrated HNO_3 before being quantitatively transferred and brought to 50 mL volume with MilliQ water in individual volumetric flasks, final concentration 3% (v/v) HNO_3. This smaller final volume was used for water column particulate samples to prevent excessive dilution of a small sample mass. This method of total digestion resulted in complete combustion of blank filter papers and contributed concentrations of the measured elements that were lower than the limit of detection.

Solutions were analysed for P spectrophotometrically, Fe by AAS, and Fe, Al, Ca, Mg, P and Mn by inductively coupled plasma – mass spectrometry, see section 2.3.4. Element recovery was determined by repeat analysis of an international sediment standard (either PACS-2 or SBC-1) and the reproducibility of the method was determined by repeat analysis of a sample, see Table 2.5.

Table 2.5 Total digestion method element recovery and reproducibility.

Recovery is based on certified values for an international sediment standard. Reproducibility is based on a repeated sample.

Analysis Method	Element	Recovery	Reproducibility (RSD)
AAS	Fe	95-97% (n=2)	4% (n=6)
Spectrophotometer	P	96-97% (n=2)	5% (n=6)
ICP-MS	Fe	107 ± 6% (n=3)	4% (n=6)
	Al	105 ± 5% (n=3)	2% (n=6)
	Ca	ND	1% (n=6)
	Mg	ND	4% (n=6)
	P	107 ± 4% (n=3)	1% (n=3)
	Mn	108 ± 5% (n=3)	2% (n=6)

2.3 Analysis

2.3.1 Spectrophotometric analysis

2.3.1.1 Phosphomolybdate blue method

The molybdenum blue reaction is one of the most common means of determining orthophosphate in environmental waters and can also be used to analyse silicate, arsenate and germanate concentrations via spectrophotometry. The basic reaction involves the reaction of phosphate with an acidified molybdate reagent, to form a phosphomolybdate heteropolyacid which is then reduced to form the coloured phosphomolybdenum blue compound, the intensity of which can be determined spectrophotometrically (Worsfold et al., 2005). There are many variations of the original method of Murphy and Riley (1962), which tend to use alternative reductants and acid strengths, but for this study ascorbic acid is used as the reductant to produce a product with a wavelength maximum of 880 nm, with the final pH of the measured solution between 1 and 2.

The reagents required for the preparation of the molybdate blue reagent are detailed in Table 2.6. Preparation of the molybdate blue reagent is detailed in Table 2.7, the solution should be transparent and a very pale yellow in colour. The molybdate blue reagent should be stored in a glass bottle in the fridge, where it can be used for 3-4 weeks.

Table 2.6 Details of reagents required for the preparation of the molybdate blue reagent.

All solutions are made in MilliQ water.

Reagent	Chemical	Concentration
Reagent 1	H_2SO_4	10% (v/v)
Reagent 2	Antimony potassium tartrate hydrate	1.48 g/L
Reagent 3	Ammonium molybdate tetrahydrate	7.92 g/L

Table 2.7 Details for the preparation of 250 mL of the molybdate blue reagent using the reagents detailed in Table 2.6.

Steps should be followed in order and the solution mixed before the addition of the next reagent. The solution should be brought to volume using MilliQ water.

Step	Reagent to be used	Volume/mass per 250 ml
I	Ascorbic acid	0.500 g
II	Reagent 1	45 mL
III	Reagent 2	31 mL
IV	Reagent 3	52 mL

Samples were prepared for analysis in microcentrifuge tubes following the additions detailed in Table 2.8. The colour was allowed to develop over 15 minutes before the solution was transferred to a cuvette and the absorbance was measured relative to a matrix matched blank using a Thermo Genesys 6 spectrophotometer at 880 nm. As mentioned previously, the optimum pH of the solutions for analysis is ~pH 1, some extractant solutions used in the P speciation method require the addition of either base or acid to achieve this

final pH. The volume required is determined by testing a range of addition volumes on the blank and 1 mg P/L matrix matched standards. The absorbance of these test solutions was measured at 15 minutes and again at 30 minutes. The optimum addition volume was chosen, on the basis of the blank solution remaining blank and the 1 mg P/L standard having a strong and stable absorbance over the analysis time.

Table 2.8 Sample preparation for analysis of P.

Matrix	**Molybdate blue volume**	**Sample/standard volume**	**pH adjustment**
Natural	200 µL	1000 µL	N/A
MilliQ	200 µL	1000 µL	N/A
1 M $MgCl_2$ (pH 8)	200 µL	1000 µL	N/A
Na Acetate (pH 4)	200 µL	1000 µL	50% (v/v) H_2SO_4
1 M HCl	200 µL	1000 µL	5 M NaOH

The relationship between absorbance and P concentration was calibrated by the analysis of matrix matched standards, with concentrations ranging from 0.075 – 1 mg P/L. The relationship was found to be linear up to ~1.5 mg P/L, and as such all samples analysed were required to have absorbance values within the calibrated range, those that had an absorbance value that exceeded this range were prepared again with a dilution (within the 1 mL sample/standard volume). For the analysis of natural solutions (i.e. water column and porewater samples), MilliQ water was used to make a blank and standard solutions for calibration.

2.3.1.2 Ferrozine method

The ferrozine method of Stookey (1970), was used to analyse Fe(II) concentrations in natural water samples and 0.5 M HCl. The ferrozine reagent reacts with divalent Fe to form a stable magenta complex, which yields a maximum absorbance at 562 nm between pH 4 and 9 (Viollier et al., 2000). A 0.05 M HEPES buffer/ 0.2 g/L ferrozine solution was made with MilliQ water

and adjusted to pH 7 with NaOH to make the ferrozine reagent. Samples were prepared for analysis in microcentrifuge tubes following the additions detailed in Table 2.9. The colour was allowed to develop before the solution was transferred to a cuvette and the absorbance was measured relative to a matrix matched blank using a Thermo Genesys 6 spectrophotometer at 562 nm.

Table 2.9 Sample preparation for the analysis of Fe(II).

Matrix	Ferrozine volume	Sample/standard volume
Natural Water Sample	500 µL	1000 µL
0.5 M HCl	2000 µL	50 µL

The relationship between absorbance and Fe(II) concentration was calibrated by the analysis of matrix matched standards (made with $(NH_4)_2Fe(SO_4)_2.6H_2O$), with concentrations ranging from 0.2 – 8 mg Fe/L and was found to be linear. All samples analysed were required to have absorbance values within the calibrated range, those that had an absorbance value that exceeded this range were prepared again with a dilution (within the sample/standard volume). For the analysis of natural solutions (i.e. water column and porewater samples), MilliQ water was used to make a blank and standard solutions for calibration.

2.3.1.3 Cline assay

Water column and porewater samples (1 mL) were fixed at the time of collection with 50 µL of 10 mM zinc acetate and stored in the fridge until analysis using the Cline assay (Cline, 1969). The reaction of hydrogen sulphide with dimethyl-*p*-phenylenediamine sulphate and ferric iron results in the formation of methylene blue, the intensity of the colour can be measured at 670 nm on a spectrophotometer and converted to sulphide concentrations following calibration. Based on previous studies, the expected sulphide concentration of all samples to be analysed was less than 40 µM, and hence the reagents used were made to the concentrations suggested for the 3 – 40 µM S(-II) range by Cline (1969), see Table 2.10.

Table 2.10 Preparation of the mixed diamine reagent for the analysis of 3-40 µM S(-II) solutions, as suggested by Cline (1969).

Diamine Concentration	Ferric Chloride Concentration	Sample Dilution Factor
0.8 g/ 200 mL	1.2 g/ 200 mL	1:1

Samples were prepared for analysis in microcentrifuge tubes as described in Table 2.11, and left for 20 minutes for the methylene blue colour to develop. The solutions were then transferred to cuvettes and the absorbance was measured relative to a matrix matched blank using a Thermo Genesys 6 spectrophotometer at 670 nm. The linear relationship between absorbance and S(-II) concentration was calibrated by the analysis of matrix matched standards (0 – 40 µM). Sulphide standards were made from a stock solution of $Na_2S.9H_2O$ dissolved in N_2 purged MilliQ water which was then fixed with 10 mM zinc acetate in the same ratio as samples. All samples had absorbance values lower than that given by the top standard.

Table 2.11 Sample preparation for the analysis of S(-II).

Diamine mixed reagent	Sample/Standard	MilliQ Water
100 µL	500 µL	500 µL

2.3.2 Atomic absorption spectroscopy

For samples analysed for Fe by AAS, a 20x dilution was made with MilliQ water prior to analysis. Samples were analysed on a Thermo Fisher iCE™ 3300 AAS bracketed by matrix matched blank and standard solutions for quality control. Sample absorbance values were converted to concentrations by calibration with matrix matched standards, ranging between 1 – 10 mg Fe/L. If samples fell outside the calibrated range further dilutions were made.

2.3.3 Ion chromatography

Dissolved sulphate concentration in natural solutions was determined using ion chromatography. Samples were passed through a 0.2 µm hydrophilic

polyethersulfone syringe filter before analysis using a Dionex Ionpac™ AS16 column, repeat analysis of a standard solution gave an RSD of <2%.

2.3.4 Inductively coupled plasma – mass spectrometry

Bulk sediment digests were analysed for Fe, Al, Ca, Mg, P and Mn using a Thermo Fisher iCAP™ Qc ICP-MS. Samples were diluted to 2 % HCl using MilliQ water and spiked with an internal rhenium standard for monitoring drift. Element concentrations were determined by calibration with matrix matched standards.

2.3.5 Inductively coupled plasma – optical emission spectrometry

CDB, CDA, ammonium oxalate and 1 M HCl solutions were analysed for P using a Thermo Fisher iCAP™ 7400 Radial ICP-OES. CDB, CDA and ammonium oxalate solutions were run with no dilution, and 1 M HCl solutions were diluted with MilliQ water to 0.5 M HCl. All samples were spiked with a 100 ppm Co internal standard to monitor drift. P concentrations were determined by calibration with matrix matched standards.

2.3.6 LECO carbon analyser

Sediment samples were analysed for C using a LECO SC-144DR Dual Range Sulfur and Carbon Analyzer. Samples and standards weighed into combustion boats were inserted into the LECO furnace (set at 1350°C) where the chamber is flooded with pure oxygen. The sample combusts releasing C as CO_2 gas which is measured via infrared detection cells. LECO software the converts these measurements to weight percent C, based on pre-entered sample masses. The CO_2 measurements are calibrated with high and medium C content soil standards, samples were also bracketed by standards for quality control. Repeated analysis (n=10) of the high and medium C content soil standards gave recoveries of 100 ± 0.5% and 101 ± 0.9% respectively.

Chapter 3 Development of the SEDEX phosphorus speciation method for modern and ancient iron-rich sediments

3.1 Introduction

Phosphorus (P) is a key element for life on Earth. A structural component of all organisms, P forms the backbone of DNA and RNA, and is crucial in the transmission of chemical energy through ATP molecules. Phosphorus supply to the oceans thus exerts a critical control on primary productivity in many areas of the global ocean, which in turn affects organic carbon production and burial, and ultimately the production of oxygen through time (Berner et al., 2003, Berner and Canfield, 1989, Berner and Maasch, 1996, Garrels and Perry, 1974). On geological timescales, P is generally considered the ultimate limiting nutrient (Codispoti, 1989, Redfield, 1958, Tyrrell, 1999, Van Cappellen and Ingall, 1996). As a consequence, the delivery and subsequent behaviour of P in marine environments has been the focus of considerable attention, both in modern (e.g., Eijsink et al., 2000, Ingall and Jahnke, 1994, Ingall et al., 1993; Ruttenberg and Berner, 1993, Slomp et al., 1996a, 2004, Van Cappellen and Ingall, 1994) and ancient settings (e.g., Bjerrum and Canfield, 2002, Boyle et al., 2014, Creveling et al., 2014, Lenton et al., 2014, März et al., 2008, Planavsky et al., 2010, Reinhard et al., 2017). Bulk sediment digestions can give useful information on the fluxes and behaviour of P in marine environments. However, this insight is limited as it does not consider the P phases that may be reactive or potentially bioavailable in the water column and during early diagenesis.

Phosphorus delivery to modern marine sediments mainly occurs in association with organic matter including fish debris, with authigenic sedimentary particles mainly as apatite and Fe (oxyhydr)oxide minerals, and with recalcitrant detrital P of igneous or metamorphic origin (generally fluorapatite) (Faul et al., 2005, Froelich et al., 1982, Schenau and De Lange, 2000, Slomp et al., 1996b, Stockdale et al., 2016). Following deposition under oxic conditions and early diagenesis, a major proportion of the labile organically-bound P (P_{org}) may be

released as dissolved inorganic P (DIP) by microbially-mediated respiration (Anderson et al., 2001, Berner and Rao, 1994, Froelich et al., 1988, Jahnke, 1996, Krom and Berner, 1981, Ruttenberg, 2003). This DIP can efflux from the sediment back into the water column or can undergo further reactions with other sedimentary components (termed “sink switching”) including adsorption and/or co-precipitation with Fe (oxyhydr)oxide and carbonate minerals, uptake by bacteria, or transformation to other secondary phases such as authigenic carbonate fluorapatite (CFA) or vivianite (Anschutz et al., 1998, Berner, 1981, Egger et al., 2015, Martens et al., 1978, Rothe et al., 2014, Ruttenberg and Berner, 1993, Slomp et al., 1996b, Van der Zee et al., 2002).

Under anoxic conditions in the water column or in deposited sediments, recycling of primary P phases may occur (Ingall and Jahnke, 1994, 1997, Van Cappellen and Ingall, 1994). Microbial remineralisation reactions (such as sulphate reduction) can result in the preferntial release of P relative to the organic C (C_{org}) from organic matter, resulting in C_{org}/P_{org} ratios that are highly elevated compared to the Redfield ratio of 106:1, up to several orders of magnitude (Burdige, 1991, Ingall and Jahnke, 1994, 1997, Roden and Edmonds, 1997). In addition, the Fe (oxyhydr)oxide P is often diminished under anoxic conditions due to reductive dissolution of Fe (oxyhydr)oxides, either via disimmilatory Fe reduction (Thamdrup, 2000) or direct reaction with dissolved sulfide (Canfield, 1989, Poulton et al., 2004b). Some DIP released from organic matter or Fe (oxyhydr)oxides during early diagenesis may be taken up by Fe (oxyhydr)oxides formed at the sediment-water interface if the overlying water column is oxic (Slomp et al., 1996b), or partially removed from solution as other secondary phases, particularly CFA (Ruttenberg and Berner, 1993). However, under anoxic water column conditions, P may be extensively recycled back to the water column, where it can subsequently stimulate further productivity (Ingall and Jahnke, 1994, 1997, Jensen et al., 1995, Van Cappellen and Ingall, 1994). In order to evaluate these diagenetic processes and to constrain the fate of P in sedimentary environments, it is essential to be able to quantify the phase partitioning of P within the sediment.

Extraction techniques have been widely employed to provide more detailed insight into the behaviour of P in the marine realm. The method of Aspila et al. (1976) allows determination of inorganic P and total P (P_T) in sediments, with the difference being attributed to organic P. However, this technique does not allow quantification of a variety of important phases, including the detrital fraction that is essentially unreactive in marine environments. A major step forward was achieved with the development of a sequential extraction procedure for P by Ruttenberg (1992). This technique (termed SEDEX) quantifies five operationally-defined sedimentary P reservoirs (Table 3.1): exchangeable P (P_{sorb}), Fe (oxyhydr)oxide-bound P (P_{Fe}), authigenic P (P_{auth}; comprising authigenic CFA, $CaCO_3$-bound P and biogenic apatite), detrital P (P_{det}), and organic P (P_{org}). SEDEX has proven to be a robust method for examining the phase distribution of P in many modern marine sedimentary settings (e.g., Egger et al., 2015, Eijsink et al., 2000, Kraal et al., 2015, Matijević et al., 2008, McParland et al., 2015, Poulton and Canfield, 2006, Ruttenberg and Berner, 1993, Schenau and De Lange, 2001, Slomp et al., 1996a, 2004). This enhanced understanding of P partitioning allows C_{org}/P_{org} ratios to be determined, and allows a potentially 'reactive' P pool to be quantified ($P_{reac} = P_{sorb} + P_{Fe} + P_{auth} + P_{org}$), which are particular strengths of the SEDEX method (Ruttenberg, 1992).

Table 3.1 Details of the P phases extracted by the SEDEX method (Ruttenberg, 1992).

P Pool	Phases Extracted
$\mathbf{P_{ex}}$	Exchangeable or loosely sorbed P
$\mathbf{P_{Fe}}$	Fe (oxyhydr)oxide-bound P
$\mathbf{P_{auth}}$	Authigenic apatite, $CaCO_3$-bound P and biogenic apatite
$\mathbf{P_{det}}$	Detrital apatite and other inorganic P phases
$\mathbf{P_{org}}$	Organic P

3.1.1 Using SEDEX to determine P speciation in samples with increased crystallinity

Due to the enhanced information on P cycling afforded by the SEDEX method, several studies have attempted to apply the method (or variations of it) to ancient sedimentary systems (e.g., Creveling et al., 2014, Huang et al., 2007, Kraal et al., 2010, März et al., 2008, Mort et al., 2007, 2008, Westermann et al., 2013). However, the original method was not developed – and is therefore not necessarily appropriate – for application to ancient sediments. Ancient sedimentary rocks often contain minerals of increased crystallinity compared with modern sediments, as well as important 'reactive' phases that may not be accounted for adequately by the original SEDEX method. For example, throughout the majority of early Earth's history, large areas of the global ocean were characterised by anoxic and Fe-containing ('ferruginous') water column conditions (Poulton and Canfield, 2011), which led to the deposition of sediments enriched in Fe (oxyhydr)oxide minerals, which are now present as crystalline hematite and magnetite (e.g., Canfield et al., 2008, Poulton et al., 2004a). Magnetite is not specifically targeted by the original SEDEX extraction scheme, while tests on highly crystalline hematite (Raiswell et al., 1994), suggest that the pH 7.6 citrate-dithionite-bicarbonate (CDB) extraction utilised in the existing SEDEX protocol (Figure 3.1) is unlikely to fully dissolve this phase in ancient rocks. These crystalline Fe (oxyhydr)oxide phases can also be present in some modern marine sediments, and thus there is also potential for incomplete recovery of 'reactive' P from modern Fe-rich settings.

3.1.1.1 Fe minerals

Fe (oxyhydr)oxides are well know for their capacity for P adsorption, which occurs through a ligand exchange mechanism (Parfitt and Russell, 1977, Sigg and Stumm, 1981) which is promoted by increasing ionic strength (Bowden et al., 1980). PO_4^{3-} adsorbs predominantly as binuclear, bidentate complexes, which bind to the surface hydroxyl groups at the corners of two adjacent octahedra (Cornell and Schwertmann, 1996). Because this process is accompanied by the uptake of protons, adsorption is strongly influenced by pH, with maximum uptake at low pH, and decreasing with rising pH. In general P adsorption also decreases within increased levels of crystallinity, such that

adsorption is greatest in ferrihydrite > lepidocrocite > goethite > hematite (Ruttenberg, 1992).

The capacity of Fe (oxyhydr)oxides for scavenging P from natural waters has been proven and uptake mechanisms identified, however when considering the P associated with more crystalline Fe minerals in ancient sedimentary rocks, one must bear in mind the fate of any adsorbed/coprecipitated P during transformations. For example during diagenesis, a large proportion of ferrihydrite precipitates are transformed into more stable, crystalline phases such as goethite and hematite. The transformation of ferrihydrite to goethite occurs through the initial dissolution of ferrihydrite resulting in the release of any scavenged P. Nucleation and then growth of goethite from the solution of Fe(III) ions then follows (Schwertmann and Murad, 1983). P released during the dissolution of the initial ferrihydrite precipitate may then follow one or more pathways. P may undergo i) subsequent coprecipitation with the new goethite mineral (although this is likely to be less efficient in scavenging P than the initial ferrihydrite); ii) readsorption onto the surface of other Fe (oxyhydr)oxides; iii) incorporation into authigenic phases such as apatite and carbonates or iv) remain in the dissolved phase. In seawater conditions, however, pH dictates that the solid state transformation of ferrihydrite to hematite is favoured over the formation of goethite (Schwertmann and Murad, 1983), a process which is also promoted by the presence of adsorbed phosphate on the surface of ferrihydrite (Barron et al., 1997, Galvez et al., 1999).

To understand the relevance of P associated with any more crystalline Fe minerals, the samples transformational history and effects those processes may have had on any associated P must be considered. A large amount of work has focused on understanding the fate of Fe-bound P during oxidation/reduction reactions, but more research should focus on aging and metamorphic transformations within natural environments.

3.1.1.2 Crystalline apatite

It has also been suggested that the solubility of the authigenic apatite (CFA) phase in Na acetate (Figure 3.1) may be decreased in ancient rocks due to recrystallization during burial diagenesis (Shemesh, 1990, Slomp, 2011),

making this phase less prone to dissolution by its target extractant (Figure 3.1). Carbonate fluorapatite, is essentially a highly substituted form of fluorapatite, where CO_3 groups substitute for PO_4 and OH within the crystal lattice. The effect of this substitution is to decrease the mineral's solubility (Chien and Black, 1976, Jahnke, 1984). This renders carbonate fluorapatite susceptible to acid dissolution in a moderately low pH buffered Na acetate solution, whereas fluorapatite is distinctly less soluble in this solution resulting in <5% of the P being extracted (Ruttenberg, 1992). The SEDEX method relies on this difference in solubility due to the substitutions in the chemical composition to separate CFA and fluorapatites of igneous or metamorphic origin. If the chemical composition and crystallinity of both CFA and fluorapatite were to change during diagenetic and metamorphic processes, then it is reasonable to assume that it may change their relative solubilities and therefore the ability of the SEDEX extraction regime to separate the two phases.

Shemesh (1990), studied sedimentary apatites from various settings and depositional ages, ranging from modern CFA formation sites to apatites deposited in the Precambrian. Fourier transform infrared spectroscopy (FT-IR) analysis revealed that the crystallinity index of recent apatites was generally low (3.0-3.6), while those of on land ancient apatites was high (4.5-7.8), indicating post-depositional recrystallization. This recrystallization process appeared to be associated with a decrease in the carbonate content substituted for PO_4 and an increase in the fluoride order within the apatite structure. In other word , the recrystallization process changes the crystal structure from the highly substituted and more soluble form that is CFA towards the stable and more recalcitrant endmember of the apatite group, fluorapatite. It follows that if CFA has undergone recrystallization, when using the SEDEX methods some CFA would likely be extracted as part of the detrital fluorapatite pool, rather than as authigenic apatite (Creveling et al., 2014), although this process is yet to be quantified.

Shemesh (1990) also postulated that FT-IR could be used to determine whether apatites have undergone recrystallization processes, and then the $\delta^{18}O$ composition of phosphate oxygen within the crystals could be used to

study depositional conditions in pristine CFA samples and diagenetic processes in those that have been recrystallized. A combination of these techniques with P speciation analysis may help to understand the potential for a transfer of CFA from the “authigenic P” pool to “detrital P” pool in ancient sediments.

Finally, it is generally unlikely that the measurement of exchangeable P (P_{sorb}), which was developed for modern marine sediment, would be particularly suitable when applied to ancient rocks that have often undergone recrystallization.

3.1.2 Proposal

Thus, considering the above discussion, to successfully apply P speciation to ancient sedimentary rocks, and indeed to those modern sediments containing measurable amounts of crystalline Fe (oxyhydr)oxide minerals, a modified method is required that focuses on the key mineralogical phases that may be present, and which also considers the possibility for incorrect partitioning of authigenic apatite.

In order to quantify a more complete spectrum of the Fe (oxyhydr)oxide phases commonly present in ancient sediments, Poulton and Canfield (2005) developed a sequential procedure for Fe, which extracts both magnetite and highly crystalline hematite (Figure 3.1). This provides a template to modify the SEDEX procedure to include P associated with these additional mineral phases. Therefore, to address the issues relating to the application of P speciation to modern and ancient Fe-rich sediments, we here initially test the efficiency of the original SEDEX method to extract hematite and magnetite. We then report the development of a revised extraction scheme for P, which we test using both synthetic Fe minerals and modern and ancient marine sediments. Finally, we consider the potential for incomplete recovery of the CFA pool in ancient sediments and suggest a protocol for dealing with this situation when interpreting P speciation data. Together, our approach provides a more robust means to quantify different operationally-defined P pools in modern and ancient Fe-rich sediments.

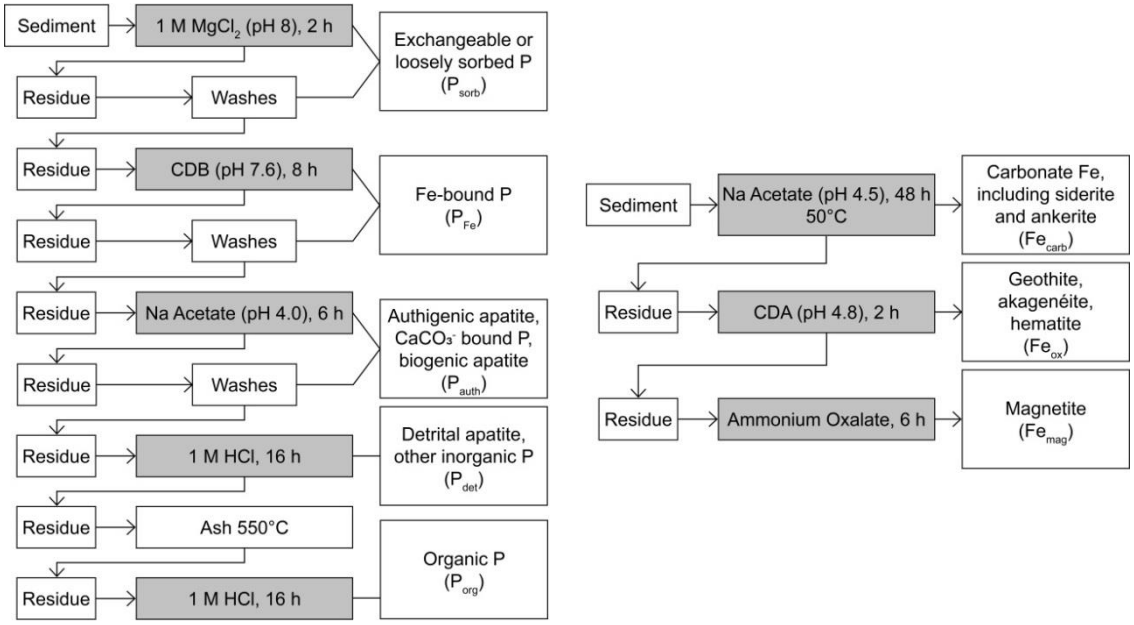

Figure 3.1 Schematic of the SEDEX sequential extraction scheme for P in modern marine sediments (left figure), as described in Ruttenberg (1992). Schematic of the Fe speciation method (right figure) for ancient sediments (Poulton and Canfield, 2005).

CDB – sodium citrate-dithionite-bicarbonate. CDA – sodium citrate-dithionite-acetate.

3.2 Samples and methods

3.2.1 Synthetic minerals

Synthetic ferrihydrite, lepidocrocite and goethite were prepared according to the standard methods of Cornell and Schwertmann (1996), and have previously been characterised (Poulton et al., 2004b) by X-ray diffraction (XRD). Hematite was provided by BDH Laboratory supplies, and its purity was confirmed by XRD (Appendix A, Figure A.1). We also analysed a magnetite-hematite composite sample. This sample was prepared via the standard method for magnetite preparation described in Cornell and Schwertmann (1996) and had previously been used in the development of a sequential Fe extraction by Poulton and Canfield (2005). Partial oxidation of magnetite to hematite during subsequent storage was confirmed by XRD (Figure A.2). HNO_3-HF-$HClO_4$ digests (see below) of this sample gave a total Fe composition of 71.8 ± 2.3 wt%, while a separate ammonium oxalate extraction aimed at dissolving magnetite (Figure 3.1; Poulton and Canfield, 2005) suggests that 79.2 ± 1.2% (56.9 wt% Fe) of the total Fe is present as magnetite.

An additional synthetic magnetite sample with co-precipitated P was prepared following the protocols of Cornell and Schwertmann (1996). 560 ml of a mixed $NaH_2PO_4 \cdot 2H_20/FeSO_4$ solution (0.39 mM:0.3 M) was heated at a constant 90°C, and 240 ml of a KOH/KNO_3 solution (3.33:0.27 M ratio) was added dropwise in an anaerobic chamber, with constant stirring. The reaction was allowed to continue for 1 h. Once cool, the mineral/solution slurry was centrifuged, and washed with MilliQ water before drying at 90°C. After drying, the solid was ground to a powder and stored frozen to prevent oxidation. XRD analysis confirmed that the only mineral phase present was magnetite (Figure A.3). Complete chemical characterisation by XRF and ICP-OES (following dissolution with 12 N HCl) confirmed a co-precipitated P content of 9.7 ± 0.7 mM/kg.

3.2.2 Natural mineral samples

A natural sample of crystalline apatite from Madagascar was analysed. XRD analyses suggest that the dominant minerals were hydroxylapatite or fluorapatite (Figure A.4). A natural sample of magnetite drilled from an Isua

Greenstone Belt banded iron formation (BIF) was used to represent crystalline magnetite found in ancient sedimentary rocks. XRD analysis showed the sample was predominantly formed of magnetite and quartz (Figure A.5). HNO_3-HF-$HClO_4$ digests of this Isua BIF sample gave a total Fe composition of 61.9 ± 1.5 wt%, and Fe speciation as described in Figure 3.1 revealed magnetite (Fe_{mag}) contributed 70.1% of total Fe (43.8 wt% Fe).

3.2.3 Modern and ancient marine sediments

Extractions were performed on modern sediments from Golfo Dulce, Costa Rica from a short core comprising Fe (oxyhydr)oxide-rich marine mud. Golfo Dulce is a 200 m deep tropical fjord where the water column is anoxic and nitrate-rich ('nitrogenous') beneath a depth of ~100 m (e.g., Thamdrup et al., 1996). Despite the reducing water column and sediment conditions, reactive Fe (oxyhydr)oxide mineral phases persist in the deposited sediment. In terms of ancient sedimentary rocks we focussed on several units from different time periods. The ~1.88-1.83 billion year old Animikie group (see Poulton et al., 2004a, 2010) was deposited in an open-ocean setting on the southwest margin of Superior Province, North America (Fralick et al., 2002, Ojakangas, 1983), and consists of low metamorphic grade black shales, which capture a record of deposition under a series of different water column redox conditions, including anoxic and sulphidic ('euxinic'), ferruginous and oxic (Poulton et al., 2004a, 2010). As such, these well-preserved core samples represent a range of key Precambrian depositional environments, making them ideal for the development and testing of our revised P speciation protocol. We additionally analysed marine sediments from ~1.65 billion year old Chuanlinggou Formation of the North China Craton, and the 715-542 million year old Kel'tminskaya-1 drill core sediment from the southern Timan Region of North Russia, The Chuanlinggou formation consists of low metamorphic grade black shales that were deposited in a semi-restricted basin in low sub tidal conditions (Li et al., 2015a, Meng et al., 2011), the samples chosen represent deposition from oxic and ferruginous water column redox conditions. The Kel'tminskaya-1 drill core is from the Mezen shallow water foreland basin, which was situated on the north-east side of the East European Platform (Maslov et al., 2008). The samples we have selected are low metamorphic grade black shales from the

Redkino and Kotlin horizons (558-542 Ma), and were also deposited in low energy sub tidal conditions. The deposition redox conditions have previously been identified as oxic or equivocal (see Johnston et al., 2012). Finally we analysed a sample from the bituminous shales section of the Whitby Mudstone at Saltwick Nab, Yorkshire, thought to be Toarcian in age (Howarth, 1962).

3.2.4 Testing the efficiency of Fe extractions

The suitability of the SEDEX method for application to Fe-rich sediments was tested on the synthetic minerals and on a suite of the natural samples described above. Firstly, all Fe minerals were subjected to a non-sequential extraction for each SEDEX step. The synthetic hematite and magnetite/hematite composite samples were also run through the original SEDEX extraction scheme sequentially. The Golfo Dulce and Animikie Basin samples were subjected to the original SEDEX procedure, with Fe measured in each step. As outlined above, we did not include the first step (P_{sorb}) of the original SEDEX method as this is unlikely to be a valid extraction for ancient rocks, although this step is still suitable for studies of modern Fe-rich sediments.

For the synthetic Fe minerals, 25-30 mg of sample was reacted at room temperature with each extractant solution of the SEDEX method (using 10 ml of extractant, except in the case of sodium dithionite extractions with hematite, where 40 ml of extractant was used to avoid saturation of the solution with respect to Fe. All extractions were carried out at least in duplicate. For the Animikie Basin and Golfo Dulce samples, 150-180 mg of sediment was extracted in 10 ml of solution for each SEDEX step. To check whether any Fe (oxyhydr)oxide minerals persisted after completing the SEDEX method, additional extractions were performed on the residual sediment, utilising a 6 h citrate-dithionite-acetate (CDA) extraction for hematite (note that a 6 h CDA extraction was performed rather than the more typical 2 h extraction (see also Canfield et al., 2007) since our aim is to target highly crystalline hematite remaining after initial extraction by CDB), followed by a 6 h ammonium oxalate extraction for magnetite (Poulton and Canfield, 2005).

3.2.5 Developing a revised method for the partitioning of P in ancient sediments

A major difference between the Fe (oxyhydr)oxide targeting steps in the SEDEX and Fe speciation methods is the pH of the dithionite extraction solution (pH 7.6 for CDB in SEDEX; pH 4.8 for CDA in Fe speciation; Figure 3.1). As outlined above, however, dithionite extractions at pH 7.6 may not effectively extract crystalline hematite, either from ancient rocks or modern sediments (Raiswell et al., 1994). In addition, neither the CDB or CDA extractions target magnetite, which is extracted via ammonium oxalate (Poulton and Canfield, 2005; Figure 3.1). Therefore, we also performed a range of extractions on our synthetic Fe minerals to determine the optimum position for the insertion of these steps into our revised P speciation scheme. Alongside these extractions, we also tested whether ammonium oxalate and CDA extracted significant P from our natural apatite sample.

The original SEDEX scheme places wash steps with either 1 M $MgCl_2$ or MilliQ water after most of the principle extraction steps, in order to reverse any secondary re-adsorption of extracted phosphate onto other remaining sedimentary phases. We also carried out this step for the measurement of any re-adsorbed P during the CDA and ammonium oxalate extractions. After all principal extraction steps, a maximum of three washes (5 ml of solution for 2 h) were performed: (i) $MgCl_2$, ii) $MgCl_2$, iii) MilliQ water. In each case, each subsequent wash was only performed if significant P was detected in the previous wash. It has been suggested that secondary adsorption of P to residual sediment is not an important process during the CDB and HCl steps of the SEDEX procedure (Figure 3.1), and only a single $MgCl_2$ extraction is required following the Na acetate extraction (Ruttenberg, 1992, Slomp et al., 1996a). However, we suggest that the number of washes should be based on whether significant P was detected in the previous wash. As a result of the above tests, an optimal extraction scheme was developed and tested, firstly in relation to the dissolution of Fe from our synthetic hematite and magnetite/hematite composite samples, and subsequently in terms of the phase partitioning of both Fe and P in Golfo Dulce sediments, and the ancient Animikie Basin samples. Finally, the revised phosphorus speciation scheme

was applied to the North China Craton, Timan Region, Russia and Saltwick Nab sedimentary rocks.

3.2.6 Chemical analyses

Following each extraction or wash step, samples were centrifuged and aliquots of the supernatants were taken for the analysis of P. All P_{auth} and P_{det} solutions, as well as $MgCl_2$ and MilliQ washes, were immediately analysed for P on a spectrophotometer via the phosphomolybdate blue method (Koroleff, 1976, Strickland and Parsons, 1972), with the solutions adjusted to a pH of 1-2 where necessary. All other P measurements (CDB, ammonium oxalate and CDA) were analysed on a Thermo Fisher iCAP 7400 Radial ICP-OES, due to interference between the solution matrix and the phosphomolybdate complex. All Fe analyses were performed by flame atomic absorption spectroscopy (AAS). The reproducibility of Fe and P extractions were determined by replicate analyses, and are reported in terms of the relative standard deviation (RSD) at appropriate points in the text below.

Digests were also performed for the determination of total P and Fe via a HNO_3–HF–$HClO_4$ extraction on ashed samples. Phosphorus was analysed via the molybdate blue method outlined above, while Fe was analysed by AAS. The precision and accuracy of the method were determined by replicate analyses of the SBC-1 USGS international sediment standard, with RSD's of 5.5% and 4.0% for Fe and P, respectively, with complete recovery for both elements (96% and 97% respectively).

3.3 Results and Discussion

3.3.1 Testing the original SEDEX method for the extraction of Fe (oxyhydr)oxides

The extraction of synthetic ferrihydrite, goethite and lepidocrocite via a single 8 h CDB solution, as performed in the first step of the SEDEX procedure, led to a recovery of 90-100% for all three minerals (Figure 3.2), in agreement with Ruttenberg (1992). However, when applied to our synthetic hematite and magnetite/hematite composite samples, the CDB extraction dissolved only 18.4 ± 0.7% of the total Fe in hematite, and only 5.6 ± 0.1% of the Fe in the

magnetite/hematite sample. In the latter case, the majority of the dissolved Fe was likely from the dissolution of hematite. Recovery of Fe from the magnetite with co-precipitated P was higher, at 17.9 ± 2.2%, most likely due to the freshly precipitated nature of the mineral. However, despite this higher Fe recovery, only ~0.1% of the P contained in the co-precipitate was extracted by the CDB reaction. No previous data for the efficiency of magnetite dissolution by CDB has been published for comparison. The efficiency for crystalline hematite was substantially lower than that found by Ruttenberg (1992), and the poor recovery for both minerals confirmed that the current SEDEX method does not efficiently extract the more crystalline Fe oxides that are often key components of ancient sedimentary rocks. By contrast, a 2 h CDA extraction dissolved 59.7 ± 3.5% of our synthetic hematite mineral, which increased to 86.0 ± 0.7% with a 6 h CDA extraction (Figure 3.2), consistent with data highlighting the resistant nature of crystalline hematite (Canfield et al., 2007, Raiswell et al., 1994). Thus, the 6 h CDA extraction extracted the majority of hematite Fe and was therefore considered the most appropriate extraction for this phase. This 6 h CDA extraction did, however, dissolve 16.1 ± 0.5% of magnetite, suggesting that the CDA extraction should be performed after the 6 h oxalate extraction, which dissolved 100.0 ± 1.6% of the Fe present as magnetite in our composite magnetite/hematite sample (Figure 3.2).

To assess the extraction efficiency of the original SEDEX method in terms of the dissolution of crystalline Fe (oxyhydr)oxide minerals, we compared the amount of Fe extracted by CDB (Ruttenberg, 1992) and CDA (Poulton and Canfield, 2005) for Animikie Basin and Golfo Dulce sediments. In both cases, the CDB extraction generally dissolved a significantly lower concentration of crystalline Fe (oxyhydr)oxide phases relative to the CDA extraction (Figure 3.3). In addition, when the Fe_{mag} pool is added to Fe extracted by CDA (Figure 3.3), it is clear that a large proportion of crystalline Fe (oxyhydr)oxide minerals was not extracted by the original SEDEX method, and this was the case for both modern sediments and ancient sedimentary rocks.

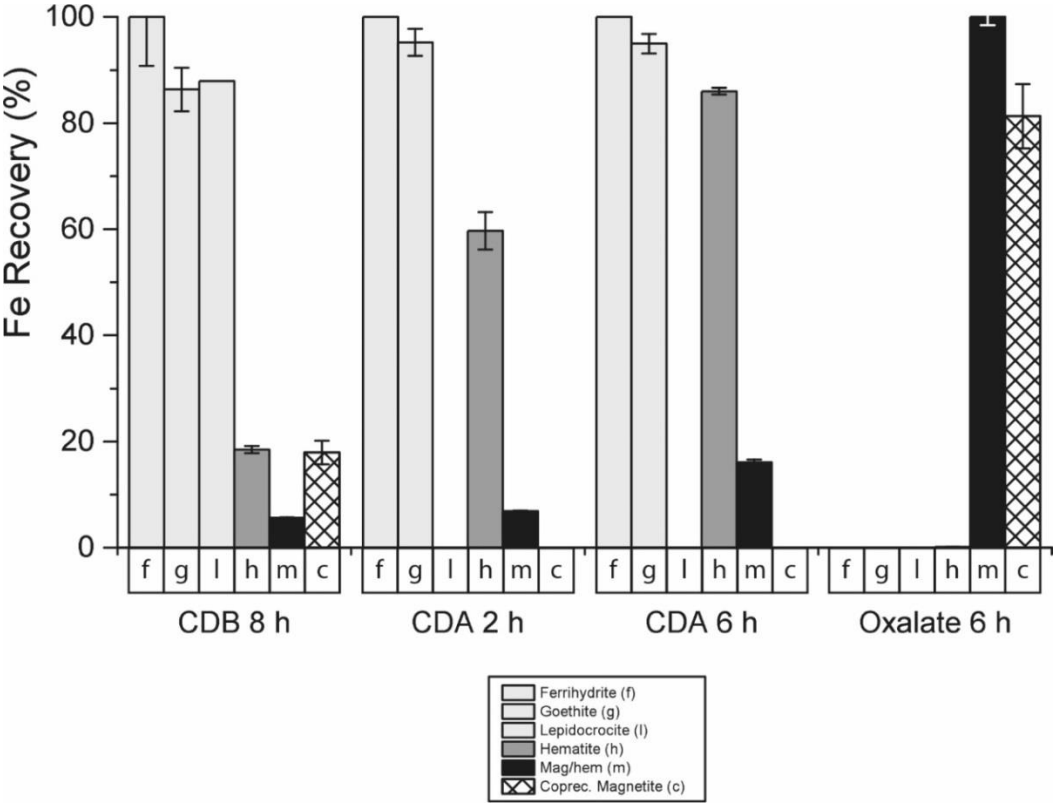

Figure 3.2 Recovery efficiencies for synthetic Fe minerals using different extractions performed non-sequentially.

Oxalate extraction data for the composite magnetite/hematite sample are expressed relative to the Fe present as magnetite. The RSD's (n=3) for these extractions are as follows: CDB 8 h – 3.7%, CDA 2 h – 3.0%, CDA 6 h – 3.2%, and ammonium oxalate 6 h – 2.9%.

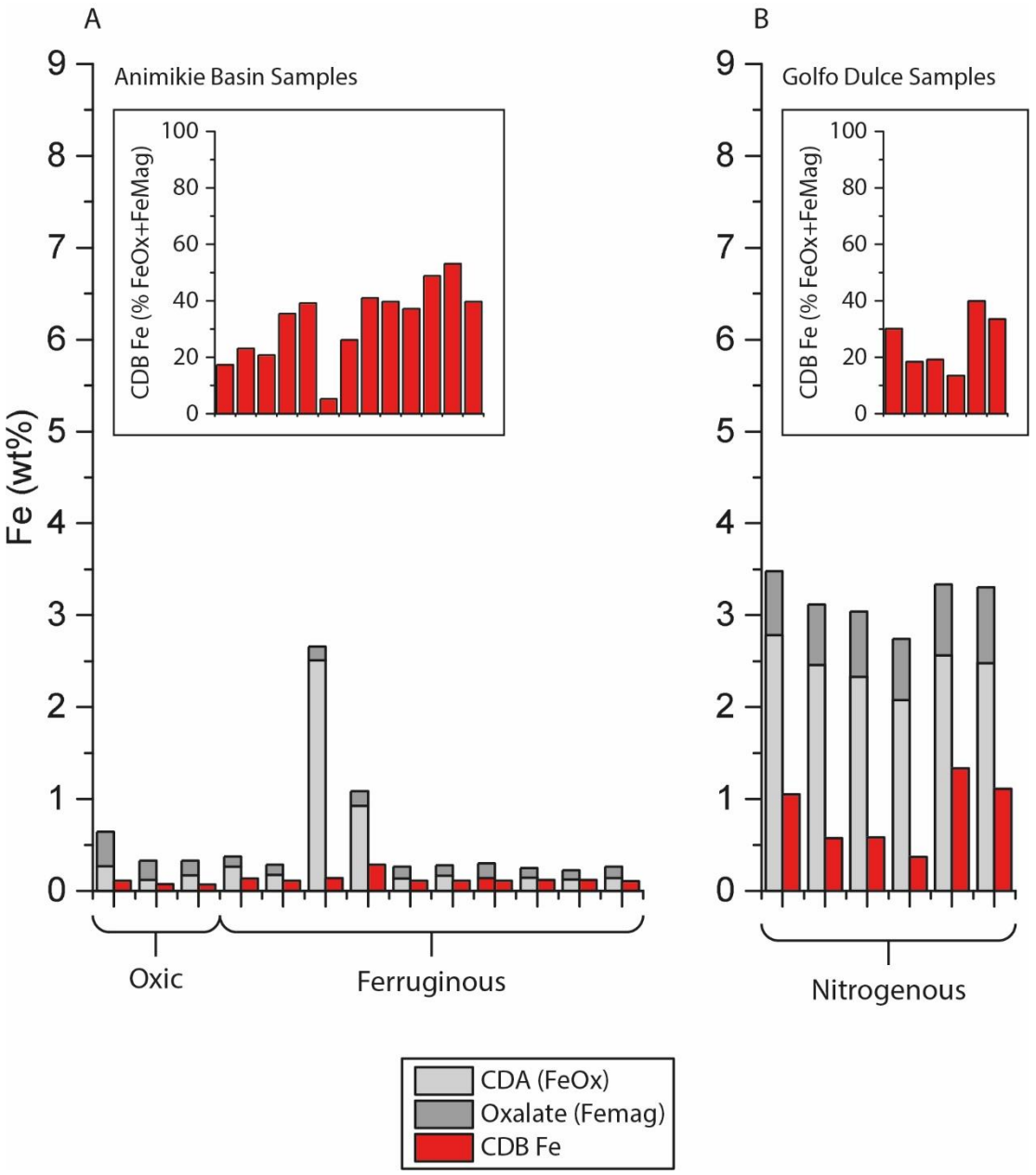

Figure 3.3 Comparison of Fe extracted from Animikie Basin (A) and Golfo Dulce (B) sediments via CDB (SEDEX procedure), with that extracted via CDA (Fe_{ox}) and ammonium oxalate (Fe_{mag}) (Poulton and Canfield, 2005).

Animikie Basin Fe_{ox} and Fe_{mag} data are from Poulton et al. (2010). The RSD (n=3) for the Fe extracted by the CDB step is 3.7%. Inset figures show the Fe extracted by an 8 h CDB extraction as a proportion of the Fe recovered by the CDA and ammonium oxalate extractions.

3.3.2 A revised method for P speciation in ancient sedimentary rocks

Having demonstrated the limitations of the existing SEDEX technique for extracting more crystalline Fe (oxyhydr)oxide phases, the next step was to consider the optimal position for the additional extractions in the sequential P method. The CDA and ammonium oxalate extractions were performed at low pH (4.8 and ~2, respectively), and hence it was not appropriate to perform these extractions prior to the pH 4.0 Na acetate extraction (which targets P_{auth}) of the SEDEX scheme (Figure 3.1). Thus, it was essential to retain the CDB extraction for the first step of the revised scheme in order to dissolve the most reactive Fe (oxyhydr)oxide minerals (hereafter termed P_{Fe1}) prior to extraction of P_{auth} (Figure 3.4). This leaves the more crystalline Fe (oxyhydr)oxide minerals, since the Na acetate extraction does not affect hematite or magnetite (Figure 3.5, also see Poulton and Canfield, 2005). Sequential extraction of our synthetic hematite and magnetite/hematite composite samples using the original SEDEX method revealed that these minerals were not appreciably dissolved by the 1 M HCl extraction used to target P_{det} (Figure 3.5). By contrast, we found that ammonium oxalate dissolved ~17% of P in the natural apatite sample from Madagascar. Thus, the ammonium oxalate and CDA extractions to determine magnetite-bound P (hereafter termed P_{mag}) and crystalline Fe (oxyhydr)oxide-bound P (hereafter termed P_{Fe2}) were placed after the 1 M HCl of the original SEDEX procedure. Furthermore, given that a 6 h CDA extraction dissolved appreciable magnetite (Figure 3.2), the 6 h CDA extraction was placed following the P_{mag} extraction. This results in the revised scheme detailed in Figure 3.4, where due to the potential for incomplete recovery by the Na acetate extraction of recrystallized P_{auth} from ancient sediments (and hence inclusion of this P as P_{det} in the subsequent step; see discussion below), we now redefine P_{det} as P_{cryst} to reflect this possibility.

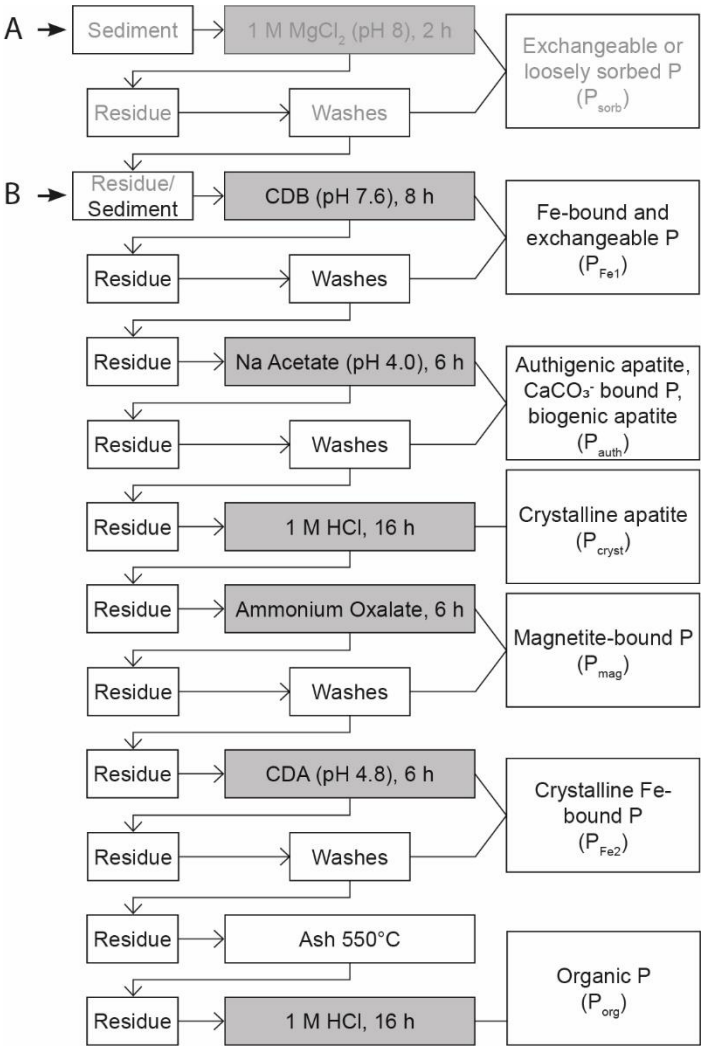

Figure 3.4 Revised method for the sequential extraction of P in modern and ancient iron-rich sediments.

Where (A) represents the starting point for modern sediments, and (B) represents the starting point for ancient rocks. Total Fe-bound P is the sum of P_{Fe1}, P_{mag} and P_{Fe2}. The P_{det} step of the original SEDEX procedure has been redefined as P_{cryst}, and represents crystalline apatite which may include recrystallized CFA and detrital apatite of igneous or metamorphic origin.

To test our revised scheme we first compare recoveries for our synthetic hematite and magnetite/hematite composite samples relative to recoveries for the original SEDEX scheme (Figure 3.5; replicate analyses (n=3) gave RSD's of 3.4% (8 h CDB), 6.4% (Na acetate), 1.0% (1 M HCl), 1.4% (ammonium oxalate), and 10.4% (CDA)).The addition of the oxalate and CDA extraction in the revised scheme significantly enhanced the total recovery of magnetite and

hematite (88.7 ± 1.1% and 76.9 ± 3.8%, respectively), relative to original scheme, suggesting that the revised scheme was more appropriate for application to modern and ancient Fe-rich sediments. The natural Isua BIF sample also showed a good recovery via the revised method (data not shown), with the P_{mag} step extracting 45.8 ± 3.0 wt% Fe, which was in good agreement with our separate determination (see earlier) of 43.8 wt% Fe_{mag} in this sample. We took this evaluation a step further by testing the ability of the ammonium oxalate extraction to recover P from magnetite, as this was one P phase that was not tested during development of the original SEDEX technique (Ruttenberg, 1992). Replicate extractions recovered 93.9 ± 1.7% of the Fe present as magnetite and 88.2 ± 12.8% of co-precipitated P, confirming the utility of this extraction for the determination of P_{mag}.

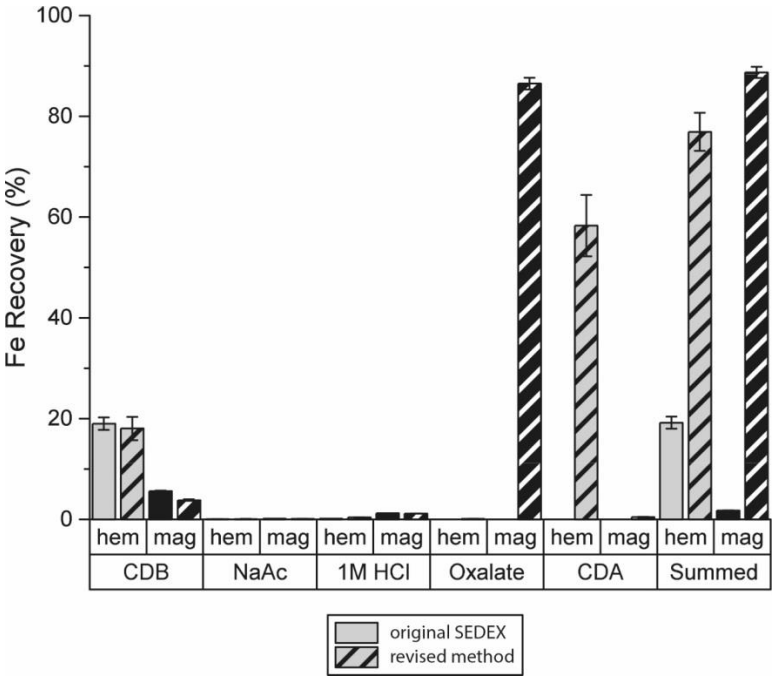

Figure 3.5 Comparison of Fe recoveries for the synthetic hematite (grey) and magnetite/hematite composite (black) samples during sequential extraction using the original SEDEX method (solid bars) and the revised method (striped bars).

The oxalate and summed recoveries for magnetite are reported relative to the concentration of magnetite Fe in the magnetite/hematite composite sample, discounting the Fe extracted by the CDB extraction, which likely largely represents hematite dissolved from this sample. Hem = hematite, mag = magnetite/hematite composite sample.

3.3.3 Application to modern and ancient sediments

After confirming that our revised method resulted in an enhanced recovery of crystalline Fe (oxyhydr)oxide minerals, we then applied the technique to determine P partitioning in Golfo Dulce (Figure 3.6) sediments and in our suite of ancient sediments (Figure 3.7). The RSD's for P extracted by each stage of the revised method are presented in Table 3.2, with each extraction displaying a high level of reproducibility. In addition, the sum of the P extracted by the revised method is highly reproducible, with a RSD of 1.8%.

Table 3.2 Reproducibility (%RSD) for each step of the revised method (n=6).

The RSD for P_{Fe2} is calculated from a different replicate sample (n=4) as PFe2 was below the limit of detection for the other replicate sample used.

Extraction	P_{Fe1}	P_{auth}	P_{det}	P_{mag}	P_{Fe2}	P_{org}	Summed P
%RSD	3.2	5.3	2.7	7.3	2.9	8.1	1.8

Clearly, our samples only capture a tiny proportion of the variability in P speciation that is possible in modern and ancient Fe-rich sediments. However, our application of the revised P speciation scheme to natural sediments does highlight the potential importance of the new scheme. In addition, this exercise also highlights possible limitations to P extraction schemes in general, which should be considered when interpreting such data-sets. Figure 3.6A shows that for the modern Golfo Dulce sediments, a significant proportion of the total P was associated with the less crystalline Fe (oxyhydr)oxide pool (P_{Fe1}; average = 41.0 ± 2.6%). However, the addition of the new Fe extraction steps increased the total recovery of Fe-bound P by up to 16%. P_{cryst} was low throughout these samples, suggesting limited recrystallization of P_{auth}. As such, the overall speciation of P as a function of reactive P (which is here calculated as the sum of P_{Fe1} + P_{auth} + P_{mag} + P_{Fe2} + P_{org}), rather than total P, showed little change (Figure 3.6B).

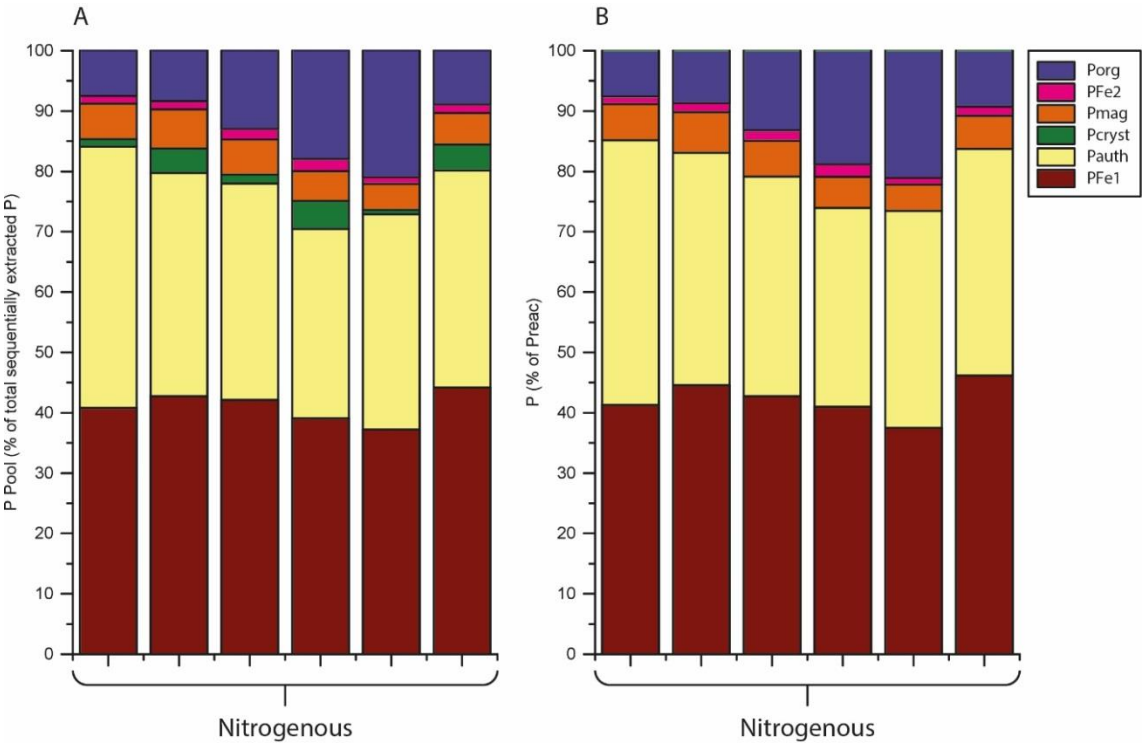

Figure 3.6 P speciation for Golfo Dulce samples using the revised method. (A) Partitioning relative to total P. (B) Partitioning relative to reactive P (defined as the sum of all phases minus P_{cryst}).

The bottom panel indicates the redox conditions in which the samples deposited.

The ancient sediments showed considerable variability in the partitioning of P (Figure 3.7A). P_{org} was particularly high in the North China Craton and Saltwick Nab samples, highlighting that P_{org} can be retained in ancient rocks that have experienced deep burial diagenesis and minor metamorphic alteration. The total proportion of Fe-bound P was relatively low in the Animikie Basin, Timan Region and Saltwick Nab sedimentary rocks. However, the North China Craton samples showed that Fe-bound P can be a major constituent of the total P pool, with up to 76% of total P occurring as Fe-bound P, of which 22% would not have been extracted using the original SEDEX scheme.

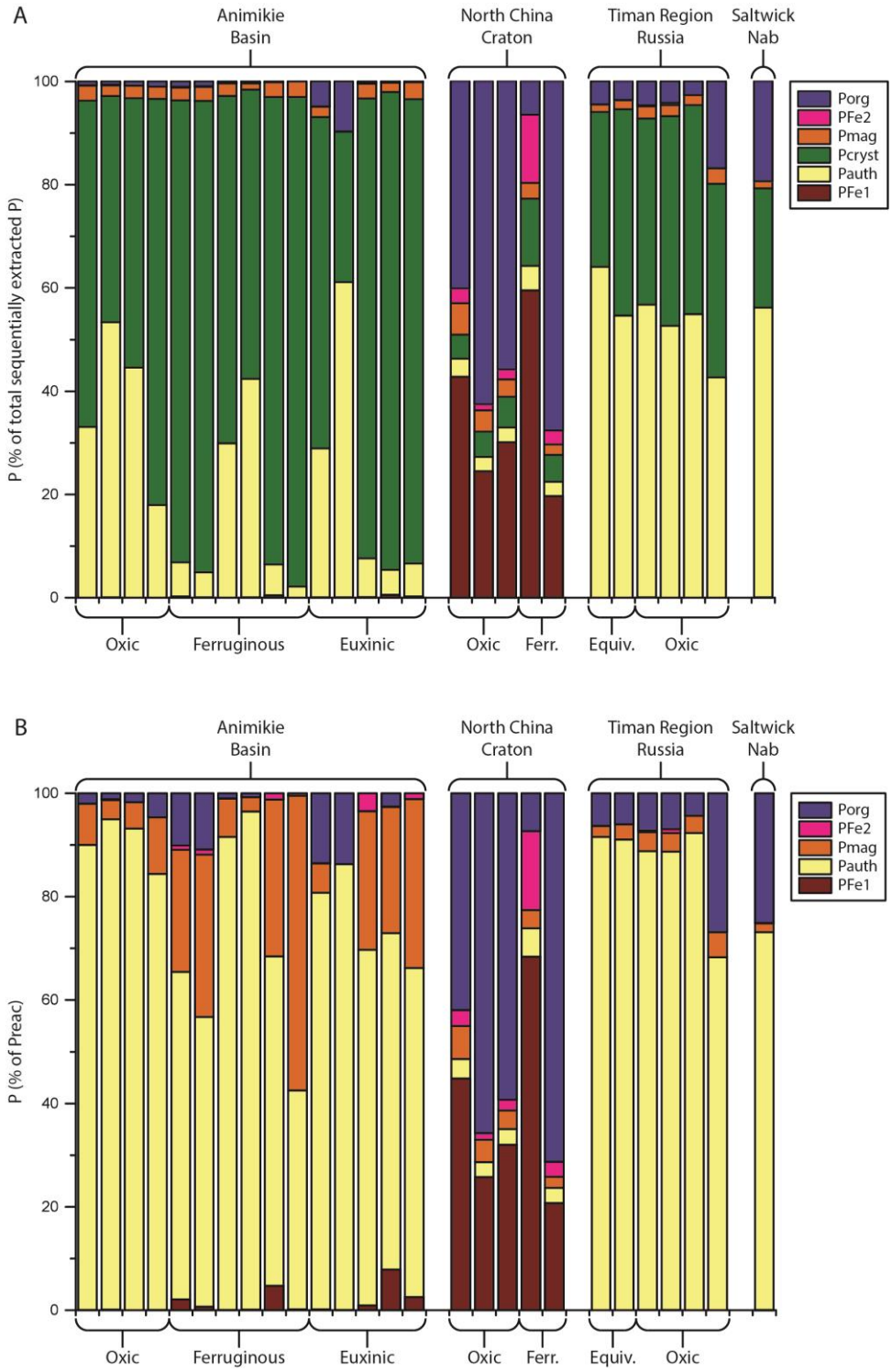

Figure 3.7 P speciation for ancient marine rocks using the revised method. (A) Partitioning relative to total P. (B) Partitioning relative to reactive P (defined as the sum of all phases minus P_{cryst}).

The bottom panel indicates the redox conditions in which the samples deposited. Ferr. = ferruginous. Equiv. = Equivocal, meaning the redox conditions were unable to be determined.

Three of the four localities had high proportions of crystalline P (Figure 3.7A). While we cannot rule out the possibility that the delivery of detrital P may have been elevated on the ancient Earth due to different weathering regimes, these high proportions of P_{cryst} do suggest probable transformation of P_{auth} to more crystalline phases. However, we note that this was not always the case, and the North China Craton samples contained much lower proportions of P_{cryst}, which were more in line with the modern sediment data (Figure 3.6A). This was likely because most of the P was partitioned into Fe-bound and organic-bound phases in this succession, and hence there was limited initial transfer of P from the sequestering phase into P_{auth} during early diagenesis. Thus, subsequent recrystallization of P_{auth} to P_{cryst} was also limited. This observation also reinforces the utility of the revised extraction scheme for robustly quantifying the organic-bound P and Fe-bound P that remains after early diagenetic 'sink-switching' to P_{auth}. After using this modified SEDEX extraction scheme, commonly used ratios such as TOC/P_{org} and P_{Fe}/P_{total} can be robustly applied to ancient rocks. In addition, it will be possible to quantify the relative roles of minerals such as hematite and magnetite in P drawdown to the sediment (e.g., see Bjerrum and Canfield, 2002; Konhauser et al., 2007).

However, while P_{Fe} (i.e., $P_{Fe1} + P_{Fe2}$), P_{mag}, and P_{org} can be considered to provide a robust quantification of these pools in ancient sediments, there will clearly be situations where P_{auth} increased significantly during early diagenesis, and hence this pool may have been affected by subsequent partial loss to the P_{cryst} pool during deep burial. Indeed, there is increasing evidence to suggest that the P_{auth} pool may also undergo progressive recrystallization during early diagenesis in modern sediments (Xiong et al., in preparation for submission). This process will be of particular significance in studies where quantification of the initial P_{reac} pool is required. We therefore suggest a general protocol whereby P_{reac} in both modern and ancient sediments is considered to fall within a minimum and maximum range. Here, a minimum value for P_{reac} may be calculated as the sum of $P_{Fe1} + P_{auth} + P_{mag} + P_{Fe2} + P_{org}$, whereas a maximum value is calculated by additionally including the P_{cryst} pool.

The ability to quantify magnetite-bound P is a novel strength of the revised speciation scheme. Over the last few years there has been increasing recognition of the major prevalence of anoxic ferruginous oceanic conditions across large periods of ancient Earth history (e.g., Canfield et al., 2008, Guilbaud et al., 2015, Johnston et al., 2010, Planavsky et al., 2011, Poulton and Canfield, 2011, Poulton et al., 2010). Under such conditions, magnetite is often a prominent mineral in the deposited sediments (e.g., Poulton et al., 2010). However, nutrient reconstructions under past ferruginous conditions have tended to focus on P uptake by Fe (oxyhydr)oxide minerals, rather than magnetite (e.g., Bjerrum and Canfield, 2002, Konhauser et al., 2007, Planavsky et al., 2010). In a recent study of a modern ferruginous water column, Zegeye et al. (2012) noted that metastable green rust was the major mineral precipitating in the water column, but this green rust subsequently commonly transfers to magnetite (e.g., Guilbaud et al., 2013, Sumoondur et al., 2008), which may begin during particle settling through the water column and continues during early diagenesis (Zegeye et al., 2012). Green rust has a particularly large adsorptive capacity for nutrient uptake (e.g., Zegeye et al., 2012), including phosphorus (Bocher et al., 2004, Hansen and Poulsen, 1999), and marine pH enhances the adsorption of anions such as phosphate (Guilbaud et al., 2013). This raises the possibility of significant retention of P as green rust transforms to magnetite. As such, magnetite-bound P in ancient shales could potentially be used as a tracer of past variability in oceanic P concentrations (see Bjerrum and Canfield, 2002; Konhauser et al., 2007; Planavsky et al., 2010). Indeed, in support of this possibility, we note that P_{mag} is much more significant than P_{Fe} in many of the ancient sediments analysed thus far (Figure 7b).

Whilst the discovery of a magnetite-bound pool of P raises important questions regarding P cycling under ferruginous conditions and the potential mechanisms of P association with Fe minerals, the origin of the magnetite itself should also be considered. As mentioned previously, there has been increased interest in the involvement of green rust in the formation of magnetite in modern ferruginous environments (Zegeye et al., 2012) and in experiments simulating Precambrian seawater reactions (Halevy et al., 2017), however, there is a large

debate about the origin of magnetite found in Fe-rich ancient sedimentary rocks (see Rasmussen and Muhling, 2018 for a recent discussion). Without some understanding of the formation mechanism of magnetite in a given sample, it is difficult to say whether any P associated with it is representative of past oceanic P concentrations.

In general there are three main mechanisms for the formation of magnetite: i) the reaction of dissolved Fe(II) and Fe (oxyhydr)oxides either in the water column or at the seafloor (Li et al., 2017); ii) reduction of Fe (III), either by dissimilatory Fe reduction coupled to organic matter oxidation (Johnson et al., 2008, Li et al., 2013a, Li et al., 2013b, Walker, 1984), or thermochemical Fe reduction of hematite and organic C (Köhler et al., 2013, Perry et al., 1973, Posth et al., 2013, but see Halama et al., 2016); and iii) the thermal decomposition of siderite, which occurs under dry condition in temperatures in excess of 400°C (French, 1971, French and Rosenberg, 1965, Gallagher and Warne, 1981) or in the presence of water at 200-300°C (Milesi et al., 2015). There seems to be a split in opinion within the scientific community with petrographic studies tending to suggest that the majority of magnetite found in iron formations is a relatively late-formed mineral, yet isotopic and experimental studies lean towards much earlier formation. Early formation of magnetite, for example through the reaction of Fe(II) with Fe (oxyhydr)oxides or dissimilatory Fe reduction, is far more likely to record ancient reactive P concentrations, whereas late-stage formation and alteration mechanisms involving extreme heat and external fluid infiltration may cause P from external or biogeochemically unreactive sources to be incorporated.

Ideally a combined approach of both geochemical and petrographic analyses would be used to determine the origin of magnetite in an Fe-rich ancient sedimentary rock along-side determining the P speciation. A highly negative δ^{56}Fe isotopic signature may indicate that dissimilatory Fe reduction was a key formation mechanism (Johnson et al., 2008), and rare earth element patterns may reveal a strong hydrothermal influence (Derry and Jacobsen, 1990), but the petrographic characteristics of a sample can also help determine whether the magnetite present is characteristic of “primary” minerals or provide textural

evidence for mineral replacement mechanisms (Ayres, 1972, LaBerge, 1964, Rasmussen and Muhling, 2018).

3.4 Conclusions

The SEDEX sequential P extraction scheme of Ruttenberg (1992) is the most commonly used technique for quantifying operationally-defined P pools in modern marine sediments, and has provided a wealth of information of P cycling in modern environments. Here, we provide a modification of this method to more specifically target important Fe phases, such as crystalline hematite and magnetite, which are common components of many ancient sediments and some Fe-rich modern sediments. We demonstrate that crystalline hematite is only partially extracted by the existing SEDEX scheme, while magnetite is not specifically targeted. Following robust calibration testing, we introduce two additional steps to the SEDEX scheme to specifically target these additional Fe-bound P phases. Testing of the revised method on modern and ancient sediments highlights the reproducible nature of the extractions and the enhanced recovery of Fe-bound P. We thus provide details of the first P speciation scheme specifically developed for application to ancient marine rocks, as well as modern Fe-rich sediments. We demonstrate the difficulties inherent in adequately quantifying the total authigenic pool of P in ancient marine rocks, and suggest a protocol for placing minimum and maximum constraints on the size of this fraction. Finally, we suggest that magnetite may have constituted a significant pool of P in many ancient ferruginous marine settings, and as such warrants further consideration in terms of its role in modifying and recording P cycling under such conditions.

Chapter 4 Iron and phosphorus cycling in the ferruginous Lake La Cruz

4.1 Introduction

4.1.1 Importance of ferruginous conditions

Whilst ferruginous conditions are a rare occurrence in the modern, oxygenated world, they were likely the prevailing ocean redox state throughout much of Earth's history (Figure 4.1; Poulton and Canfield, 2011), as documented in the geological record. Banded iron formations (BIFs) are a common feature of Precambrian deposits, and while the mechanisms for their formation are still under discussion (see Braterman et al., 1983, Konhauser et al., 2007, Klein, 2005) it is in general agreement that they are a prominent signature of ferruginous oceans. It was originally thought that the cessation of these BIFs in the sedimentary record ~1.8 Ga (Bekker et al., 2010) indicated a shift from ferruginous oceans to either euxinic (Canfield, 1998) or oxic oceans (Holland, 1984). However, there is mounting evidence from marine shales that ferruginous conditions may have been an important feature of the deep ocean through the mid-late Proterozoic and even into the Cambrian (Canfield et al., 2008, Partin et al., 2013, Planavsky et al., 2011, Poulton et al., 2010, Reinhard et al., 2013, Sperling et al., 2015) with euxinic conditions restricted to productive ocean margins (Li et al., 2010, Poulton and Canfield, 2011, Poulton et al., 2010).

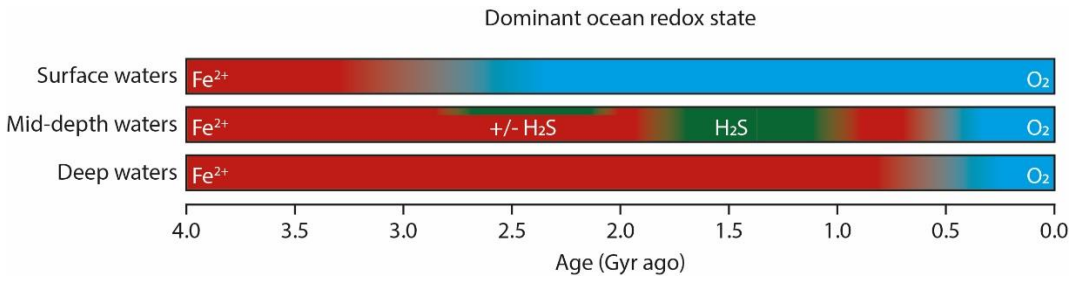

Figure 4.1 Dominant ocean redox state through time for surface, mid-depth and deep waters. After Poulton (2017).

4.1.2 Use of modern environments as analogues

Geochemists can use many different tools to help develop our understanding of biogeochemical processes on ancient Earth, including studying the original rock record, and simulating certain conditions in laboratory experiments. Whilst the first approach can be challenged by post-depositional processes, the latter is unlikely to reflect the full complexity of the natural environment. As such, modern environments that have more adequate physical, geochemical and microbial characteristics can be used alongside the rock record and laboratory simulations to provide crucial information. Locations that reflect the euxinic ocean margins of the Proterozoic, such as the Black Sea, Baltic Sea, and Lake Cadagno, are being increasingly studied (Canfield et al., 2010, Dahl et al., 2010, Dijkstra et al., 2014, Lukkari et al., 2009, Meyer and Kump, 2008, Mort et al., 2010, Wirth et al., 2013), yet it is much harder to find environments that reflect the periods of ferruginous oceans, and these are limited to freshwater systems due to the high concentration of SO_4 in the modern ocean.

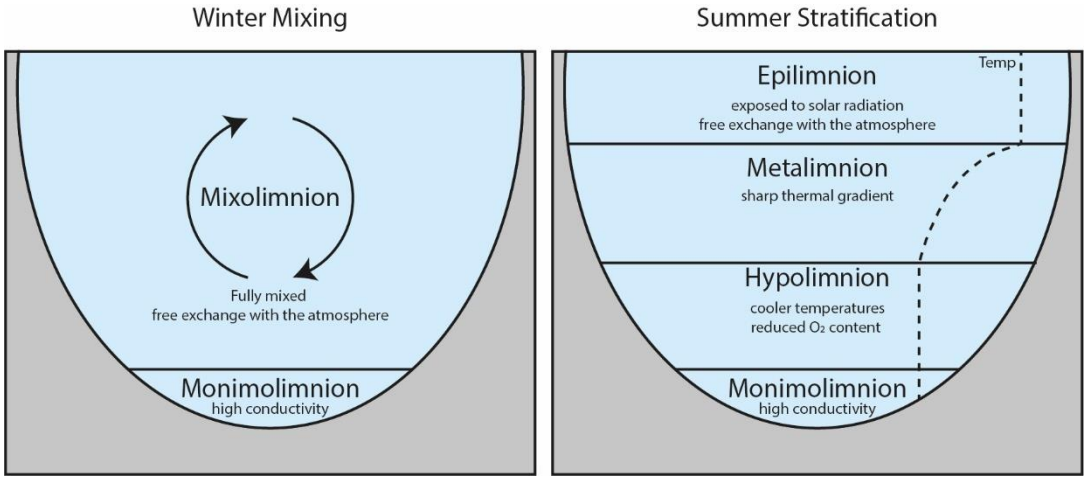

Figure 4.2 Stratification patterns of a meromictic lake, during winter mixing and summer stratification.

The most widely studied ferruginous systems are all meromictic lakes, meaning they are seasonally stratified with an additional chemically distinct bottom layer (called the monimolimnion, see Figure 4.2) that has not been recirculated in over a year, which in these cases is ferruginous. Lake Pavin, France and Lake Matano, Indonesia have been specifically targeted by studies with the purpose

of developing models of Precambrian oceans (Bura-Nakic et al., 2009, Busigny et al., 2014, Crowe et al., 2008a, Crowe et al., 2014, Zegeye et al., 2012), but both Lake La Cruz, Spain and Kabuno Bay of Lake Kivu, Democratic Republic of Congo have also been shown to be suitable environments for an Archean ocean analogue (Lliros et al., 2015, Walter, 2011, Walter et al., 2014), and a comparison of water column chemistry can be seen in Table 4.1. The merits of using these modern environments as ancient analogues have been reviewed recently by Koeksoy et al. (2016) and Camacho et al. (2017). These previous studies have mainly focused on iron isotopes and identifying photoferrotrophy in the water columns of these environments, but so far there has been little investigation into the cycling of the limiting nutrient phosphorus. Lakes with ferruginous conditions that extend down through the water column, through the sediment-water interface and into the sediment, provide a perfect environment for researching the mechanisms that control P drawdown and release under the redox conditions that were so prevalent throughout much of Earth's history.

Table 4.1 Comparison of water chemistry of the anoxic layers of modern ferruginous lakes and estimates for the Archean.

a) Walter et al. (2014), b) Rodrigo et al. (2001) c) Crowe et al. (2008), d) Bura-Nakic et al. (2009) e) Busigny et al. (2014), f) Canfield (2005), g) Bjerrum and Canfield (2002), h) Crowe et al. (2014), i) Konhauser et al. (2007a) j) Saito et al. (2003) and k) Grotzinger and Kasting (1993)

	Lake La Cruz[a]	Lake Matano[c]	Lake Pavin[d]	Archean
O_2 (µM)	0	0	0	<0.3[c]
Fe(II) (µM)	230	140	1000	40-120f
PO_4^{3-} (µM)	<1.6	9	340[e]	0.03-0.29[g]
SO_4^{2-} (µM)	<25	<0.1	<5.0	0.06-0.08[h]
SiO_2 (µM)	550[b]	420	556-1130	670-2200[i]
pH	7	7	6.08	>6.5[j]
T (°C)	6	25-28	4	40-70[k]

4.1.3 Lake La Cruz

4.1.3.1 Setting

Lake La Cruz (Laguna de la Gitana) is an iron-rich meromictic lake situated in the Lagunas de Cañada del Hoyo National Park, Spain. One of many lakes in the area that lie in sink holes within dolomitic ($CaMg(CO_3)_2$) substrate ~1000 m above sea level, Lake La Cruz has a mean diameter of 122 m and a maximum depth of 25 m. The sinkhole itself has a larger diameter (170 m), creating walls standing 16-25 m above the waterline (Romero-Viana et al., 2010) (Figure 4.3). These steep walls act as a barrier to wind, reducing wind-driven currents and hence vertical mixing.

Figure 4.3 (Left) Aerial view of lake La Cruz, with the bathymetry of Vicente and Miracle (1988) overlaid.

The red viewpoint indicates where the photo (right) was taken from during the sampling for this study in 2014. The rib seen in the middle is the sampling location.

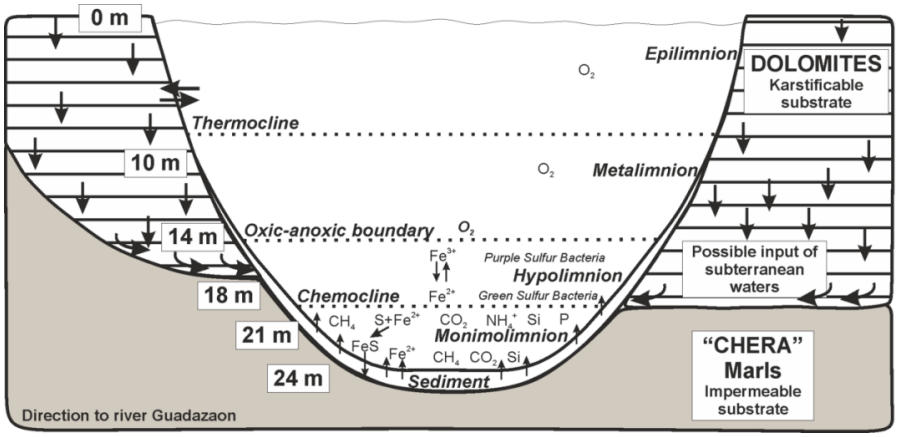

Figure 4.4 Schematic of the vertical structure of Lake La Cruz during periods of thermal stratification (summer-autumn). After Rodrigo et al. (2001)

Lake La Cruz has a negligible catchment area and no connection with running waters (Rodrigo et al., 2001). Instead, the lake is largely subterranean fed by lateral sources (Santisteban, 1994) which transport dissolved species from the surrounding substrate which is mainly dolomites, marls and clays. This region of Spain receives unpredictable, generally low levels of rainfall which is unevenly distributed. This causes the lake's hydrology to be strongly dictated by both annual and seasonal changes climatological conditions. As is expected for a meromictic lake, there is a general progression of thermal stratification throughout the year, increasing throughout the summer before collapsing on winter mixing, however the timing and physical characteristics of the stratification patterns can vary significantly year on year. This was best demonstrated by Rodrigo et al. (2001), when the lake was sampled every 1-2 months over a 17 month period. Warmer than average temperatures in winter and increased rainfall in spring in the 2nd year lead to large interannual variation in the two thermal stratification periods (Figure 4.5).

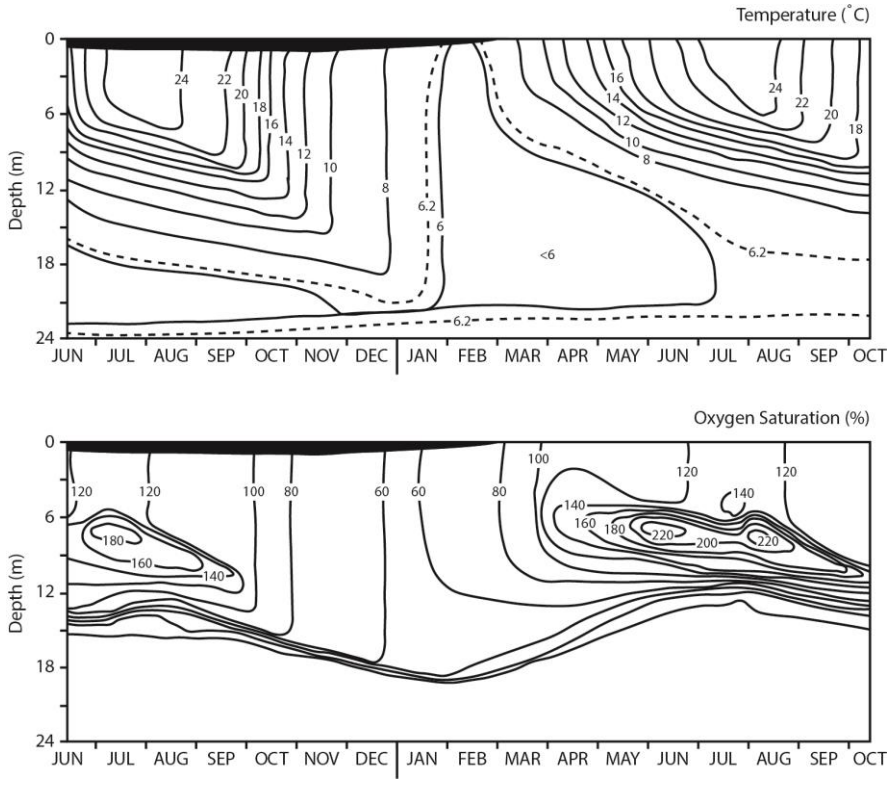

Figure 4.5 Time and depth distributions of temperature and O_2 saturation in Lake La Cruz over two stratification events. After Rodrigo et al. (2001)

The lake has a strong chemical stratification all year round due to high concentrations of bicarbonate, calcium and magnesium (sourced from the surrounding substrate) in the monimolimnion below ~19 m depth, relative to maximum depth (Rodrigo et al., 2001). Lake La Cruz is one of a series of sink hole lakes in the area, but is the only one with a permanent monimolimnion; El Tejo for example, a lake only 150 m from Lake La Cruz, is deeper and has the same protective steep walls, but is subject to full convective mixing during autumn cooling. It is thought the location of subterranean inflow to the lake is crucial in determining whether the lakes have a permanent monimolimnion or a seasonal hypolimnion. At El Tejo, the inflow is directly from the bottom of the basin, and it has been suggested that this destabilises the deep water preventing a monimolimnion from forming (Rodrigo et al., 2001). Due to the impermeable layer of Fe-rich marls surrounding the bottom 4-5m of Lake La Cruz (Figure 4.4), the subterranean inflow is located just above this stratum (Santisteban, 1994), allowing an undisturbed monimolimnion to form below. The high level of both chemical and physical stratification reduces mixing and with it, the oxygen penetration depth.

Sulphate concentrations are low (30 µM in the monimolimnion; Miracle et al. 1992) due to the lack of gypsum in the surrounding area and limited pyrite oxidation. This limits the production of sulphide via sulphate reduction, allowing Fe(II), originating from the underlying marl (Julia et al., 1998), to accumulate below the chemocline creating ferruginous conditions. When there is excess organic matter following iron reduction and limited sulphate reduction, mineralisation can be driven to methanogenesis (Romero-Viana et al., 2010).

The Lake also undergoes an annual summer “whiting” event around July/August, where there is short-term massive precipitation of $CaCO_3$ due to changes in temperature and photosynthetic activity (Romero-Viana et al., 2008). This is a widespread phenomenon in hardwater lakes, and can have several effects on the biology and chemistry of the system due to coprecipitation/adsorption reactions and also distinct changes in the light penetration with depth. Unless the whiting events are the focus of any

research, sampling of lake during summer stratification is best conducted from September onwards, when the system has returned to normal.

4.1.3.2 Previous studies

Previous work has found evidence of anoxygenic phototrophic prokaryotes both in the present water column (Rodrigo et al., 2000), and throughout the lake's history in the sediment record (Romero-Viana et al., 2010); with mass mortality events occurring due to oxygen exposure when the thermal stratification collapses (Romero et al., 2006). Dense populations of purple and green anoxygenic phototrophic sulphur bacteria have been identified despite the low sulphate and sulphide concentrations. It has been shown that these communities survive through photoferrotrophy, using Fe(II) as an electron donor instead of sulphur (Ehrenreich and Widdel, 1994, Heising et al., 1999, Walter, 2011) which is a potential mechanism for the deposition of BIFs prior to the evolution of oxygenic photosynthesis (Kappler et al., 2005, Konhauser et al., 2005)).

Whilst the previous work by Walter et al. (2014) provides an excellent insight into biologically mediated reactions occurring in the ferruginous water column of Lake La Cruz, the investigation into the sediments is limited. Previously, the sediments have been described as sulphidic, due to the lack of 0.5 M HCl extractable Fe(III) and the accumulation of Fe(II), FeS and FeS_2 phases (Walter, 2011, Walter et al., 2014). From this, they conclude that the presence of FeS rich sediments in the geological record should not be taken as evidence that they were deposited from a euxinic or eutrophic water column, as they believe FeS minerals are the main sedimentary feature of this ferruginous oligo-mesotrophic lake (Walter, 2011). However, in general, the presence of FeS in sediments is not the only factor considered when assessing the depositional redox conditions, but rather the degree of sulphidisation of reactive Fe in the sediment. This can be assessed using either the original method of Berner (1970), or with the complimentary indicator of Fe_{py}/ Fe_{HR} using the more detailed extraction scheme of Poulton and Canfield (2005). Previously in Lake La Cruz, only a 0.5 M extraction was used to quantify the reactive Fe pool in

sediments (Walter, 2011), which is a much weaker extraction than those suggested by Berner (1970) or Poulton and Canfield (2005). This resulted in the extraction of highly reducible ferric oxides only, likely leading to an underestimation of other reactive Fe phases. However, considering the high concentration of Fe(II) and the relatively low concentration of sulphide in the water column, it seems unreasonable to assume that all the solid phase Fe(II) accumulated in the sediment is sulphidised. Full Fe speciation by the method of Poulton and Canfield (2005) will more accurately determine whether Lake La Cruz sediments give a ferruginous or euxinic signal.

Because of the ferruginous redox structure (especially in the monimolimnion) and the presence of anoxygenic phototrophic communities, Lake La Cruz has been thought to be a good analogue for the Neoarchean ocean (Camacho et al., 2017, Koeksoy et al., 2016, Walter, 2011). For these reasons, it also provides a perfect location to investigate the iron minerals that form under ferruginous conditions, and how they interact with nutrients, specifically phosphorus. Fe mineral interactions with P are strongly influenced by dissolved silica concentrations due to competition for available sorption sites on Fe (oxyhydr)oxides (Konhauser et al., 2007b), and hence it is imperative that the silica concentrations present in any analogue system are comparable to those estimated for the Archean. Lake La Cruz has a relatively high concentration of SiO_2 in the ferruginous monimolimnion, which is close the range estimated for the Archean (Konhauser et al., 2007a) (see Table 4.1), making the lake a good natural laboratory for studying the potential P/Fe interactions of the Archean.

4.1.4 Objectives

To investigate Fe and P cycling in the ferruginous conditions of Lake La Cruz, the following objectives were set.

1. Identify the partitioning of Fe and P in both the sediment and water column particulates between common operationally defined pools.
2. Determine if dissolved P released from the mineralisation of organic matter and the reduction of Fe minerals is recycled to the water column from the sediment or retained in authigenic mineral phases.

3. If dissolved P and Fe are released from the sediment, ascertain the fate of these dissolved constituents in the water column.
4. Consider the potential importance of our findings in relation to the stimulation/limitation of primary productivity under meso-oligotrophic ferruginous continental margins.

4.2 Methods

All samples were collected from a central sampling station (see Figure 4.3, right) on the lake between 4^{th}-11^{th} September 2014, in collaboration with N.R. Posth, A.-E. Rotaru, R.P. Cox, M.R. Miracle, and E. Vicente. This sampling period was after the lake had recovered from the annual whiting event and during a period of strong stratification. During this time, the maximum water depth was ~ 20 m.

4.2.1 Sample collection and processing

A physicochemical survey of the water column was conducted prior to any disturbance caused by physical sampling using a CTD probe (conductivity/temperature/density probe). *In situ* measurements of temperature, O_2 saturation and conductivity were recorded approximately every 50 cm. This provided information on the current stratification of the lake and allowed identification of the thermo- and redoxcline prior to sampling of the water column, our sampling strategy was then decided based on this (Table 4.2). Water column samples were taken from the centre of the lake at the depths outlined in Table 4.2 and three sediment cores of ~30 cm length were recovered from the centre of the lake.

Following collection, water column samples were processed for the analysis of dissolved and total Fe(II), P, S(-II) and SO_4 concentrations. Water column particulate matter was collected from each water column sample and stored under anoxic conditions. Of the three cores, one was frozen intact for future work and two were immediately processed in an anaerobic atmosphere for the separation of bulk sediment and porewaters. Porewaters were divided up for immediate analysis of dissolved Fe(II), P and storage of S(-II) and SO_4.

Sediment samples remained frozen during transport back to Leeds, where they were freeze dried and then stored in the freezer. Full details of sample collection and processing methods can be found in Chapter 3, section 3.1.1.

Table 4.2 Water column sampling strategy.

Sample ID	Sample depth (m)	Water Column Zone
WC1	4	Oxic
WC2	6.5	
WC3	9	O_2 peak
WC4	10	Redoxcline
WC5	10.5	
WC6	11	
WC7	11.5	
WC8	12.5	Anoxic
WC9	14	
WC10	15	
WC11	16	
WC12	17	
WC13	17.5	
WC14	18	
WC15	19	

4.2.2 Techniques

Full details of analytical techniques and methods can be found in Chapter 2, only an outline of the data collected is mentioned here.

4.2.2.1 Aqueous chemistry

Total (unfiltered) and dissolved (filtered, 0.2 µm) Fe(II) and P were analysed immediately using the ferrozine (Stookey, 1970, Viollier et al., 2000) and the phosphomolybdate blue (Murphy and Riley, 1962) methods respectively. For S(-II) analysis, samples were fixed with 50 µl of 10 mM Zinc Acetate, and were

analysed in Leeds following the Cline assay (Cline, 1969). Subsamples kept for SO_4 analysis were analysed by ion chromatography.

4.2.2.2 Solid chemistry

Bulk chemistry of sediments and water column particulates was determined by a HNO_3-HF-$HClO_4$-H_3BO_3-HNO_3 digestion of freeze dried sediment or pre-weighed filters respectively. Solutions were then analysed for P by the phosphomolybdate blue method, Fe(III) by AAS, and Al, Ca, Mg and Mn by ICP-MS. Total carbon (TC) and total organic carbon (TOC) were determined on separate splits of freeze dried sediment and analysed on a C analyser.

Fe speciation (Canfield et al., 1986, Poulton and Canfield, 2005) as described in Chapter 2 was completed on freeze dried sediment and segments of water column filters. The weight of sample on the filter sections was unknown prior to extractions so wt% Fe cannot be directly measured as it is for sediment samples. The method does, however, give the proportion of the Fe pools for each sample, which can then be applied to the total Fe concentration obtained through digestion of a whole filter (with known sample mass) to give wt% Fe.

P speciation was determined for sediment and water column particulates using the SEDEX method (Ruttenberg, 1992), as described in detail in Chapter 2. All solutions were analysed for P using the phosphomolybdate blue method, apart from the P_{Fe} – CDB (sodium citrate/dithionite/bicarbonate) solution which requires analysis by ICP-OES due to the interference of citrate with the molybdate complex, Fe was also analysed in this solution. As with the Fe speciation, P speciation on the water column particulates collected on filters can only give the proportion of each P pool, but this can be used in combination with total P to give wt% P.

4.2.2.3 Geochemical modelling

Estimates of the diffusive flux of Fe(II) and P from the sediment surface can be made using Fick's first law:

$$J = -\frac{\varphi}{\theta^2} D_0(S,T) \frac{\partial C}{\partial x}$$

J	*Flux of dissolved constituent*
φ	*Sediment porosity*
θ^2	*Correction factor for sediment tortuosity* ($\theta^2 = 1 - 2ln(\varphi)$)
$D_0(S,T)$	*Molecular diffusion coefficient for the measured salinity (S) and temperature (T)*
C	*Porewater concentration*
x	*Depth in sediment*

The surface sediment diffusive flux for both Fe(II) and P were calculated using measured data from the top 8 cm of the core and D_0 values calculated using the R package CRAN: marelac (Soetaert et al., 2016) which is based on Boudreau (1997). Details of the parameters used in the calculation can be found in Table 4.3.

Table 4.3 Parameters used in diffusive flux calculations.

The diffusion coefficient is based bottom water salinity, temperature and pressure.

Parameter		Fe(II)	P
Porosity	(v/v)	0.94	0.94
$\frac{\partial C}{\partial x}$	($\mu mol/dm^3/cm^{-1}$)	12.5	1.5
$D_0(S,T)$ (S = 0.69, T = 5.8°C, P = 20.9 bar)	(m^2/s^1)	4.18×10^{-10}	3.45×10^{-10}

The saturation index of the monimolimnion with respect to vivianite was calculated using PHREEQC Interactive 3.3.7, using the databases of Appelo et al. (2014) and Laliberté (2009). Calculations were based on measured input values of dissolved Fe(II) and P, temperature, pH and eH.

4.3 Results

4.3.1 Physical parameters

In situ measurements of the water column revealed a well-defined, physicochemically stratified water column (Figure 4.6). A well-mixed epilimnion extends down to 6.5 m, with consistent temperature, O_2 saturation and conductivity. The metalimnion is then defined by the start of the thermocline, which extends over 5.5 m, decreasing from 23.6°C down to 7.9°C at 12 m depth. The first 2 m of the metalimnion are characterised by a distinct peak in O_2 saturation up to 208%, most likely indicating peak photosynthesis and the reduced mixing of water in the thermocline. O_2 concentrations then rapidly decrease across a 3 m redoxcline to the point of oxygen extinction at 12 m. Conductivity increases gradually throughout the metalimnion, particularly across the redoxcline, this slow increase in dissolved solids continues in the anoxic hypolimnion below 12 m depth and temperature stabilises around 7°C. A marked increase in conductivity is not seen until 15 m, which is most likely due to the combined influence of redox chemistry, the sediment/water interface, and the subterranean water input ~5 above the bottom. This is consistent with previous suggestions of a permanent monimolimnion existing in the bottom 5 m of the lake. The maximum conductivity measured was 868 µS/cm at 16.5 m, where measurements ceased due to proximity to the lake bottom. The average temperature of the monimolimnion was 5.8°C.

4.3.2 Water column

4.3.2.1 Dissolves species

Dissolved Fe(II) is negligible throughout the epi- and metalimnion, increasing only slightly to 9.1 µM in the hypolimnion (Figure 4.7). A significant gradient is seen in the monimolimnion, increasing to 252.3 µM over 2 m. Dissolved P concentrations follow a similar pattern to Fe(II), with concentrations below the detection limit in the both the epi- and metalimnion, but also extending through the hypolimnion (Figure 4.7). Dissolved P only becomes detectable at 15 m but, at only 0.04 µM, concentrations remain very low until 18 m where there is a

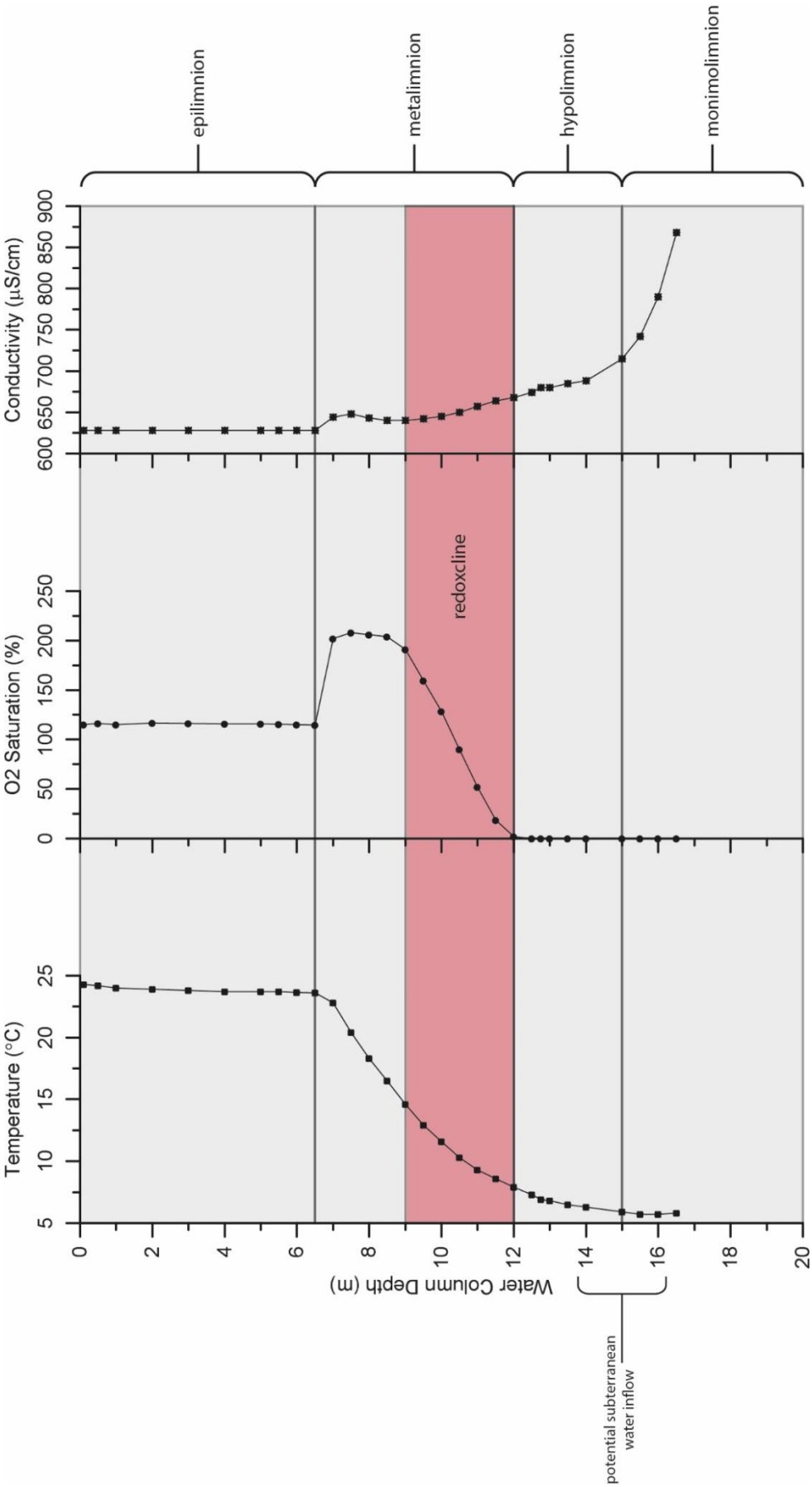

Figure 4.6 Water column physical parameters

sharp increase towards the sediment in the bottom 2 m up to a maximum of 2.54 µM. Dissolved S(-II) remains negligible throughout the oxygenated epi- and metalimnion, and increases marginally below the point of oxygen extinction at 14 m (Figure 4.7). Like Fe(II) and P, dissolved S(-II) concentrations display a sharp increase towards the sediment in the monimolimnion, but remain low, with a maximum of 3.7 µM at 19 m. There does appear to be a drop in sulphide to 0.5 µM at 17.5 m, but it is not clear whether this is an analytical artefact. Sulphate concentrations in the epi- and upper metalimnion decrease from 30 to 20 µM with depth, but then increase again to ~29 µM in the redoxcline between 10 and 11 m depth (Figure 4.7). Concentrations then decrease again through the hypolimnion, and appear to stabilise around 4 µM in the monimolimnion.

4.3.2.2 Particulate species

Particulate Fe(II) is insignificant in the epi- and metalimnion due to high O_2 concentrations, but reaches more detectable levels throughout the redoxcline, averaging 0.4 µM (Figure 4.8). At the base of the redoxcline and the point of O_2 extinction, Fe(II) bearing particles precipitate, reaching concentrations of 1.5 µM in the hypolimnion. In general, concentrations then increase in the monimolimnion reaching a maximum of 3.8 µM, but also become more variable with concentrations ranging by 3.1 µM. Particulate P concentrations are low but detectable in the epi- and metalimnion, averaging around 0.04 µM, but peak suddenly to 0.35 µM at 12.5 m, just below the redoxcline (Figure 4.8).

Concentrations then fall below the limit of detection until 17 m depth where they then remain elevated at depth, but ~10 times lower than dissolved P in the monimolimnion. Particulate S(-II) concentrations are close to detection limits throughout the upper water column, becoming more prevalent in the redoxcline, increasing with depth and reaching a maximum of 1.29 µM in the monimolimnion (Figure 4.8). In this permanently anoxic zone of the lake, particulate sulphide concentrations appear to be tightly coupled with particulate Fe(II), with a distinct trough at 17-17.5 m depth.

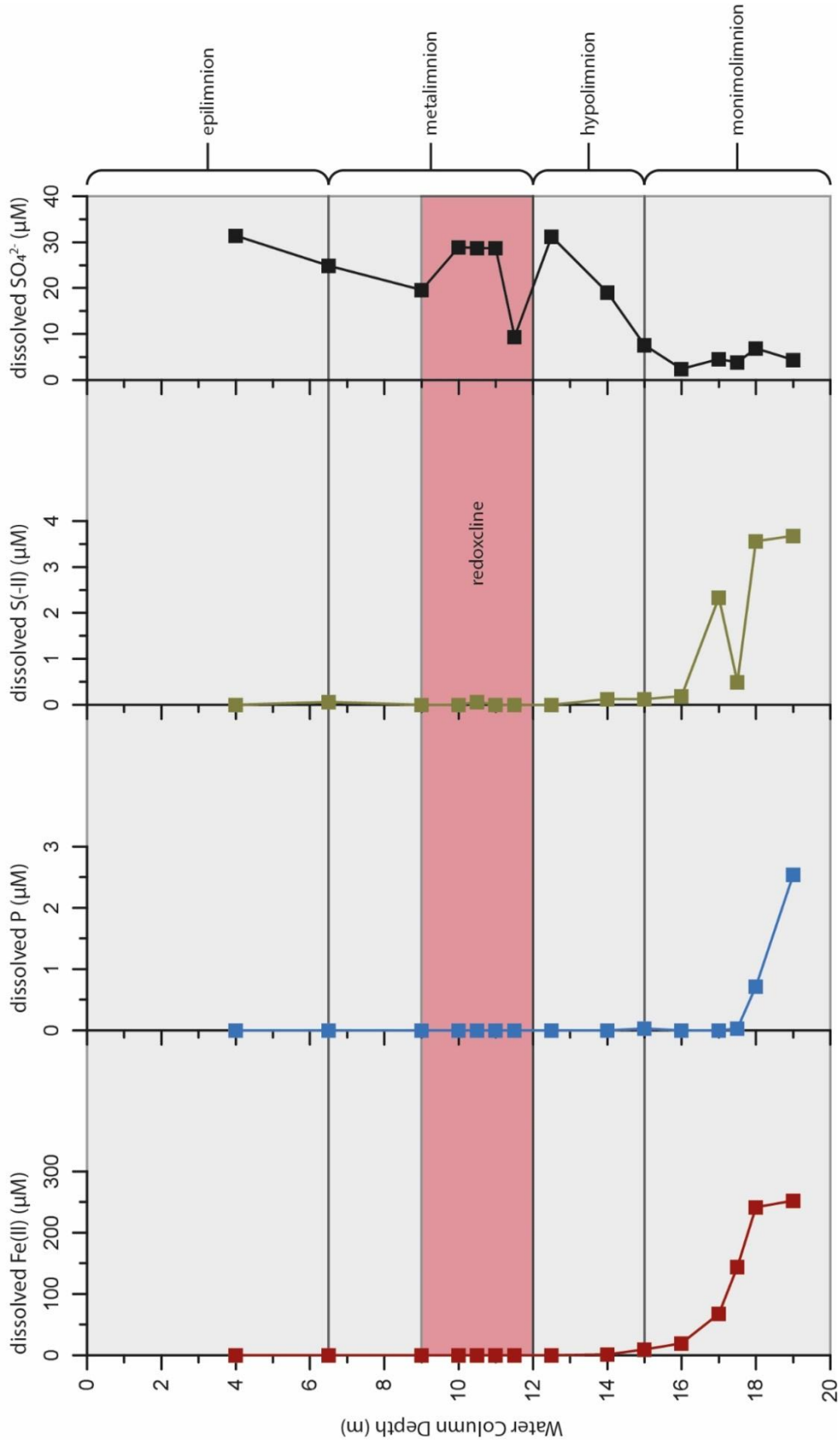

Figure 4.7 Water column dissolved species

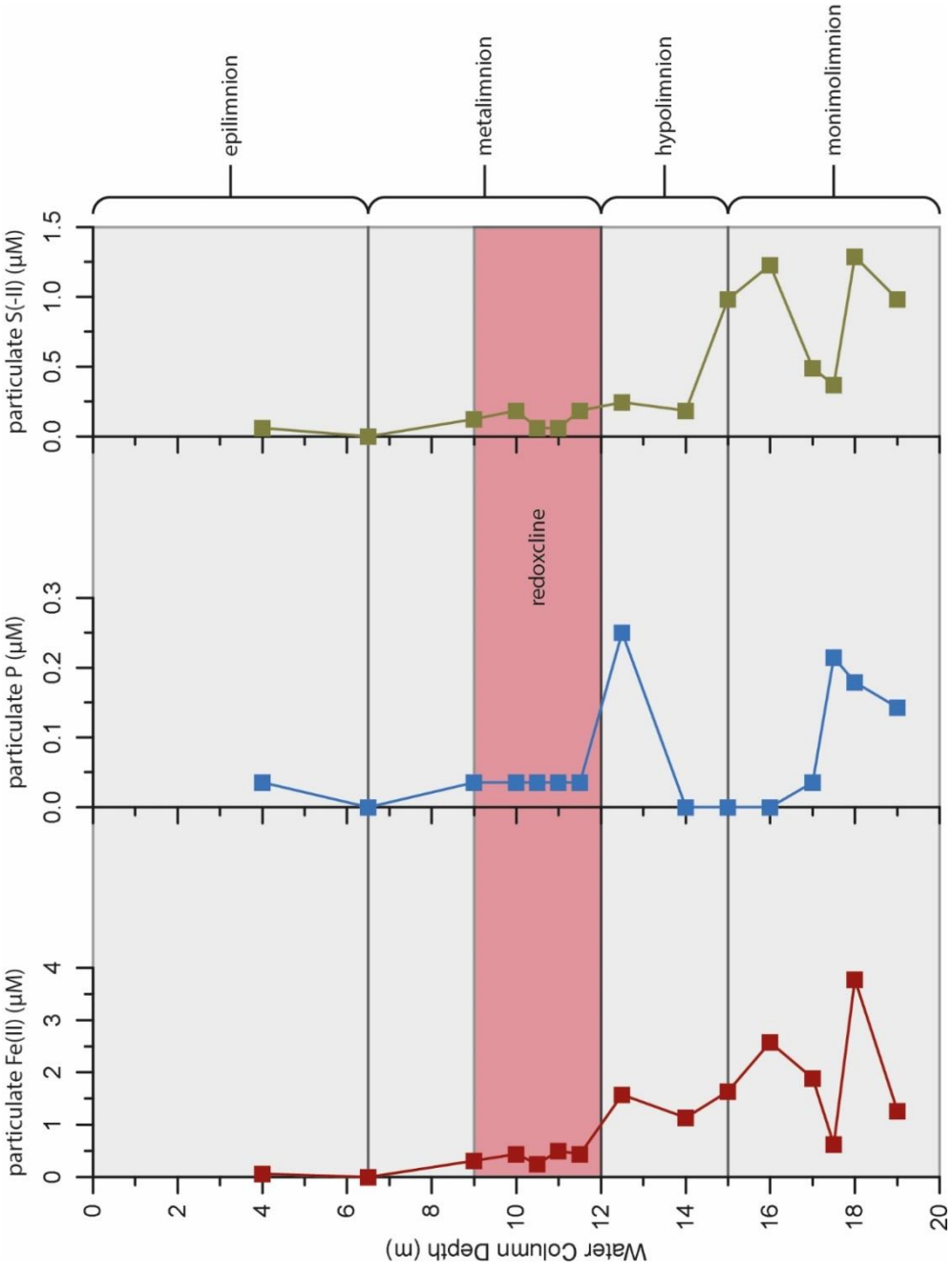

Figure 4.8 Water column particulate species

4.3.2.3 Bulk particle analysis

The bulk composition of water column particulates can be seen in Figure 4.9. Total Fe (Fe_T) exhibits a general increase with depth, from 0.7 wt% at 4 m up to 6.5 wt% at 17 m depth. The exception to this is in the top metre of the redoxcline, where Fe_T drops to 0.3 wt% between 9 and 10 m depth. There is then a strong gradient in concentrations between the base of the redoxcline, through the hypolimnion to concentrations greater than 2.7 wt% in the monimolimnion. This behaviour is mirrored by total P (P_T), with concentrations increasing from 0.2 wt% at 4 m depth to 0.7 wt% at 17 m depth. P_T also decreases in the redoxcline, dropping to 0.1 wt% at 9 and 10.5 m depth, before increasing through the hypolimnion to the maximum concentrations in the monimolimnion, although the concentration gradient is less pronounced than for Fe_T. Al, Ca and Mg all display similar trends, with relatively consistent concentrations throughout the water column apart from distinct increases in the redoxcline at 10.5 m depth.

4.3.2.4 Particulate Fe speciation

Filters from the upper 9 m of the water column did not collect enough particulate matter in order to conduct Fe speciation, and therefore results are only available from 10 m depth onwards (Figure 4.10). Fe_{AVS} and FePy were not determined for the water column particulate samples and as such, Fe(II) in this case also includes Fe_{AVS}. Fe(II) increases slightly across the redoxcline as O_2 saturation decreases to 0%, but then remains to contribute a steady 30% of the particulate Fe pool throughout out the hypolimnion. In the monimolimnion, Fe(II) drops to 19% of extracted Fe at 17 m, reflecting the pattern seen in particulate Fe(II) concentrations (Figure 4.8). Fe_{Ox1} increases as a proportion of Fe with depth from 11% to 68%, becoming the dominant pool of Fe in the monimolimnion. There is a small decrease in the deepest sample at 18 m which is taken up into the Fe(II) pool. In contrast, Fe_{Ox2} decreases with depth, going from the most dominant pool in the metalimnion, contributing on average 42% of Fe, to being 3rd in magnitude in the monimolimnion, contributing just 12%. Changes in Fe_{Ox2} in the meta- and hypolimnion are largely balanced by

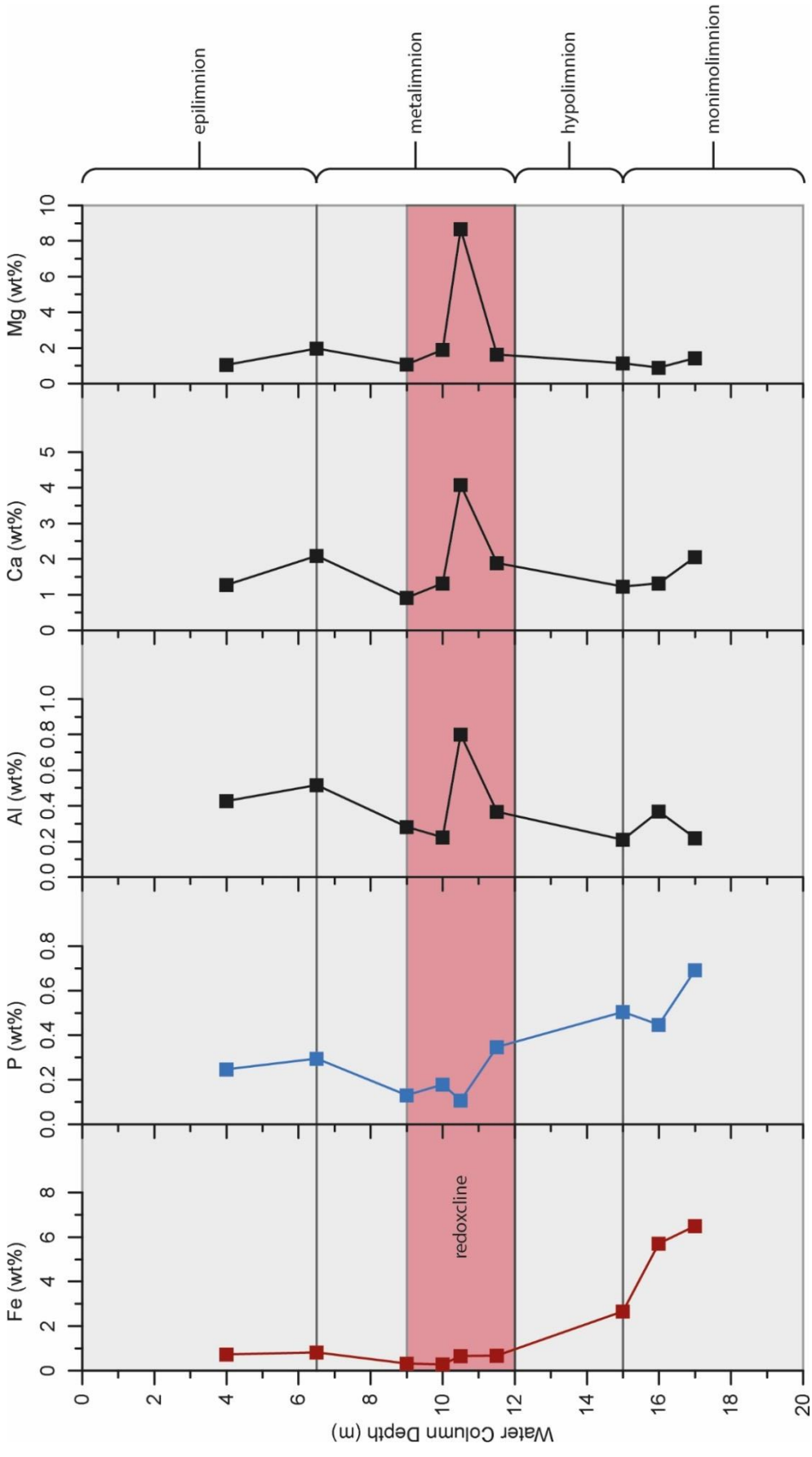

Figure 4.9 Bulk composition of water column particulate matter collected on filters

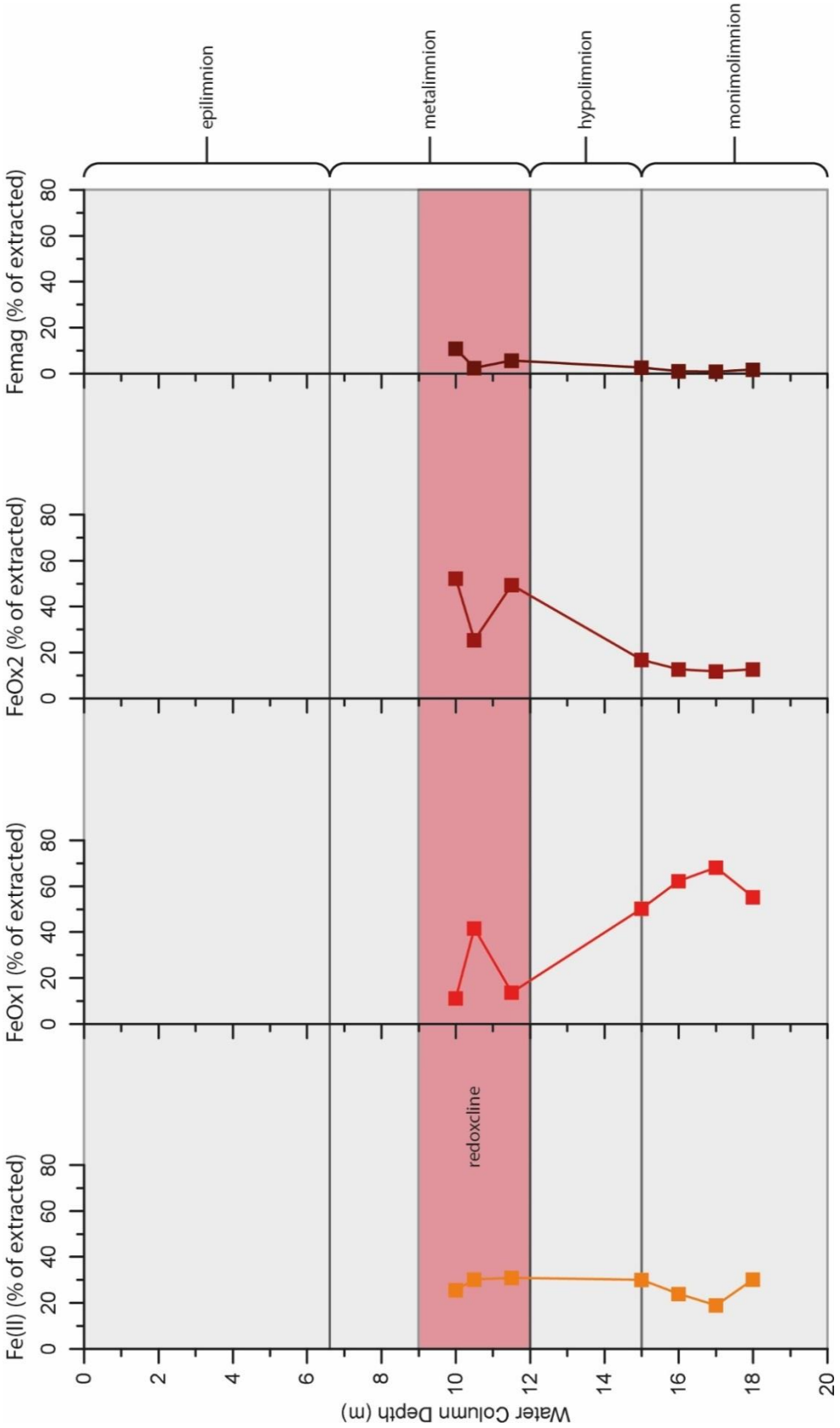

Figure 4.10 Fe speciation of the water column particulates collected on filters

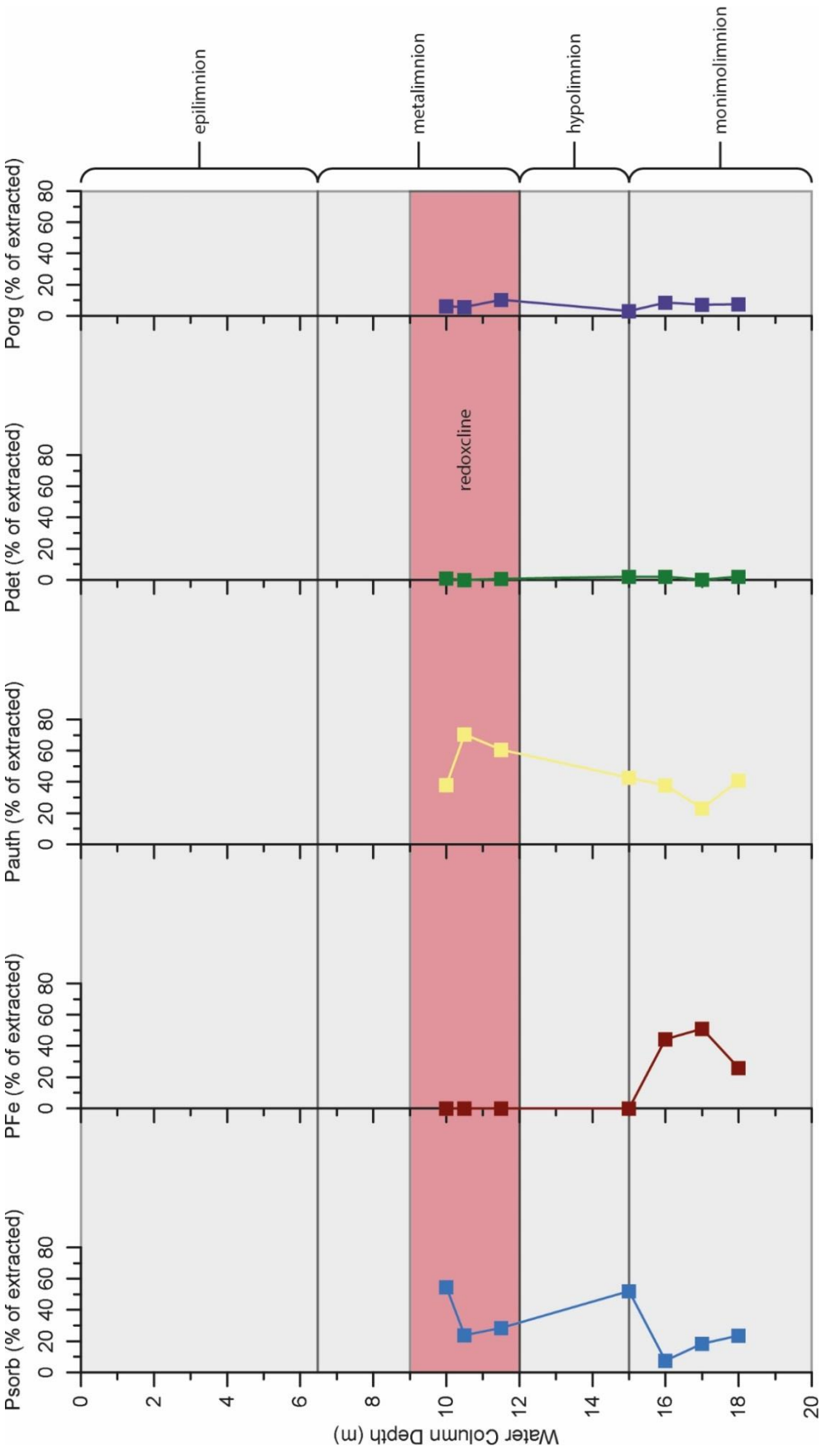

Figure 4.11 P speciation of water column particulate matter collected on filters

the Fe_{Ox1} pool, and partially the Fe(II) pool in the redoxcline. Fe_{mag} is consistently the smallest pool extracted by Fe speciation, contributing a maximum of 11% of particulate Fe in the redoxcline, steadily decreasing to a minimum of 1% at 17 m depth in the monimolimnion. It does exhibit a small increase to 2% in the deepest sample at the same time as the Fe(II) pool increases.

4.3.2.5 Particulate P speciation

As for Fe speciation, there was only sufficient particles collected to complete P speciation from 10 m onwards, and therefore no data will be presented for the surface 9 m (Figure 4.11). Initial observations see that P_{sorb} and P_{auth} are the dominant pools in the meta- and hypolimnion, and in the redoxcline they generally account for each other's variations. P_{sorb} contributes 24-55% of extracted P in the meta- and hypolimnion, but this drops to just 17% in the monimolimnion. This decrease in P_{sorb} just below the hypo-/monimolimnion boundary is balanced by the appearance of P_{Fe}, which goes from being below detection in the upper water column to forming 44% of P at 16 m. This results in the dominant pools changing to P_{Fe} and P_{auth} in the monimolimnion. P_{Fe} increases to a maximum of 51% at 17m, dominating particulate P, before dropping at 18 m to half this value. P_{auth} shows an initial increase from 38-70% of extracted P in the redoxcline before decreasing to 43% at the start of the monimolimnion, where it continues to drop before becoming the dominant pool again in the deepest sample, contributing 41%. As a proportion of P, P_{det} is consistently low with depth, contributing 0-2%. P_{org} is consistently one of the smallest pools of P, varying between 3 and 10%.

4.3.3 Sediment

4.3.3.1 Porewater dissolved species

Dissolved Fe(II) within sediment porewaters increases with depth from 197.6 µM to 509.6 µM at 26.75 cm depth (Figure 4.12). This is followed by a notable decrease between 28 and 30 cm, dropping to ~400 µM before stabilising at ~500 µM below this depth. Dissolved P follows a similar trend to Fe(II) in the surface sediments, increasing from 5.8 µM to 27.3 µM at 14.75 cm. Beyond this, concentrations stabilise around ~26 µM down to ~22 cm, where dissolved

P then generally decreases with depth to 17.2 µM at 32.75 cm. Concentrations of dissolved S(-II) remain low throughout the core, exhibiting a small decrease from 1.3 µM at the surface to 0.4 µM at 17.75 cm. Dissolved sulphide then peaks significantly at 20.75 cm, with a maximum concentration of 3.1 µM, before immediately dropping back down to 0.8 µM at 22.25 cm. Porewater S(-II) then stabilises at ~0.4 µM down to 32.75 cm depth where it exhibits a small increase to 1.1 µM at 34.5 cm before the base of the core. Dissolved sulphate concentrations exhibit a sharp decrease in the surface 6 cm of sediment, decreasing from a maximum of 8.9 µM at 0.75 cm to 1.2 µM at 5.75 cm depth. Concentrations then remain remarkably consistent with depth averaging1.4 µM. Porewater measurements of Fe(II) and P indicate a flux from the sediment into the water column of 37.3 µmol/m^2/d and 3.8 µmol/m^2/d^1 respectively.

4.3.3.2 Bulk sediment analysis

Bulk sediment concentrations of major and minor elements can be seen in Figure 4.13. Total Fe (Fe_T) decreases slightly in the surface 5 cm dropping from 0.9 wt% to 0.8 wt%. Fe_T then averages 1.1 wt% between 7.25 cm and 34.5 cm depth, with large fluctuations between 0.9 and 1.4 wt%. Al has a relatively narrow range of concentrations in the sediment, as in the water column, varying between 1.2 and 1.8 wt%, increasing with depth. Ca concentrations are considerably higher in the sediment than the water column, ranging between 16.5 and 23.2 wt%. Ca initially increases from 20.8 wt% at the top of the core to 23.2 wt% at 4.25 cm depth, where concentrations then gradually decrease to 18.7 wt% at 10.25 cm depth. From this depth down, Ca concentrations average 18.8 wt%, with the only notable feature occurring between 20.75 and 25.25 cm depth, where the concentration drops to 16.5 wt% at 22.25 cm. Sedimentary Mg concentrations are ~4 times higher than in water column particulates (discounting the discrete maximum of 8.7 wt% at 10.5 m water depth), ranging between 4.6 and 8.3 wt%. Mg increases from 6.9 to 8.3 wt% in the top 21 cm, where concentrations drop to 4.9 wt% at 23.75 cm depth. From there to the base of the core, Mg concentrations are considerably lower than the rest of the core, averaging 5.3 wt%, but remain higher than water column particulate content.

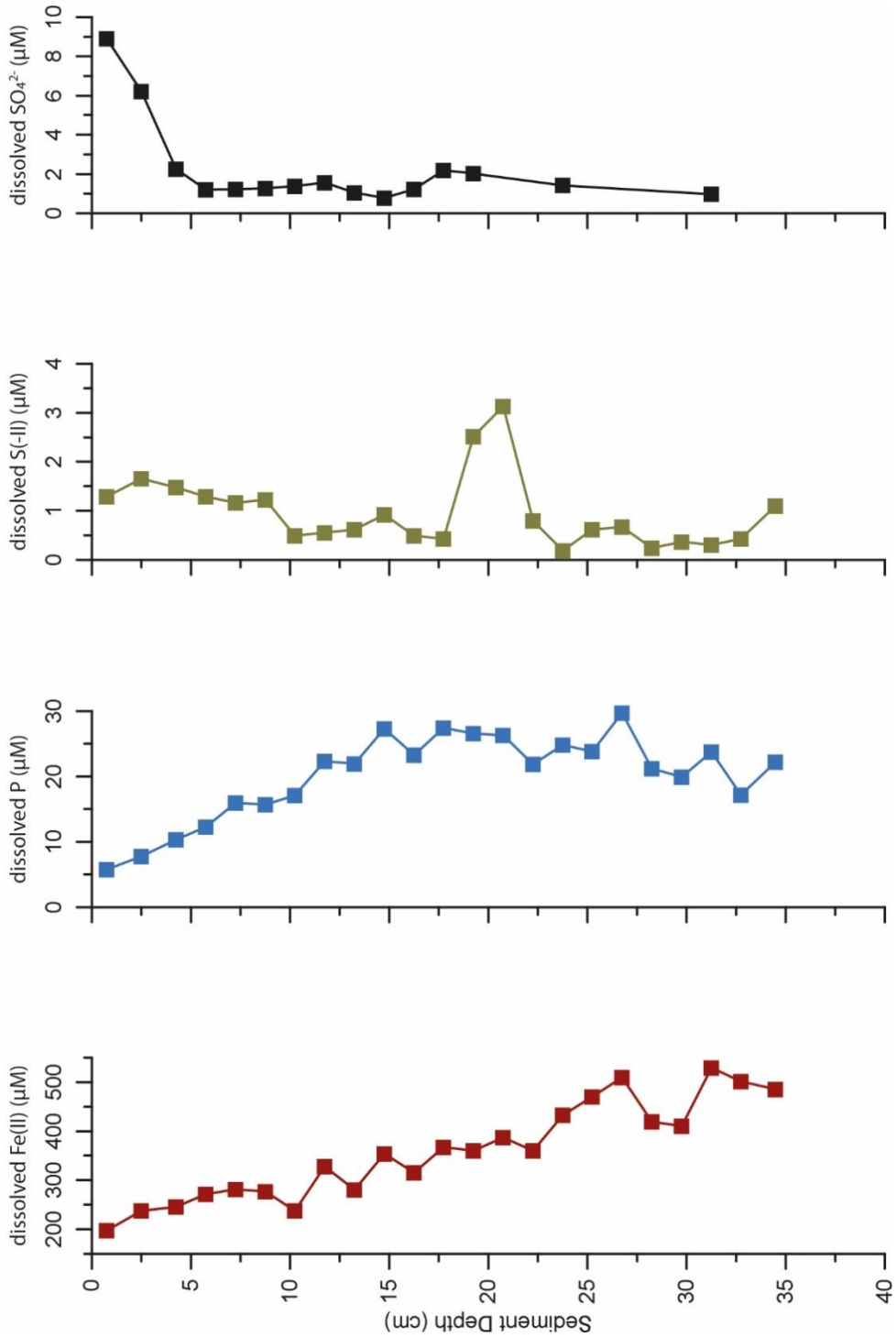

Figure 4.12 Dissolved sediment porewater species

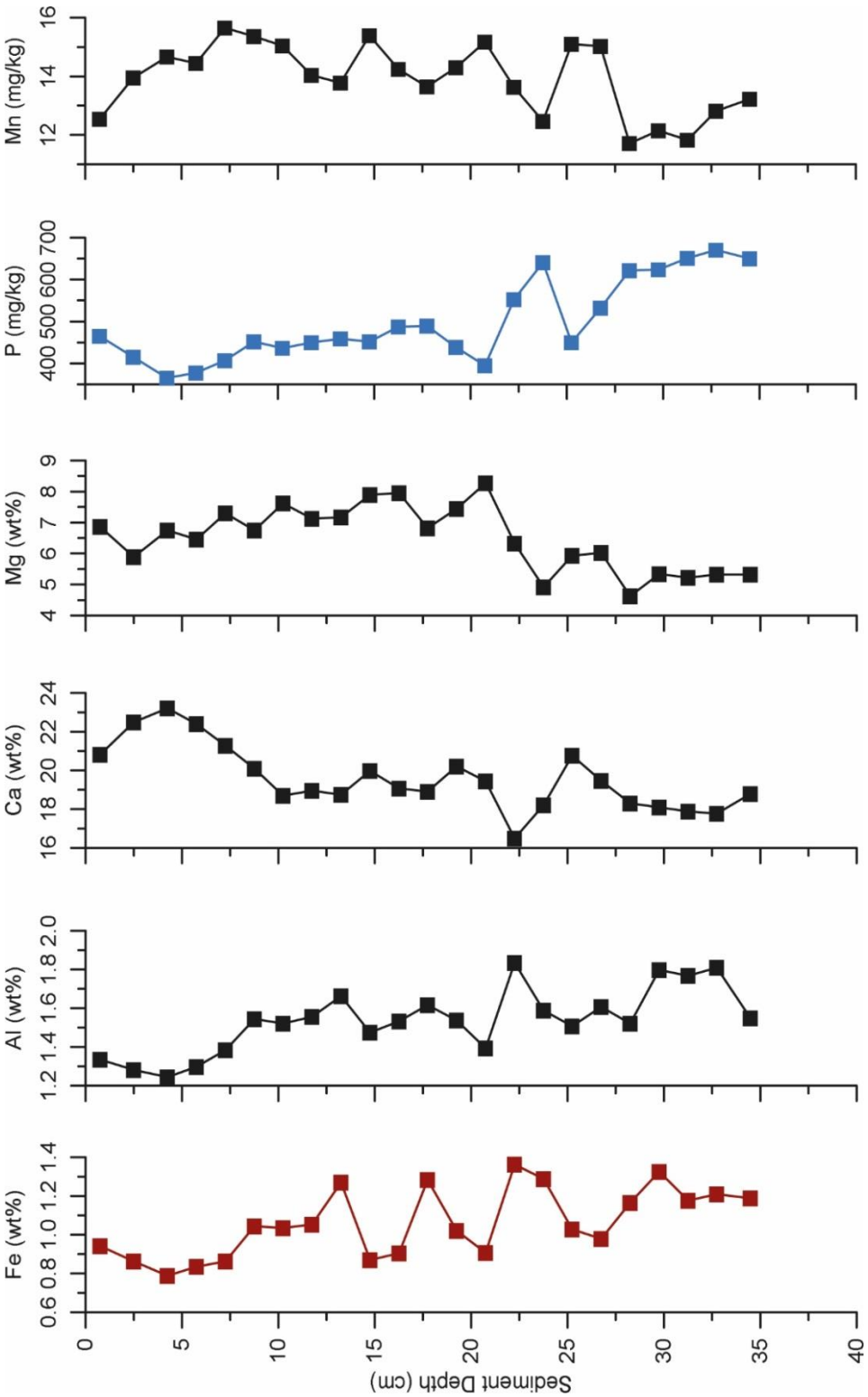

Figure 4.13 Bulk sediment chemistry

P_T concentrations are ~10 times lower in the sediment (Figure 4.13) compared to water column particulates (Figure 4.9), ranging from 365 mg/kg to 671 mg/kg. P concentrations initially decrease over the surface 5 cm of the sediment core, from 465 to 365 mg/kg. Beyond this depth P_T increases with depth to the maximum of 671 mg/kg at the base of the core, apart from between 17.75 and 28.25 cm where there is a large excursion from the trend. P_T drops to 395 mg/kg at 20.75 cm before sharply increasing to 641 mg/kg at 23.75 cm, where it then immediately drops to 450 mg/kg at 25.25 cm depth before returning to the general down core increasing trend. Mn concentrations vary over a range of 4 mg/kg, increasing over the top 8 cm of the core from 12.5 mg/kg to a maximum concentration of 15.7 mg/kg at 7.25 cm depth. Concentrations then fluctuate but show an overall trend of decreasing with depth, down to a minimum of 11.7 mg/kg at 18.25 cm. Mn then appears to increase with depth to the base of the core.

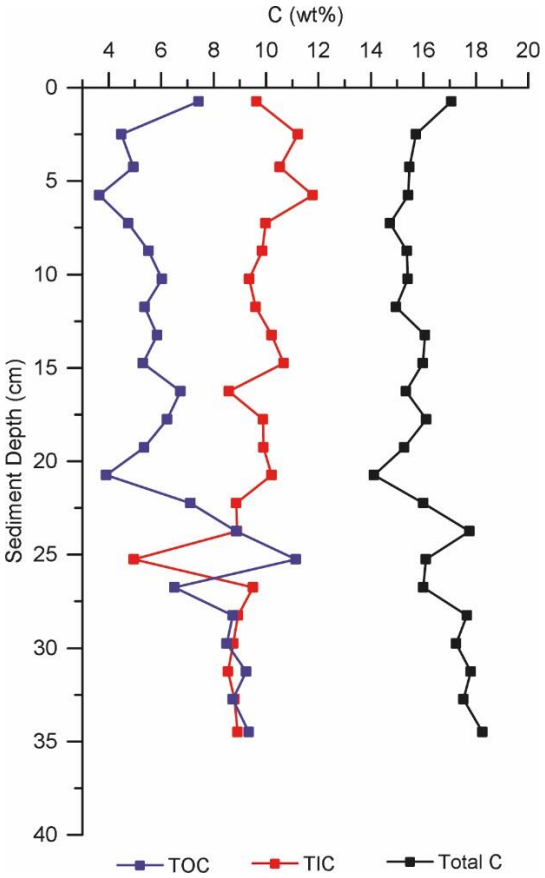

Figure 4.14 Sediment total, inorganic and organic C concentration

TC ranges between 14.1 and 18.3 wt% C (Figure 4.14). There is an initial drop from 17.1 to 15.7 in the first 3 cm, but then TC remains relatively constant with depth, averaging 15.5 wt% between 2.5 and 19.25 cm. At 20.75 cm, TC reaches its minimum of 14.1 wt.% C before a sharp increase to 17.8 wt% C at 23.75 cm. TC concentrations then follow an increasing trend up to a maximum of 18.3 wt% C at 34.5 cm depth. For the majority of the core TIC dominates, contributing ~65% of TC, averaging 9.5 wt%. However, the increase seen in TC with depth can largely be attributed to increases in TOC, especially the notable increase at 20-25 cm depth. Beyond this depth, TIC and TOC contributions are relatively equal, averaging 8.5 and 8.9 wt% respectively.

4.3.3.3 Fe speciation

Within the sediments, reduced and unsulphidised solid phase Fe(II) is the dominant pool of Fe, averaging 0.47 wt% Fe (Figure 4.15) and 63% of Fe_{HR} (not shown). There is an initial decrease from 0.48 wt% at the surface down to a minimum of 0.28 wt% at 4.25 cm depth, but Fe(II) then increases again to 0.51 wt% Fe(II) at 7.25 cm. Between 10 – 30 cm depth, Fe(II) averages 0.50 wt%, but ranges between 0.32 and 0.63 wt%, peaking and troughing regularly. Below 30 cm depth, Fe(II) concentrations are more consistent and average a little a higher, 0.54 wt%. Fe_{Ox1} is below the limit of detection for the majority of the core, with reducible ferric oxides peaking at 5.75 and 23.75 cm contributing just 0.02 wt% Fe at each depth. Whilst the sediments appear to be lacking in Fe_{Ox1} minerals such as ferrihydrite and lepidocrocite, the more crystalline ferric oxides of Fe_{Ox2} contribute on average 0.08 wt% and 10% of Fe_{HR}. Fe_{mag} contributions are low throughout the core averaging just 0.004 wt%. Both Fe_{AVS} and Fe_{Py} increase smoothly from the surface to 13.25 cm, reaching concentrations of 0.14 and 0.19 wt% respectively. Both pools of S-associated Fe go through a zone of high variability, fluctuating between minimum and maximum concentrations of the core, before establishing a more consistent range concentration below 28.25 cm depth (Fe_{AVS} averaging 0.11 wt% and Fe_{Py} averaging 0.08 wt%).

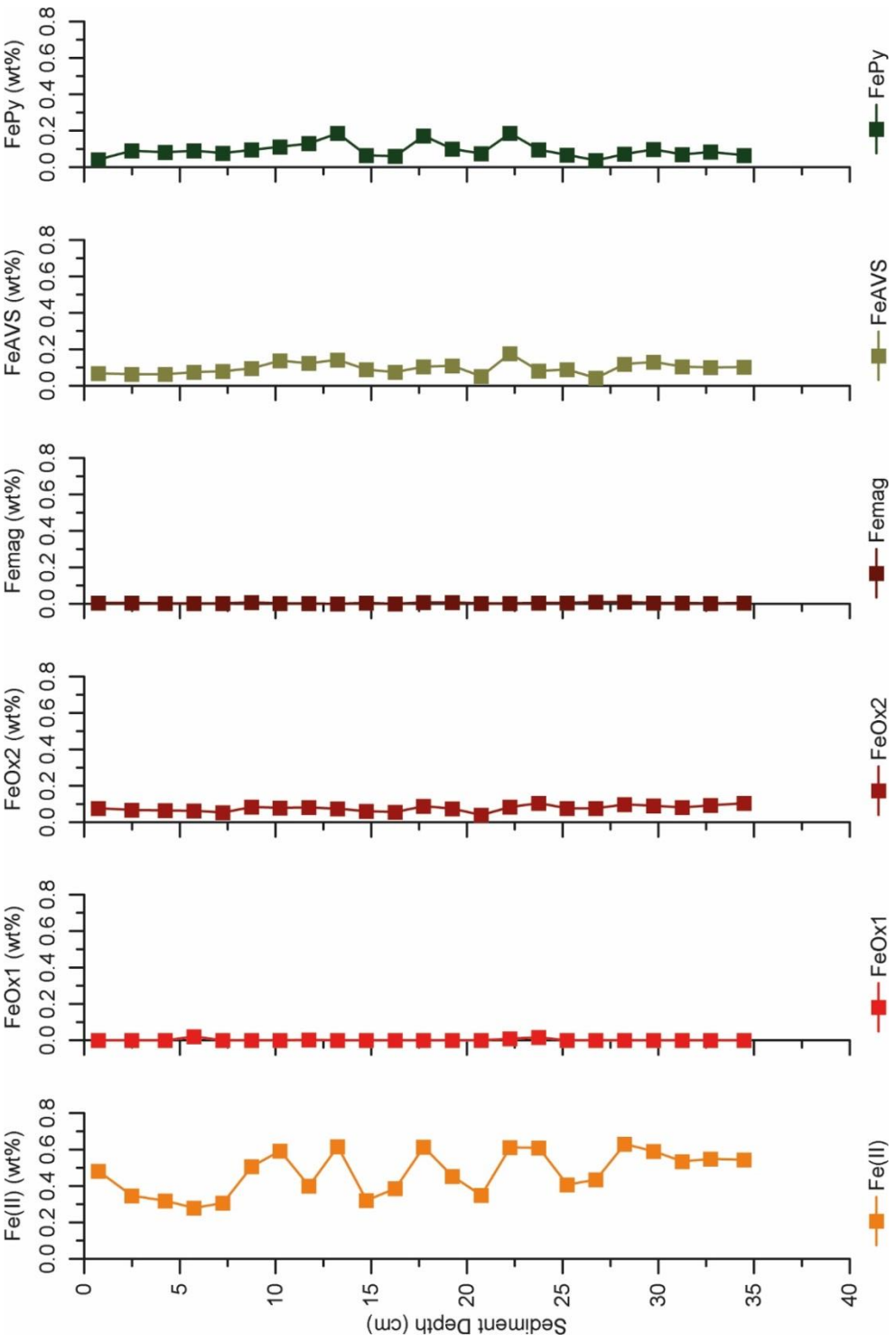

Figure 4.15 Sediment Fe speciation

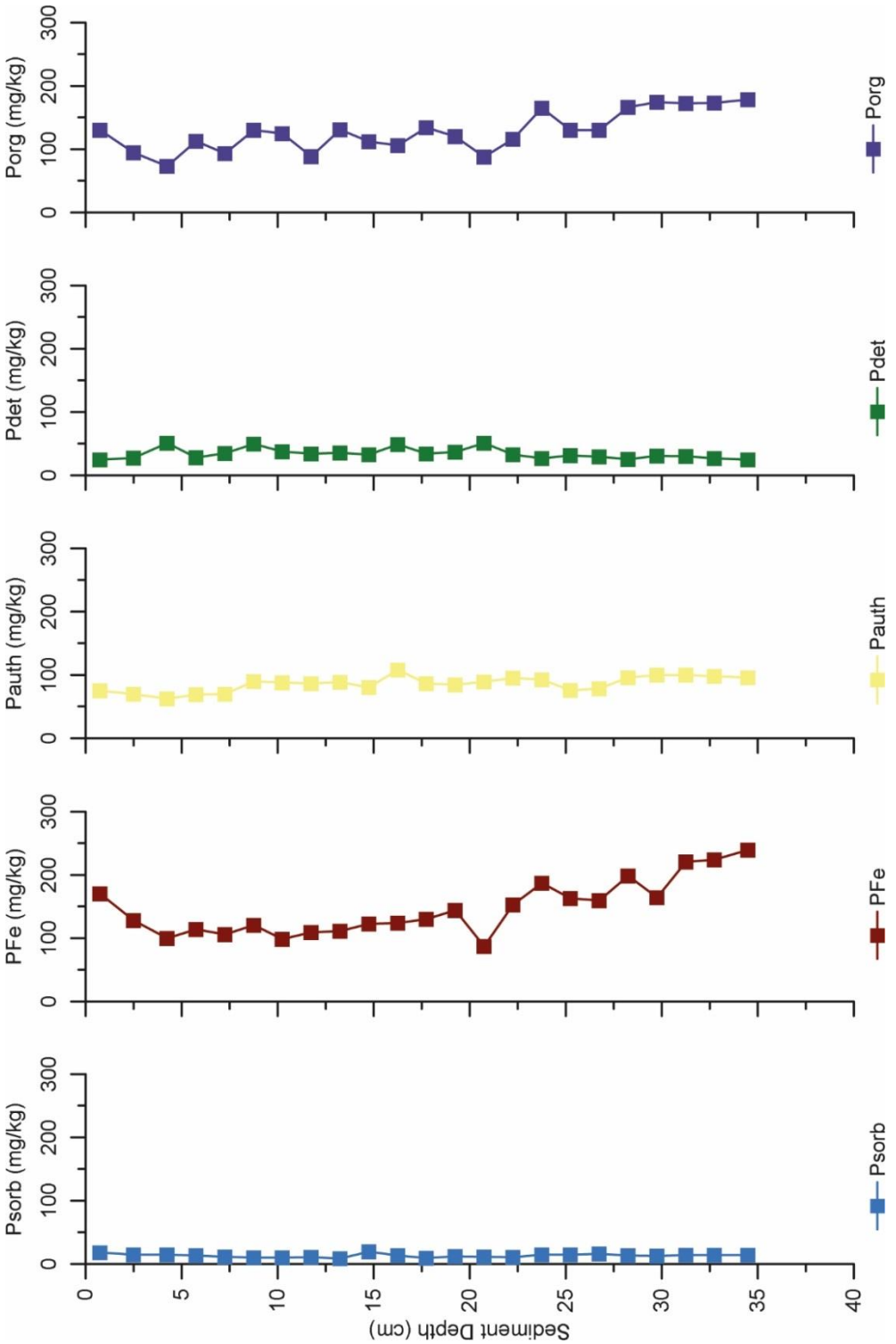

Figure 4.16 Sediment P speciation

4.3.3.4 P speciation

Within the sediments, loosely sorbed P (P_{sorb}) is the smallest pool of P averaging just 13.2 mg/kg (Figure 4.16). P_{Fe} is generally the dominant pool of P in these sediments ranging between 87.4 and 239.8 mg/kg equating to 27-35% of total extracted P. P_{Fe} concentrations initially decrease with depth in the first 5 cm, from 170.7 mg/kg to 99.9 mg/kg, where they then gradually increase up to 144.3 mg/kg at 19.25 cm depth, before exhibiting a sharp decrease to the minimum concentration of 87.4 mg/kg at 20.75 cm. From 20.75 cm, P_{Fe} returns to concentrations of 153.0 mg/kg at 22.25 cm and increases in a more fluctuating manner, to a maximum of 239.8 mg/kg at the bottom of the core. P_{auth} is relatively constant with depth, averaging 86.1 mg/kg and 21% of P. P_{det} is consistently the 2nd smallest pool of P, contributing between 5 and 17% of total extracted P. P_{det} initially exhibits an increase in concentration over the first 5 cm of the core, increasing from 25.0 to 50.9 mg/kg, but then is largely consistent, only displaying a slight decreasing trend with depth and averaging 34.2 mg/kg. Organic P is the 2nd largest pool of P in these sediments, ranging between 72.9 and 178.7 mg/kg. Like P_{Fe} and P_{auth}, P_{org} initially decreases in the first 5 cm before generally increasing with depth. Between 5 and 27 cm depth, the increase is characterised by fluctuations in concentration of up to ~80 mg/kg in magnitude, but then below this point, P_{org} stabilises in the deepest 13 cm of the core, varying by only 12.3 mg/kg in the deepest 13 cm.

4.4 Discussion

4.4.1 Sediment geochemistry

Due to the annual “whiting” event that occurs within Lake La Cruz, the sediments have a very high inorganic C content, which is assumed to mainly be $CaCO_3$. These annual mass depositions of $CaCO_3$ create varves within the sediment that can be seen on the millimetre scale, the thickness of which reveals considerable inter-annual variability in these events (Romero-Viana et al., 2008). Whilst the individual varves are unlikely to influence the results of this study due to the coarser sampling regime (1-2 cm sediment slice per sample point), the high overall concentration of $CaCO_3$ results in the considerable dilution of other elements within the sediment. Variations in this dilution within the core could mask true down core trends of other elements, The effects of $CaCO_3$ dilution can be removed by plotting data on a $CaCO_3$ free basis (assuming all TIC is present as $CaCO_3$), however in this instance, doing this had little influence on the interpretation of the trends observed and hence all original data is discussed.

The decreasing concentrations of total P and Fe with depth in the surface sediments of Lake La Cruz are most likely due to release of P during organic matter degradation and reductive dissolution of Fe (oxyhydr)oxide minerals during early diagenesis. The result of this can be seen in increasing concentrations of the relevant porewater constituents over the same depth range (Figure 4.17). The concentration gradient formed by these early diagenetic processes is indicative of a diffusive flux of dissolved P and Fe(II) to the overlying water column, which has been estimated to be 3.8 µmol/m^2/d and 37.3 µmol/m^2/d^1 respectively using Fick’s first law. Bacterial sulphate reduction has previously been documented in the water column of Lake La Cruz (see Walter et al., 2014), and sulphide produced in the sediments would result in dissolution of Fe_{Ox1} minerals (Canfield et al., 1992, Poulton et al., 2004b), ultimately producing the small but evident Fe_{Py} and Fe_{AVS} pools (Figure 4.17). However, due to the low sulphate concentrations (Figure 4.17), sulphate reduction is likely to be limited and anaerobic methanogenesis (documented by

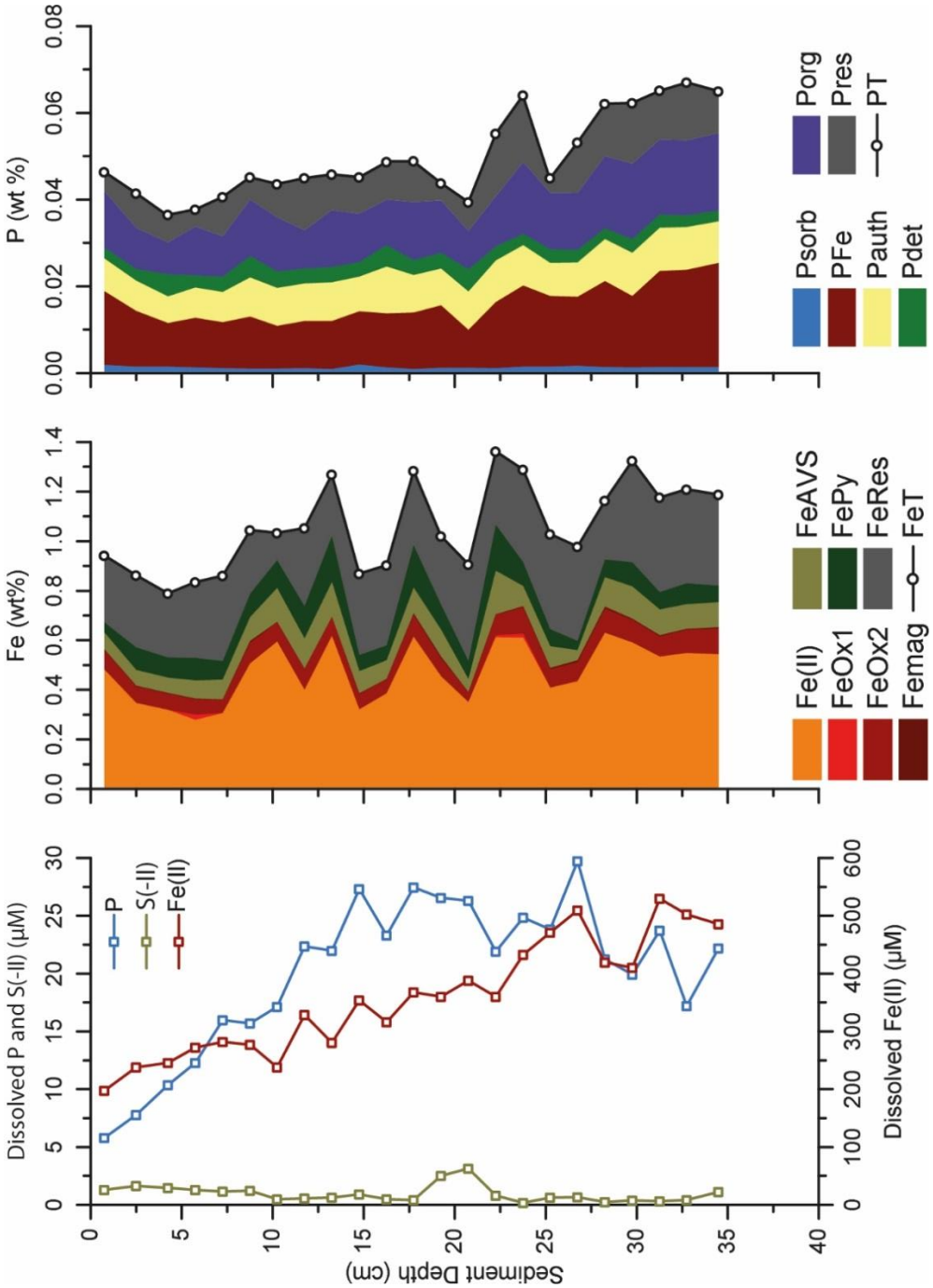

Figure 4.17 Porewater S(-II), P and Fe(II), Fe speciation and P speciation

Romero-Viana et al., 2010) coupled with dissimilatory Fe reduction is likely to play a role in producing the high concentration of unsulphidised Fe(II) minerals that contribute on average ~63% of Fe_{HR}. Whilst Fe_{Ox1} minerals are almost entirely consumed in the sediments, the more crystalline Fe_{Ox2} phases persist at low concentrations with depth.

The partitioning of sedimentary Fe is relatively constant with depth, with the only significant changes seen in solid phase Fe(II) concentrations, which are reflected in fluctuations of the total Fe content. As such, it seems the only major mineralogical Fe transformations occurring within the sediment are those affecting the partitioning of Fe(II) between the sediment and porewaters. Despite the low Fe oxide (Fe_{Ox1} and Fe_{Ox2}) of the sediments, the full Fe speciation method reveals that Fe_{HR}/FeT enrichments are high, averaging 0.70 ± 0.08, and therefore are indicative of deposition from an anoxic water column (Poulton et al., 2004a, Poulton and Raiswell, 2002, Raiswell and Canfield, 1998, Raiswell et al., 2001). Furthermore, the degree of sulphidisation is very low with $(Fe_{Py}+Fe_{AVS})/Fe_{HR}$ averaging 0.25 ± 0.05, correctly recording deposition from a ferruginous water column (Anderson and Raiswell, 2004, Poulton et al., 2004a). As such, whilst it is fair to say these sediments contain Fe sulphides, to say they do not record the ferruginous water column above due to a lack of Fe(III) (oxyhydr)oxide accumulation as suggested by Walter et al. (2014), is incorrect. Full evaluation of the partitioning of Fe in these sediments does record deposition in a ferruginous water column.

Under anoxic conditions, porewater P resulting from the break-down of organic matter and dissolution of Fe minerals can be released to the overlying water column (Ingall and Jahnke, 1994, 1997, Van Cappellen and Ingall, 1994) and/or sequestered in the sediments via the formation of authigenic mineral phases (Ruttenberg and Berner, 1993, Slomp et al., 1996a). Assessing the ratio of organic C to P in sediments can indicate whether P has been retained or lost from the sediment, as preferential release of P from organic matter remineralisation can result in the molar TOC:P_{org} of the remaining sediment to be high relative to that of 106:1 established for marine phytoplankton by

Redfield (1958), evidence of which has been summarised by Anderson et al. (2001).

Throughout the sediments of Lake La Cruz, TOC:P_{org} is highly elevated, averaging 1307 (Figure 4.18), with large fluctuations in the top half of the core, ranging from 833 to 1748 over the upper 6 cm. Ingall and Van Cappellen (1990), compiled TOC:P_{org} data from a range of sedimentary environments and found sediments deposited at an intermediate rate (between 0.002 and 1 cm/yr) had elevated ratios, up to 600. With a sedimentation rate of 0.1-0.5 cm/yr (Romero-Viana et al., 2010), Lake La Cruz sediments fall within this intermediate rate range but exhibit TOC:P_{org} ratios well in excess of 600, indicating increased preservation of C over P, compared to the majority of modern settings included in that study. This could be explained by the intermediate nature of ferruginous conditions compared to the extreme redox endmembers of oxic or sulphidic sediments. Oxidation of organic matter by oxygen or sulphate is far more efficient than by Fe oxyhydroxides, which requires 4 moles of FeOOH to oxidise 1 mole of CH_2O. Indeed, anoxic and low sulphate conditions have been connected with the exceptional preservation of fossil biota in the Burgess Shale, due the limited availability of oxidants for organic matter remineralisation (Gaines et al., 2012). Whilst TOC:P_{org} ratios are high in La Cruz sediments, they are lower than those observed in shales deposited from a euxinic water column (>3000; Ingall et al., 1993, Slomp et al., 2004), where the flux of organic matter to the sediment is high due to increased productivity, but elevated levels of bacterial sulphate reduction cause the preferential release of P.

Lake La Cruz TOC:P_{reac} ratios are still raised, compared to the Redfield ratio, but are much lower, averaging 445. These values remain above the Redfield ratio despite the fact that P_{reac} is also likely sourced via water column draw down of P_{sorb}, P_{Fe} and P_{auth} (Figure 4.11). Together, these observations suggest that whilst a large amount of P may be lost from the sediment, some of the P released to solution during early diagenesis is also retained by other secondary phases. CFA formation is a primary mechanism for draw down of porewater P and has been shown to account for 30-40% of total P in oxic

continental margins, appearing to form at the expense of P_{org} (Ruttenberg and Berner, 1993). However, such a clear relationship between P_{org} and P_{auth} is not evident in the sediments of Lake La Cruz, with P_{auth} constituting just ~20% of total P. Fe bound P, however, accounts for 27-43% of total P, and increases with depth, potentially providing a sink for some previously released P. This range is higher than that previously found for oxic continental margins, with P_{Fe} ranging from below the limit of detection (Ruttenberg and Berner, 1993) to <30% of total P (Slomp et al., 1996a).

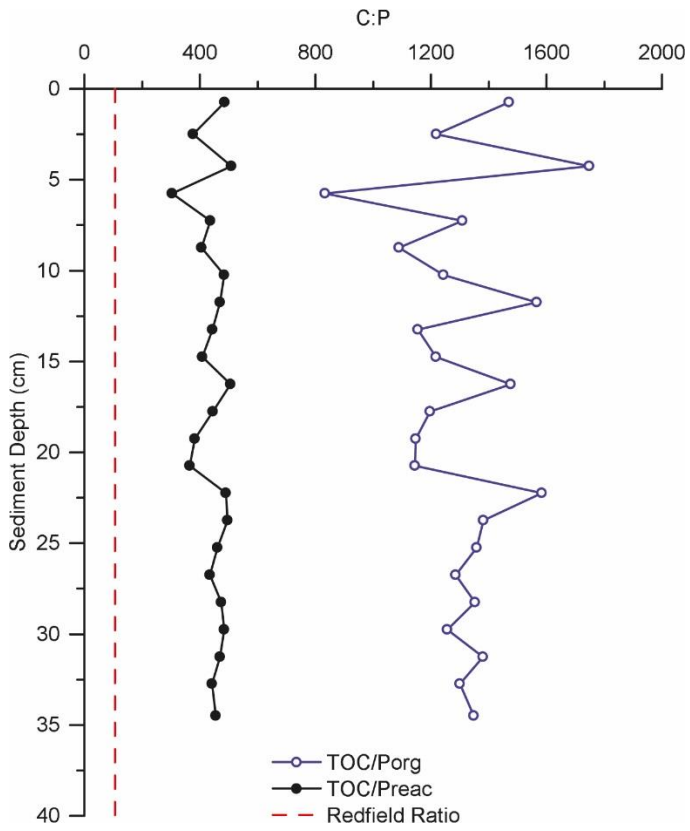

Figure 4.18 Sediment TOC/P ratios for organic P and reactive P, compared to the Redfield ratio of 106C:1P

Porewater P decreases with depth from ~15 cm onwards (Figure 4.17), suggesting removal of P from the dissolved phase, through either adsorption processes or authigenic mineral formation. The lack of an increase in P_{sorb} suggests surface re-adsorption is unlikely, although previously, P extracted by the CDB (P_{Fe}) step has been shown to include P adsorbed to $CaCO_3$ surfaces

in environments with high $CaCO_3$ content (Kraal et al., 2017). This was partly inferred from similarities in the P_{Fe} and $CaCO_3$ profiles, and Fe:P ratios in the CDB extract being lower than those expected for Fe(III)- or Fe(II)- bound P minerals. Whilst the $CaCO_3$ content of the sediments at Lake La Cruz is high, there are no such similarities between P_{Fe} and $CaCO_3$, and there is an excess of Fe (average Fe:P of P_{Fe} = 18) relative to the required Fe:P ratios for Fe-phosphate minerals (Jensen and Thamdrup, 1993, Slomp et al., 1996b). The increase in P_{Fe} with depth (Figure 4.17) supports the formation of an Fe-phosphate mineral, and due to the lack of increase seen in the Fe_{Ox1} or Fe_{Ox2} pools, and the increasing dominance of Fe(II), it is likely that the increase in P_{Fe} is due to the formation of a reduced Fe-phosphate such as vivianite.

Fe phosphates are most likely forming below 5 cm depth, where porewater sulphate decreases to very low levels, minimising sulphide production. An increase in dissolved P is not seen initially (between 5 and 15 cm) as it is being produced at a faster rate than it is being precipitated. As the release P from organic matter and Fe oxides decreases with depth, the rate of P precipitation exceeds that of dissolved P production, resulting in a decrease in porewater P at greater depths. Attempts to locate and identify the mineral by both X-ray diffraction and scanning electron microscopy with energy-dispersive X-ray spectroscopy as previous studies have done (see Rothe et al., 2016) were thwarted by the dominance of quartz, calcite, aragonite, dolomite, kaolinite and muscovite.

The porewater and solid phase geochemistry of the ferruginous sediments of Lake La Cruz suggests some retention of P in Fe-bound phases, most likely Fe(II)-phosphates, but despite this there is extensive mobilisation of both P and Fe to the overlying water column. In terms of understanding the potential influence this release of Fe and P might have on primary productivity the fate of these dissolved elements once in the overlying water column must be determined.

4.4.2 Water column P and Fe cycling

Dissolved Fe(II) concentrations (Figure 4.19-A) are in good agreement with Walter et al. (2014), but lower than those found in the monimolimnion by

Rodrigo et al. (2001). Whilst SO_4 concentrations (Figure 4.7) are within a similar range to those recorded by both Rodrigo et al. (2001) and Walter et al. (2014), ranging between ~5-35 µM, water column sulphide concentrations detected during this study (Figure 4.19-A) are far lower than those recorded by Walter et al. (2014), and are much more in line with those stated by Rodrigo et al. (2001). Previously published measurements of P are scarce, but the maximum concentration of 2.5 µM dissolved P at 19 m depth (Figure 4.19-A) is much lower than the average of 53 µM found by Rodrigo et al. (2001).

Dissolved Fe(II) and P both continue to decrease across the sediment-water interface, but reach barely detectable levels by the hypolimnion. The flux of P appears to be exhausted prior to Fe(II), dipping below the limit of detection at 17.5 m depth, whereas dissolved Fe(II) is low but detectable up to the hypolimnion boundary at 15 m depth (Figure 4.19-A). The particulate concentrations of both Fe(II) and P are highest in the monimolimnion (Figure 4.19-B) coinciding with the flux of the dissolved constituents from the sediment, presumably due to precipitation. This is reflected in the high concentrations of Fe and P in wt% of the particulate matter collected on filters from the monimolimnion (Figure 4.19- C and D).

Looking at the P speciation of the particulate matter collected, initial precipitation of P in the monimolimnion is mostly in association with Fe, but both P_{sorb} and P_{auth} phases also contribute a substantial proportion of P (Figure 4.19-D). The depth range within the monimolimnion that particulate P speciation is presented (15 – 18 m depth), is undersaturated with respect to the reduced Fe phosphate vivianite (Figure 4.19-E), suggesting the Fe-bound P present at this depth may P associated with Fe (oxyhydr)oxides. Below 18 m the geochemical data suggest that the water column is saturated with respect to vivianite, suggesting that this mineral may form above the sediment-water interface.

Above 15 m depth, dissolved Fe(II) very low, and as such precipitation of Fe-bound P ceases and P_{Fe} falls below the limit of detection, instead particulate P is dominated by the P_{sorb} and P_{auth}. This shift of P from P_{Fe} to P_{sorb} above the monimolimnion may not mean P is no longer associated with Fe, P_{sorb} includes

P loosely sorbed to the surface of Fe minerals; it does, however, suggest a change in the mechanism of P association with Fe. Minerals targeted by the P_{Fe} extraction could be formed by coprecipitation, whereas P extracted during the P_{sorb} step may be loosely sorbed to the surface of previously precipitated Fe minerals or other phases. It is generally thought that P_{auth} is formed within the sediments or at the sediment-water interface, where P released from organic matter and/or Fe (oxyhyr)oxides, causes significant enrichment of P and Ca leading to CFA precipitation. In Lake La Cruz we see significant contributions from the P_{auth} pool within the water column, which according to the SEDEX protocol, could include authigenic and biogenic apatite, and $CaCO_3$ -bound P (Ruttenberg, 1992). Due to the surrounding dolomitic substrate and the occurrence of seasonal “whiting” events, the concentration of Ca in the water column is high, reaching 4 mM in the monimolimnion (Rodrigo et al., 2001), this combined with the increase of dissolved P towards the sediment may provide the right conditions for precipitation of CFA in the water column, but it is most likely that the P_{auth} contribution to water column particulate matter is $CaCO_3$-bound P or biogenic apatite.

The vertical extent of dissolved P, Fe(II) and particulate P_{Fe} appears to coincide with the approximate location of the subterranean water inflow (4-6 m above the lake bottom). Whilst this could indicate that the input of groundwater at this level is critical in the precipitation of P_{Fe} in the monimolimnion, it is unlikely to be the source of the mineral constituents required, as the flux of dissolved P and Fe(II) is clearly supplied from the sediment. The subterranean water is thought to contribute to the chemically-induced stability of the monimolimnion (Rodrigo et al., 2001), and it could be that it influences the background chemistry of the monimolimnion, such that the conditions are poised for Fe-phosphate precipitation. The chemistry of the subterranean water is yet to be described, and investigation of this along with the calculation of saturation indexes for more key mineral phases throughout the water column, should clarify the impact this influx has on mineralogical process occurring in the monimolimnion of Lake La Cruz.

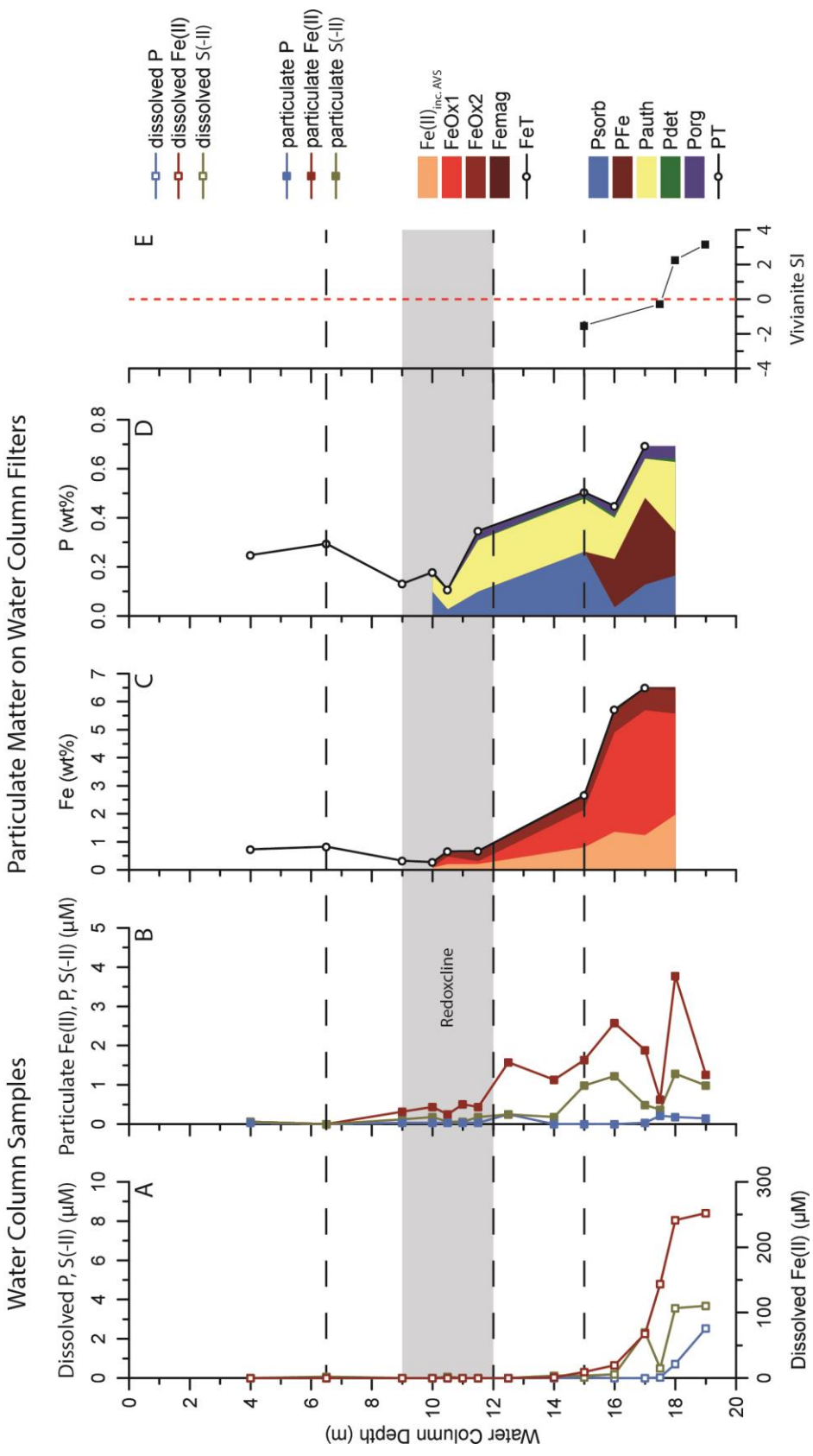

Figure 4.19 (A) Dissolved and (B) particulate Fe(II), P and S(-II) concentrations in the water column. (C) Fe and (D) P speciation of particulate matter collected on water column filters. (E) Saturation index for vivianite in the monimolimnion. Dashed lines indicate the boundaries of the stratification layers.

Fe precipitation in the monimolimnion is dominated by the Fe_{Ox1} pool (Figure 4.19-C) which is distinctly different from the speciation in the underlying sediment (Figure 4.17) where this pool is negligible. Fe(II) phases (potentially including AVS for the water column particulate speciation) also account for a large proportion of particulate Fe in the monimolimnion especially closest to the sediment-water interface. This suggests the initial formation of ferrihydrite and goethite, along with some Fe(II) phases, with the more crystalline phases attributed to Fe_{Ox2} becoming of greater importance in the metalimnion with increased distance from the source of dissolved Fe(II) and the increasing concentration of O_2 across the redoxcline. Particulate sulphide and Fe(II) concentrations (Figure 4.19, B and C respectively) follow similar trends in the monimolimnion, indicating that Fe sulphide phases could contribute a large proportion of the Fe(II) pool in these samples. Bura-Nakic et al. (2009) found that in the hypolimnion of the ferruginous Lake Pavin, 80% of the methylene blue reactive sulphides were amorphous FeS, produced by the reaction of Fe(II) with sulphide.

The occurrence of Fe oxides below the redoxcline, is likely due to the oxidation of Fe(II) by anoxygenic phototrophs, such as *Chlorobium clathratiforme* and *Lamprocystis purpurea*, which have previously been identified by (Walter et al., 2014). During water column sampling, water collected from just below the redoxcline at 12.5 m depth had a distinct purplish hue, which is characteristic of purple sulphur bacteria, and is within the depth range of the biomass maxima for *Lamprocystis purpurea* previously documented (Rodrigo et al., 2000, Walter et al., 2014). Biologically mediated Fe-oxidation was also proposed for the anoxic and ferruginous water column of Lake Pavin (Cosmidis et al., 2014), and more specifically was linked to the formation of Fe-phosphates, due to the frequent observation of Fe-phosphates that had morphologies reminiscent of encrusted microbial shapes.

4.5 Summary and future work

This study is the first to assess Fe and P partitioning for both the water column and sediments of a ferruginous system. Furthermore, the observations and conclusions drawn from this work could reasonably be applied to ancient, ferruginous oceanic settings, due to its similar water column chemistry (Walter et al., 2014). Figure 4.20 depicts the key aspects of water column and sediment Fe and P cycling in Lake La Cruz, as suggested by this study. As previously predicted and demonstrated for ferruginous settings, sedimentary phosphorus in Lake La Cruz is mainly bound with Fe minerals, and based on the Fe content of the sediments these are likely to mainly be reduced Fe phosphates such as vivianite (Busigny et al., 2016, Cosmidis et al., 2014, Derry, 2015). Despite the formation of these Fe phosphate phases, TOC:P_{reac} ratios are highly elevated in comparison to the Redfield ratio, suggesting release of P from the sediment and this is supported by a net flux of both porewater Fe(II) and P from the sediment into the water column.

This flux of dissolved Fe(II) and P is rapidly titrated in the monimo- and hypolimnion, precipitating mainly as reduced solid phase Fe, highly reducible Fe (oxyhydr)oxides, and Fe-bound P. The association of P with Fe minerals has previously been observed in the ferruginous Lake Pavin by XRD, SEM, TEM and STXM techniques (Cosmidis et al., 2014), where the precipitation of Fe-phosphates below the chemocline is thought to play a role in limiting P concentrations in the oxic photic zone. Whilst the exact nature of the Fe phosphate minerals found in Lake La Cruz has not been determined here, it is clear that whilst substantial amounts of P are released from the sediment, this flux is highly modulated by precipitation in association with the “Fe-wheel” that exists below the redoxcline, most likely in processes mediated by bacteria. Whilst dissolved P concentrations are extremely low in the photic zone of Lake La Cruz, this Mesotrophic lake, with an inorganic C assimilation of ~180 g $C/m^2/y$ (Camacho et al., 2017, Rodrigo et al., 2001) clearly is not nutrient limited. P_{sorb} and P_{auth} are present in water column particulates above the point where P_{Fe} desists, and may represent a source of P for photosynthesis when recycled within the water column, but the

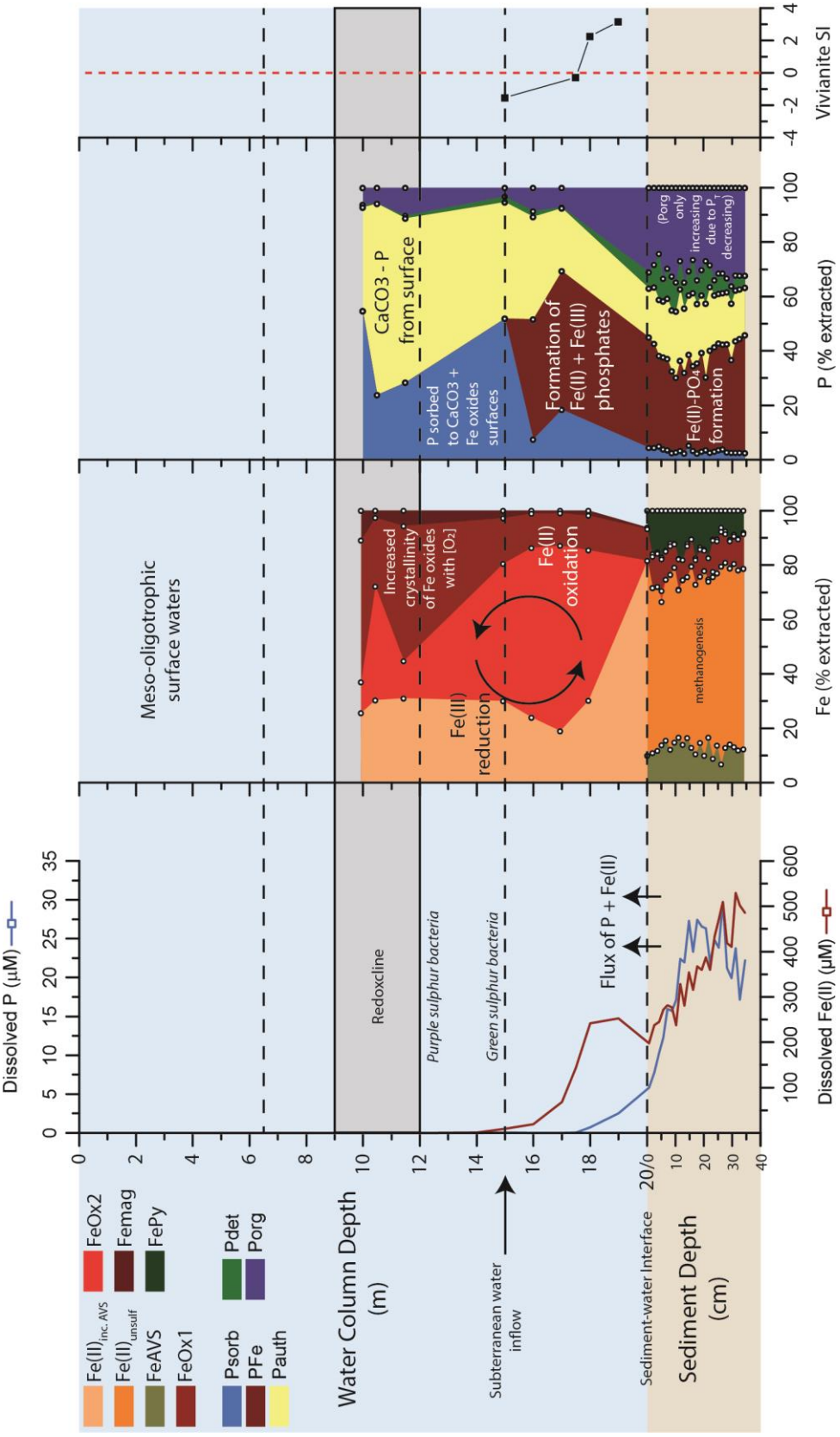

Figure 4.20 Key aspects of water column and sediment Fe and P cycling in Lake La Cruz overlaying dissolved concentrations and Fe an P speciation of solid matter. SI stands for saturation index.

released dissolved P is utilised rapidly and hence dissolved P does not accumulate in surface waters.

When considering whether ferruginous conditions such as those in Lake La Cruz could limit or stimulate primary productivity in other environments, the key factor is whether the flux of dissolved P from the sediment can reach the photic zone. For this to occur, dissolved P would need to be transported beyond the “iron wheel” precipitation mechanism, which could be achieved by the vertical diffusive flux being assisted by physical transport. Regions of upwelling, particularly upwelling continental margins, where the sediment-water interface is shallower and closer to the photic zone compared to the open ocean (Figure 4.21-A) may be a prime location for benthic P to reach the photic zone and stimulate low level productivity in ferruginous ancient oceans. In deeper water depths, the effects of the “Fe wheel” in removing P from solution and limiting productivity would be far greater.

The supply of SO_4 from continental weathering is greatest at the continental margin, so as this flux increased with increased atmospheric oxygenation (Kendall et al., 2010, Reinhard et al., 2009, Scott et al., 2011) it would fuel the mineralisation of organic matter produced due to benthic P stimulation of primary production (Figure 4.21-B). Enhanced levels of bacterial sulphate would yield free sulphide which would rapidly titrate Fe(II) from the dissolved system, lowering the Fe:P ratio and supressing the formation of Fe (oxyhydr)oxides and Fe phosphates. This could result in an increased flux of P to the photic zone further stimulating primary productivity, forming a positive feedback and the development of euxinic water column conditions along continental margins (Figure 4.21-C), as previously envisaged for large periods of the Proterozoic (Poulton and Canfield, 2011, Poulton et al., 2010).

Lake La Cruz is a Mesotrophic ferruginous lake which exhibits significant fluxes of P from the sediment to the water column, which have the potential to stimulate primary productivity in the photic zone. However, the benthic flux of P is highly modulated by Fe phosphate formation and the association of P with Fe (oxyhydr)oxide phases in the water column the extent of which will vary in different localities according to the precise fluxes of P and Fe. Lake La Cruz is

situated between the end members of eutrophic euxinic conditions promoting high levels of P recycling, and oligotrophic global ferruginous oceans where P is extensively draw down in association with Fe minerals, and as such provides a natural laboratory for an intermediate system that may help to elucidate Fe and P cycling in a large range of scenarios.

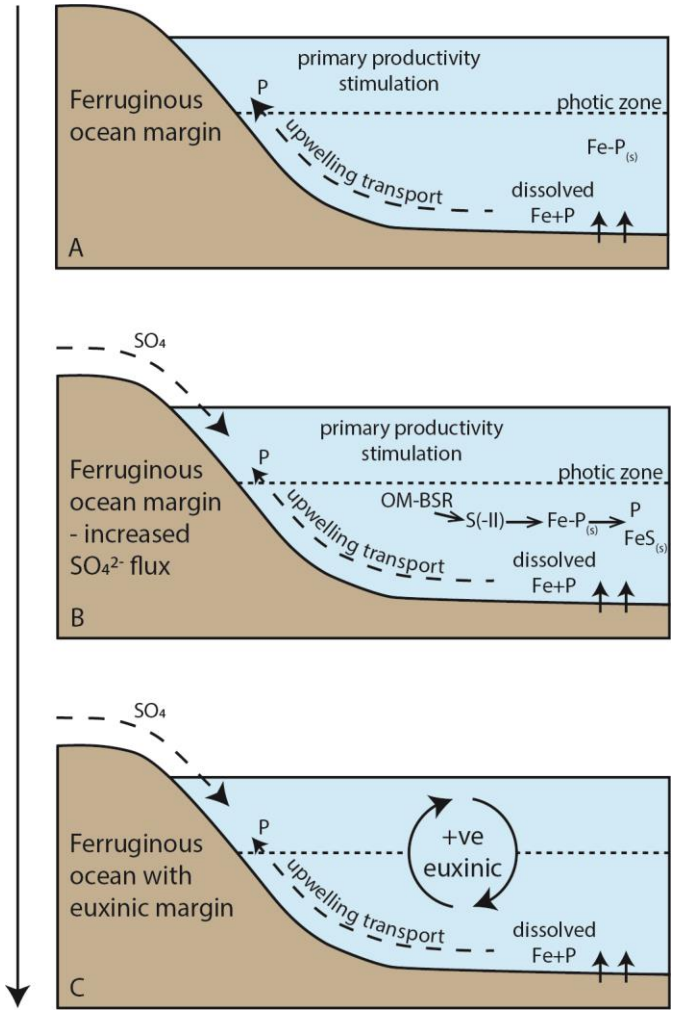

Figure 4.21 Potential mechanism of primary productivity stimulation on a ferruginous ocean margin.

A) Transport of benthic P to the photic zone by upwelling, stimulating primary productivity. B) Increased continental SO_4 input increases oxidation of organic matter by bacterial sulphate reduction (OM-BSR), producing S(-II) promoting the formation of $FeS_{(s)}$ rather than Fe-$P_{(s)}$. C) Inhibited Fe-P(s) formation increases the dissolved flux of P to the photic zone, further stimulating primary production and OM-BSR, creating a positive feedback for euxinic water column conditions along the upwelling margin.

Chapter 5 Phosphorus cycling in the Animikie Basin

5.1 Introduction

Our understanding of the redox evolution of the Precambrian ocean has altered dramatically over the last decade, with increased datasets using improved chemical and isotopic proxy techniques. Whilst the precise timing of the emergence of oxygenic photosynthesis is still vigorously debated (see Lyons et al., 2014), with evidence ranging from ~3.7 (Rosing and Frei, 2004) to 2.35 (Kirschvink and Kopp, 2008) billion years ago, it has become clear that the production of oxygen resulted in an increase in oxidative weathering of continental sulphide minerals, and hence an increased supply of sulphate to the ocean (Kendall et al., 2010, Reinhard et al., 2009, Scott et al., 2011). This enhanced sulphate influx promoted the development of expansive euxinic mid-depth waters along productive continental margins by ~1.8 Ga (Canfield, 1998, Poulton et al., 2004a, Poulton et al., 2010). However, beneath oxic surface waters, this euxinic wedge overlaid deeper waters that remained anoxic and ferruginous (Planavsky et al., 2011, Poulton and Canfield, 2011). The 1.88-1.83 billion-year old Animikie Basin (Superior Region, North America) captures this redox structure as it developed, providing a superb setting for investigating the driving forces and consequences of this major change in ocean chemistry. It is thought that these stratified redox conditions prevailed until ~1.0 Ga (Canfield et al., 2008, Guilbaud et al., 2015, Johnston et al., 2010) after which ferruginous conditions dominated through much of the Neoproterozoic, with relatively little evidence for continental margin euxinia (Guilbaud et al., 2015, Raiswell and Canfield, 2012, but see also Thomson et al., 2015).

The cycling of phosphorus under this stratified redox structure, typical of continental margins between 1.8 and 1.0 Ga, is poorly understood, and hence feedback mechanisms associated with P stimulation or limitation of primary productivity, organic C burial and, ultimately, oxygen production, are poorly constrained. Previous studies have used biogeochemical modelling (Boyle et al., 2014, Lenton et al., 2014), P/Fe ratios in iron-rich chemical sediments

(Bjerrum and Canfield, 2002, Planavsky et al., 2010), P speciation methods developed for modern sediments (Creveling et al., 2014, März et al., 2008), or bulk P contents (Reinhard et al., 2017) to investigate P cycling in ancient settings, and whilst these methods provide useful insight, they all have their limitations. Biogeochemical models are an immensely important tool for reconstructing past ocean conditions, and are particularly useful when testing hypotheses, but in order to build these models we must seek evidence from the natural system (both modern analogues and ancient rock records) to gain understanding of the mechanisms that control key biogeochemical cycles. The molar P/Fe ratio in iron-rich chemical sediments has been used to infer oceanic dissolved P concentrations at the time of deposition (Bjerrum and Canfield, 2002, Konhauser et al., 2007b, Planavsky et al., 2010), although variations in the way this has been calculated has led to a wide range of results. This approach is also inherently limited by the lack of a continuous iron-rich chemical sediment record through time (Poulton, 2017), and hence studies have moved towards utilising shales.

A recent compilation of bulk P data from shales spanning the past 3.5 billion years by Reinhard et al. (2017), identified a fundamental shift around 800 million years ago, with sediments deposited after this point containing on average four times the amount of P relative to the more ancient settings. The authors interpret this increase in bulk P as a shift from marginal siliciclastics sediments containing predominantly detrital P prior to the Cryogenian, to a substantial contribution from authigenic P beyond this point. Whilst simulations using an ocean-sediment biogeochemical model appear to support this hypothesis, identification of the detrital and reactive pools of P using P speciation methods would help provide more information on the nature of the reactive pool present. Both März et al. (2008) and Creveling et al. (2014) analysed ancient sediments using modified versions of the SEDEX P speciation method, originally designed for use with modern sediments, and were able to identify distinct patterns in the cycling of P and crucially, reactive P. As previously discussed in Chapter 3, the SEDEX method is not optimised for use with ancient sediments and as such, it has been shown to underestimate Fe-bound P by not targeting P associated with more crystalline

Fe minerals such as magnetite and hematite that are often prevalent in ancient sedimentary rocks. For a more complete evaluation of P speciation in ancient sediments, a revised version of the SEDEX method designed to target these phases (as developed in Chapter 3) should be used.

Here, the speciation of phosphorus is examined through six cores from the Animikie Basin using this revised method, providing a detailed picture of the spatial and temporal variability in phosphorus cycling during the evolution of this dominant continental margin redox structure.

5.2 Materials and methods

5.2.1 Sample origin

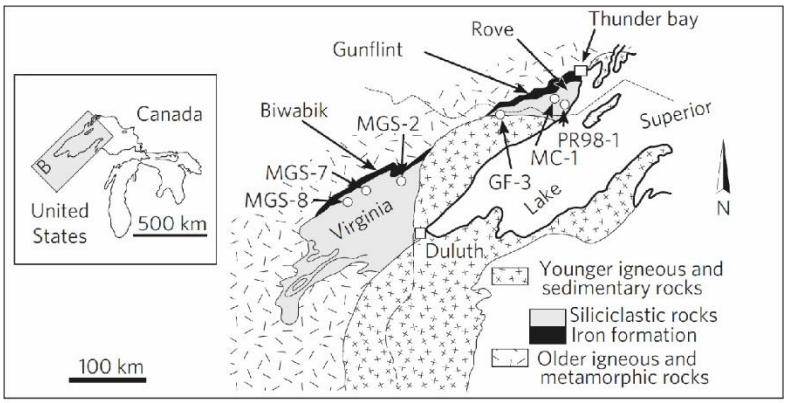

Figure 5.1 (Top) Core locations, from Poulton et al. (2010). (Bottom) In core sample location, depositional redox setting and stratigraphic categorisation.

The ~1.88-1.83 billion-year old Animikie group (see Poulton et al., 2010, 2004) was deposited in an open-ocean setting on the southwest margin of Superior Province, North America (Fralick et al., 2002, Ojakangas, 1983), and consists of chemical and siliciclastic sedimentary rocks. Based on palaeocurrents, the shoreline is thought to have been aligned approximately east-west (Morey, 1973), and the six drill cores sampled in this study form a NNE-SSW transect at approximately 30° to this (Figure 5.1), with the most distal core lying approximately 200 km from the palaeoshoreline (Poulton et al., 2010). The

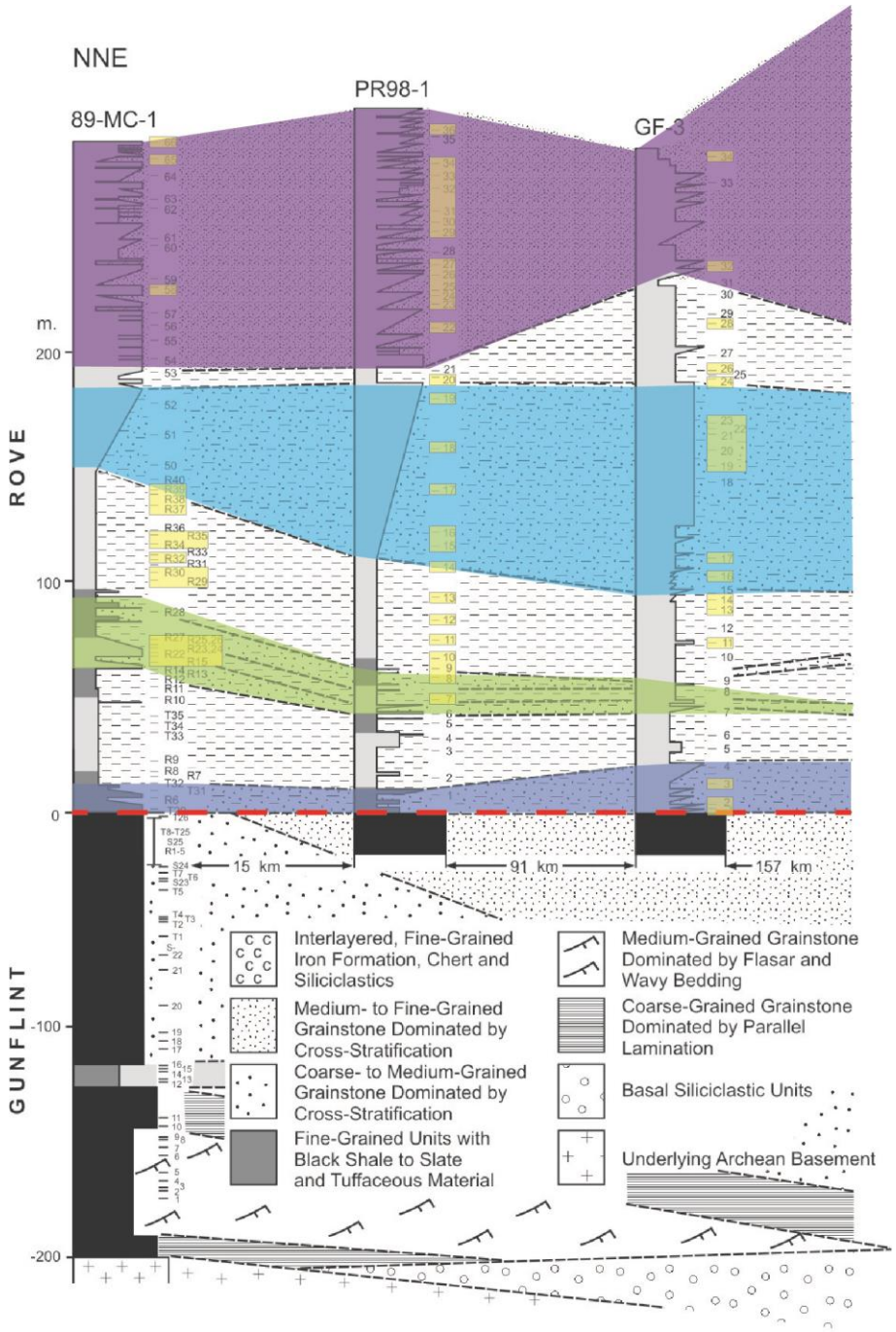

Figure 5.2 (a) Stratigraphy and sample positions for the Gunflint-Rove Formations (after Poulton et al., 2010, supplementary information)

Complete lithological legend information can be found opposite in Figure 5.2 (b) . Samples highlighted in yellow are those used in this study. Other shaded regions are highlighted to aid recognition from in text discussion.

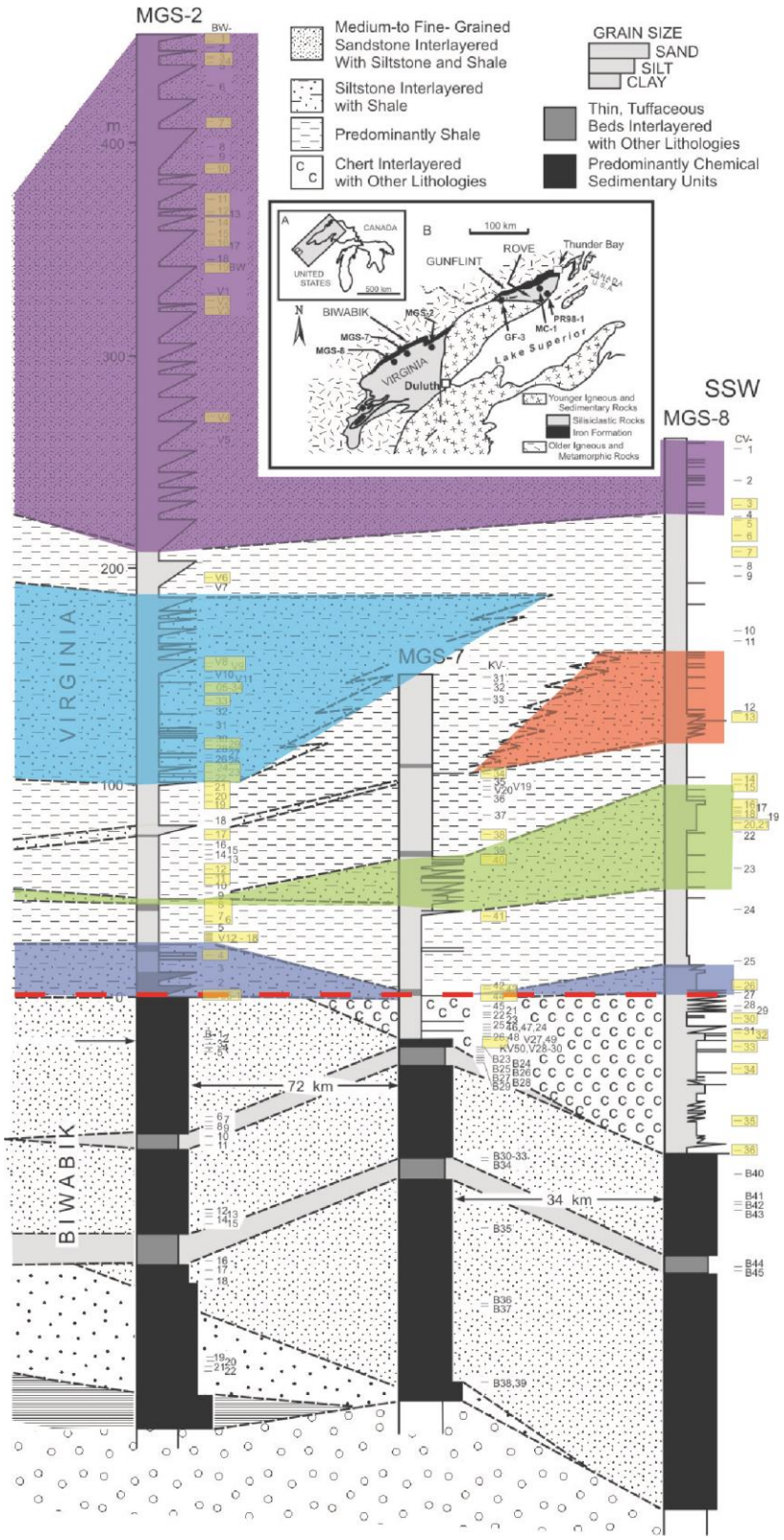

Figure 5.2 (b) Stratigraphy and sample positions for the Biwabik-Virginia Formations (after Poulton et al., 2010, supplementary information)

Samples highlighted in yellow are those used in this study. Other shaded regions are highlighted to aid recognition from in text discussion.

base of the drill cores used in this study intersect the correlative Gunflint Iron Formation in the North and the Biwabik Iron Formation in the South (below 0 m core height), and continue up through the overlying siliciclastic Rove and Virginia Formations, respectively (Figure 5.2 a and b).

The underlying Gunflint and Biwabik formations (1878 Ma) are separated (Figure 5.2, red dashed line) from the overlying Rove and Virginia formation (1835 Ma) by a major hiatus in deposition, most likely due to a change from a tensional to a compressive regime during the Penokean Orogeny, which led to upraising of the back arc area and withdrawal of the sea during this period (Poulton et al., 2010, supplementary information). The lower 5 – 10 m of the Rove and Virginia formations (Figure 5.2, shaded dark blue) consists of shales containing siltstones, thin tuffaceous layers and sandstones, most likely deposited during the resubmergence of the area due to unramped orogenic load (Maric and Fralick, 2005). The occurrence of the coarser grained material then decreases and fissile black shale dominates almost completely for the nect 100 – 150 m of the succession. This section of shales is only interrupted midway by a basin-wide interval rich in siltstone and very fine-grained sandstone (Figure 5.2, shaded green), possibly marking another period with low water levels (Poulton et al., 2010, supplementary information). The carbonaceous shales above this interval are also split in the Virginia Formation by a southward thickening wedge of shale interlayered with siltstones and rarer sandstones, potentially derived from upraised portions of the Penokean Belt (Maric and Fralick, 2005). Above 100-150 m, the shales transition into a coarsening upwards succession approximately 100 m thick (Figure 5.2, shaded light blue), before massive graded beds of sandstone begin to appear (Figure 5.2, shaded purple). This sandstone-shale bed consists of a stacked assemblage of individual parasequences, each containing graded, commonly massive, fine-grained sandstones separated by thin (mm-cm thick) sections of shale. The shale layers separating parasequences are up to 2 m thick, with both current and wave ripples present (Maric and Fralick, 2005).

Previous interpretations of these units have generally agreed that the Rove and Virginia formations were most likely deposited the lower- to mid-fan portions of

a submarine fan (Lucente and Morey, 1983, Maric and Fralick, 2005, Poulton et al., 2010), with the Rove Formation containing similar lithofacies and lithofacies sequencing to distal bars of modern delta dominated shorelines (Maric and Fralick, 2005). Water depths are difficult to determine, although they are unlikely to exceed a few hundred metres due to the continental position of the basin (Poulton et al., 2010). Tidal deposits identified in correlative units in the southern portion of the basin suggest that the Rove and Virginia formations were probably deposited whilst the basin was connected to the open ocean (Ojakangas, 1983).

137 samples were selected from the six well preserved drill cores, representing a range of depositional environments based on stratigraphy and previously published Fe speciation data (Poulton et al., 2010). The majority of samples were taken from the siliciclastics of the Rove and Virginia formations (Figure 5.2 a and b), with only 9 samples located in the chemical sediments of the Biwabik formation (MGS-7 and MGS-8, <0 m, Figure 5.2 b). Previously, sediments situated in the first 20 m and 86 m below 0 m of the two most distal cores (MGS-7 and MGS-8 respectively) were classed as the base of the Virginia Formation based on their total Fe content (Lucente and Morey, 1983). However, these are in fact chemical sediments and have more recently been reassigned to the chemical sediments of the Biwabik Formation (Poulton et al., 2010), although they are chemically distinct from the underlying iron formation.

For the purpose of comparison, samples have been separated into three zones, as depicted in Figure 5.3. A region characterized by oscillations between ferruginous and euxinic conditions was previously identified in the lower portion of the Rove Formation (Poulton et al., 2004a), which was stratigraphically correlated across all the cores (Poulton et al., 2010). Samples falling within this region are in the “transitional zone”. Below the transition zone, samples are categorised as “chemical sediments”. Above the transition zone, the “stable zone” is characterized by more permanent and stable redox conditions across the basin.

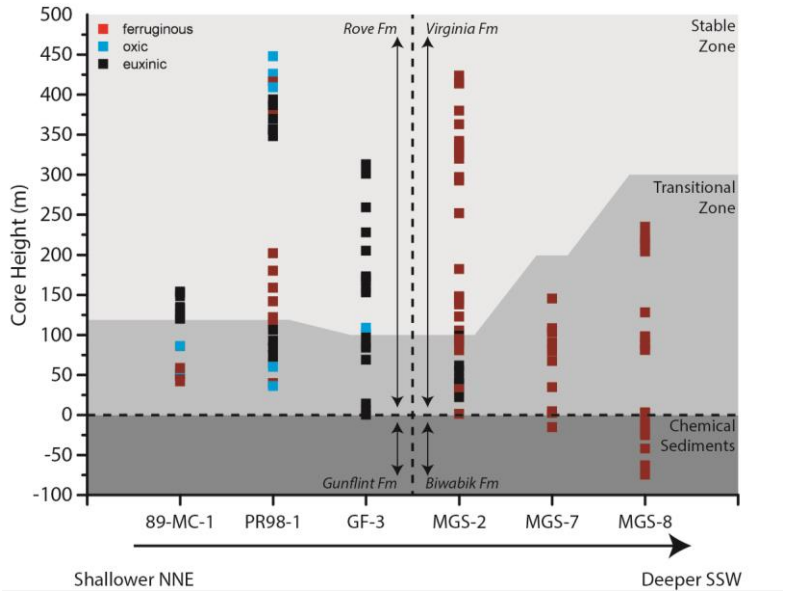

Figure 5.3 In core sample location, depositional redox setting and stratigraphically correlated categorisation based on (Poulton et al., 2010)

5.2.2 Techniques

Bulk sediment chemistry was determined by total digest as described in Chapter 2, section 2.2.4.. Total Fe, Al, P and Mn concentrations were analysed using ICP-MS, and the accuracy and reproducibility were assessed using an international sediment standard (n=3) and a repeated sample (n=6) respectively. A revised method of phosphorus speciation, as developed in Chapter 3, was applied to 160-190 mg of these ancient sedimentary rock samples. One sample was repeated six times to calculate the reproducibility of the method for these samples. Phosphorus was separated into the six pools listed in **Error! Reference source not found.** and a minimum estimate of "reactive P" (P_{reac}) is given by the sum of all pools excluding P_{cryst}. Total Fe-bound P is the sum of P_{Fe1}, P_{mag} and P_{Fe2}.

5.2.3 Statistics

Comparison of one population of data to a standard value, such as average shale element/Al ratios, or the Redfield ratio, was performed by a one-sample t-Test at a 0.05 significance level, with equal variance assumed. The comparison of two data populations was done using a two-sampled t-Test at a 0.05 significance level. In the text, a two-tailed test is indicated by “tt” and a single-tailed test is indicated by a “st”.

5.3 Results

5.3.1 Bulk chemistry

TOC data taken from Poulton et al. (2010) are presented in Figure 5.4 Total organic C content taken from for completeness although were not reanalysed in this study. The average Al content across all cores was 9.2 ± 2.2 wt% (Figure 5.5). Aluminium contents were generally relatively consistent, but large variability was observed in a few samples from the transitional zone in the 3 cores most proximal to the palaeoshoreline, especially in GF-3 (ranging from 5 to 8 wt%) near the contact between the Gunflint and Rove Formations. Another fluctuation can be seen at ~150 m height in the two most proximal cores. These deviations from the mean could indicate changes in the supply of detrital material to the basin.

Total Fe concentrations were highest in the chemical sediments of the two most distal cores, averaging 8.2 ± 1.8 wt%, with large fluctuations situated across the boundary into the siliciclastic sediments above (Figure 5.6). The average Fe content for samples in the transitional and stable zones across all cores was 5.5 ±1.6 wt%. As for Al, the largest fluctuations can be seen in the transition zone of the three most proximal cores.

Total P concentrations were also increased in the chemical sediments, averaging 0.1 ± 0.5 wt% below 0 m height in MGS-8, whereas the average siliciclastic P content was lower at 0.07 ± 0.4 wt% (Figure 5.7). There were two notable peaks in GF-3, one in the transition zone and one in the stable zone,

with total P reaching 0.26 and 0.31 wt% respectively. Total P content also seemed to show some variability between 300-425 m height in MGS-2.

Total Mn concentrations were relatively constant over the first four cores, averaging 0.05 ± 0.07 wt%, but were considerably enhanced in the deeper samples of MGS-7 and MGS-8 (Figure 5.8). These enhanced Mn concentrations of up to 2.6 wt% were mainly located in the chemical sediments below 0 m height, but the maximum concentration was actually seen in the lower transition zone of MGS-7 at 34.8 m height. There were also elevated and variable total Mn concentrations seen around 86 m in 89-MC-1, where the core was sampled on the mm scale, although the maximum concentration reached at this point (0.5 wt%) was far lower than those seen in the chemical sediments.

To determine if the fluctuations seen in total Fe, P and Mn were merely features of detrital inputs, these elements were normalised to Al concentrations. Comparison of these values with the average element ratios for shales, as determined using values from Turekian and Wedepohl (1961), can indicate whether these elements are enriched or depleted in these samples (Figure 5.9).

On average across all samples, Fe/Al ratios indicate enrichment of Fe relative to average shale, although there was a large range of values. As expected, Fe/Al ratios in the chemical sediments were highly enriched compared to the average shale values, with a mean value of 1.0 ± 0.3. Such values were also reached by samples from the top of the transition zone in 89-MC-1 and MGS-8. Samples from cores PR98-1, GF-3, MGS-2 and the siliciclastic samples from MGS-7 all had a narrow range of Fe/Al values, falling very close to that of average shale. In contrast, high variability was seen in the most proximal core (89-MC-1) with ratios ranging from 0.2 to 1.9 (Figure 5.9).

The mean P/Al ratio across all samples fell inline with average shale, although there were some key deviations from this value (Figure 5.9). The majority of samples in PR98-1 fell below average shale, averaging just 0.005 ± 0.001, indicating possible depletion of P. The chemical sediments at the base of MGS-

7 and MGS-8 exhibited some of the highest ratios seen across all samples, averaging 0.013 ± 0.006.

For Mn, the majority of siliciclastic sediments were within the range of average shale, with a mean Mn/Al ratio of 0.01 ± 0.04, although large excursions from this were seen in the upper transition zone of 89-MC-1, where the samples were taken on the mm scale (Figure 5.9). As for Fe and P, Mn/Al ratios of the chemical sediments were distinctly higher with increased variability, averaging 0.05 ± 0.06, these high values also seemed to continue through in the lower siliciclastic samples of MGS-7, with values as high as 0.23 seen at 34.8 m core height.

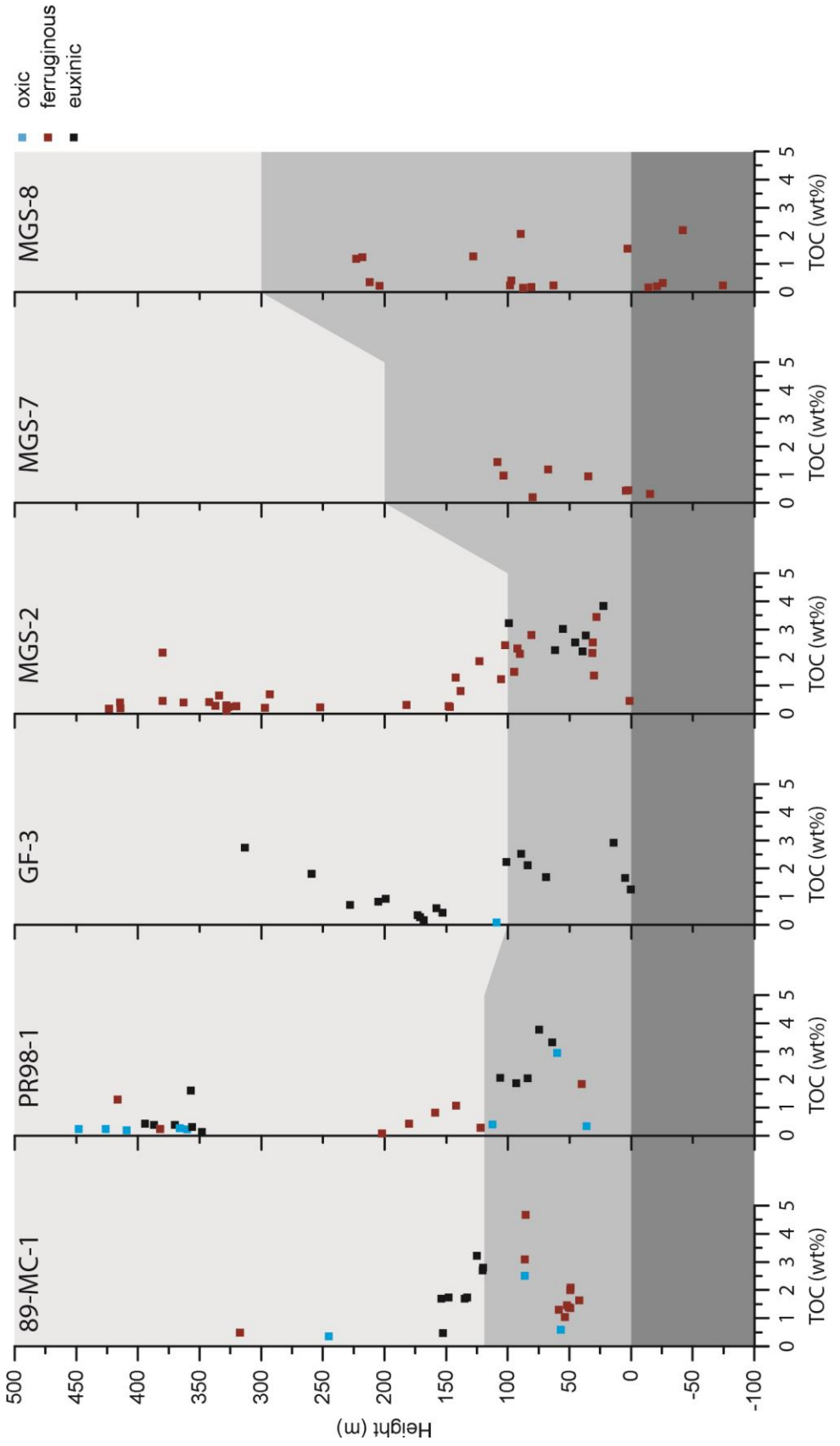

Figure 5.4 Total organic C content taken from Poulton et al. (2010)

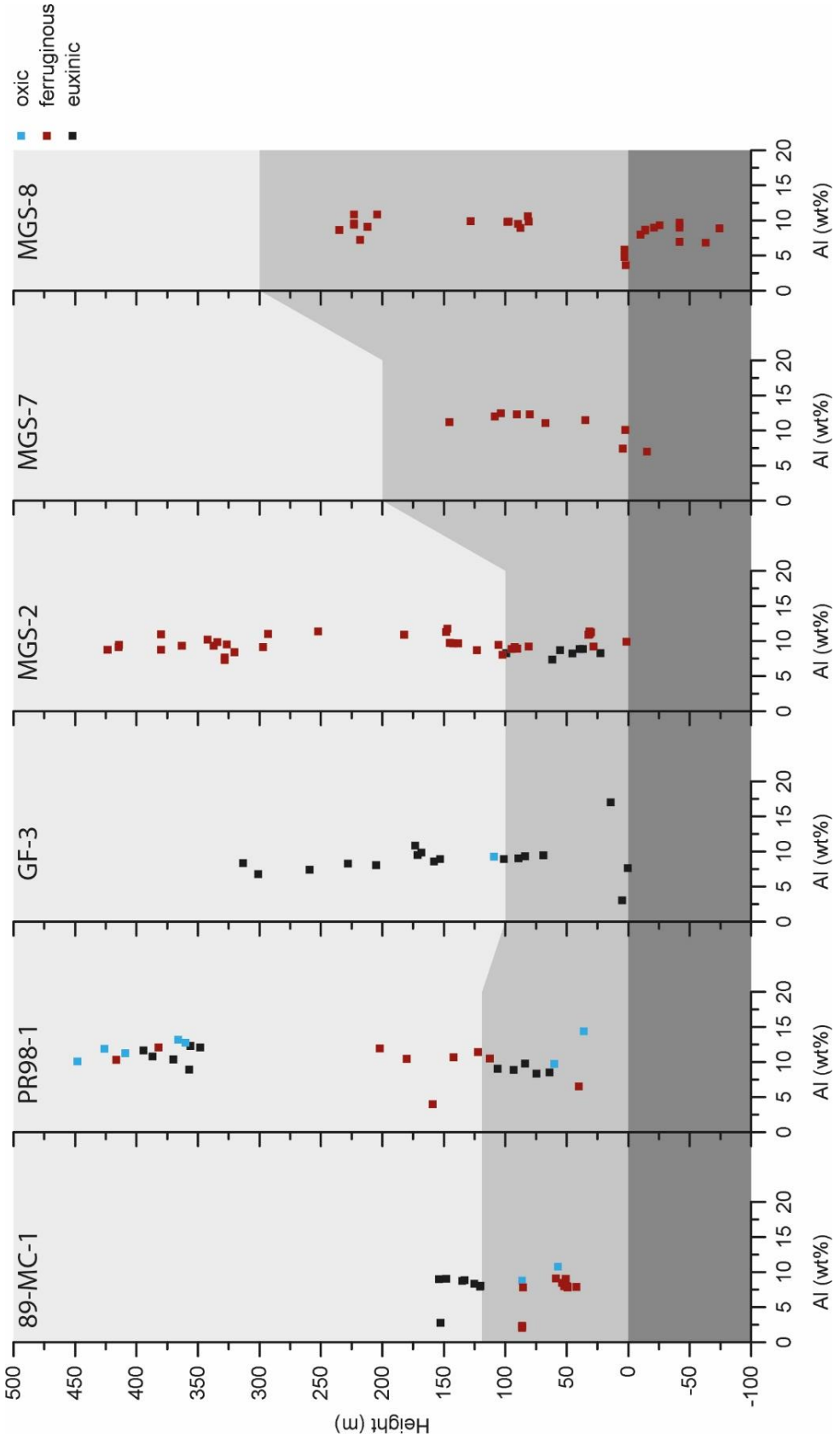

Figure 5.5 Total Al concentrations

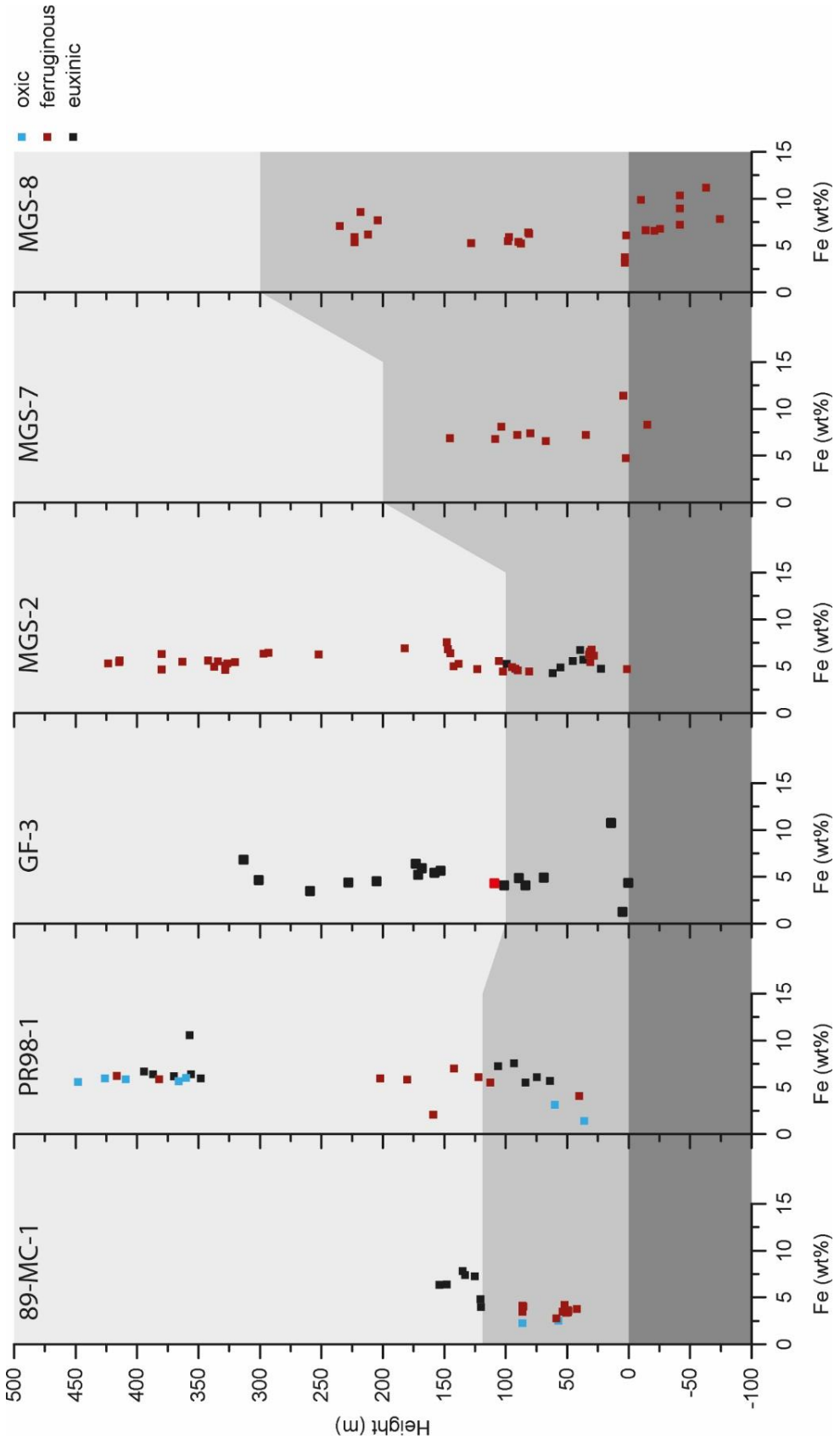

Figure 5.6 Total Fe concentrations

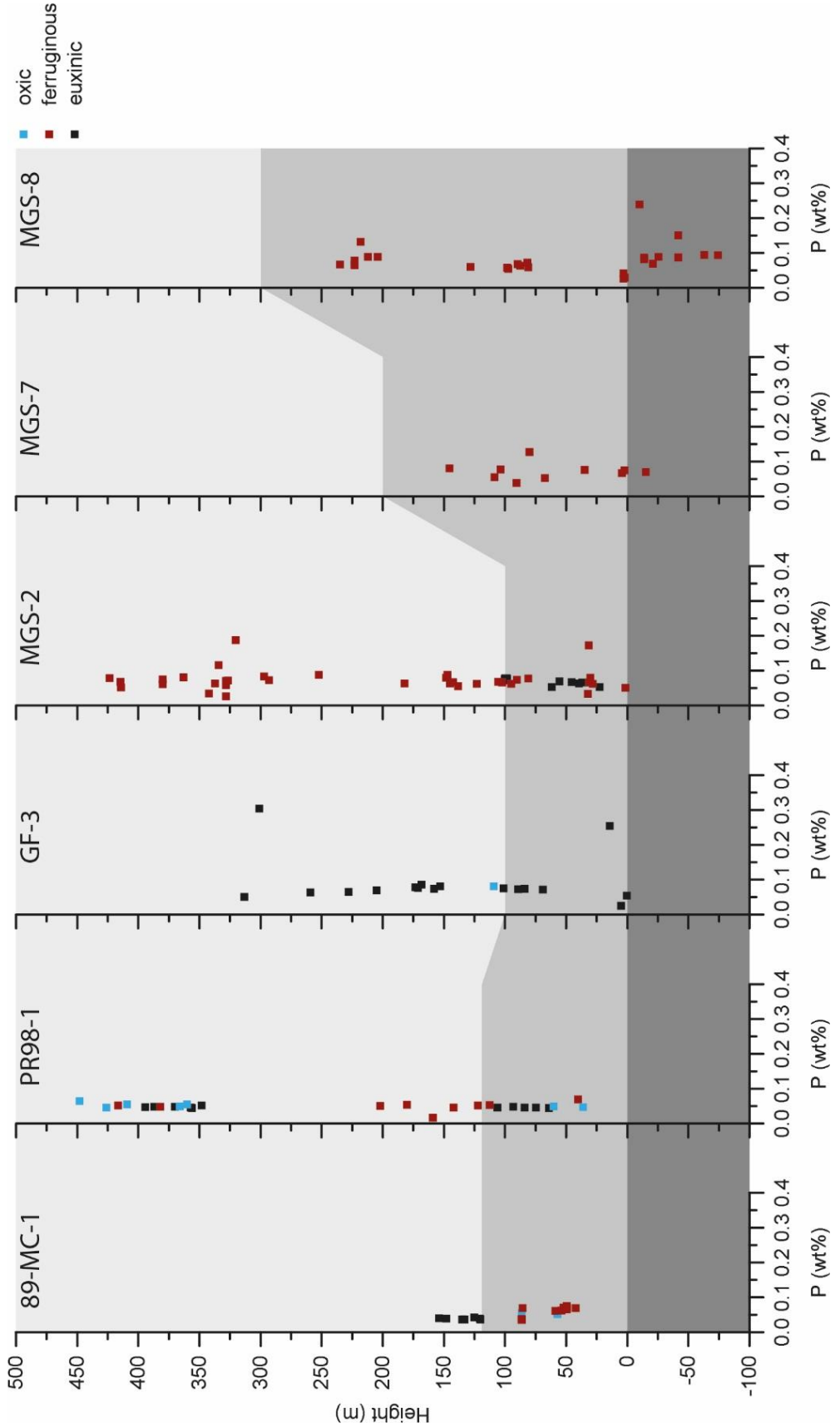

Figure 5.7 Total P concentrations

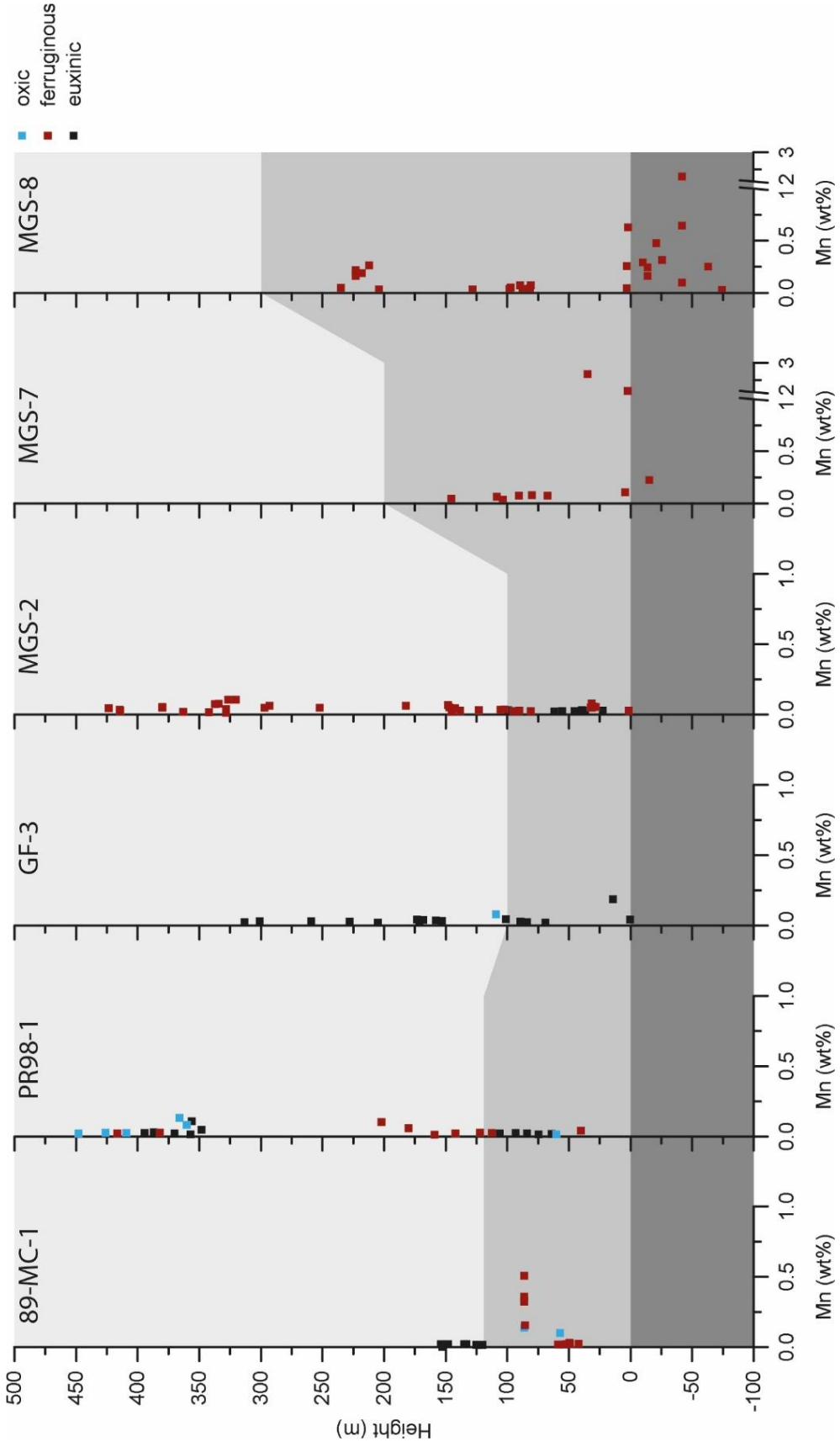

Figure 5.8 Total Mn concentrations. Note the scale break for MGS-7 and MGS-8

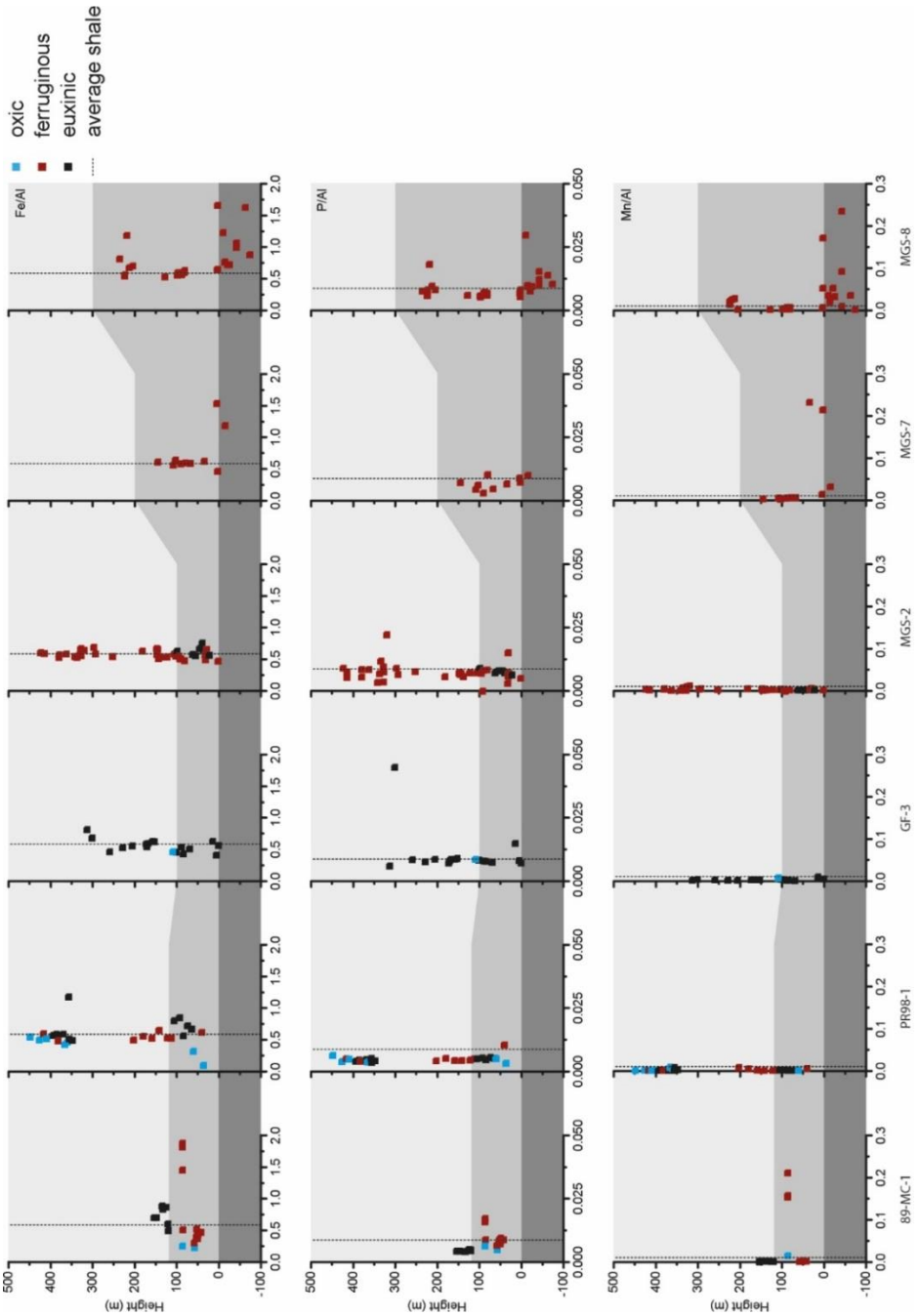

Figure 5.9 Total Fe (top), P (middle) and Mn (bottom) concentrations normalised to Al.

Average shale ratios based on values given in Turekian and Wedepohl (1961) are indicated by the dashed lines.

5.3.2 P Speciation

On average, P speciation recovered 94.1 ± 16.8% of P extracted by total digestion. P_{cryst} contributed 73.5 ± 14.1% of this and as such, the remaining P_{reac} pool was generally small, averaging 26.5 ± 14.1% of extracted P across all samples (Figure 5.10). P_{Fe1} was generally low (Figure 5.11 and 5.9), averaging 1.1 ± 2.8 mg/kg across cores 89-MC-1, MGS-2,7 and 8. Sediments in the GF-3 core generally exhibited higher concentrations, averaging 8.7 ± 5.0 mg/kg and range of substantial enrichments in P_{Fe1} were seen in the transition zone of PR98-1, reaching a maximum of 12.4 mg/kg (Figure 5.11).

P_{auth} was generally the second largest pool of P across all cores, although there is a lot of scatter, averaging 130.3 ± 67.5 mg/kg (Figure 5.11 and 5.9). P_{auth} concentrations appeared to be lower in the chemical sediments, averaging just 36.4 ± 28.0 mg/kg (Figure 5.12).

P_{cryst} was consistently the largest pool of P, with the lowest concentrations seen in the stable zone of the two most proximal cores (~250 mg/kg, Figure 5.11). Large excursions were seen in the transition zone of 89-MC-1, MGS-2 and 8, reaching a maximum concentration of 1283.8 mg/kg (Figure 5.12).

Pmag, generally the largest pool of Fe-bound P (not including P_{Fe1} in the transition zone of PR98-1), had an average concentration of 14.3 ± 6.4 mg/kg. Highest concentrations were seen in the transition zone of MGS-2, up to 27.5 mg/kg (Figure 5.12).

P_{Fe2} contributions were low (<2 mg/kg) and generally less than 0.5 mg/kg. Highest P_{Fe2} concentrations generally coincided with the transition zone (e.g. 89-MC-1, PR98-1 and MGS-2), although similar excursions were also detected in the upper sediments of PR98-1 (Figure 5.11 and 5.9).

P_{org} concentrations were very low and mainly only detectable in the three most proximal cores (Figure 5.11). There were no distinct patterns and concentrations averaged 1.5 ± 3.0 mg/kg across all cores.

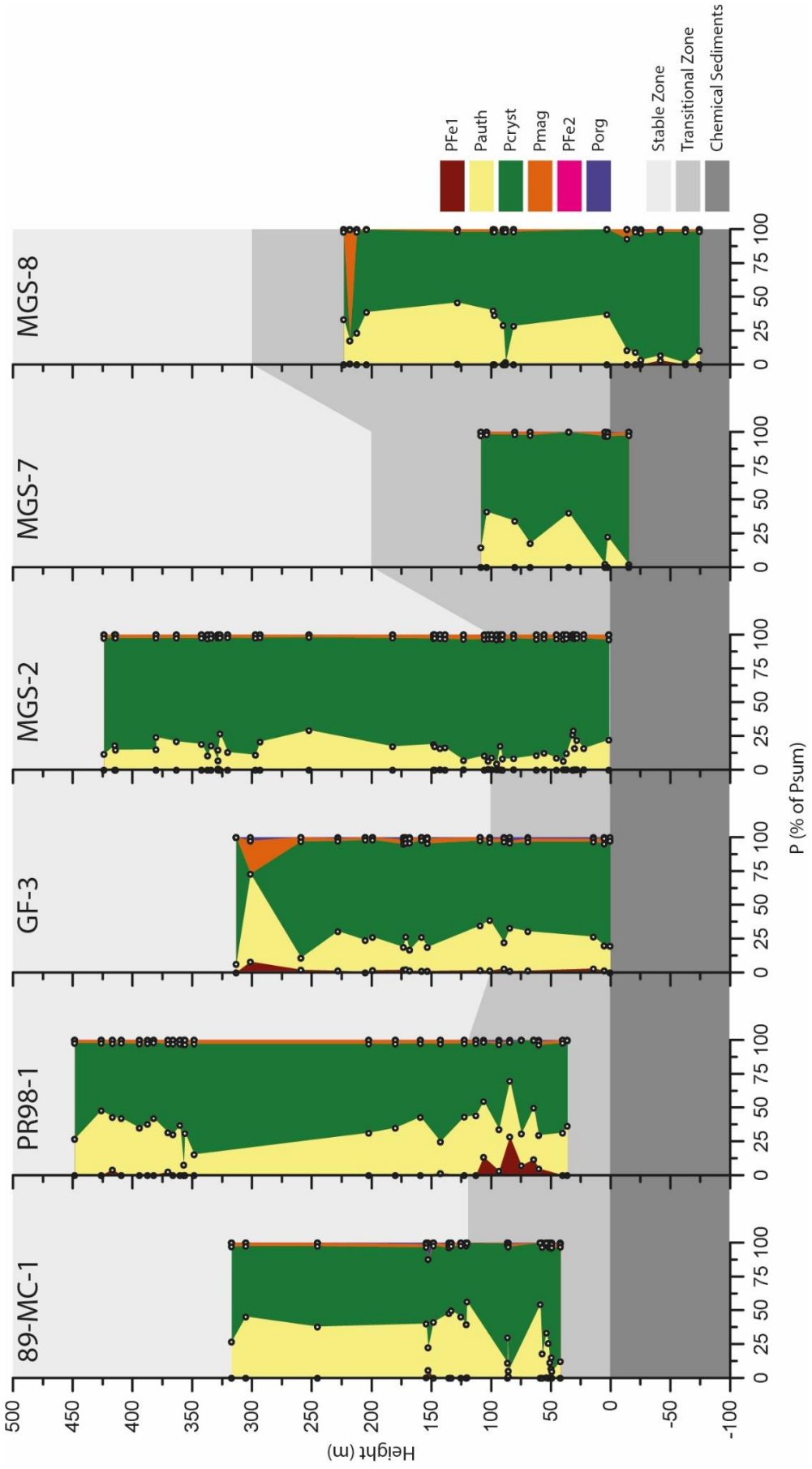

Figure 5.10 P Speciation as a proportion of total extracted P (P_{sum})

Since it is reactive P that is considered potentially bioavailable and capable of stimulating or limiting primary productivity, the initial analysis of the results will mainly consider reactive P partitioning, but the likelihood that some P_{auth} has been transferred to P_{cryst} as suggested in Chapter 3 will subsequently be discussed.

Across all the cores, reactive P was generally dominated by P_{auth}, averaging 81.4 ± 15.6% of P_{reac}, although total Fe-bound P was elevated in some samples, particularly in the chemical sediments (Figure 5.13). P_{org} was very low in the majority of samples and often below the limit of detection, averaging 1.3 ± 3.8 % of P_{reac}, with maximum concentrations seen in the chemical sediments of MGS-8 (max 12% of P_{reac}) and the transition zone of 89-MC-1 (max 35% of P_{reac}) (Figure 5.13). P_{Fe1} was generally low apart from in the transition zone of the two most proximal cores and throughout the entirety of GF-3. The highest concentrations of P_{Fe1} were seen in the transition zone of PR98-1 and contributed up to 40% of P_{reac}, but were more consistent across the full height of GF-3, providing on average 6% of P_{reac} (Figure 5.13). A more ubiquitous pool of Fe-bound P in terms of concentration was P_{mag}, but P_{mag} as a proportion of the P_{reac} pool varied greatly, from 1- 82%. P_{mag} was consistently high in the chemical sediments of MGS-8, contributing 36 ± 18 % of P_{reac} (Figure 5.13). However, despite this high contribution to the P_{reac} pool (Figure 5.13), this is likely due to diminished contributions of all other P_{reac} components, rather than significantly enhanced P_{mag} contents (Figure 5.12). This is supported by the particularly low contributions of P_{auth} (Figure 5.12). P_{Fe2} was negligible in across all samples only contributing a maximum of 3.5% in GF-3.

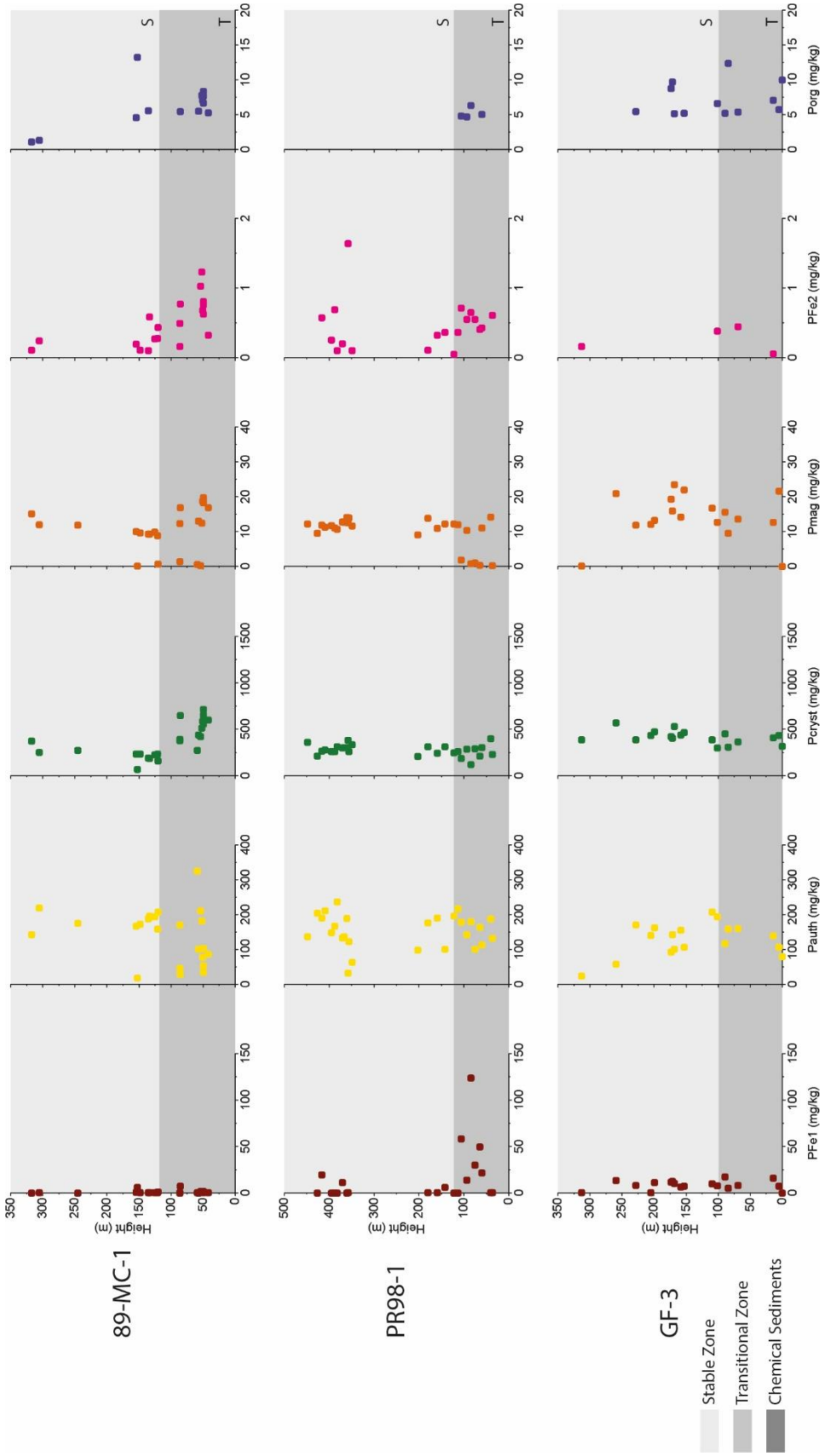

Figure 5.11 P speciation in mg/kg for the 3 most proximal cores. Note the different scales for each pool.

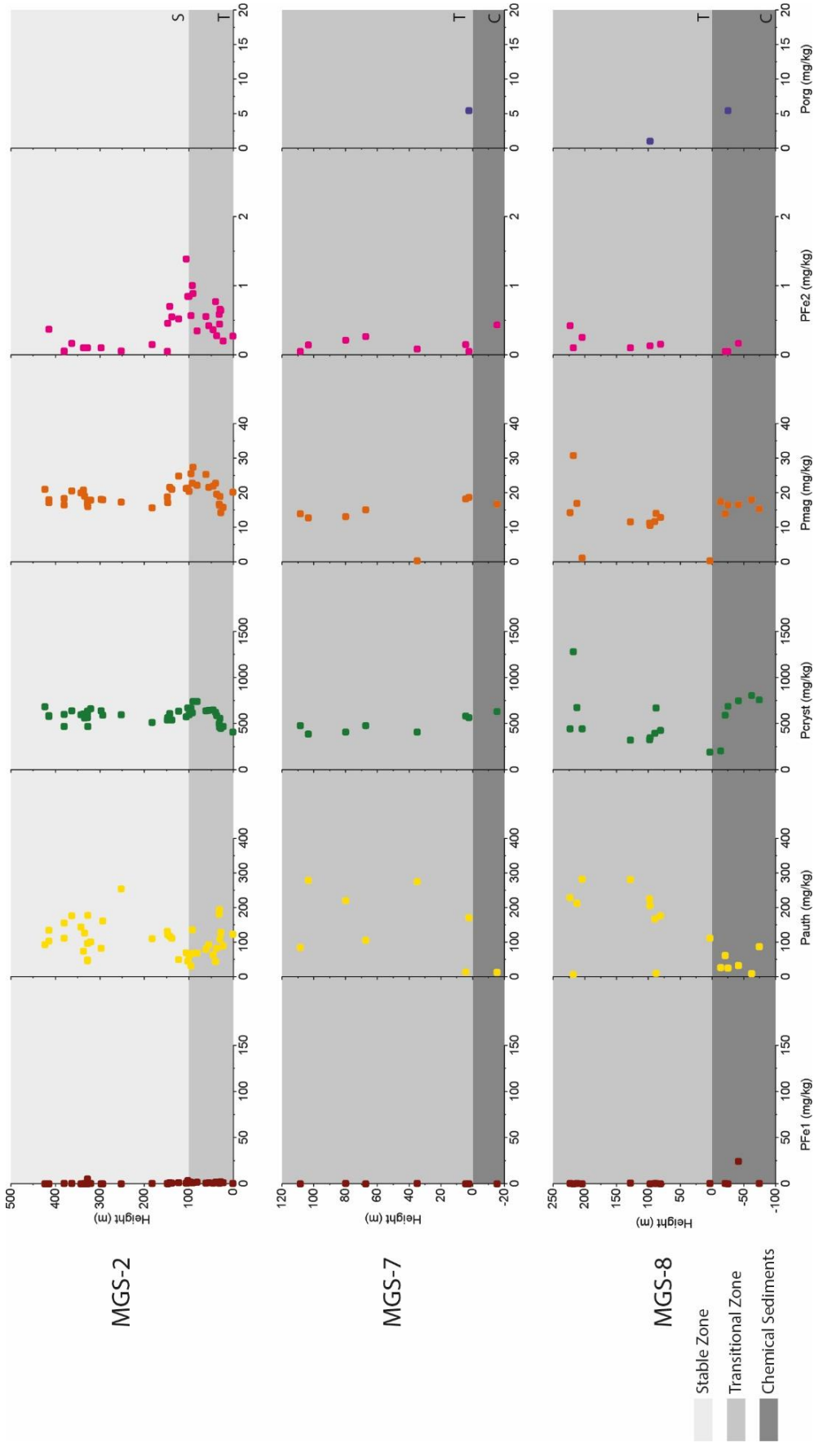

Figure 5.12 P speciation in mg/kg for the 3 most distal cores. Note the different scales for each pool.

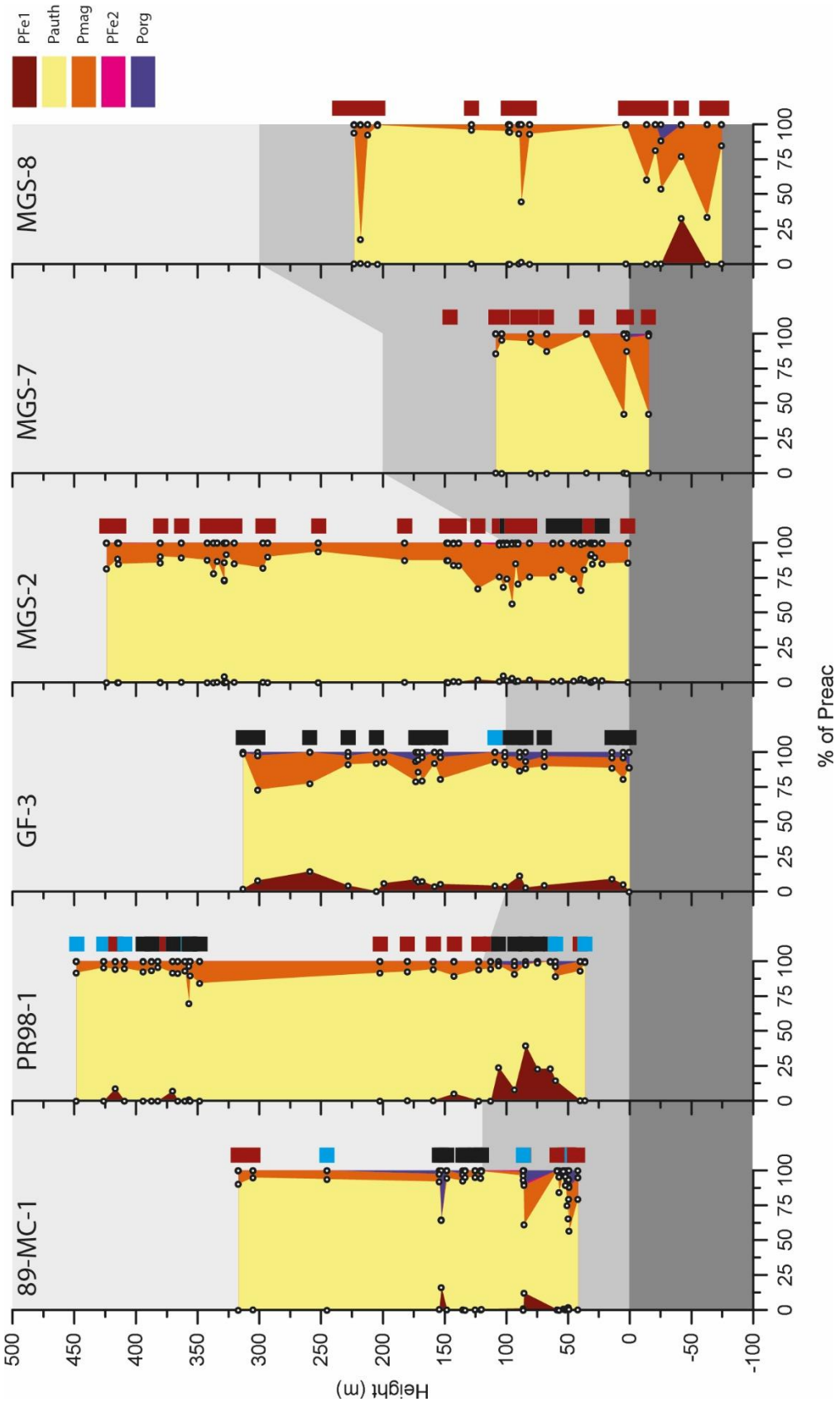

Figure 5.13 Reactive P speciation

5.4 Discussion

In Chapter 3, the potential for P_{auth} to become more crystalline and hence be extracted by the P_{cryst} step was discussed. As shown in Figure 5.10, P_{cryst} is an overwhelmingly dominant pool in these ancient sedimentary rocks, and while it could represent a high flux of detrital material to the basin during this period, it could also signify substantial transformation of P_{auth} to more crystalline phases. Theoretically, true detrital P should correlate well with Al, an indicator of detrital flux, however in these sedimentary rocks, no such correlation is found. Furthermore, P_{auth} is the dominant pool of reactive P in the majority of samples, and when comparing the concentration profiles of P_{cryst} and P_{auth}, they strongly mirror each other in a number of places (Figure 5.14), providing support for a significant conversion of P_{auth} to P_{cryst}.

A method of determining the extent of P_{auth} recrystallization has not yet been developed, and as such, only minimum and maximum estimates of Preac can be considered; the minimum being the values we have previously assessed (P_{reac} = Fe-bound P + P_{auth} + P_{org}), and the maximum given by additionally including P_{cryst}, denoted here as P_{sum} (P_{sum} = P_{reac} + P_{cryst}). The minimum estimate of P_{reac} can be confidently discussed with regard to the partitioning of P between the reactive pools, and will be discussed initially. Consideration of a maximum estimate of P_{reac} and its implications for P cycling in the Animikie Basin will follow.

To understand P cycling during the transition from a fully ferruginous ocean to the development of euxinic mid-depth waters and oxic surface waters along the margin in the Animikie Basin, it is important to consider the basin as a whole system as opposed to looking at the data on a core by core basis. Poulton et al. (2010) defined a zone across all cores which encompasses a region of variable redox states in the most proximal cores. Stratigraphically correlated across all six cores, this “transitional” zone can be taken to be a time slice of the Animikie basin during which the euxinic margin was developing. Above this zone, sediments were deposited in more stable redox conditions, once the euxinic wedge had been established at mid-depths. The chemical sediments in the

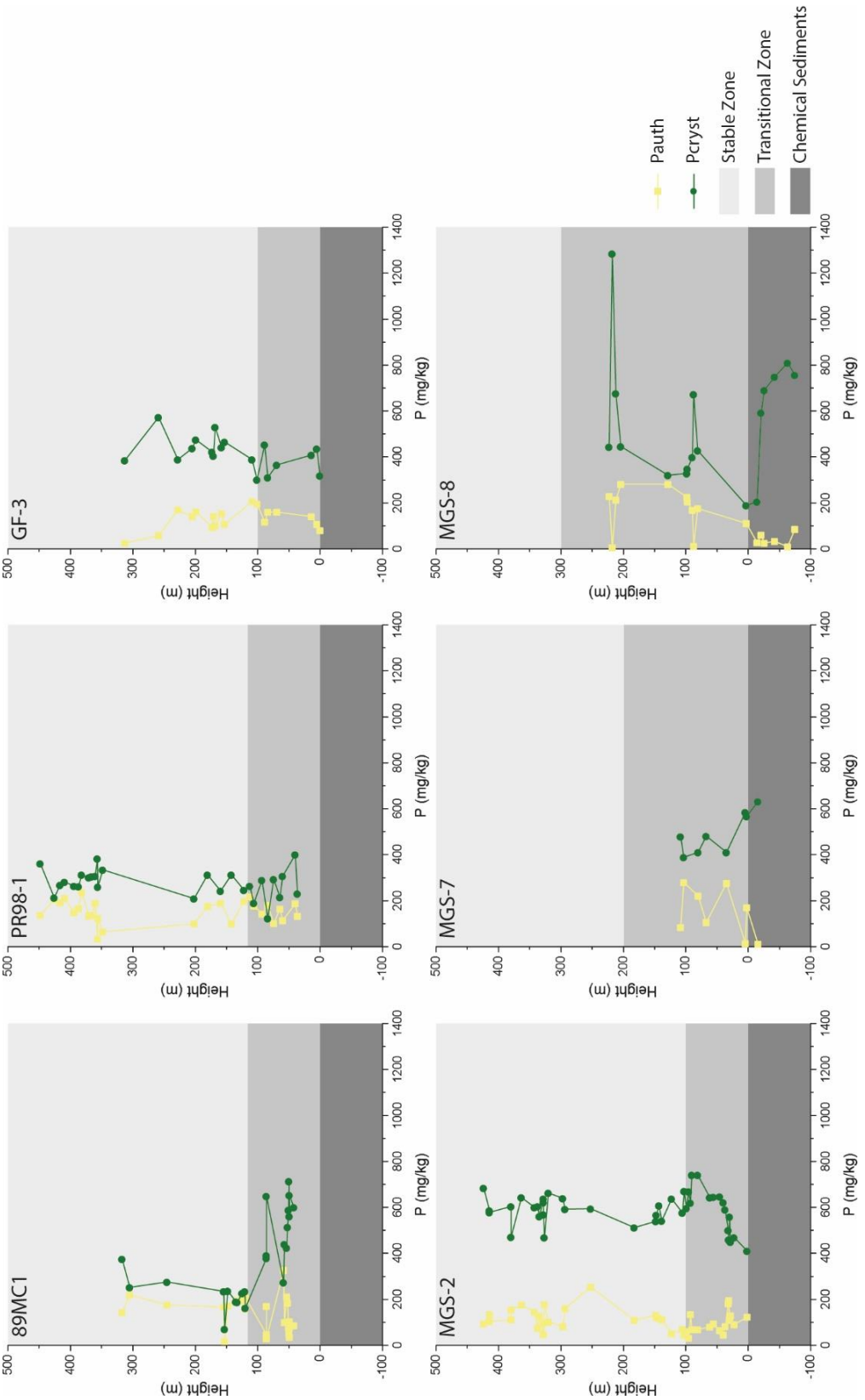

Figure 5.14 Comparison of P_{auth} and Pc_{ryst} concentrations in the sediment.

most distal cores represent a distinct period of time, prior to the deposition of the siliciclastic sediments of the overlying Rove and Virginia formations. These zones, representing different time periods during the evolution of the Animikie Basin, can then be subdivided into regions of oxic, ferruginous and euxinic conditions to determine differences in P cycling under different spatial and temporal depositional redox conditions.

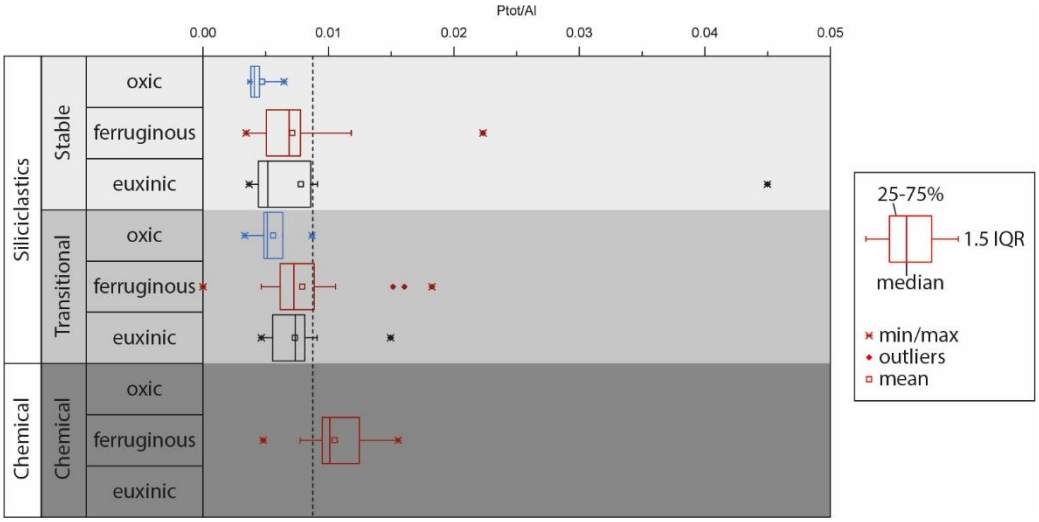

Figure 5.15 Comparison of Ptot/Al values for each zone and redox setting.

The ratio for average shale is indicated by the dashed line.

For an initial insight into the cycling of P during the development of the Animikie Basin, total P concentrations normalised to Al content can reveal changes in bulk P. No statistically significant differences were seen sorting samples by redox conditions, however, when split by sediment type (siliciclastic or chemical), P_{tot}/Al ratios in the chemical sediments were greater than those in the siliciclastics (st, *p* 0.04) (Figure 5.15). This suggests a significant enrichment in total P in the chemical sediments compared to the overlying siliciclastic sediments, with no difference seen between the transitional and stable zone. Whilst this enrichment is clear, it does not necessarily represent an increased retention of bioavailable P, as it could also reflect higher P-containing detrital fluxes. Indeed, Figure 5.10 shows that P_{reac} concentrations contribute far less in the chemical sediments than in the siliciclastics,

suggesting that the unreactive, detrital component of P_{tot} was relatively increased (assuming P_{cryst} is accurately partitioning detrital apatite).

TOC/P_{org} ratios are commonly used to determine the loss or retention of P_{org} from sediments by comparison with the Redfield molar ratio (C:P) of 106:1 (Berner, 1980, Ingall and Van Cappellen, 1990). In these sediments, P_{org} was very low and often below the limit of detection. For samples where P_{org} was measurable, TOC/P_{org} was quantified and extremely elevated (~7000), suggesting extensive preferential loss of P relative to C during mineralization. Anderson et al. (2001) suggest that the ratio of TOC/P_{reac} can provide insights into the fate of organic matter-derived P, i.e. whether it is trapped during the formation of authigenic phases, such as apatite and Fe minerals, or lost to the overlying water column. Therefore, the TOC/P_{reac} ratio may provide more insight into the potential recycling of P back to the water column after diagenetic release from organic matter and Fe oxide minerals. However, given that it is likely that a significant amount of Pcryst was originally Preac, TOC/Preac will only provide a minimum estimate of original TOC/Preac ratios, and hence the main focus here will be on comparing relative differences in TOC/Preac ratios between oxic, ferruginous and euxinic parts of the three sediment zones.

When categorised by redox setting alone, TOC/P_{reac} values for oxic samples were not significantly different to the Redfield ratio (tt, p 0.92), whereas both ferruginous and euxinic samples were greater than the Redfield ratio (st, $<<0.05$), indicating possible loss of P from the sediments. The difference between ferruginous and euxinic samples was not statistically significant. When samples were categorised by their depositional zone, results suggest that chemical sediments and stable zone samples were not statistically different from the Redfield ratio (tt, $p > 0.05$), but samples from the transition zone were depleted in P relative to the Redfield ratio (st, $p << 0.05$).

When the zones are subdivided into depositional redox categories, some clear differences can be seen (Figure 5.16). Within the transitional zone, TOC/P_{reac} values across all redox conditions generally plot above the Redfield ratio, as previously suggested by the bulk zone analysis. However, oxic samples

present ratios which are not different to the 106:1 value. Both the ferruginous and euxinic samples are significantly higher (st, p <<0.05) than the Redfield ratio, but are not statistically different from each other on a 0.05 significance level. Based on bulk zone analysis, samples from the stable zone were not statistically different to the Redfield ratio, but when subdivided into redox settings, there were some distinct patterns. On average, oxic samples in the

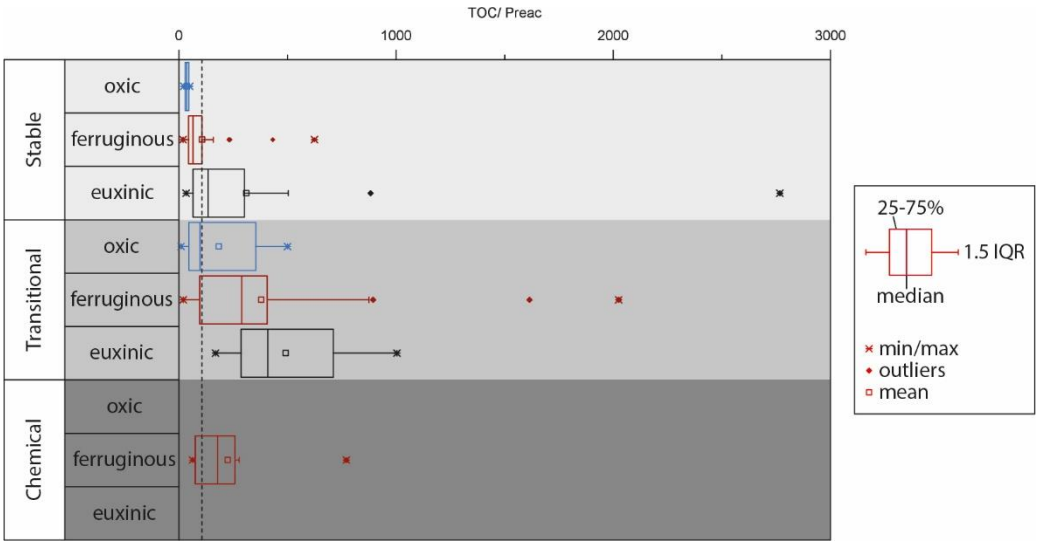

Figure 5.16 TOC/P_{reac} values for each zone and redox setting.

The dashed line represents the Redfield ratio.

stable zone have TOC/P_{reac} values lower than 106 (st, p <<0.05), ferruginous samples are not statistically different from the Redfield ratio and euxinic samples are greater than 106 (st, p 0.04).

Samples deposited under the same redox conditions through the different zones were also compared. Oxic samples in the transitional zone have statistically higher TOC/P_{reac} values than in the stable zone (st, p 0.049), which is also the case for ferruginous samples (transitional > stable, st, p <<0.05). However, there is no statistical difference in TOC/P_{reac} values for euxinic samples between these two zones (tt, p >0.05).

5.4.1 Inferences about P cycling over time in the Animikie Basin from P speciation and TOC/P_{reac} ratios

5.4.1.1 Chemical sediments

Despite total P enrichments in the chemical sediments, relative to both average shales and the overlying siliciclastic sediments, the proportion contributing P_{reac} was very low, averaging only 8.2 ± 4.7% of P_{sum}, and less than 103 mg/kg (Figure 5.10). TOC/P_{reac} ratios for these sediments as a whole were not statistically different from the Redfield ratio (Figure 5.16), although on a sample by sample basis, some ratios reached values as high as ~750, suggesting a loss of reactive P in some samples. A large proportion of the remaining P_{reac} in these sediments is magnetite bound (Figure 5.13), with P_{auth} playing a far less dominating role in the retention of P than in the overlying sediments. Without using the revised P speciation method developed in Chapter 3, this P_{mag} pool would have gone undetected, leading to underestimation of the role of Fe minerals in the cycling of P in these sediments. Instead we have shown magnetite bound P as a key sink for P during deposition of chemical sediments under ferruginous conditions.

5.4.1.2 Transitional zone

Samples in the transitional zone were deposited during the development of a euxinic wedge extending from the shoreline. Low P_{tot}/Al and high TOC/P_{reac} ratios across this zone suggest preferential P loss during the development of the euxinic wedge (Figure 5.15 and Figure 5.16). Whilst depositional redox conditions oscillated between oxic, ferruginous and euxinic conditions, P appears to have been drawn down in line with the Redfield ratio under oxic periods, but extensively recycled during ferruginous and euxinic conditions, as indicated by high TOC/P_{reac} ratios in anoxic samples. It is possible that the loss of P from sediments relative to organic C was enhanced by repeated switches from ferruginous to euxinic conditions, drawing down high concentrations of P associated with Fe minerals during ferruginous conditions, which was then released back to the water column during euxinic episodes (Figure 5.17 – A).

5.4.1.3 Stable zone

Once the redox conditions became more stable following the establishment of the euxinic wedge, the difference in P cycling between different redox environments became more distinct. In this stable zone, sediments deposited under euxinic conditions continue to have elevated TOC/P_{reac} values (although they are lower than those for euxinic samples in the transition zone), whereas samples deposited under ferruginous conditions (generally found further offshore) had TOC/P_{reac} values more in line with the Redfield ratio, in stark contrast to the transition zone. This suggests a loss of reactive P from sediments to the water column under the euxinic conditions, in agreement with modern euxinic environments (e.g. Ingall and Jahnke, 1994; Colman and Holland, 2000) and retention in line with the Redfield ratio (possibly leaning towards enhanced draw down of P) under the more distal ferruginous environments (Figure 5.17 – B). In the few samples that indicate deposition from oxic surface waters, TOC/P_{reac} ratios suggest enhanced P drawdown relative to the Redfield ratio.

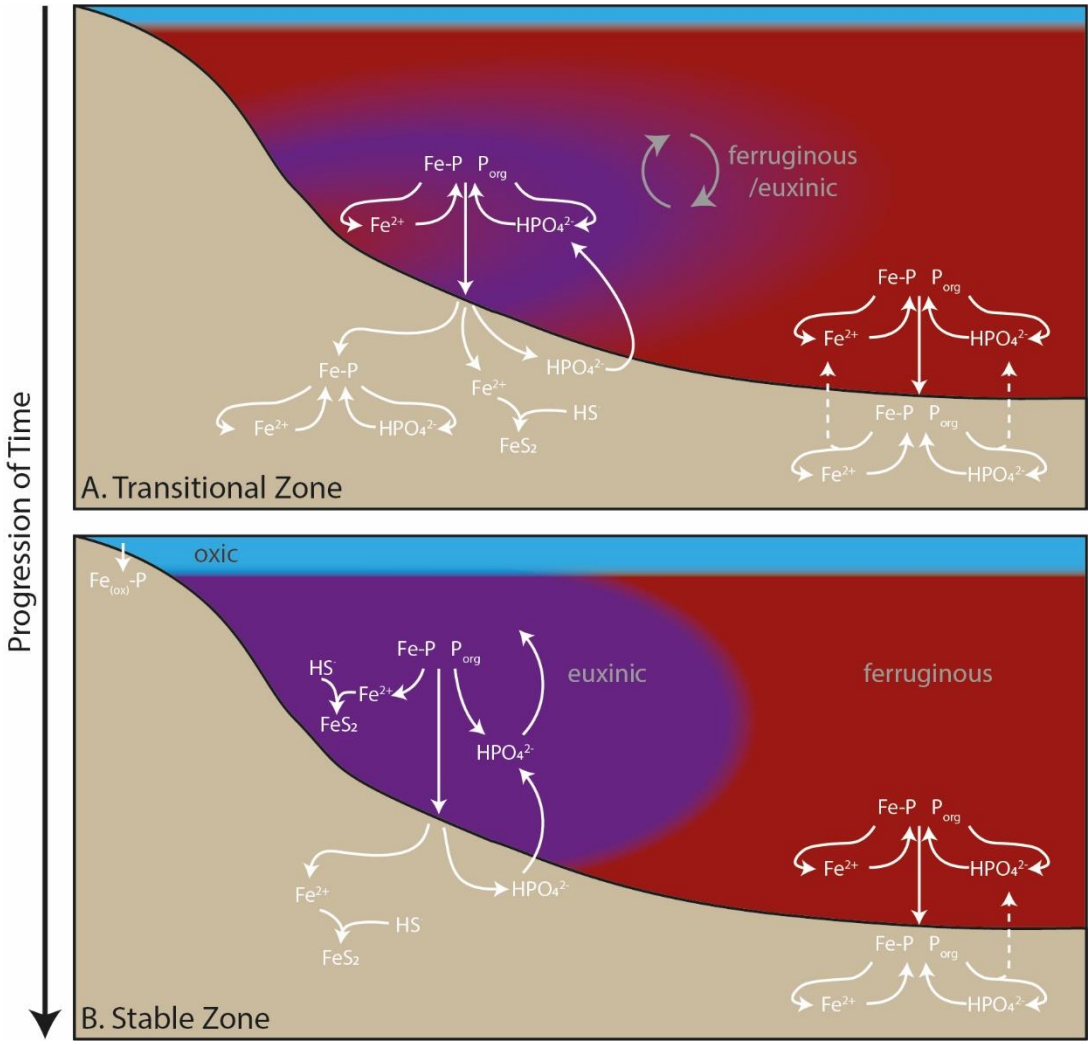

Figure 5.17 Schematic of proposed P cycling during the evolution of the Animikie Basin

5.4.1.4 Defining Reactive P from P speciation

Considering a maximum estimate of P_{reac} as described previously, TOC/P_{sum} ratios fall below the Redfield ratio for the majority of samples, but the general pattern of higher values in euxinic sample compared to ferruginous and oxic samples (Figure 5.18) is nevertheless maintained. In all likelihood, the true TOC/P_{reac} ratios lie somewhere between the minimum and maximum scenarios (Figure 5.16 and Figure 5.18, respectively), but most likely still reflecting enhanced recycling of P during euxinic depositional periods and enhanced P retention under ferruginous conditions.

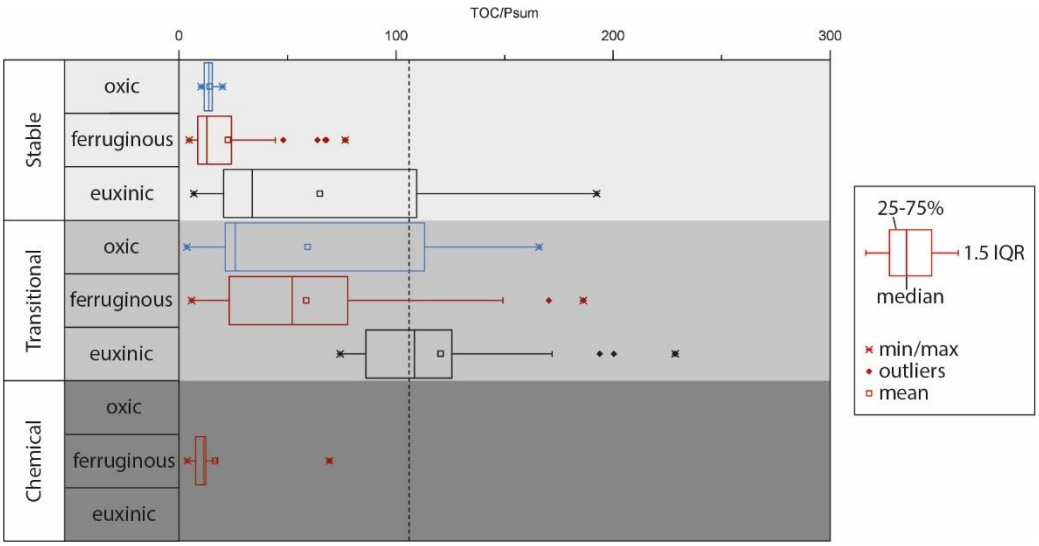

Figure 5.18 TOC/P_{sum} values for each zone and redox setting.

P_{sum} represents the maximum possible value of P_{reac} if all P_{cryst} was originally authigenic apatite. The dashed line represents the Redfield ratio.

5.5 Conclusions

This study used a newly revised P speciation method (Chapter 3), specifically designed for use with ancient sedimentary rocks, and is the first to describe P speciation in a Precambrian environment. The 1.88 – 1.83 billion-year old Animikie Basin provides a suite of samples which capture the transition from a fully ferruginous water column, to euxinic conditions along the continental margin and ferruginous deeper waters. By assessing the P speciation of these ancient sedimentary rocks, we were able to gain insight into the cycling of this key nutrient during the evolution of redox conditions in this region, which is thought to be representative of many continental margins during this period of Earth's history.

We suggest that fluctuations between ferruginous and euxinic conditions along continental margins during the development of euxinic wedges may have resulted in enhanced recycling of reactive P from the sediments to the overlying water column. The resulting benthic flux could have potentially stimulated primary productivity in these areas, leading to increased organic carbon burial, providing a positive feedback mechanism that would have helped establish

stable euxinic conditions in shallow coastal waters (Van Cappellen and Ingall, 1994, Handoh and Lenton, 2003). With ferruginous conditions prevailing in the deeper waters further offshore due to limited sulphate supply, P in these regions would be drawn down in line with or in excess of Redfield proportions, potentially limiting primary productivity to lower levels in more distal regions.

Once the redox structure of euxinic margins and ferruginous deep waters became established, the differing P cycling regimes for ferruginous and euxinic conditions became more distinct. Ferruginous deep waters resulted in enhanced draw down of P significantly in excess of the Redfield ratio, most likely originally in association with reduced and mixed valance Fe minerals such as vivianite (see Chapter 4), green rust (Zegeye et al., 2012) and magnetite, due to the high concentration of Fe(II) but also in association with Fe (oxyhrdroxides) through adsorption, therefore limiting surface water P concentrations, organic carbon burial and ultimately oxygen production. This sequestered Fe-bound P may have remained in more crystalline forms such as magnetite (as suggested by the presence of P_{mag} in these sedimentary rocks) or undergone sink switching to the P_{auth} pool during early diagenetic reactions on burial in the sediments (as indicated by the dominance of P_{reac} by P_{auth}). Petrographic analysis of these samples would improve our understanding of this magnetite-bound pool of P, helping to elucidate whether the associated P is primary or a result of re-oxidation and/or late stage adsorption processes. Stable euxinic conditions along continental margins, resulted in recycling of P back to the water column, although perhaps less substantial than during fluctuating redox conditions as the delivery of Fe-bound P to the sediments would be limited, and hence the benthic flux mainly consisted of P released from organic matter.

The extent of the euxinic margins would have had an impact on the net O_2 production associated with oceanic organic C burial, with elevated organic C burial along the eutrophic euxinic margins, and limited organic C burial in the more oligotrophic ferruginous deep waters offshore. The balance between these two regimes would be affected by many environmental changes, including fluctuations in the sulphate and highly reactive iron influxes to the

ocean (Poulton and Canfield, 2011, Canfield et al., 2008, Guilbaud et al., 2015). It is possible that the relative size of the euxinic margin and the ferruginous open oceans and their associated P and C regimes may have remained delicately poised, so as to keep atmospheric O_2 at low levels for a protracted period of time after the advent of oxygenic photosynthesis.

Chapter 6 Conclusions

6.1 Summary

6.1.1 Fe and P partitioning in ferruginous environments

Fe-bound P contributes a significant proportion of particulate P in the ferruginous water column of Lake La Cruz, whilst Fe minerals are predominantly unsulphidised solid phase Fe(II) and highly reactive Fe (oxyhydr)oxides, suggesting the Fe-bound P is likely to be a reduced Fe phosphate such as vivianite and P associated with the surface of Fe (oxyhydr)oxides. The varying proportions of the two main Fe mineral phases below the redoxcline indicates cycling of Fe through reduction and oxidation reactions and, as this also coincides with the zone where green and purple sulphur bacteria have previously been identified, this is likely to play a critical role in Fe and P cycling in the lake. During these redox reactions the mixed valance Fe mineral green rust could potentially be formed, which has a large capacity of P adsorption and could therefore play a significant role along with vivianite in water column P cycling.

Within the ferruginous sediments of the lake, a small amount of Fe sulphide minerals persist due to the low levels of SO_4^{2-} available, although they contribute a very low proportion of the Fe in the sediments and have very little influence on the interactions between Fe and P. Solid phase unsulphidised Fe(II) increases in dominance in the sediments whereas the highly reactive Fe (oxyhydr)oxides that were prevalent in the water column are almost completely reduced and only a small proportion of the more crystalline Fe oxides persist. P is still predominantly Fe-bound, with authigenic Ca-P and organic-bound P also contributing significant proportions. Due to the dominance of Fe(II) minerals over Fe(III) minerals and in light of evidence from the ferruginous lake Pavin, the sedimentary Fe-bound P is expected to be vivianite.

Ferruginous sediments overlain by ferruginous waters result in a substantial flux of dissolved Fe and P from the sediments into the water column, and this is considered likely to have a strong control on the particulates formed. In this

short (~20 m) water column, some of this dissolved P is likely to stimulate productivity, although this is rapidly consumed. However, when applying the knowledge gained from this modern system to the ferruginous oceans of the Precambrian, the differences in the physical environment must be considered. The vastly increased water depth of open oceans and even continental margins in comparison to the lake would probably cause Fe-phosphate mineral formation in the water column to limit the vertical extent of this flux, resulting in less P reaching the photic zone, hence exerting a strong control on primary production in oligotrophic ferruginous oceans.

6.1.2 P in ancient sediments

Use of the original SEDEX method for determining P speciation in modern sediments results in incomplete extraction of Fe minerals and any associated P from ancient sedimentary rocks, due to the presence of highly crystalline hematite and magnetite in these samples. The method has therefore been modified to rectify this with the insertion of two additional extractions which target these more crystalline Fe minerals that are prevalent in ancient sedimentary rocks but also in modern Fe-rich environments. Crystalline Fe oxides and magnetite are shown to contribute considerable pools of reactive P in ancient sedimentary rocks sourced from four different localities and in the modern Fe-rich sediments of the Gulfo Dulce. Magnetite-bound P, in particular, constitutes a significant proportion of reactive P in ferruginous environments which previously has not been identified and, as such, warrants further consideration in terms of its role in recording P cycling under such conditions.

Using this revised method to look at the ~1.8 Ga Animikie Basin has revealed that magnetite-bound P is an important pool in sediments formed in many depositional settings, particularly in chemical sediments and during periods of cycling between ferruginous and euxinic water column conditions. Authigenic Ca-P and crystalline apatite are the main contributors of sedimentary P across the basin and there are indications that there has been considerable recrystallization of P_{auth}, resulting in the transfer of reactive P to the P_{cryst} pool. This makes it difficult to distinguish P that was once reactive and potentially available for use during productivity from detrital P, and future work should focus on a way of determining this in ancient sediments. For the present, the

revised method developed here has enabled minimum and maximum estimates of reactive P for the Animikie basin sediments to be made and differences in P cycling between different redox settings to be identified.

Oscillations between euxinic and ferruginous conditions along the shelf slope resulted in decreased burial of reactive P and a substantial flux of dissolved P to the overlying water column. In the near-shore environments, this enhanced recycling of P could potentially have stimulated primary productivity, leading to increased organic carbon burial, thereby strengthening euxinic conditions where the supply of sulphate was sufficient. During stable redox circumstances, ferruginous conditions offshore caused significant retention of reactive P within the sediments relative to the euxinic conditions closer to the shore, which is most likely to have resulted in severely P-limited oligotrophic open oceans. Whilst the partitioning of reactive P in these ancient sedimentary rocks is predominantly as authigenic Ca-P (most likely CFA), the presence of magnetite-bound P in these rocks and the dominance of Fe-bound P in the analogous water column and sediments of the ferruginous Lake La Cruz, suggests the original drawdown of P was likely to have been in association with Fe minerals, which have since undergone sink switching to form the authigenic Ca-P present today. These conclusions are based on the minimum estimate of reactive P within these ancient sedimentary rocks; the retention of P under ferruginous conditions could be even greater when considering that some of the original reactive P may have transformed into fluorapatite during recrystallization processes, which is often assumed to be terrigenous in origin.

6.1.3 The influence of water column and sediment redox on primary productivity

By combining the P speciation data of the ~1.8 billion-year old Animikie Basin with the observations of Fe-P interactions in the ferruginous Lake La Cruz, an overarching theory of the influence depositional redox has on nutrient availability can be suggested. Where sulphate supply is sufficient to cause the water column to become euxinic, sulphidation of Fe minerals causes substantial amounts of P to be recycled from the sediments back to the water column, potentially causing surface waters to become eutrophic. In the ferruginous open oceans where nutrient delivery is negligible, P is drawn down

in association with Fe minerals (most likely to be reduced Fe phosphates such as vivianite or mixed valance phases such as green rusts and magnetite). During diagenesis, it is suggested that large proportions of this Fe-bound sedimentary P, are likely to undergo sink switching but that the P is retained within the sediments, maintaining oligotrophic conditions in the surface waters. Under Ferruginous conditions, where the nutrient supply is slightly higher and therefore rates of primary productivity are increased (e.g. closer to shore), organic matter degradation can result in significant fluxes of P back into the water column. This certainly has the potential to stimulate more productivity, but the process is highly modulated by Fe phosphate formation. This mineralogical control on P availability starts in the water column and its strength will vary in different localities according to the precise fluxes of Fe and P. Lake La Cruz is an analogue environment for this mesotrophic, intermediate situation, and provides a highly valuable natural laboratory for investigating a wide range of scenarios under ferruginous conditions.

6.2 Future Work

To fully understand Fe and P cycling and its direct influence on primary productivity in Lake La Cruz, a field campaign needs to focus on collection of both water column and sediment samples for the purpose of identifying the Fe and P mineral phases present. Sample collection, preservation and analysis during this campaign should be guided by previous studies where vivianite has been identified using X-ray techniques (e.g. Cosmidis et al., 2014, Egger et al., 2015, Rothe et al., 2014). Water column particulate organic matter concentrations should also be quantified, enabling TOC/P_{org} ratios in the water column to be determined. Sediment traps may be of particular use for this and would also provide information about the sedimentation rates of different types of particulate matter.

P speciation in a range of ancient sedimentary rocks spanning the Precambrian should be examined using the newly modified method presented here. This would provide a far more accurate and detailed view of P cycling through time than the previously used methods of assessing bulk P or P in BIFs. Attempts should be made to develop a way of determining the extent of authigenic

apatite recrystallization in a given ancient sedimentary rock, as this would vastly improve our estimates of reactive P burial. Petrographic observations and correlation with indicators of detrital influx, can identify whether recrystallization may have occurred but, at present, can not be used to quantify the extent of this process.

This work has highlighted the importance of reduced and mixed valance Fe minerals in the cycling of P under ferruginous conditions. The formation and subsequent transformations of these minerals under a variety of different conditions needs to be investigated in more detail with laboratory experiments, the results of which then need to be incorporated into the biogeochemical models used to study ancient environments.

Together, these suggested future studies could go a long way to improving our understanding of primary production and organic carbon burial during the Precambrian, and hence elucidate the mechanisms behind the evolution of atmospheric oxygen through this critical part of Earth’s history.

References

Ahn, J. H. & Buseck, P. R. 1990. Hematite Nanospheres of Possible Colloidal Origin from a Precambrian Banded Iron Formation. *Science,* 250**,** 111-113.

Albani, A. E., Bengtson, S., Canfield, D. E., Bekker, A., Macchiarelli, R., Mazurier, A., Hammarlund, E. U., Boulvais, P., Dupuy, J.-J., Fontaine, C., Fürsich, F. T., Gauthier-Lafaye, F., Janvier, P., Javaux, E., Ossa, F. O., Pierson-Wickmann, A.-C., Riboulleau, A., Sardini, P., Vachard, D., Whitehouse, M. & Meunier, A. 2010. Large colonial organisms with coordinated growth in oxygenated environments 2.1 Gyr ago. *Nature,* 466**,** 100-104.

Allwood, A. C., Walter, M. R., Kamber, B. S., Marshall, C. P. & Burch, I. W. 2006. Stromatolite reef from the Early Archaean era of Australia. *Nature,* 441**,** 714-718.

Anderson, L. A. & Sarmiento, J. L. 1994. Redfield Ratios of Remineralization Determined by Nutrient Data-Analysis. *Global Biogeochemical Cycles,* 8**,** 65-80.

Anderson, L. D., Delaney, M. L. & Faul, K. L. 2001. Carbon to phosphorus ratios in sediments: Implications for nutrient cycling. *Global Biogeochemical Cycles,* 15**,** 65-79.

Anderson, T. F. & Raiswell, R. 2004. Sources and mechanisms for the enrichment of highly reactive iron in euxinic Black Sea sediments. *American Journal of Science,* 304**,** 203-233.

Anschutz, P., Zhong, S., Sundby, B., Mucci, A. & Gobeil, C. 1998. Burial efficiency of phosphorus and the geochemistry of iron in continental margin sediments. *Limnology and Oceanography,* 43**,** 53-64.

Appelo, C. A. J., Parkhurst, D. L. & Post, V. E. A. 2014. Equations for calculating hydrogeochemical reactions of minerals and gases such as CO2 at high pressures and temperatures. *Geochimica et Cosmochimica Acta,* 125**,** 49-67.

Aspila, K. I., Agemian, H. & Chau, A. S. Y. 1976. A semi-automated method for the determination of inorganic, organic and total phosphate in sediments. *Analyst,* 101**,** 187-197.

Ayres, D. E. 1972. Genesis of Iron-bearing Minerals in Banded Iron Formation Mesobands in The Dales Gorge Member, Hamersley Group, Western Australia. *Economic Geology,* 67**,** 1214-1233.

Barron, V., Galvez, N., Hochella, M. F. & Torrent, J. 1997. Epitaxial overgrowth of goethite on hematite synthesized in phosphate

media: A scanning force and transmission electron microscopy study. *American Mineralogist,* 82**,** 1091-1100.

Bekker, A., Slack, J. F., Planavsky, N., Krapez, B., Hofmann, A., Konhauser, K. O. & Rouxel, O. J. 2010. Iron Formation: The Sedimentary Product of a Complex Interplay among Mantle, Tectonic, Oceanic, and Biospheric Processes. *Economic Geology,* 105**,** 467-508.

Berner, R. A. 1970. Sedimentary Pyrite Formation. *American Journal of Science,* 268**,** 1-&.

Berner, R. A. 1980. *Early Diagenesis: A Theoretical Approach,* New Jersey, USA, Princeton University Press.

Berner, R. A. 1981. A new geochemical classification of sedimentary environments. *Journal of Sedimentary Petrology,* 51**,** 359-365.

Berner, R. A., Beerling, D. J., Dudley, R., Robinson, J. M. & Wildman, R. A. 2003. Phanerozoic atmospheric oxygen. *Annual Review of Earth and Planetary Sciences,* 31**,** 105-134.

Berner, R. A. & Canfield, D. E. 1989. A new model for atmospheric oxygen over Phanerozoic time. *American Journal of Science,* 289**,** 333-361.

Berner, R. A. & Maasch, K. A. 1996. Chemical weathering and controls on atmospheric O_2 and CO_2: Fundamental principles were enunciated by J.J. Ebelmen in 1845. *Geochimica et Cosmochimica Acta,* 60**,** 1633-1637.

Berner, R. A. & Rao, J. L. 1994. Phosphorus in sediments of the Amazon River and estuary: Implications for the global flux of phosphorus to the sea. *Geochimica et Cosmochimica Acta,* 58**,** 2333-2339.

Beukes, N. J. & Gutzmer, J. 2008. Origin and Paleoenvironmental Significance of Major Iron Formations at the Archean-Paleoproterozoic Boundary. *In:* Hagemann, S., Rosière, C. A., Gutzmer, J. & Beukes, N. J. (eds.) *Banded Iron Formation-Related High-Grade Iron Ore.* Society of Economic Geologists.

Bjerrum, C. J. & Canfield, D. E. 2002. Ocean productivity before about 1.9 Gyr ago limited by phosphorus adsorption onto iron oxides. *Nature,* 417**,** 159-162.

Bocher, F., Gehin, A., Ruby, C., Ghanbaja, J., Abdelmoula, M. & Genin, J. M. R. 2004. Coprecipitation of Fe(II-III) hydroxycarbonate green rust stabilised by phosphate adsorption. *Solid State Sciences,* 6**,** 117-124.

Boudreau, B. P. 1997. Chapter 4. Constitutive Equations. *Diagenetic models and their implementation. Modelling transport and reactions in aquatic sediments.* Berlin: Springer.

Bowden, J. W., Nagarajah, S., Barrow, N. J., Posner, A. M. & Quirk, J. P. 1980. Describing the Adsorption of Phosphate, Citrate and Selenite on a Variable-Charge Mineral Surface. *Australian Journal of Soil Research,* 18**,** 49-60.

Boyle, R. A., Dahl, T. W., Dale, A. W., Shields-Zhou, G. A., Zhu, M., Brasier, M. D., Canfield, D. E. & Lenton, T. M. 2014. Stabilization of the coupled oxygen and phosphorus cycles by the evolution of bioturbation. *Nature Geoscience,* 7**,** 671-676.

Braterman, P. S., Cairnssmith, A. G. & Sloper, R. W. 1983. Photooxidation of Hydrated Fe^{2+} - Significance for Banded Iron Formations. *Nature,* 303**,** 163-164.

Brocks, J. J., Logan, G. A., Buick, R. & Summons, R. E. 1999. Archean molecular fossils and the early rise of eukaryotes. *Science,* 285**,** 1033-1036.

Bura-Nakic, E., Viollier, E., Jezequel, D., Thiam, A. & Ciglenecki, I. 2009. Reduced sulfur and iron species in anoxic water column of meromictic crater Lake Pavin (Massif Central, France). *Chemical Geology,* 266**,** 311-317.

Burdige, D. J. 1991. The kinetics of organic matter mineralization in anoxic marine sediments. *Journal of Marine Research,* 49**,** 727-761.

Busigny, V., Jézéquel, D., Cosmidis, J., Viollier, E., Benzerara, K., Planavsky, N. J., Albéric, P., Lebeau, O., Sarazin, G. & Michard, G. 2016. The Iron Wheel in Lac Pavin: Interaction with Phosphorus Cycle. *In:* Sime-Ngando, T., Boivin, P., Chapron, E., Jezequel, D. & Meybeck, M. (eds.) *Lake Pavin: History, geology, biogeochemistry, and sedimentology of a deep meromictic maar lake.* Cham: Springer International Publishing. 205-220.

Busigny, V., Planavsky, N. J., Jézéquel, D., Crowe, S., Louvat, P., Moureau, J., Viollier, E. & Lyons, T. W. 2014. Iron isotopes in an Archean ocean analogue. *Geochimica et Cosmochimica Acta*.

Camacho, A., Walter, X. A., Picazo, A. & Zopfi, J. 2017. Photoferrotrophy: Remains of an Ancient Photosynthesis in Modern Environments. *Frontiers in Microbiology,* 8.

Canfield, D. E. 1989. Reactive iron in marine sediments. *Geochimica et Cosmochimica Acta,* 53**,** 619-632.

Canfield, D. E. 1998. A new model for Proterozoic ocean chemistry. *Nature,* 396**,** 450-453.

Canfield, D. E. 2004. The evolution of the Earth surface sulfur reservoir. *American Journal of Science,* 304**,** 839-861.

Canfield, D. E. 2005. The early history of atmospheric oxygen: Homage to Robert A. Garrels. *Annual Review of Earth and Planetary Sciences,* 33**,** 1-36.

Canfield, D. E. 2014. *Oxygen: a four billion year history,* Oxfordshire, Princeton University Press.

Canfield, D. E., Farquhar, J. & Zerkle, A. L. 2010. High isotope fractionations during sulfate reduction in a low-sulfate euxinic ocean analog. *Geology,* 38**,** 415-418.

Canfield, D. E., Poulton, S. W., Knoll, A. H., Narbonne, G. M., Ross, G., Goldberg, T. & Strauss, H. 2008. Ferruginous conditions dominated later neoproterozoic deep-water chemistry. *Science,* 321**,** 949-952.

Canfield, D. E., Poulton, S. W. & Narbonne, G. M. 2007. Late-Neoproterozoic deep-ocean oxygenation and the rise of animal life. *Science,* 315**,** 92-95.

Canfield, D. E., Raiswell, R. & Bottrell, S. 1992. The Reactivity of Sedimentary Iron Minerals toward Sulfide. *American Journal of Science,* 292**,** 659-683.

Canfield, D. E., Raiswell, R., Westrich, J. T., Reaves, C. M. & Berner, R. A. 1986. The use of chromium reduction in the analysis of reduced inorganic sulfur in sediments and shales. *Chemical Geology,* 54**,** 149-155.

Canfield, D. E. & Thamdrup, B. 2009. Towards a consistent classification scheme for geochemical environments, or, why we wish the term 'suboxic' would go away. *Geobiology,* 7**,** 385-392.

Chien, S. H. & Black, C. A. 1976. Free-Energy of Formation of Carbonate Apatites in Some Phosphate Rocks. *Soil Science Society of America Journal,* 40**,** 234-239.

Cline, J. D. 1969. Spectrophotometric determination of hydrogen sulfide in natural waters. *Limnology and Oceanography,* 14**,** 454-458.

Cloud, P. 1972. WORKING MODEL OF PRIMITIVE EARTH. *American Journal of Science,* 272**,** 537-548.

Cloud, P. E. 1968. Atmospheric and Hydrospheric Evolution on Primitive Earth. *Science,* 160**,** 729-&.

Codispoti, L. A. 1989. Phosphorus vs. nitrogen limitation of new and export production. *In:* Berger, W. H., Smetacek, V. S. & Wefer, G. (eds.) *Productivity of the ocean: present and past.* New York: John Wiley and Sons. 377-394.

Colman, A. S. & Holland, H. D. 2000. The global diagenetic flux of phosphorus from marine sediments to the oceans: redox sensitivity and the control of atmospheric oxygen levels. *In:* Glenn, C. R., Lucas, J. & Prévôt-Lucas, L. (eds.) *Marine*

Authigenesis: from Global to Microbial. SEPM Spec. Pub. 53-75.

Conley, D. J., Humborg, C., Rahm, L., Savchuk, O. P. & Wulff, F. 2002. Hypoxia in the Baltic Sea and basin-scale changes in phosphorus biogeochemistry. *Environmental Science & Technology,* 36**,** 5315-5320.

Cornell, R. M. & Schwertmann, U. 1996. *The Iron Oxides: Structure, Properties, Reactions, Occurrence and Uses.,* Weinheim, Germany, VCH Publishers.

Cosmidis, J., Benzerara, K., Morin, G., Busigny, V., Lebeau, O., Jézéquel, D., Noël, V., Dublet, G. & Othmane, G. 2014. Biomineralization of iron-phosphates in the water column of Lake Pavin (Massif Central, France). *Geochimica et Cosmochimica Acta,* 126**,** 78-96.

Creveling, J. R., Johnston, D. T., Poulton, S. W., Kotrc, B., März, C., Schrag, D. P. & Knoll, A. H. 2014. Phosphorus sources for phosphatic Cambrian carbonates. *GSA Bulletin,* 126**,** 145-163.

Crowe, S. A., Dossing, L. N., Beukes, N. J., Bau, M., Kruger, S. J., Frei, R. & Canfield, D. E. 2013. Atmospheric oxygenation three billion years ago. *Nature,* 501**,** 535-+.

Crowe, S. A., Jones, C., Katsev, S., Magen, C., O'Neill, A. H., Sturm, A., Canfield, D. E., Haffner, G. D., Mucci, A., Sundby, B. & Fowle, D. A. 2008a. Photoferrotrophs thrive in an Archean Ocean analogue. *Proceedings of the National Academy of Sciences of the United States of America,* 105**,** 15938-15943.

Crowe, S. A., Maresca, J. A., Jones, C., Sturm, A., Henny, C., Fowle, D. A., Cox, R. P., Delong, E. F. & Canfield, D. E. 2014. Deep-water anoxygenic photosythesis in a ferruginous chemocline. *Geobiology,* 12**,** 322-339.

Crowe, S. A., O'Neill, A. H., Katsev, S., Hehanussa, P., Haffner, G. D., Sundby, B., Mucci, A. & Fowle, D. A. 2008b. The biogeochemistry of tropical lakes: A case study from Lake Matano, Indonesia. *Limnology and Oceanography,* 53**,** 319-331.

Czaja, A. D., Johnson, C. M., Beard, B. L., Roden, E. E., Li, W. Q. & Moorbath, S. 2013. Biological Fe oxidation controlled deposition of banded iron formation in the ca. 3770 Ma Isua Supracrustal Belt (West Greenland). *Earth and Planetary Science Letters,* 363**,** 192-203.

Dahl, T. W., Anbar, A. D., Gordon, G. W., Rosing, M. T., Frei, R. & Canfield, D. E. 2010. The behavior of molybdenum and its isotopes across the chemocline and in the sediments of

sulfidic Lake Cadagno, Switzerland. *Geochimica Et Cosmochimica Acta,* 74**,** 144-163.

Dahl, T. W., Canfield, D. E., Rosing, M. T., Frei, R. E., Gordon, G. W., Knoll, A. H. & Anbar, A. D. 2011. Molybdenum evidence for expansive sulfidic water masses in ~750 Ma oceans. *Earth and Planetary Science Letters,* 311**,** 264-274.

Delaney, M. L. 1998. Phosphorus accumulation in marine sediments and the oceanic phosphorus cycle. *Global Biogeochemical Cycles,* 12**,** 563-572.

Derry, L. A. 2015. Causes and consequences of mid-Proterozoic anoxia. *Geophysical Research Letters,* 42**,** 8538-8546.

Derry, L. A. & Jacobsen, S. B. 1990. The chemical evolution of Precambrian seawater: Evidence from REEs in banded iron formations. *Geochimica et Cosmochimica Acta,* 54**,** 2965-2977.

Dijkstra, N., Kraal, P., Kuypers, M. M. M., Schnetger, B. & Slomp, C. P. 2014. Are Iron-Phosphate Minerals a Sink for Phosphorus in Anoxic Black Sea Sediments? *Plos One,* 9.

Ebelman, J. J. 1845. Sur les produits de la décomposition des espèces minérales de la famille des silicates. *Annales des Mines,* 7**,** 3-66.

Egger, M., Jilbert, T., Behrends, T., Rivard, C. & Slomp, C. P. 2015. Vivianite is a major sink for phosphorus in methanogenic coastal surface sediments. *Geochimica et Cosmochimica Acta,* 169**,** 217-235.

Ehrenreich, A. & Widdel, F. 1994. Anaerobic Oxidation of Ferrous Iron by Purple Bacteria, a New-Type of Phototrophic Metabolism. *Applied and Environmental Microbiology,* 60**,** 4517-4526.

Eijsink, L. M., Krom, M. D. & Herut, B. 2000. Speciation and burial flux of phosphorus in the surface sediments of the eastern Mediterranean. *American Journal of Science,* 300**,** 483-503.

Faul, K. L., Paytan, A. & Delaney, M. L. 2005. Phosphorus distribution in sinking oceanic particulate matter. *Marine Chemistry,* 97**,** 307-333.

Filippelli, G. M. 1997a. Controls on phosphorus concentration and accumulation in oceanic sediments. *Marine Geology,* 139**,** 231-240.

Filippelli, G. M. 1997b. Intensification of the Asian monsoon and a chemical weathering event in the late Miocene early Pliocene: Implications for late Neogene climate change. *Geology,* 25**,** 27-30.

Fralick, P., Davis, D. W. & Kissin, S. A. 2002. The age of the Gunflint Formation, Ontario, Canada: single zircon U-Pb age

determinations from reworked volcanic ash. *Canadian Journal of Earth Sciences,* 39**,** 1085-1091.

French, B. M. 1971. Stability Relations of Siderite ($FeCO_3$) in System Fe-C-O. *American Journal of Science,* 271**,** 37-&.

French, B. M. & Rosenberg, P. E. 1965. Siderite ($FeCO_3$): Thermal Decomposition in Equilibrium with Graphite. *Science,* 147**,** 1283-1284.

Froelich, P. N., Arthur, M. A., Burnett, W. C., Deakin, M., Hensley, V., Jahnke, R., Kaul, L., Kim, K. H., Roe, K., Soutar, A. & Vathakanon, C. 1988. Early diagenesis of organic matter in Peru continental margin sediments: Phosphorite precipitation. *Marine Geology,* 80**,** 309-343.

Froelich, P. N., Bender, M. L., Luedtke, N. A., Heath, G. R. & DeVries, T. 1982. The marine phosphorus cycle. *American Journal of Science,* 282**,** 474-511.

Froelich, P. N., Klinkhammer, G. P., Bender, M. L., Luedtke, N. A., Heath, G. R., Cullen, D., Dauphin, P., Hammond, D., Hartman, B. & Maynard, V. 1979. Early Oxidation of Organic-Matter in Pelagic Sediments of the Eastern Equatorial Atlantic - Suboxic Diagenesis. *Geochimica Et Cosmochimica Acta,* 43**,** 1075-1090.

Gaines, R. R., Hammarlund, E. U., Hou, X. G., Qi, C. S., Gabbott, S. E., Zhao, Y. L., Peng, J. & Canfield, D. E. 2012. Mechanism for Burgess Shale-type preservation. *Proceedings of the National Academy of Sciences of the United States of America,* 109**,** 5180-5184.

Gallagher, P. K. & Warne, S. S. 1981. Thermomagnetometry and Thermal-Decomposition of Siderite. *Thermochimica Acta,* 43**,** 253-267.

Galvez, N., Barron, V. & Torrent, J. 1999. Effect of phosphate on the crystallization of hematite, goethite, and lepidocrocite from ferrihydrite. *Clays and Clay Minerals,* 47**,** 304-311.

Garrels, R. M. & Perry, E. A. 1974. Cycling of carbon, sulfur and oxygen through geologic time. *In:* Goldberg, E. D. (ed.) *The Sea, vol. 5.* New York: Wiley Intersci. 303-336.

Grotzinger, J. P. & Kasting, J. F. 1993. New Constraints on Precambrian Ocean Composition. *Journal of Geology,* 101**,** 235-243.

Guilbaud, R., Poulton, S. W., Butterfield, N. J., Zhu, M. & Shields-Zhou, G. A. 2015. A global transition to ferruginous conditions in the early Neoproterozoic oceans. *Nature Geoscience,* 8**,** 466-470.

Guilbaud, R., White, M. L. & Poulton, S. W. 2013. Surface charge and growth of sulphate and carbonate green rust in aqueous media. *Geochimica Et Cosmochimica Acta,* 108**,** 141-153.

Halama, M., Swanner, E. D., Konhauser, K. O. & Kappler, A. 2016. Evaluation of siderite and magnetite formation in BIFs by pressure-temperature experiments of Fe(III) minerals and microbial biomass. *Earth and Planetary Science Letters,* 450**,** 243-253.

Halevy, I., Alesker, M., Schuster, E. M., Popovitz-Biro, R. & Feldman, Y. 2017. A key role for green rust in the Precambrian oceans and the genesis of iron formations. *Nature Geoscience,* 10**,** 135-139.

Hansen, H. C. B. & Poulsen, I. F. 1999. Interaction of synthetic sulphate "Green rust" with phosphate and the crystallization of vivianite. *Clays and Clay Minerals,* 47**,** 312-318.

Harder, H. 1978. Synthesis of Iron Layer Silicate Minerals under Natural Conditions. *Clays and Clay Minerals,* 26**,** 65-72.

Heising, S., Richter, L., Ludwig, W. & Schink, B. 1999. Chlorobium ferrooxidans sp nov., a phototrophic green sulfur bacterium that oxidizes ferrous iron in coculture with a "Geospirillum" sp strain. *Archives of Microbiology,* 172**,** 116-124.

Hofmann, H. J., Grey, K., Hickman, A. H. & Thorpe, R. I. 1999. Origin of 3.45 Ga coniform stromatolites in Warrawoona Group, Western Australia. *Geological Society of America Bulletin,* 111**,** 1256-1262.

Holland, H. D. 1978. *The chemistry of the atmosphere and oceans,* New York, John Wiley and Sons.

Holland, H. D. 1984. *The Chemical Evolution of the Atmosphere nad Oceans,* Princeton New Jersey, Princeton University Press.

Holland, H. D. 2002. Volcanic gases, black smokers, and the Great Oxidation Event. *Geochimica Et Cosmochimica Acta,* 66**,** 3811-3826.

Howarth, M. K. 1962. The Jet Rock Series and the Alum Shale Series of the Yorkshire coast. *Proceedings of the Yorkshire Geological and Polytechnic Society,* 33**,** 381.

Huang, Y., Wang, C. & Chen, X. 2007. Response of reactive phosphorus burial to the sedimentary transition from cretaceous black shales to oceanic red beds in southern tibet. *Acta Geologica Sinica - English Edition,* 81**,** 1012-1018.

Ingall, E. & Jahnke, R. 1994. Evidence for enhanced phosphorus regeneration from marine sediments overlain by oxygen depleted waters. *Geochimica et Cosmochimica Acta,* 58**,** 2571-2575.

Ingall, E. & Jahnke, R. 1997. Influence of water-column anoxia on the elemental fractionation of carbon and phosphorus during sediment diagenesis. *Marine Geology,* 139**,** 219-229.

Ingall, E. D., Bustin, R. M. & Van Cappellen, P. 1993. Influence of water column anoxia on the burial and preservation of carbon and phosphorus in marine shales. *Geochimica et Cosmochimica Acta,* 57**,** 303-316.

Ingall, E. D. & Van Cappellen, P. 1990. Relation between Sedimentation-Rate and Burial of Organic Phosphorus and Organic-Carbon in Marine-Sediments. *Geochimica Et Cosmochimica Acta,* 54**,** 373-386.

Isley, A. E. & Abbott, D. H. 1999. Plume-related mafic volcanism and the deposition of banded iron formation. *Journal of Geophysical Research-Solid Earth,* 104**,** 15461-15477.

Jahnke, R. A. 1984. The Synthesis and Solubility of Carbonate Fluorapatite. *American Journal of Science,* 284**,** 58-78.

Jahnke, R. A. 1996. The global ocean flux of particulate organic carbon: Areal distribution and magnitude. *Global Biogeochemical Cycles,* 10**,** 71-88.

Jensen, H. S., Mortensen, P. B., Andersen, F. O., Rasmussen, E. & Jensen, A. 1995. Phosphorus cycling in a coastal marine sediment, Aarhus Bay, Denmark. *Limnology and Oceanography,* 40**,** 908-917.

Jensen, H. S. & Thamdrup, B. 1993. Iron-Bound Phosphorus in Marine-Sediments as Measured by Bicarbonate-Dithionite Extraction. *Hydrobiologia,* 253**,** 47-59.

Johnson, C. M., Beard, B. L., Klein, C., Beukes, N. J. & Roden, E. E. 2008. Iron isotopes constrain biologic and abiologic processes in banded iron formation genesis. *Geochimica Et Cosmochimica Acta,* 72**,** 151-169.

Johnston, D. T., Poulton, S. W., Dehler, C., Porter, S., Husson, J., Canfield, D. E. & Knoll, A. H. 2010. An emerging picture of Neoproterozoic ocean chemistry: Insights from the Chuar Group, Grand Canyon, USA. *Earth and Planetary Science Letters,* 290**,** 64-73.

Johnston, D. T., Poulton, S. W., Goldberg, T., Sergeev, V. N., Podkovyrov, V., Vorob'eva, N. G., Bekker, A. & Knoll, A. H. 2012. Late Ediacaran redox stability and metazoan evolution. *Earth and Planetary Science Letters,* 335**,** 25-35.

Julia, R., Burjachs, F., Dasi, M. J., Mezquita, F., Miracle, M. R., Roca, J. R., Seret, G. & Vicente, E. 1998. Meromixis origin and recent trophic evolution in the Spanish mountain lake La Cruz. *Aquatic Sciences,* 60**,** 279-299.

Kappler, A., Pasquero, C., Konhauser, K. O. & Newman, D. K. 2005. Deposition of banded iron formations by anoxygenic phototrophic Fe(II)-oxidizing bacteria. *Geology,* 33**,** 865-868.

Kaufman, A. J., Hayes, J. M. & Klein, C. 1990. Primary and Diagenetic Controls of Isotopic Compositions of Iron-Formation Carbonates. *Geochimica Et Cosmochimica Acta,* 54**,** 3461-3473.

Kendall, B., Gordon, G. W., Poulton, S. W. & Anbar, A. D. 2011. Molybdenum isotope constraints on the extent of late Paleoproterozoic ocean euxinia. *Earth and Planetary Science Letters,* 307**,** 450-460.

Kendall, B., Reinhard, C. T., Lyons, T., Kaufman, A. J., Poulton, S. W. & Anbar, A. D. 2010. Pervasive oxygenation along late Archaean ocean margins. *Nature Geoscience,* 3**,** 647-652.

Kirschvink, J. L. & Kopp, R. E. 2008. Palaeoproterozoic ice houses and the evolution of oxygen-mediating enzymes: the case for a late origin of photosystem II. *Philosophical Transactions of the Royal Society B-Biological Sciences,* 363**,** 2755-2765.

Klein, C. 2005. Some Precambrian banded iron-formations (BIFs) from around the world: Their age, geologic setting, mineralogy, metamorphism, geochemistry, and origin. *American Mineralogist,* 90**,** 1473-1499.

Koeksoy, E., Halama, M., Konhauser, K. O. & Kappler, A. 2016. Using modern ferruginous habitats to interpret Precambrian banded iron formation deposition. *International Journal of Astrobiology,* 15**,** 205-217.

Kohler, I., Konhauser, K. O., Papineau, D., Bekker, A. & Kappler, A. 2013. Biological carbon precursor to diagenetic siderite with spherical structures in iron formations. *Nature Communications,* 4.

Konhauser, K. O., Amskold, L., Lalonde, S. V., Posth, N. R., Kappler, A. & Anbar, A. 2007a. Decoupling photochemical Fe(II) oxidation from shallow-water BIF deposition. *Earth and Planetary Science Letters,* 258**,** 87-100.

Konhauser, K. O., Hamade, T., Raiswell, R., Morris, R. C., Ferris, F. G., Southam, G. & Canfield, D. E. 2002. Could bacteria have formed the Precambrian banded iron formations? *Geology,* 30**,** 1079-1082.

Konhauser, K. O., Lalonde, S. V., Amskold, L. & Holland, H. D. 2007b. Was there really an Archean phosphate crisis? *Science,* 315**,** 1234.

Konhauser, K. O., Newman, D. K. & Kappler, A. 2005. The potential significance of microbial Fe(III) reduction during deposition of Precambrian banded iron formations. *Geobiology,* 3**,** 167-177.

Konhauser, K. O., Pecoits, E., Lalonde, S. V., Papineau, D., Nisbet, E. G., Barley, M. E., Arndt, N. T., Zahnle, K. & Kamber, B. S. 2009. Oceanic Nickel depletion and a methanogen famine before the Great Oxidation Event. *Geochimica Et Cosmochimica Acta,* 73**,** A678-A678.

Konhauser, K. O., Planaysky, N. J., Hardisty, D. S., Robbins, L. J., Warchola, T. J., Haugaard, R., Lalonde, S. V., Partin, C. A., Oonk, P. B. H., Tsikos, H., Lyons, T. W., Bekker, A. & Johnson, C. M. 2017. Iron formations: A global record of Neoarchaean to Palaeoproterozoic environmental history. *Earth-Science Reviews,* 172**,** 140-177.

Koroleff, F. 1976. Determination of Nutrients. *In:* Grasshoff, K. E. A. (ed.) *Methods of seawater analysis.* 2nd ed.: Verlag-Chimie. 117-156.

Kraal, P., Bostick, B. C., Behrends, T., Reichart, G.-J. & Slomp, C. P. 2015. Characterization of phosphorus species in sediments from the Arabian Sea oxygen minimum zone: Combining sequential extractions and X-ray spectroscopy. *Marine Chemistry,* 168**,** 1-8.

Kraal, P., Dijkstra, N., Behrends, T. & Slomp, C. P. 2017. Phosphorus burial in sediments of the sulfidic deep Black Sea: Key roles for adsorption by calcium carbonate and apatite authigenesis. *Geochimica Et Cosmochimica Acta,* 204**,** 140-158.

Kraal, P., Slomp, C. P., Forster, A. & Kuypers, M. M. M. 2010. Phosphorus cycling from the margin to abyssal depths in the proto-Atlantic during oceanic anoxic event 2. *Palaeogeography, Palaeoclimatology, Palaeoecology,* 295**,** 42-54.

Krom, M. D. & Berner, R. A. 1981. The Diagenesis of Phosphorus in a Nearshore Marine Sediment. *Geochimica Et Cosmochimica Acta,* 45**,** 207-216.

Kump, L. R. & Seyfried, W. E. 2005. Hydrothermal Fe fluxes during the Precambrian: Effect of low oceanic sulfate concentrations and low hydrostatic pressure on the composition of black smokers. *Earth and Planetary Science Letters,* 235**,** 654-662.

LaBerge, G. L. 1964. Development of magnetite in iron formations of the Lake Superior region. *Economic Geology,* 59**,** 1313-1342.

Laliberté, M. 2009. A Model for Calculating the Heat Capacity of Aqueous Solutions, with Updated Density and Viscosity Data. *Journal of Chemical & Engineering Data,* 54**,** 1725-1760.

Lebo, M. E. 1991. Particle-Bound Phosphorus Along an Urbanized Coastal-Plain Estuary. *Marine Chemistry,* 34**,** 225-246.

Lenton, T. M., Boyle, R. A., Poulton, S. W., Shields-Zhou, G. A. & Butterfield, N. J. 2014. Co-evolution of eukaryotes and ocean oxygenation in the Neoproterozoic era. *Nature Geoscience,* 7**,** 257-265.

Li, C., Love, G. D., Lyons, T. W., Fike, D. A., Sessions, A. L. & Chu, X. L. 2010. A Stratified Redox Model for the Ediacaran Ocean. *Science,* 328**,** 80-83.

Li, C., Planavsky, N. J., Love, G. D., Reinhard, C. T., Hardisty, D., Feng, L. J., Bates, S. M., Huang, J., Zhang, Q. R., Chu, X. L. & Lyons, T. W. 2015a. Marine redox conditions in the middle Proterozoic ocean and isotopic constraints on authigenic carbonate formation: Insights from the Chuanlinggou Formation, Yanshan Basin, North China. *Geochimica et Cosmochimica Acta,* 150**,** 90-105.

Li, P., Cui, W. Y. & Bai, H. L. 2013a. An approach to reduce the antiferromagnetic coupling of antiphase boundaries in half-metallic magnetite films. *Journal of Applied Physics,* 114.

Li, T. J., Huang, C. C., Ruan, P. W., Chuang, K. Y., Huang, K. J., Shieh, D. B. & Yeh, C. S. 2013b. In vivo anti-cancer efficacy of magnetite nanocrystal-based system using locoregional hyperthermia combined with 5-fluorouracil chemotherapy. *Biomaterials,* 34**,** 7873-7883.

Li, W. Q., Beard, B. L. & Johnson, C. M. 2015b. Biologically recycled continental iron is a major component in banded iron formations. *Proceedings of the National Academy of Sciences of the United States of America,* 112**,** 8193-8198.

Li, Y.-L., Konhauser, K. O. & Zhai, M. 2017. The formation of magnetite in the early Archean oceans. *Earth and Planetary Science Letters,* 466**,** 103-114.

Lliros, M., Garcia-Armisen, T., Darchambeau, F., Morana, C., Triado-Margarit, X., Inceoglu, O., Borrego, C. M., Bouillon, S., Servais, P., Borges, A. V., Descy, J. P., Canfield, D. E. & Crowe, S. A. 2015. Pelagic photoferrotrophy and iron cycling in a modern ferruginous basin. *Scientific Reports,* 5.

Lucente, M. E. & Morey, G. B. 1983. Stratigraphy and Sedimentology of the Lower Proterozoic Virginia Formation, Northern Minnesota. *Report of investigations.* Minnesota Geological Survey, University of Minnesota. 28, 28.

Lucotte, M. & Danglejan, B. 1983. Forms of Phosphorus and Phosphorus Iron Relationships in the Suspended Matter of the St-Lawrence-Estuary. *Canadian Journal of Earth Sciences,* 20**,** 1880-1890.

Luff, R. & Moll, A. 2004. Seasonal dynamics of the North Sea sediments using a three-dimensional coupled sediment-water model system. *Continental Shelf Research,* 24**,** 1099-1127.

Lukkari, K., Leivuori, M., Vallius, H. & Kotilainen, A. 2009. The chemical character and burial of phosphorus in shallow coastal sediments in the northeastern Baltic Sea. *Biogeochemistry,* 94**,** 141-162.

Lyons, T. W., Reinhard, C. T. & Planavsky, N. J. 2014. The rise of oxygen in Earth's early ocean and atmosphere. *Nature,* 506**,** 307-315.

Lyons, T. W. & Severmann, S. 2006. A critical look at iron paleoredox proxies: New insights from modern euxinic marine basins. *Geochimica et Cosmochimica Acta,* 70**,** 5698-5722.

Maric, M. & Fralick, P. W. 2005. Sedimentology of the Rove and Virginia Formations and their tectonic significance. *Institute on Lake Superior Geology,* 51**,** 41-42.

Martens, C. S., Berner, R. A. & Rosenfeld, J. K. 1978. Interstitial water chemistry of anoxic Long Island Sound sediments. 2. Nutrient regeneration and phosphate removal 1. *Limnology and Oceanography,* 23**,** 605-617.

März, C., Poulton, S. W., Beckmann, B., Kuster, K., Wagner, T. & Kasten, S. 2008. Redox sensitivity of P cycling during marine black shale formation: Dynamics of sulfidic and anoxic, non-sulfidic bottom waters. *Geochimica et Cosmochimica Acta,* 72**,** 3703-3717.

Maslov, A. V., Grazhdankin, D. V., Podkovyrov, V. N., Ronkin, Y. L. & Lepikhina, O. P. 2008. Composition of sediment provenances and patterns in geological history of the Late Vendian Mezen Basin. *Lithology and Mineral Resources,* 43**,** 260-280.

Matijević, S., Kušpilić, G., Kljaković-Gašpić, Z. & Bogner, D. 2008. Impact of fish farming on the distribution of phosphorus in sediments in the middle Adriatic area. *Marine Pollution Bulletin,* 56**,** 535-548.

McParland, E., Benitez-Nelson, C. R., Taylor, G. T., Thunell, R., Rollings, A. & Lorenzoni, L. 2015. Cycling of suspended particulate phosphorus in the redoxcline of the Cariaco Basin. *Marine Chemistry,* 176**,** 64-74.

Meng, Q. R., Wei, H. H., Qu, Y. Q. & Ma, S. X. 2011. Stratigraphic and sedimentary records of the rift to drift evolution of the northern North China craton at the Paleo- to Mesoproterozoic transition. *Gondwana Research,* 20**,** 205-218.

Meyer, K. M. & Kump, L. R. 2008. Oceanic euxinia in Earth history: Causes and consequences. *Annual Review of Earth and Planetary Sciences,* 36**,** 251-288.

Milesi, V., Guyot, F., Brunet, F., Richard, L., Recham, N., Benedetti, M., Dairou, J. & Prinzhofer, A. 2015. Formation of CO_2, H_2 and condensed carbon from siderite dissolution in the 200-300°C range and at 50 MPa. *Geochimica Et Cosmochimica Acta,* 154**,** 201-211.

Miracle, M. R., Vicente, E. & Pedros-Alio, C. 1992. Biological studies of Spanish meromictic and stratified karstic lakes. *Limnetica,* 8**,** 59-77.

Morey, G. B. 1973. Stratigraphic framework of Middle Proterozoic rocks in Minnesota. *In:* Young, G. M. (ed.) *Huronian Stratigraphy and Sedimentation: Geological Association of Canada Special Paper 12.* Pierre Des Marais. 211-249.

Mort, H. P., Adatte, T., Föllmi, K. B., Keller, G., Steinmann, P., Matera, V., Berner, Z. & Stüben, D. 2007. Phosphorus and the roles of productivity and nutrient recycling during oceanic anoxic event 2. *Geology,* 35**,** 483-486.

Mort, H. P., Adatte, T., Keller, G., Bartels, D., Föllmi, K. B., Steinmann, P., Berner, Z. & Chellai, E. H. 2008. Organic carbon deposition and phosphorus accumulation during Oceanic Anoxic Event 2 in Tarfaya, Morocco. *Cretaceous Research,* 29**,** 1008-1023.

Mort, H. P., Slomp, C. P., Gustafsson, B. G. & Andersen, T. J. 2010. Phosphorus recycling and burial in Baltic Sea sediments with contrasting redox conditions. *Geochimica Et Cosmochimica Acta,* 74**,** 1350-1362.

Murphy, J. & Riley, J. P. 1962. A modified single solution method for determination of phosphate in natural waters. *Analytica Chimica Acta,* 26**,** 31-&.

Ojakangas, R. W. 1983. Tidal deposits in the early Proterozoic basin of the Lake Superior region - The Palms and the Pokegama Formations: Evidence for subtidal-shelf deposition of Superior-type banded iron-formation. *In:* Medaris, J. L. G. (ed.). Geological Society of America Memoir 160. 49-66.

Parfitt, R. L. & Russell, J. D. 1977. Adsorption on Hydrous Oxides .4. Mechanisms of Adsorption of Various Ions on Goethite. *Journal of Soil Science,* 28**,** 297-305.

Partin, C. A., Bekker, A., Planavsky, N. J., Scott, C. T., Gill, B. C., Li, C., Podkovyrov, V., Maslov, A., Konhauser, K. O., Lalonde, S. V., Love, G. D., Poulton, S. W. & Lyons, T. W. 2013. Large-scale fluctuations in Precambrian atmospheric and oceanic

oxygen levels from the record of U in shales. *Earth and Planetary Science Letters,* 369**,** 284-293.

Perry, E. C., Tan, F. C. & Morey, G. B. 1973. Geology and Stable Isotope Geochemistry of Biwabik Iron Formation, Northern Minnesota. *Economic Geology,* 68**,** 1110-1125.

Planavsky, N. J., Asael, D., Hofmann, A., Reinhard, C. T., Lalonde, S. V., Knudsen, A., Wang, X., Ossa Ossa, F., Pecoits, E., Smith, A. J. B., Beukes, N. J., Bekker, A., Johnson, T. M., Konhauser, K. O., Lyons, T. W. & Rouxel, O. J. 2014a. Evidence for oxygenic photosynthesis half a billion years before the Great Oxidation Event. *Nature Geosci,* 7**,** 283-286.

Planavsky, N. J., McGoldrick, P., Scott, C. T., Li, C., Reinhard, C. T., Kelly, A. E., Chu, X. L., Bekker, A., Love, G. D. & Lyons, T. W. 2011. Widespread iron-rich conditions in the mid-Proterozoic ocean. *Nature,* 477**,** 448-451.

Planavsky, N. J., Reinhard, C. T., Wang, X., Thomson, D., McGoldrick, P., Rainbird, R. H., Johnson, T., Fischer, W. W. & Lyons, T. W. 2014b. Low Mid-Proterozoic atmospheric oxygen levels and the delayed rise of animals. *Science,* 346**,** 635-638.

Planavsky, N. J., Rouxel, O. J., Bekker, A., Lalonde, S. V., Konhauser, K. O., Reinhard, C. T. & Lyons, T. W. 2010. The evolution of the marine phosphate reservoir. *Nature,* 467**,** 1088-1090.

Posth, N. R., Köhler, I., D. Swanner, E., Schröder, C., Wellmann, E., Binder, B., Konhauser, K. O., Neumann, U., Berthold, C., Nowak, M. & Kappler, A. 2013. Simulating Precambrian banded iron formation diagenesis. *Chemical Geology,* 362**,** 66-73.

Poulton, S. W. 2017. BIOGEOCHEMISTRY Early phosphorus redigested. *Nature Geoscience,* 10**,** 75-76.

Poulton, S. W. & Canfield, D. E. 2005. Development of a sequential extraction procedure for iron: implications for iron partitioning in continentally derived particulates. *Chemical Geology,* 214**,** 209-221.

Poulton, S. W. & Canfield, D. E. 2006. Co-diagenesis of iron and phosphorus in hydrothermal sediments from the southern East Pacific Rise: Implications for the evaluation of paleoseawater phosphate concentrations. *Geochimica et Cosmochimica Acta,* 70**,** 5883-5898.

Poulton, S. W. & Canfield, D. E. 2011. Ferruginous conditions: A dominant feature of the ocean through Earth's history. *Elements,* 7**,** 107-112.

Poulton, S. W., Fralick, P. W. & Canfield, D. E. 2004a. The transition to a sulphidic ocean ~1.84 billion years ago. *Nature,* 431**,** 173-177.

Poulton, S. W., Fralick, P. W. & Canfield, D. E. 2010. Spatial variability in oceanic redox structure 1.8 billion years ago. *Nature Geoscience,* 3**,** 486-490.

Poulton, S. W., Krom, M. D. & Raiswell, R. 2004b. A revised scheme for the reactivity of iron (oxyhydr)oxide minerals towards dissolved sulfide. *Geochimica et Cosmochimica Acta,* 68**,** 3703-3715.

Poulton, S. W. & Raiswell, R. 2002. The low-temperature geochemical cycle of iron: From continental fluxes to marine sediment deposition. *American Journal of Science,* 302**,** 774-805.

Raiswell, R. 2006. An evaluation of diagenetic recycling as a source of iron for banded iron formations. *Evolution of Early Earth's Atmosphere, Hydrosphere, and Biosphere: Constraints from Ore Deposits,* 198**,** 223-238.

Raiswell, R. & Canfield, D. E. 1998. Sources of iron for pyrite formation in marine sediments. *American Journal of Science,* 298**,** 219-245.

Raiswell, R. & Canfield, D. E. 2012a. The Iron Biogeochemical Cycle Past and Present. *Geochemical Perspectives,* 1**,** 1-220.

Raiswell, R. & Canfield, D. E. 2012b. Section 9. The History of the Iron Biogeochemical Cycle. *Geochemical Perspectives,* 1**,** 115-149.

Raiswell, R., Canfield, D. E. & Berner, R. A. 1994. A comparison of iron extraction methods for the determination of degree of pyritisation and the recognition of iron-limited pyrite formation. *Chemical Geology,* 111**,** 101-110.

Raiswell, R., Newton, R. & Wignall, P. B. 2001. An indicator of water-column anoxia: Resolution of biofacies variations in the Kimmeridge Clay (Upper Jurassic, UK). *Journal of Sedimentary Research,* 71**,** 286-294.

Rasmussen, B., Krapež, B. & Meier, D. B. 2014a. Replacement origin for hematite in 2.5 Ga banded iron formation: Evidence for postdepositional oxidation of iron-bearing minerals. *Geological Society of America Bulletin,* 126**,** 438-446.

Rasmussen, B., Krapez, B. & Muhling, J. R. 2014b. Hematite replacement of iron-bearing precursor sediments in the 3.46-b.y.-old Marble Bar Chert, Pilbara craton, Australia. *Geological Society of America Bulletin,* 126**,** 1245-1258.

Rasmussen, B., Krapez, B., Muhling, J. R. & Suvorova, A. 2015. Precipitation of iron silicate nanoparticles in early

Precambrian oceans marks Earth's first iron age. *Geology,* 43**,** 303-306.

Rasmussen, B. & Muhling, J. R. 2018. Making magnetite late again: Evidence for widespread magnetite growth by thermal decomposition of siderite in Hamersley banded iron formations. *Precambrian Research,* 306**,** 64-93.

Rasmussen, B., Muhling, J. R., Suvorova, A. & Krapez, B. 2016. Dust to dust: Evidence for the formation of "primary" hematite dust in banded iron formations via oxidation of iron silicate nanoparticles. *Precambrian Research,* 284**,** 49-63.

Redfield, A. C. 1934. *In:* Daniel, R. J. (ed.) *James Johnston Memorial Volume.* University Press of Liverpool. 176-792.

Redfield, A. C. 1958. The biological control of chemical factors in the environment. *American Scientist,* 46**,** 230A, 205-221.

Reinhard, C. T., Planavsky, N. J., Gill, B. C., Ozaki, K., Robbins, L. J., Lyons, T. W., Fischer, W. W., Wang, C., Cole, D. B. & Konhauser, K. O. 2017. Evolution of the global phosphorus cycle. *Nature,* 541**,** 386-389.

Reinhard, C. T., Planavsky, N. J., Robbins, L. J., Partin, C. A., Gill, B. C., Lalonde, S. V., Bekker, A., Konhauser, K. O. & Lyons, T. W. 2013. Proterozoic ocean redox and biogeochemical stasis. *Proceedings of the National Academy of Sciences,* 110**,** 5357-5362.

Reinhard, C. T., Raiswell, R., Scott, C., Anbar, A. D. & Lyons, T. W. 2009. A Late Archean Sulfidic Sea Stimulated by Early Oxidative Weathering of the Continents. *Science,* 326**,** 713-716.

Roden, E. & Edmonds, J. 1997. Phosphate mobilization in iron-rich anaerobic sediments: microbial Fe (III) oxide reduction versus iron-sulfide formation. *Archiv für Hydrobiologie,* 139**,** 347-378.

Rodrigo, M. A., Miracle, M. R. & Vicente, E. 2001. The meromictic Lake La Cruz (Central Spain). Patterns of stratification. *Aquatic Sciences,* 63**,** 406-416.

Rodrigo, M. A., Vicente, E. & Miracle, M. R. 2000. The role of light and concentration gradients in the vertical stratification and seasonal development of phototrophic bacteria in a meromictic lake. *Archiv Fur Hydrobiologie,* 148**,** 533-548.

Romero-Viana, L., Julia, R., Camacho, A., Vicente, E. & Miracle, M. R. 2008. Climate signal in varve thickness: Lake La Cruz (Spain), a case study. *Journal of Paleolimnology,* 40**,** 703-714.

Romero-Viana, L., Keely, B. J., Camacho, A., Vicente, E. & Miracle, M. R. 2010. Primary production in Lake La Cruz (Spain) over the last four centuries: reconstruction based on sedimentary

signal of photosynthetic pigments. *Journal of Paleolimnology,* 43**,** 771-786.

Romero, L., Camacho, A., Vicente, E. & Miracle, M. R. 2006. Sedimentation patterns of photosynthetic bacteria based on pigment markers in meromictic Lake La Cruz (Spain): paleolimnological implications. *Journal of Paleolimnology,* 35**,** 167-177.

Rosing, M. T. & Frei, R. 2004. U-rich Archaean sea-floor sediments from Greenland - indications of > 3700 Ma oxygenic photosynthesis. *Earth and Planetary Science Letters,* 217**,** 237-244.

Rothe, M., Frederichs, T., Eder, M., Kleeberg, A. & Hupfer, M. 2014. Evidence for vivianite formation and its contribution to long-term phosphorus retention in a recent lake sediment: a novel analytical approach. *Biogeosciences,* 11**,** 5169-5180.

Rothe, M., Kleeberg, A. & Hupfer, M. 2016. The occurrence, identification and environmental relevance of vivianite in waterlogged soils and aquatic sediments. *Earth-Science Reviews,* 158**,** 51-64.

Ruttenberg, K. C. 1992. Development of a sequential extraction method for different forms of phosphorus in marine sediments. *Limnology and Oceanography,* 37**,** 1460-1482.

Ruttenberg, K. C. 1993. Reassessment of the Oceanic Residence Time of Phosphorus. *Chemical Geology,* 107**,** 405-409.

Ruttenberg, K. C. 2003. 8.13 - The Global Phosphorus Cycle. *In:* Holland, H. D. & Turekian, K. K. (eds.) *Treatise on Geochemistry.* Oxford: Pergamon. 585-643.

Ruttenberg, K. C. & Berner, R. A. 1993. Authigenic apatite formation and burial in sediments from non-upwelling, continental margin environments. *Geochimica et Cosmochimica Acta,* 57**,** 991-1007.

Saito, M. A., Sigman, D. M. & Morel, F. M. M. 2003. The bioinorganic chemistry of the ancient ocean: the co-evolution of cyanobacterial metal requirements and biogeochemical cycles at the Archean-Proterozoic boundary? *Inorganica Chimica Acta,* 356**,** 308-318.

Santisteban, C. 1994. Control estructural del sistema cárstico de la zona de los lagos de Cañada del Hoyo (Cuenca). Simposium sobre los ecosistemas acuáticos de Castilla-La Mancha, 1994. Book of abstracts, pp. 45.

Schenau, S. J. & De Lange, G. J. 2000. A novel chemical method to quantify fish debris in marine sediments. *Limnology and Oceanography,* 45**,** 963-971.

Schenau, S. J. & De Lange, G. J. 2001. Phosphorus regeneration vs. burial in sediments of the Arabian Sea. *Marine Chemistry,* 75**,** 201-217.

Schwertmann, U. & Murad, E. 1983. Effect of pH on the Formation of Goethite and Hematite from Ferrihydrite. *Clays and Clay Minerals,* 31**,** 277-284.

Scott, C., Lyons, T. W., Bekker, A., Shen, Y., Poulton, S. W., Chu, X. & Anbar, A. D. 2008. Tracing the stepwise oxygenation of the Proterozoic ocean. *Nature,* 452**,** 456-459.

Scott, C. T., Bekker, A., Reinhard, C. T., Schnetger, B., Krapež, B., Rumble, D. & Lyons, T. W. 2011. Late Archean euxinic conditions before the rise of atmospheric oxygen. *Geology,* 39**,** 119-122.

Shemesh, A. 1990. Crystallinity and diagenesis of sedimentary apatites. *Geochimica et Cosmochimica Acta,* 54**,** 2433-2438.

Sigg, L. & Stumm, W. 1981. The Interaction of Anions and Weak Acids with the Hydrous Goethite (α-Feooh) Surface. *Colloids and Surfaces,* 2**,** 101-117.

Slomp, C. P. 2011. 5.06 - Phosphorus Cycling in the Estuarine and Coastal Zones: Sources, Sinks, and Transformations. *In:* Wolanski, E. & Mclusky, D. (eds.) *Treatise on Estuarine and Coastal Science.* Waltham: Academic Press. 201-229.

Slomp, C. P., Epping, E. H. G., Helder, W. & Raaphorst, W. V. 1996a. A key role for iron-bound phosphorus in authigenic apatite formation in North Atlantic continental platform sediments. *Journal of Marine Research,* 54**,** 1179-1205.

Slomp, C. P., Thomson, J. & De Lange, G. J. 2004. Controls on phosphorus regeneration and burial during formation of eastern Mediterranean sapropels. *Marine Geology,* 203**,** 141-159.

Slomp, C. P., Van der Gaast, S. J. & Van Raaphorst, W. 1996b. Phosphorus binding by poorly crystalline iron oxides in North Sea sediments. *Marine Chemistry,* 52**,** 55-73.

Soetaert, K., Petzoldt, T. & Meysman, F. J. R. 2016. marelac : Tools for aquatic sciences, R package version 2.1.6, https://CRAN.R-project.org/package=marelac.

Sperling, E. A., Wolock, C. J., Morgan, A. S., Gill, B. C., Kunzmann, M., Halverson, G. P., Macdonald, F. A., Knoll, A. H. & Johnston, D. T. 2015. Statistical analysis of iron geochemical data suggests limited late Proterozoic oxygenation. *Nature,* 523**,** 451-454.

Stockdale, A., Krom, M. D., Mortimer, R. J. G., Benning, L. G., Carslaw, K. S., Herbert, R. J., Shi, Z. B., Myriokefalitakis, S., Kanakidou, M. & Nenes, A. 2016. Understanding the nature of

atmospheric acid processing of mineral dusts in supplying bioavailable phosphorus to the oceans. *Proceedings of the National Academy of Sciences of the United States of America,* 113**,** 14639-14644.

Stookey, L. L. 1970. Ferrozine - a new spectrophotometric reagent for iron. *Analytical Chemistry,* 42**,** 779-781.

Strickland, J. D. H. & Parsons, T. R. 1972. A practical handbook of seawater analysis. *Fisheries Research Board of Canada, Ottawa,* Bulletin 167 (2nd edition)**,** 45-64.

Stumm, W. & Morgan, J. J. 1970. *Aquatic chemistry: An introduction emphasizing chemical equilibria in natural waters,* New York, Wiley Interscience.

Sumoondur, A., Shaw, S., Ahmed, I. & Benning, L. G. 2008. Green rust as a precursor for magnetite: an in situ synchrotron based study. *Mineralogical Magazine,* 72**,** 201-204.

Sun, S., Konhauser, K. O., Kappler, A. & Li, Y. L. 2015. Primary hematite in Neoarchean to Paleoproterozoic oceans. *Geological Society of America Bulletin,* 127**,** 850-861.

Thamdrup, B. 2000. Bacterial manganese and iron reduction in aquatic sediments. *In:* Schink, B. (ed.) *Advances in Microbial Ecology.* Boston, MA: Springer US. 41-84.

Thamdrup, B., Canfield, D. E., Ferdelman, T. G., Glud, R. N. & Gundersen, J. K. 1996. A biogeochemical survey of the anoxic basin Golfo Dulce, Costa Rica. *Revista De Biologia Tropical,* 44**,** 19-33.

Thomson, D., Rainbird, R. H., Planavsky, N., Lyons, T. W. & Bekker, A. 2015. Chemostratigraphy of the Shaler Supergroup, Victoria Island, NW Canada: A record of ocean composition prior to the Cryogenian glaciations. *Precambrian Research,* 263**,** 232-245.

Tice, M. M. & Lowe, D. R. 2004. Photosynthetic microbial mats in the 3,416-Myr-old ocean. *Nature,* 431**,** 549-552.

Tice, M. M. & Lowe, D. R. 2006. Hydrogen-based carbon fixation in the earliest known photosynthetic organisms. *Geology,* 34**,** 37-40.

Tosca, N. J. & Guggenheim, S. Experimental Constraints on Precambrian Seawater Chemistry: Solubility in the Fe^{2+}-SiO_2(aq) System. Goldschmidt, 2014 Sacramento. Abstract 2502.

Tosca, N. J., Guggenheim, S. & Pufahl, P. K. 2016. An authigenic origin for Precambrian greenalite: Implications for iron formation and the chemistry of ancient seawater. *GSA Bulletin,* 128**,** 511-530.

Tyrrell, T. 1999. The relative influences of nitrogen and phosphorus on oceanic primary production. *Nature,* 400**,** 525-531.

Tyrrell, T. & Law, C. S. 1997. Low nitrate:phosphate ratios in the global ocean. *Nature,* 387**,** 793.

Van Cappellen, P. & Ingall, E. D. 1994. Benthic phosphorus regeneration, net primary production, and ocean anoxia - a model of the coupled marine biogeochemical cycles of carbon and phosphorus. *Paleoceanography,* 9**,** 677-692.

Van Cappellen, P. & Ingall, E. D. 1996. Redox stabilization of the atmosphere and oceans by phosphorus-limited marine productivity. *Science,* 271**,** 493-496.

Van der Zee, C., Slomp, C. P. & Van Raaphorst, W. 2002. Authigenic P formation and reactive P burial in sediments of the Nazare canyon on the Iberian margin (NE Atlantic). *Marine Geology,* 185**,** 379-392.

Vicente, E. & Miracle, M. R. 1988. Physicochemical and microbial stratification in a meromictic karstic lake of Spain. *Verhandlungen des Internationalen Verein Limnologie,* 23**,** 522-529.

Viollier, E., Inglett, P. W., Hunter, K., Roychoudhury, A. N. & Van Cappellen, P. 2000. The ferrozine method revisited: Fe(II)/Fe(III) determination in natural waters. *Applied Geochemistry,* 15**,** 785-790.

Walker, J. C. G. 1984. Suboxic Diagenesis in Banded Iron Formations. *Nature,* 309**,** 340-342.

Walter, X. A. 2011. *Anaerobic Iron Cycling in a Neoarchean Ocean Analogue.* PhD Thesis PhD Thesis, University of Neuchâtel.

Walter, X. A., Picazo, A., Miracle, M. R., Vicente, E., Camacho, A., Aragno, M. & Zopfi, J. 2014. Phototrophic Fe(II)-oxidation in the chemocline of a ferruginous meromictic lake. *Frontiers in Microbiology,* 5.

Ward, L. M., Kirschvink, J. L. & Fischer, W. W. 2016. Timescales of Oxygenation Following the Evolution of Oxygenic Photosynthesis. *Origins of Life and Evolution of Biospheres,* 46**,** 51-65.

Westermann, S., Stein, M., Matera, V., Fiet, N., Fleitmann, D., Adatte, T. & Föllmi, K. B. 2013. Rapid changes in the redox conditions of the western Tethys Ocean during the early Aptian oceanic anoxic event. *Geochimica et Cosmochimica Acta,* 121**,** 467-486.

Wheat, C. G., Feely, R. A. & Mottl, M. J. 1996. Phosphate removal by oceanic hydrothermal processes: An update of the phosphorus budget in the oceans. *Geochimica Et Cosmochimica Acta,* 60**,** 3593-3608.

Wirth, S. B., Gilli, A., Niemann, H., Dahl, T. W., Ravasi, D., Sax, N., Hamann, Y., Peduzzi, R., Peduzzi, S., Tonolla, M., Lehmann, M. F. & Anselmetti, F. S. 2013. Combining sedimentological, trace metal (Mn, Mo) and molecular evidence for reconstructing past water-column redox conditions: The example of meromictic Lake Cadagno (Swiss Alps). *Geochimica Et Cosmochimica Acta,* 120**,** 220-238.

Worsfold, P. J., Gimbert, L. J., Mankasingh, U., Omaka, O. N., Hanrahan, G., Gardolinski, P. C. F. C., Haygarth, P. M., Turner, B. L., Keith-Roach, M. J. & McKelvie, I. D. 2005. Sampling, sample treatment and quality assurance issues for the determination of phosphorus species in natural waters and soils. *Talanta,* 66**,** 273-293.

Xiong, Y., Guilbaud, R., Peacock, C. L., Cox, R. P., Canfield, D. E., Krom, M. D. & Poulton, S. W. 2017. Phosphorus cycling in Lake Cadagno, Switzerland: A low sulfate euxinic ocean analogue. *In review with Geochimica et Cosmochimica Acta*.

Zegeye, A., Bonneville, S., Benning, L. G., Sturm, A., Fowle, D. A., Jones, C., Canfield, D. E., Ruby, C., MacLean, L. C., Nomosatryo, S., Crowe, S. A. & Poulton, S. W. 2012. Green rust formation controls nutrient availability in a ferruginous water column. *Geology,* 40**,** 599-602.

Zhang, Y., Jacob, D. J., Horowitz, H. M., Chen, L., Amos, H. M., Krabbenhoft, D. P., Slemr, F., St. Louis, V. L. & Sunderland, E. M. 2016. Observed decrease in atmospheric mercury explained by global decline in anthropogenic emissions. *Proceedings of the National Academy of Sciences,* 113**,** 526-531.

Appendix A – X-ray diffraction patterns

This section contains the XRD patterns for the minerals used to develop the revised P speciation method in Chapter 3.

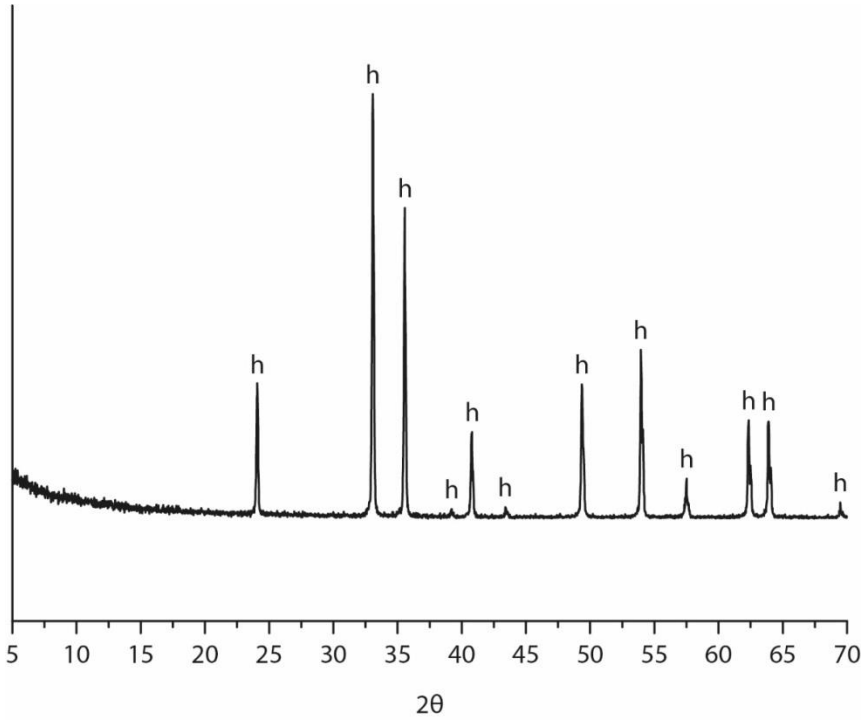

Figure A.1 XRD scan of synthetic hematite.

Peaks labelled "h" correspond with those of the reference pattern for synthetic hematite (PDF 33-0664, α-Fe_2O_3). Y axis is relative intensity.

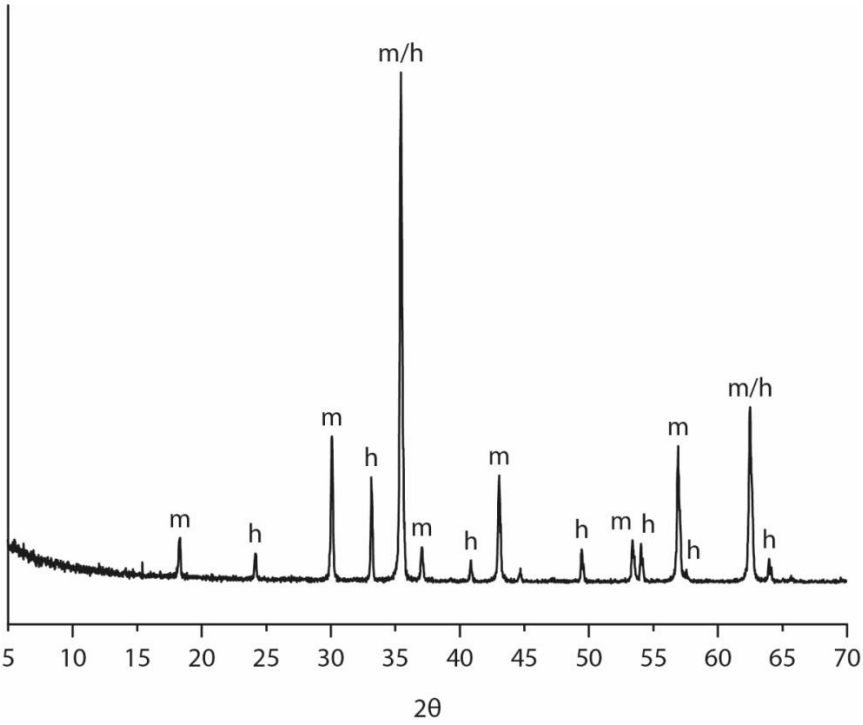

Figure A.2 XRD scan of the magnetite/hematite composite sample.

Peaks labelled “m” and “h” correspond with those of the reference pattern for synthetic magnetite and hematite respectively (magnetite PDF 19-0629, Fe_3O_4 and hematite PDF 33-0664, α-Fe_2O_3). Y axis is relative intensity.

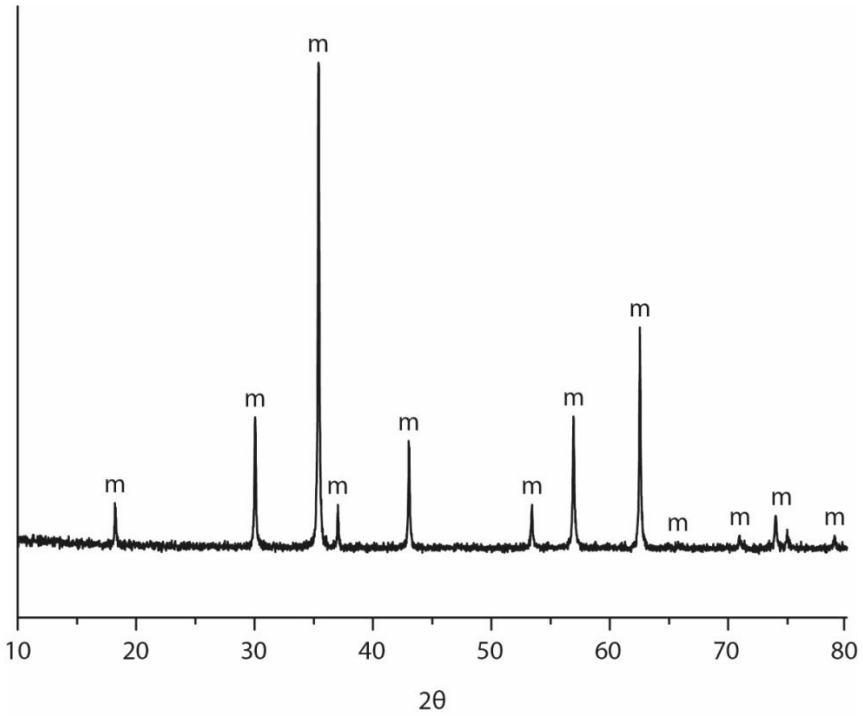

Figure A.3 XRD scan on the synthetic magnetite sample with co-precipitated P.

Peaks labelled “m” correspond with those of the reference pattern for synthetic magnetite (PDF 19-0629, Fe_3O_4). Y axis is relative intensity.

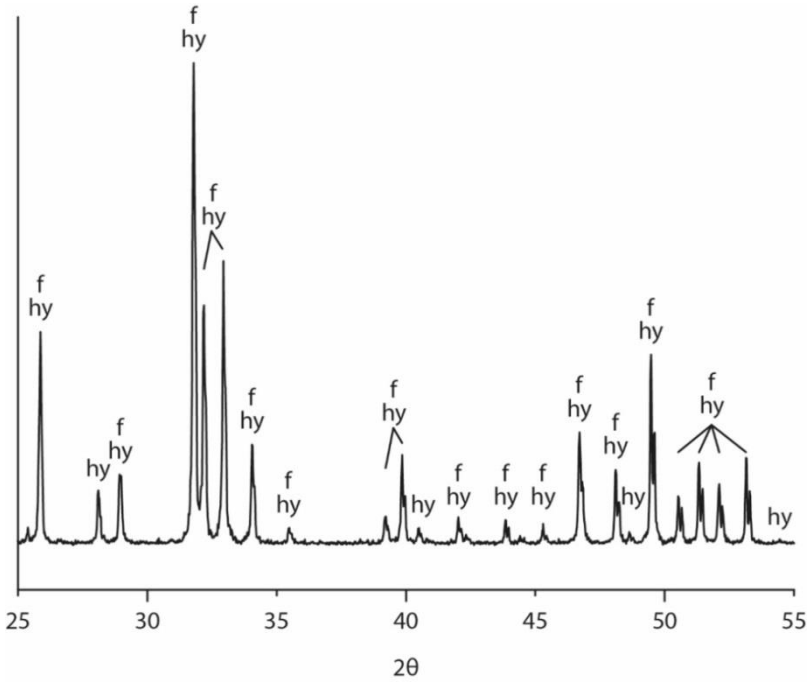

Figure A.4 XRD scan of Madagascan apatite.

Peaks labelled “f” and “hy” correspond with those of the reference pattern for fluorapatite and synthetic hydroxylapatite respectively (fluorapatite PDF 03-0736, $Ca_5(PO_4)_3F$ and hydroxylapatite PDF 09-0432, $Ca_5(PO_4)_3(OH)$. Y axis is relative intensity.

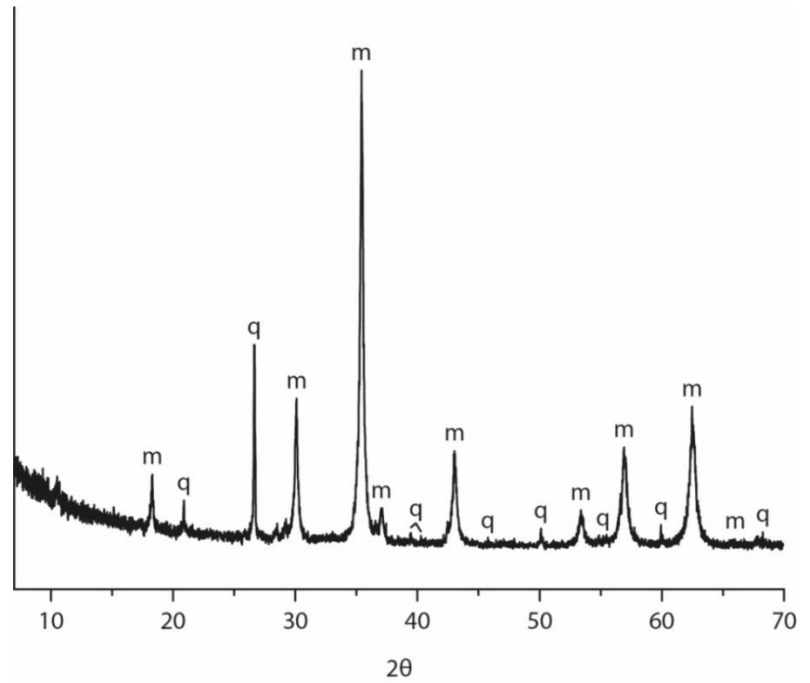

Figure A.5 XRD scan of BIF sample, Isua Greenstone Belt.

Peaks labelled “m” and “q” correspond with those of the reference pattern for synthetic magnetite and quartz respectively (magnetite PDF 19-0629, Fe_3O_4 and quartz PDF 33-1161, SiO_2). Y axis is relative intensity.